University of Tasmania

TRACTION CONTROL USING ARTIFICIAL NEURAL NETWORKS

David Andrew Butler, BEng. (Hon.)

Submitted in fulfilment of the requirements for the degree of Masters of Engineering Science (MEngSc)

Engineering (Civil & Mechanical)

March 2002

- Strictly Confidential -

DECLARATION

The thesis contains no material which has been previously accepted for a degree or diploma by the university or any other institution, except by way of background information and has been duly acknowledged in the thesis, and to the best of the author's knowledge and belief no material has been previously published or written by any other person except where due acknowledgment is made in the text of the thesis.

Signed: 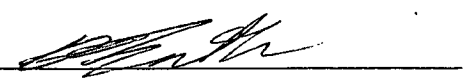

Dated this thirteenth day of September 2002

AUTHORITY OF ACCESS

This thesis contains confidential information and is not to be disclosed or made available for loan or copy without the express written permission from the University of Tasmania (i). Once released the thesis may be made available for loan and limited copying in accordance with the *Copyright Act 1968*.

(i) Enquiries should be directed to the Research and Development Office.

Signed: 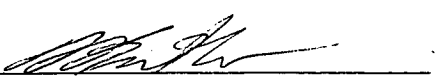

Dated this thirteenth day of September 2002

ACKNOWLEDGMENTS

This study was conducted as part of the "Intelligent Car" series of projects undertaken at the University of Tasmania aimed at incorporating artificial intelligent techniques into automotive applications. Such investigation could not be accomplished without a very enthusiastic research team and expert supervision.

As our research supervisor, Dr Vishy Karri has provided this and more. His perseverance in obtaining research grants and media attention, as well as providing help in any form where and when needed, is unparalleled in my experience. There is no doubt in my mind that his resent Prime Minster's Award for University Teaching was well deserved and completely justified.

Further, I'd like to extend my gratitude to Garth Heron, who cooperatively helped me throughout the design and construction of the Intelligent car. For his help in the design and development of the frame, suspension, wheel assembly, drive train, seat, steering, gear changer and other numerous sub-systems, as well as all of the workshop hours he put in, I am truly indebted. In particular, I'd like to thank him for constantly pushing for the unconventional approaches and high standards that make the Intelligent car the success it is.

Thanks must also be extended to Cranston Polson, Tim Moore and Bent Rosenkilde, who were primarily responsible for installing the fuel injection system and other engine associated equipment, and Helen Cunningham for sorting out all of the subsequent wiring problems and installing the dash components. Nick Jones and Robert Neben should also be complimented for their work in installing and calibrating the data acquisition system and associated sensors.

Finally, I should also note the help extended by the engineering technical and administration staff, as well as a number of local racers who gave us invaluable advice.

ABSTRACT

Modern traction control techniques manage driven wheel speed from data obtained through a small number of sensors from around an automobile. This data is then fed into an onboard computer that has been specially programmed to attempt to maximise driven wheel traction from its information base. Problems can arise, however, when abnormal conditions are encountered. The small number of sensors used as controller inputs and the various assumptions made during the conventional controller programming can lead to erroneous correction commands – with an increased risk of spinout and other undesirable situations.

The incorporation of artificial neural networks into the traction controller command logic has the scope to bring a two-fold advantage. The first stems from a neural network's ability to learn. It can be programmed through experimental data, and thus removes the need for tedious mathematics programming of the vehicle dynamics, which can be used to reduce controller cost and also brings about the possibility of continual reprogramming as the vehicle's condition alters due to wear, etc. The second is its ability to cope with data from a large number of sensors. With more sensors in place, the NN has a large base of information on which to make decisions on how to optimise traction. The result, hopefully, will be a traction control response that will provide superior traction solutions and be readily programmed to suit different applications.

This study aims at conducting preliminary research into the accuracy and application limitations of artificial neural networks in the interests of determining their feasibility for use in closed loop traction control applications. This includes selecting parameters to be predicted, as well as model input variables, network architectures and the collection of network training data for off-line control. To this end the accuracy of backpropagation and general regression neural networks will be compared using 14 input, single output architectures in the interests of predicting longitudinal acceleration, lateral acceleration and yaw angle, which are identified as crucial factors in vehicle dynamics control. The study also includes the complete construction of a test vehicle, in which the sensors are mounted and data acquisition systems used to gather the network training and testing data, from which this investigation is based. This work is a step towards establishing the applications of artificial neural networks to automobile applications on a sound mathematical and quantitative basis.

TABLE OF CONTENTS

LIST OF TABLES

LIST OF FIGURES

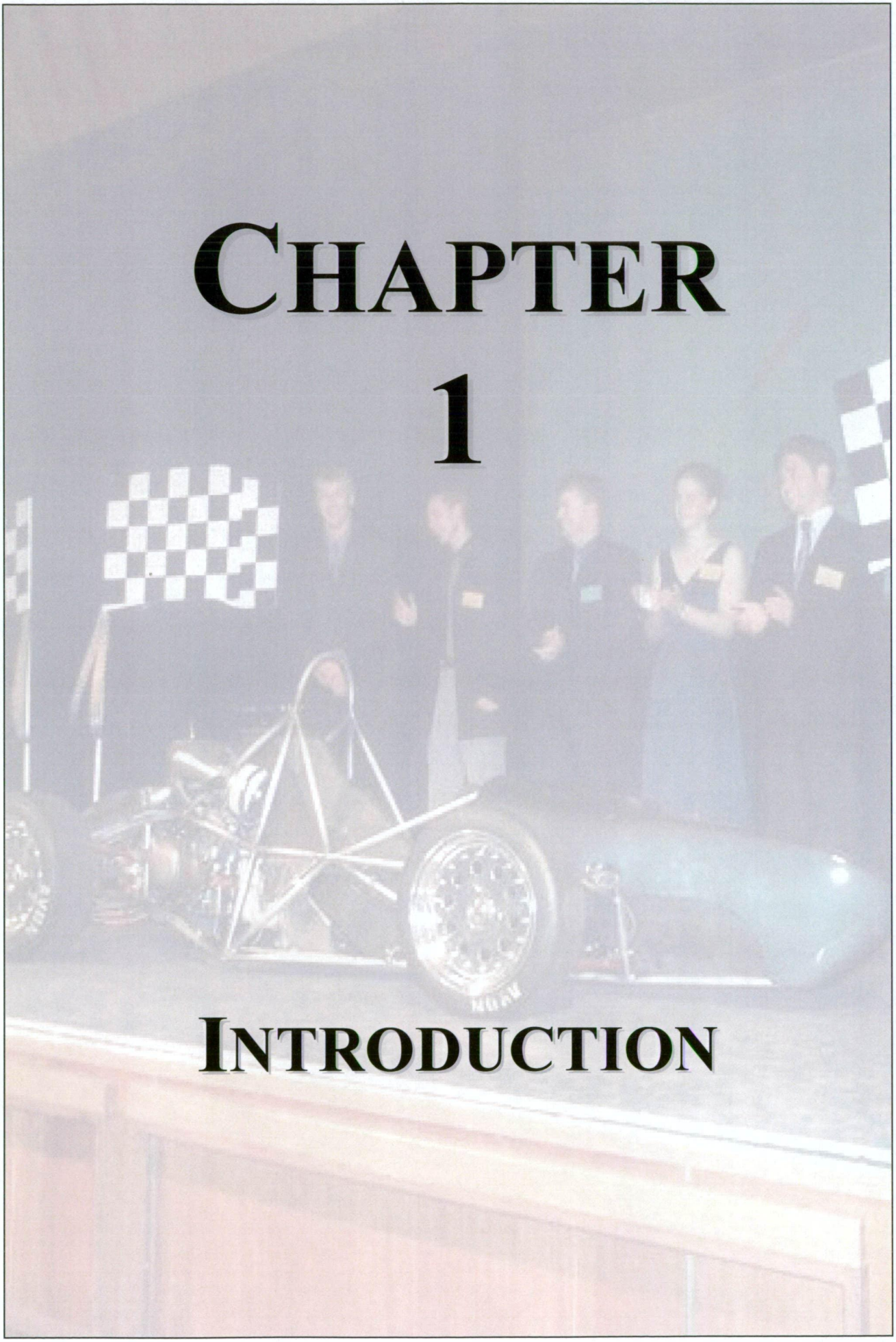

CHAPTER 1

INTRODUCTION

The road / vehicle / driver interface is a very complex system and accidents occur when the three do not work well together. A road is subject to all types of environmental conditions including varying pavement surfaces, weather and traffic density. The vehicle can be at varying levels of condition comprising of tyre pressure and tread depth, suspension wear, amount of loading, and a host of other factors. And lastly different drivers operate at very diverse skill levels, states of mind and physical conditions. The reduction in the frequency and severity of accidents stemming from these factors is of a prime concern to the automotive industry [1, 2, 3].

The most common way of increasing driver safety has been the consideration of passive safety systems, which are designed to prevent accidents and their risk of injury by improving driving conditions and by increasing safety during an accident. These include constructing roads with clear markings and signage, safety barriers, minimal obstacles such as trees and telegraph poles and good pavement surfaces with good drainage properties. It also includes automotive systems such as seat belts and air bags as well as general safety considerations in vehicle design [1, 2, 4].

The design of passive safety systems has, however, reached a 'point of diminishing returns', with investments of large amounts of resources resulting in marginal increases in safety. It is the driver, as the control unit, that has long been the unknown element. In fact, 80 and 90% of automotive accidents stem from driver error, including inappropriate speed, not driving to weather conditions, failure to maintain safety margins and disputes over right-of-way, as suggested by Gohring [5]. It has also been noted that the introduction of such systems has effected driver behaviour in subtle ways. As an example, studies have shown that a 1% increase in vehicle speed resulted from the introduction of seat belts. The introduction of other systems has also been linked to higher travel speeds. Evens [6] shows that it is evident that by increasing the margins of safety, drivers soon adjust their behaviour to one that they perceive contains an acceptable level of risk. Conversely, it has also been observed that the introduction of these safety systems has had the overall effect of reducing accident frequency and severity. This shows that, ultimately, the addition of any type of safety systems gives the driver the choice to use its performance benefits to either drive more aggressively or to drive within a larger safety envelope [6]. Education campaigns have been the

mainstay of efforts to influence driver behaviour to err on the side of safety in this respect. Advanced driver courses are also prevalent, teaching drivers to foresee unexpected driving conditions and react in the most appropriate way. The fact remains, however, that drivers make mistakes and most do not know how to control their vehicle optimally during critical situations.

Most drivers rarely experience emergency situations while driving and as such are seriously lacking in ability when a critical driving condition occurs. In the event of an imminent accident this means that most drivers will not react in the most appropriate way. This could stem from slow reaction times, the driver's inability to recognise the vehicle's level of instability, a lack of knowledge of the vehicle's dynamic behaviour under such conditions or by making corrections that are either erroneous or of incorrect magnitude. For instance, it has been shown that drivers with reaction times half a second faster than average times experience 60% less rear-end collisions, 50% less collisions at intersections and 30% less frontal crashes [3, 4, 5, 7].

It can be seen that there is a need to provide the driver with support during these critical situations. To this end, active safety systems have been developed to fulfil driver shortcomings so that the automobile will avoid an accident with the largest margin of safety, in contrast to passive systems which only seek to fulfil shortcomings in road and automotive design with respect to accident frequency and severity. This means that active safety systems must assess when to automobile is about to be involved in an accident, register the driver's inputs and implement the most appropriate course of action, possibly by overriding driver control [1, 2, 4, 8]. Current systems in use presently include the:

- Anti-lock Braking System (ABS)
- Traction Control System (TCS) and Acceleration Slip Regulation System (ASR)
- Vehicle Dynamics Control System (VDC) and Electronic Stability Program (ESP)

To varying levels of ability, these systems can identify the stability of a vehicle and alter the driver's inputs during critical situations to emulate the abilities of a well trained, professional driver. The goal being to provide a vehicle control system that will enable the driver to drive their automobile to its physical limit, in a predictable manner, as emergency situations dictate [1, 2, 7].

It can be seen that, since the stability of the vehicle is ultimately determined at the tyre / road interface, the operation of these systems must make best use out of the tractive forces available at the tyres. ABS controls the hydraulic pressure to the brakes to increase steering control and avoid wheel skid during panic braking situations. TCS seeks to optimise the available traction at each driven wheel to improve stability and acceleration through the control of wheel torques using engine, brake and/or differential intervention. And VDC advances both ABS and TCS technologies to provide broad stability control over a range of situations by controlling individual wheel torques, including braking wheels to help steer through corners when travelling too fast.

Of course, the interface between the road and the tyres are subject to a large variety of influences that effect their ability to provide accelerative and centripetal forces to the vehicle. The dynamics of a vehicle is far from a simple problem. A vehicle is subject to numerous forces including propulsive forces, aerodynamic drag, rolling resistance, crosswinds and centrifugal forces. This, coupled with other complex elements such as tyre grip and deformation, suspension movement, weight distribution and steering angle make the dynamics extremely difficult to predict mathematically and even harder to control. As such, the active control of a vehicle must measure a large variety of parameters for efficient control, and make numerous assumptions when parameter measurement and integration into a control system is either too impractical or too expensive. ABS and TCS generally only measure wheel speeds in their control logic, while VDC also integrates steering angle, yaw rate and lateral acceleration measurements into the system, in order to gain a greater understanding of the dynamics of the vehicle. This limited number of sensory inputs has been shown to provide enough data for proficient automotive control in most conditions, where the general assumptions made hold with reasonable accuracy, but can fall down in abnormal situations, resulting in flawed control.

Matues [9] suggests that future trends in active control systems seek to fill this gap by improving the usage of available traction under complex real road conditions and extend their range of performance. This includes an increase of sensory input and the control of additional vehicle parameters such as rear wheel steering, automatic load distribution, real time damping, active suspension and active camber change [4, 10, 11]. Of course, this also means a significant increase in the complexity of the necessary control algorithms, which grow in size exponentially with the inclusion of additional parameters, as illustrated by Bannatyne [12].

Focusing on TCS, it can be seen there are numerous situations when its operation does not represent optimum control, in fact many systems include the facility to deactivate the system when driving in abnormal conditions because its operation can be so erroneous [3]. The addition of extra sensory data can result on more compressive control in TCS operation scenarios, which includes combined longitudinal and lateral acceleration at a range of speeds and surface conditions. The complexity of the system, however, means that the inclusion of increased data would also require extensive investigation and algorithm development to model the effects on the vehicle dynamics using conventional techniques.

Artificial neural networks (ANN) offer an alternative approach to this method. ANNs have been in use by the manufacturing industry for some time and offer numerous advantages. Firstly, the controlled system does not have to be fully understood by the programmer because the ANN 'trains' itself from historical data, enabling the modelling of complex systems with minimal effort. Secondly, the statistical model of the ANN is more complex than conventional models, enabling it to handle a wider variety of operating conditions. Thirdly, as sensory input deteriorates (ie. as a result of sensor failure) the ANN will continue to operate with diminished accuracy, unlike conventional models that may give highly erroneous commands. And finally, because most of the computing has been done in the 'training' stage of programming, ANNs can provide control results with minimal computing power, in real time.

The goal of this study is to test the appropriateness of using ANNs for traction control by investigating their accuracy using additional sensory data during off-line control testing. This includes the construction of a test vehicle and the addition of numerous sensors for both chassis dynamics measurement and engine control data collection. The parameters measured total 40 and include:

- Steering wheel angle
- Hydraulic brake pressure on front and rear circuits
- Throttle position
- Engine speed
- Individual wheel speeds
- Independent suspension travel
- Acceleration in three dimensions
- Yaw, pitch and roll rates
- Yaw, pitch and roll angles

The following chapters will review the approach taken to measure as many parameters as possible that may have had an effect on TCS operation and identify which values produce the most accurate representation of the vehicle dynamics. Different ANN architectures will then be compared to the collected data to gain an estimate of their accuracy and scope for future development.

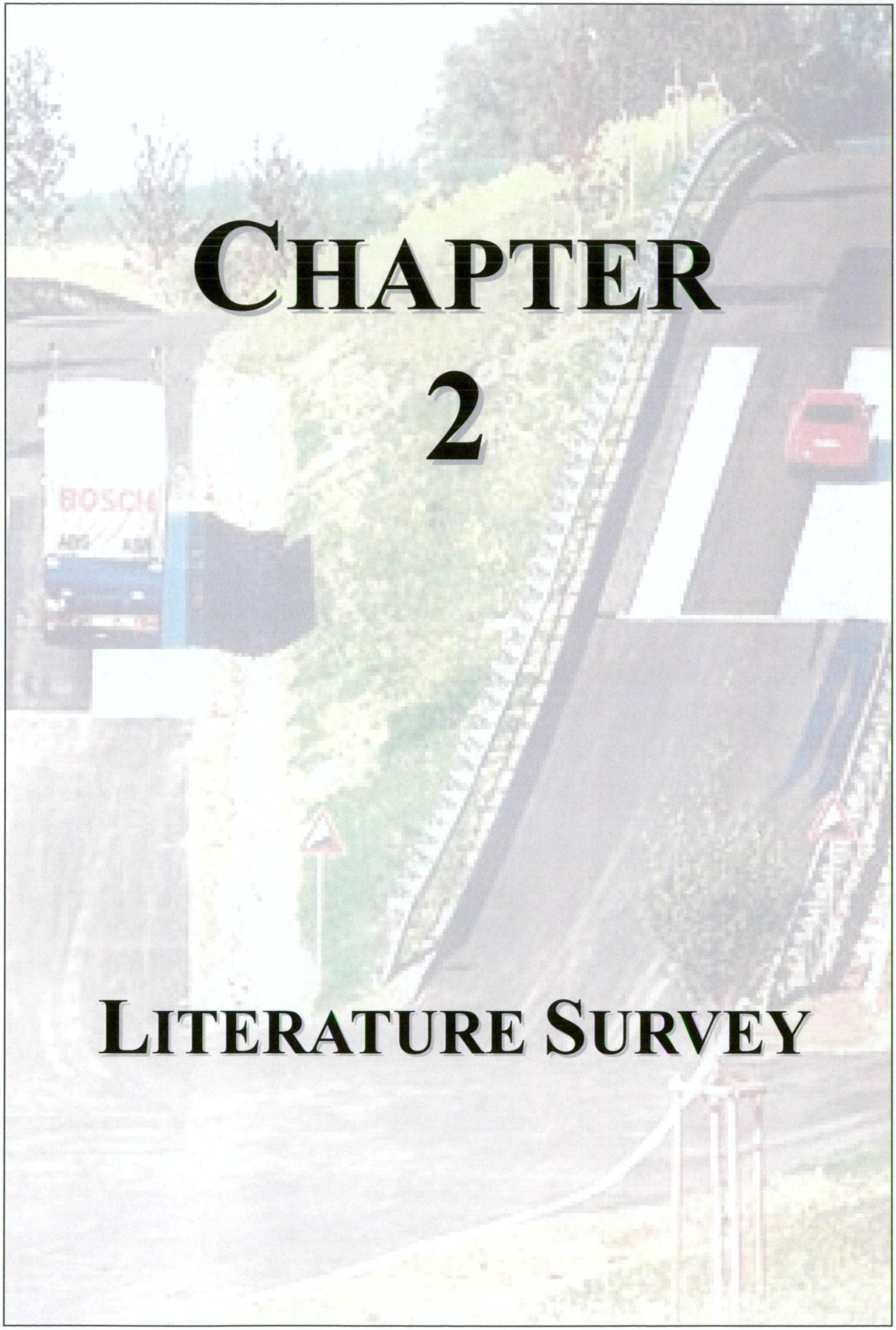

CHAPTER 2

LITERATURE SURVEY

How well tyres grip the road ultimately defines vehicular stability, and as such, this chapter will first introduce the reader to the fundamental principles behind tyre dynamics. The effects of the tyre forces with respect to vehicle dynamics will then be discussed, along with the inclusion of several standard performance tests. This will then lead to the examination of operational theory behind ABS, TCS and VDC, with the sensory and control requirements between each system highlighted in relation to traction control. Some alternative control logic research will also be presented before introducing the applications and basic operational principles of artificial neural networks.

2.1. Tyre Dynamics

Tyres are obviously an important consideration in determining vehicle dynamics and stability. They are the connecting element, linking the vehicle to the road surface, and must provide sufficient propulsive, braking and lateral forces in the current environmental conditions before the vehicle can complete any type of manoeuvre. Matues [9] expresses this by stating that the efficiency with which the tyre patches are utilised in a limit handling situation determines the performance envelope of the vehicle. As such, a study into vehicle dynamics must first consider the tyre / road interface and its effects on performance. This includes the effects of normal tyre forces, slip values and slip angles on longitudinal and lateral force combinations, as discussed in the following sections [1, 2, 13, 14].

2.1.1. Normal Tyre Forces

The normal tyre force (F_N) is defined as the downward force exerted between the tyre and the road. The force is generally the result of vehicle mass, but also varies depending on how the automobile is sitting on its suspension. As an example, uneven surfaces will effect normal tyre forces at individual wheels whereas cornering will produce higher loads on the outside wheels.

The contact patch between the tyre and the road is partially defined by the normal forces applied to it. The area of this patch and the way it transfers the tyre forces to the road define the tyre's effectiveness. Tyre pressure, tread compound and wear, the effect of sidewall deflection and speed all effect the tyre in different ways. Figure 2.1 shows the trapezoidal distribution of the normal tyre forces that arise primarily because of the deformation of the sidewalls [10].

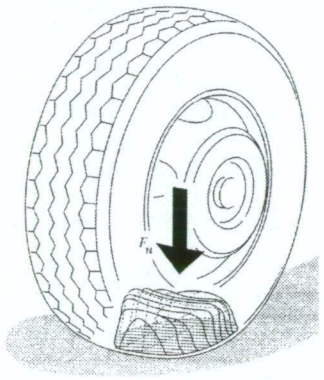

Figure 2.1: Contact patch pressure distribution from normal loading (radial tyre) [1, 2]

2.1.2. Longitudinal Tyre Forces

Straight line braking, acceleration and rolling resistance produce longitudinal forces on tyres. Figure 2.2 shows that for a wheel travelling with longitudinal velocity (v_x) the braking torque (M_B) produces a longitudinal force (F_L) which is transferred through the tyre to the road.

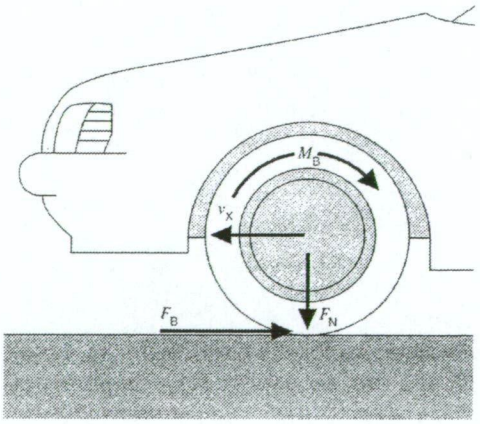

Figure 2.2: Longitudinal forces applied to a wheel [1,2, 10, 36]

Inspection also shows that the maximum braking force that can be achieved will be:

$$F_{L\,max} = F_N \mu_L$$

where μ_L = longitudinal coefficient of friction between tyre and road

Eqn 2.1

Further inspection also shows that in this case:

$$v_x \neq \omega r$$

where ω = rotational speed of wheel

r = radius of tyre

Eqn 2.2

This is because of the deformation of the contact patch. As the tyre rotates the contact patch deforms to varying magnitudes and the vehicle will travel less distance than the tyre's revolution would infer. This relationship between longitudinal wheel speed and vehicle speed is called tyre slip (λ_L) and defines the level of force transfer from a tyre to the road. It should be noted, however, that the definition of λ_L varies depending on whether the wheel is under braking or accelerating forces [3].

Under brakes

$$\lambda_L = \lambda_B = (v_x - \omega r) / v_x$$

where $\omega r \leq v_x$

Eqn 2.3

Under acceleration

$$\lambda_L = \lambda_A = (\omega r - v_x) / \omega r$$

where $\omega r \geq v_x$

Eqn 2.4

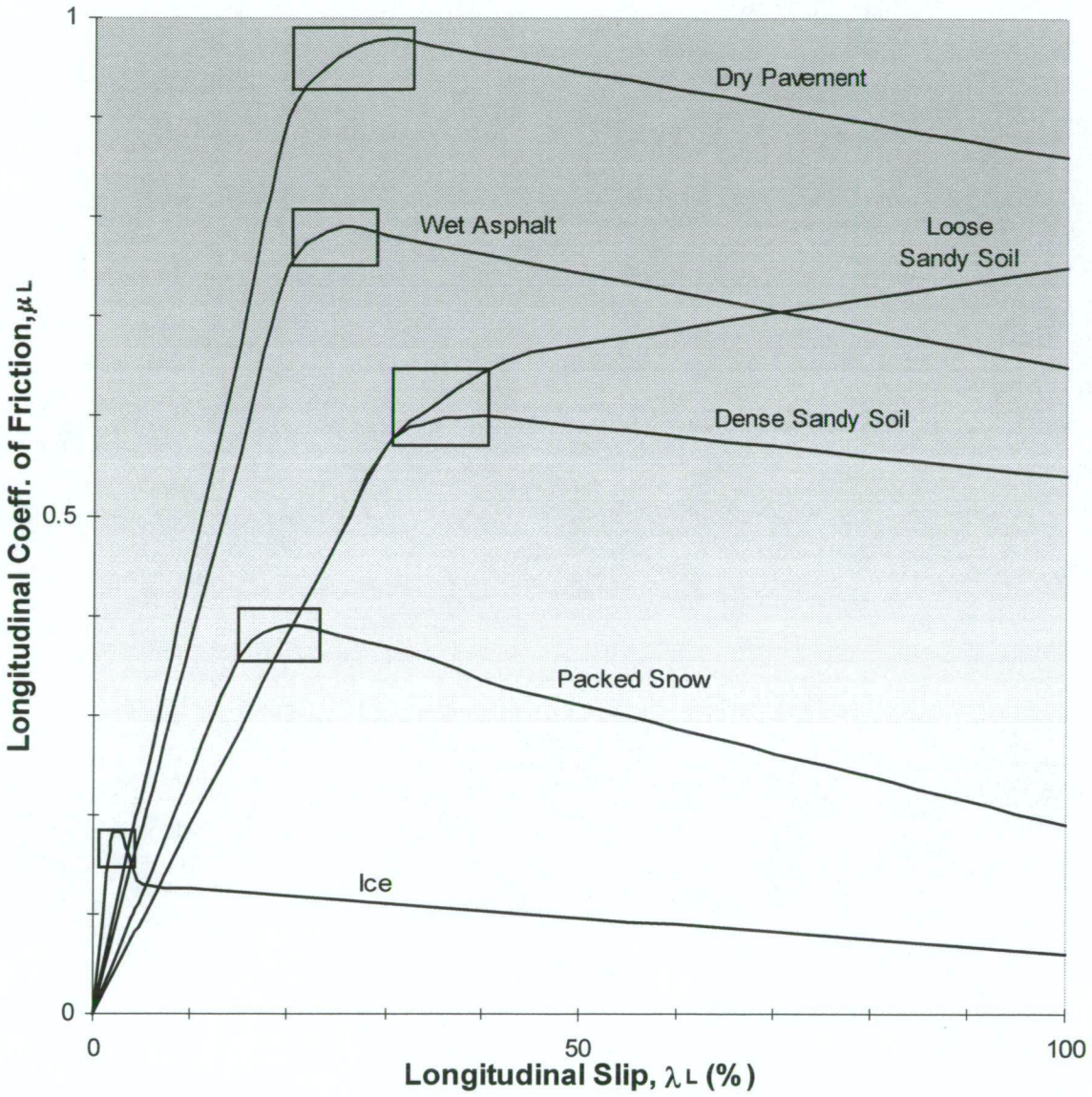

Figure 2.3: Operation of longitudinal slip on different surfaces [1, 2, 3, 15]

In relation to vehicle dynamics, slip operates in three modes, as shown in Figure 2.3. The foremost is in the linear region at low slip values, in which most driving conditions occur. When vehicles are driven within this region, demands for more braking or acceleration can be easily met by the tyres, resulting in stable driving conditions. The region following this is the transition region (boxed) where the tyres reach their maximum level of adhesion. In this region tyres are operating at their very limit but are difficult to control without going into the final region, the unstable region. In the unstable region increases of slip generally result in reduced adhesion, the result being a

locked wheel under brakes or a rapidly spinning wheel under acceleration, both of which are undesirable and are causes of loss of control situations [3, 10].

Looking at the figure we can see that this interpretation is a generalisation. It is true for most driving situations but falls down for driving on loose surfaces. However in these cases the soil can not transmit the higher tractive forces without tearing apart. The result being that tyres 'dig' themselves into the road with reduced traction than the curve would suggest [1, 2].

This effect, however, has its advantages on some surfaces. Consider an unsealed road that has a firm clay base covered in loose gravel. The coefficient of friction curve suggests that a vehicle should realise very low levels of adhesion on the gravel surface at any rate of slip, which is not the case. The ability of the tyres to 'dig' into the road at high levels of slip has the advantage of removing the loose gravel and exposing the clay surface of the road. The effect is a marked increase in traction to the road.

2.1.3. Lateral Tyre Forces

Longitudinal force relationships only apply to vehicles travelling in a straight line. Lateral forces (F_S) must be provided through the tyres to enable an automobile to turn, and results in a deformation of the tyre sidewalls, as can be seen in Figure 2.4.

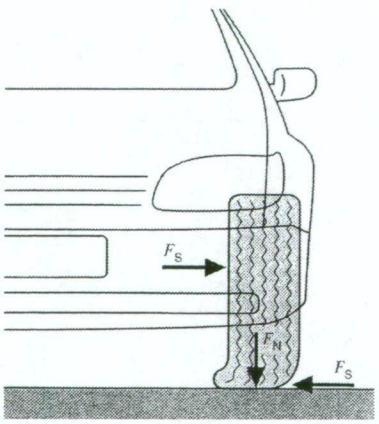

Figure 2.4: Tyre flex as a resultant of lateral forces [1, 2, 5]

This deformation causes the whole tyre to move with a velocity component in the lateral direction (v_y), termed lateral slip (λ_S).

$$\lambda_S = v_y / v_x \qquad \textit{Eqn 2.5}$$

The slip angle (α) can also be defined by these values. It is the angle separating the resultant wheel speed (v_α) and the longitudinal wheel speed (v_x), as shown in Figure 2.5.

$$|v_\alpha| = \sqrt{(v_x^2 + v_y^2)} \qquad \textit{Eqn 2.6}$$

$$\alpha = \tan^{-1} (v_y / v_x)$$
$$= \tan^{-1} (\lambda_S) \qquad \textit{Eqn 2.7}$$

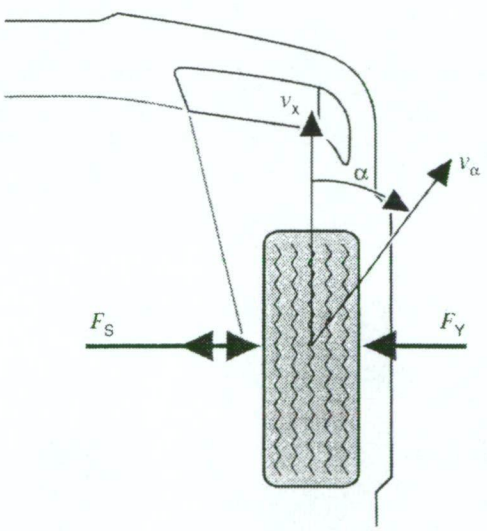

Figure 2.5: Lateral forces and slip applied to a wheel [1, 2, 4, 10]

The magnitude of the lateral force that can be transferred to the road is defined by the coefficient of lateral force (μ_S) according to the relation:

$$F_S = F_N \mu_S \qquad \textit{Eqn 2.8}$$

However it should be noted that because of the complexities in tyre deflection under lateral loads that μ_S is particularly sensitive to the magnitude of the normal load (F_N) during accelerating and braking, as well as to slip angle (α) and road surface. Figure 2.6 shows an example of this relationship. This is in contrast to the longitudinal coefficient of friction (μ_L), which is primarily dependent only on road surface [1, 2, 4, 10].

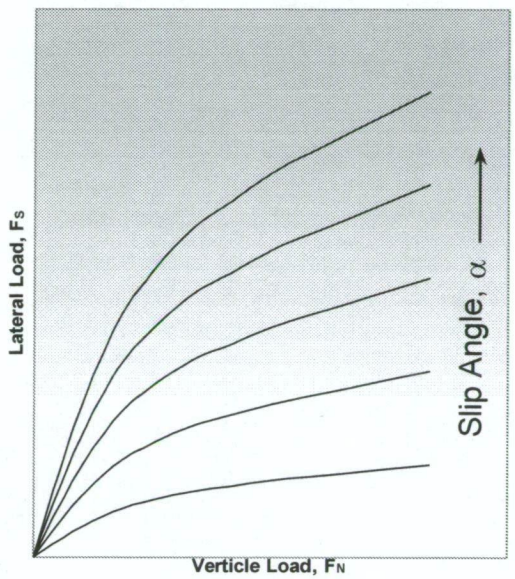

Figure 2.6: Variation of lateral force as a function of vertical load and slip angle [4]

2.1.4. Effects of Slip

Obviously, cases of just longitudinal or just lateral forces acting on a vehicle are special cases that do not reflect all aspects of driving, especially in emergency situations. Stability requires the precise control of differing combinations of longitudinal and lateral forces under all conditions. This is made harder by the fact that the maximum achievable longitudinal forces change with the amount of current lateral forces and vice-versa as shown in Figure 2.7.

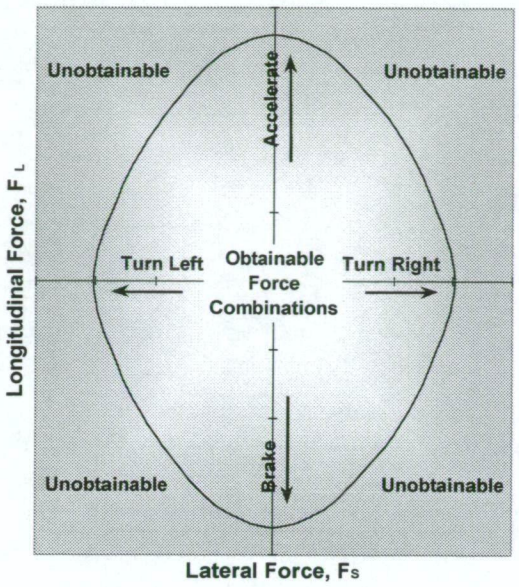

Figure 2.7: Variation of available lateral and longitudinal forces [4]

This figure shows the field of longitudinal and lateral forces available to the tyres, and thus to the vehicle, under specific driving conditions. The size and shape of this field varies dramatically depending on factors such as road condition, tyre condition and vehicle setup, as shown in Figure 2.8 which compares the available acceleration field of a luxury FWD vehicle to that of a performance RWD.

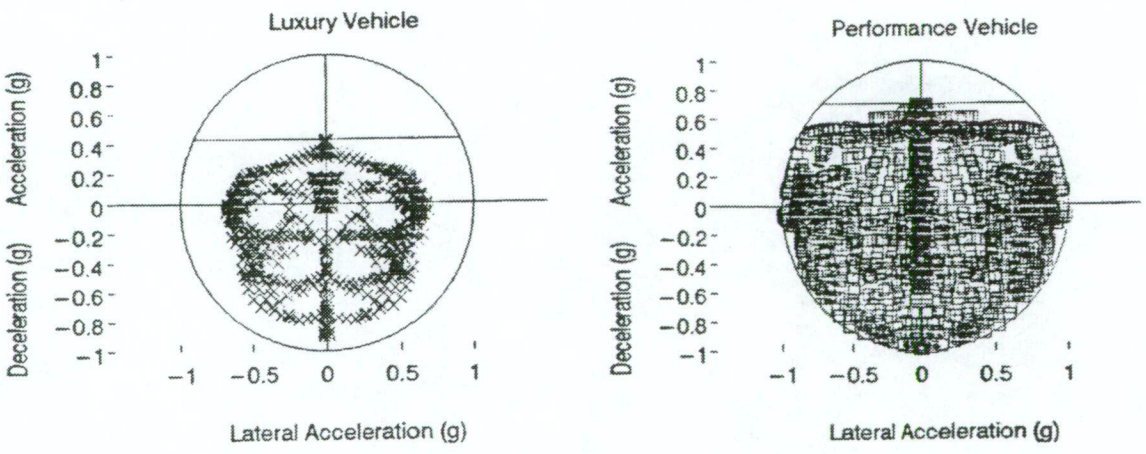

Figure 2.8: Comparison of acceleration fields for different vehicles [4]

This diagram of longitudinal and lateral forces can then be incorporated into the above lateral and normal force diagram (Figure 2.6) to gain a diagram that incorporates the

entire field of tyre loads. Figure 2.9, thus, shows the entire capabilities of each tyre to transmit force to the specific road surface as a function of vertical loading which arises due to driving conditions.

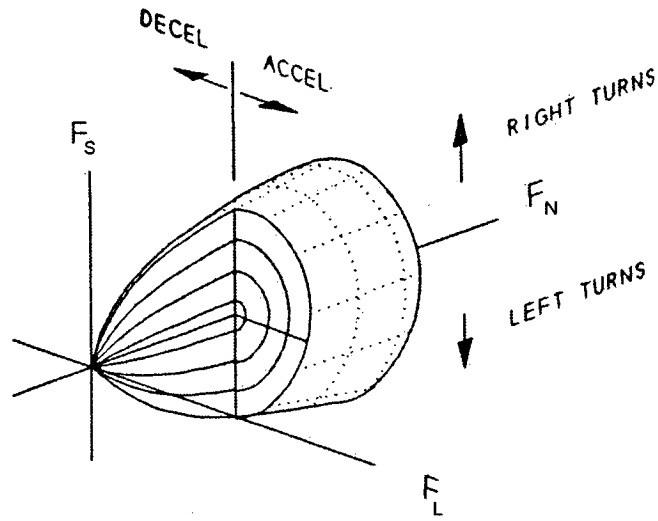

Figure 2.9: Total tyre force capability map [4]

The reasons for the complexity of these force relationships are due to slip, as shown in Figure 2.10. It can be seen that any increase of longitudinal force within the stable region (below 10% longitudinal slip) results in a corresponding reduction in lateral adhesion. It can also be seen that increasing rates of slip angle reduces available longitudinal forces but increases possible lateral loads.

This means that the tyre's ability to transfer the required level of adhesion is a function primarily of normal load (F_N), longitudinal slip (μ_L), slip angle (α), surface condition and tyre condition.

$$F_L, F_S = f(F_N, \mu_L, \alpha, \text{surface condition, tyre condition})$$

Eqn 2.9

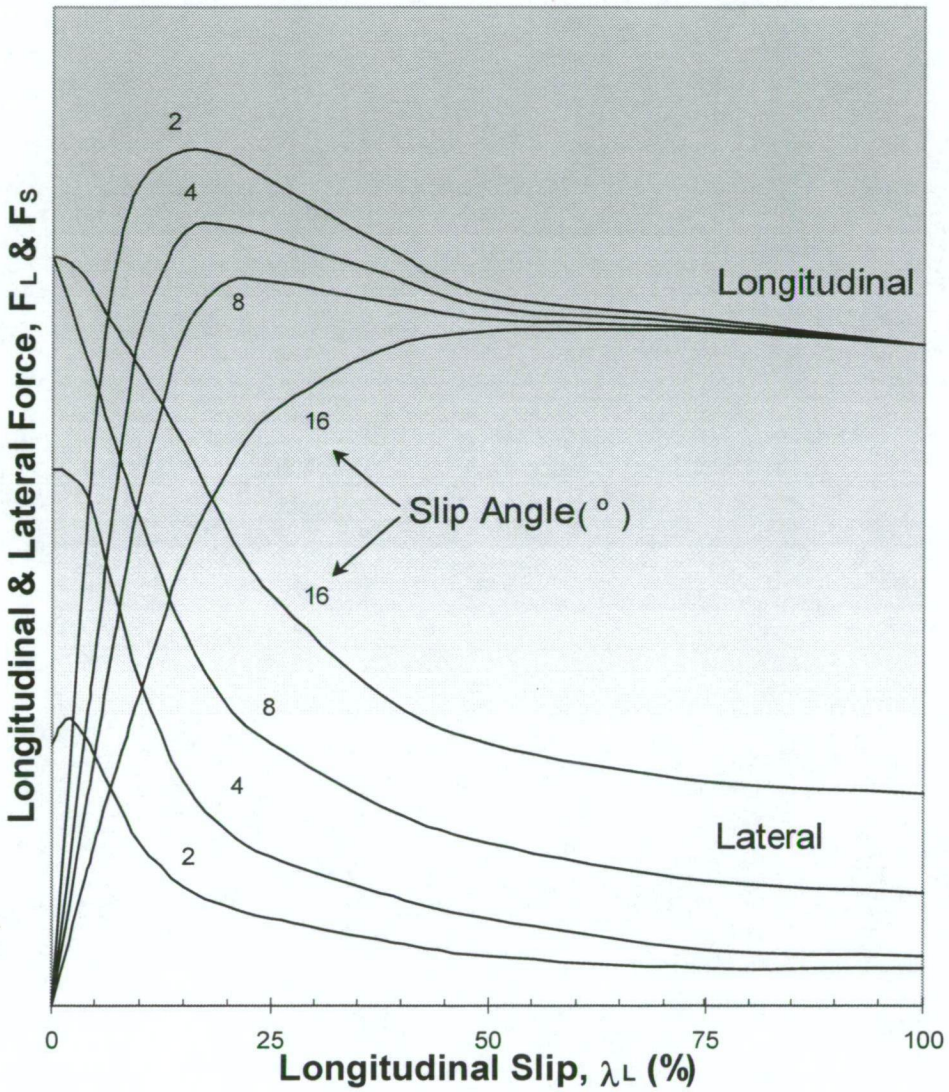

Figure 2.10: Longitudinal and lateral forces as a function of slip and slip angle [3, 16, 18, 23, 28, 33]

2.2. Vehicle Dynamics

Now having an understanding of the behaviour of individual tyres, analysis can proceed into the dynamics of the complete vehicle. Figure 2.11 shows the common simplified two-dimensional vehicle system.

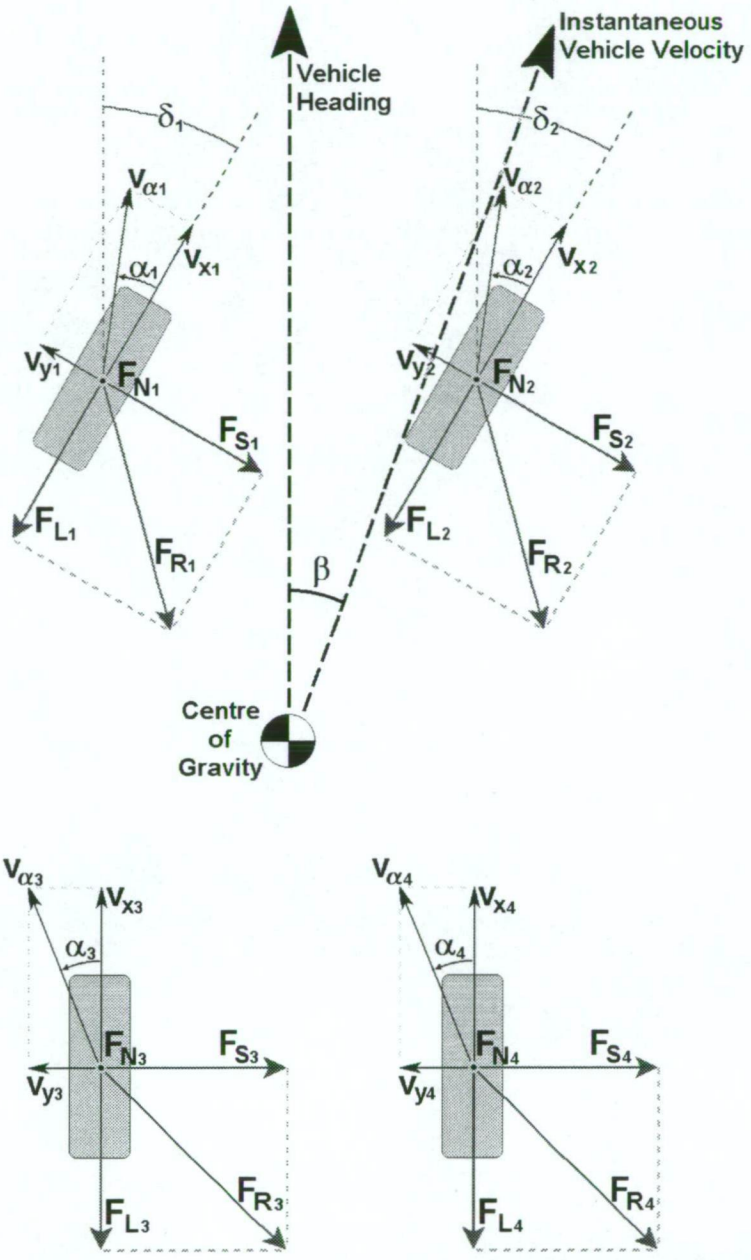

where F_R = resultant of F_L & F_S

δ = steered angle

β = yaw (drift) angle

Figure 2.11: Vehicle parameters

The model describes a vehicle, with two wheel steering, as a body in which all loads are transmitted to it by the four tyres. The steered angle (δ) of the front wheels as well as normal, longitudinal and lateral loads, wheel velocities, slip value and slip angle are all used to model the dynamics of each wheel. The resultant forces (F_R) of each tyre are

then translated to obtain the dynamics of the vehicle mass, with the position of its centre of gravity defined by vehicle wheel base and track width. The overall vehicle dynamics can then be defined through the motion of its centre of gravity, including its yaw angle (β), as stated by Mohan et al. [10].

Of course, due to the two-dimensional nature of this model, it is very simplified and does not include factors such as rollover probability. A comprehensive model of vehicle dynamics should include the parameters shown in Figure 2.12 which include:

- Three dimensional position of centre of gravity
- Acceleration in three axes
- Yaw, pitch and roll
- Suspension travel
- Body loading such as aerodynamic drag and crosswind effects
- Wheel rotational speed
- Vehicle velocity

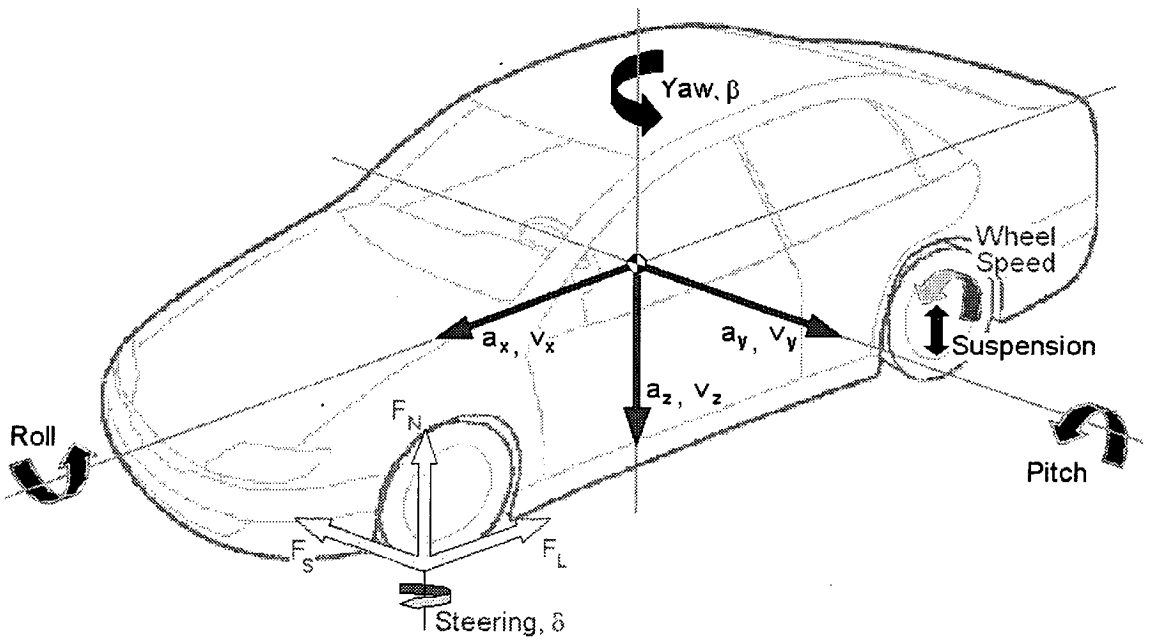

Figure 2.12: Three dimensional parameters for vehicle dynamics

However, difficulties arise with the inclusion of all of these parameters into a vehicle model. The dynamics of an automobile are extremely complex and as such would

require extensive and expensive work to gain an accurate model under all driving conditions using current techniques. Vehicle control systems also require result sets many times a second in real time. This sort of demand on such a complex model would require large amounts of computing power to obtain results that would be of use to any current control system. Coupled with the fact that the sensors required to measure all of these parameters has been considered too expensive by manufactures to be included in commercially available automobiles has resulted in extremely little publicly available research publications into the problem [3, 12].

2.2.1. Stability

Tyres must remain sure-footed on the road surface without excessive slippage to provide stability to a vehicle. The consequence is that a vehicle must be able to maintain a path that reflects the driver's steering angle, to itself be considered stable. The vehicle's yaw angle (β) and yaw rate (dβ/dt) must correlate to its intended heading, dynamic lateral response is the critical factor [1, 2, 3, 4, 17].

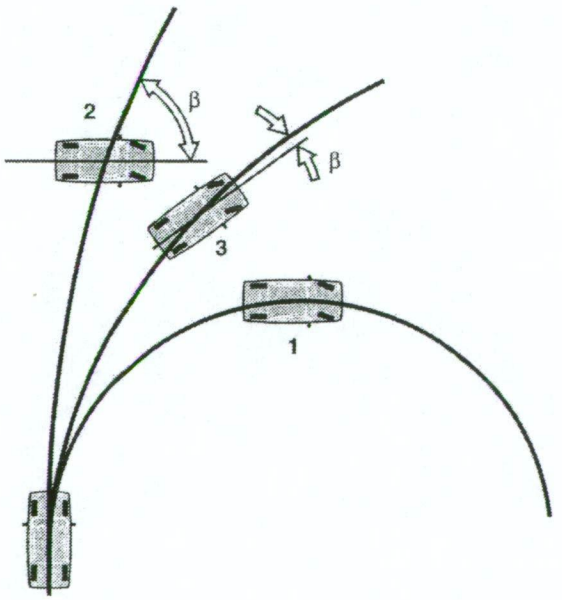

Figure 2.13: Dynamic lateral response [1, 2, 3, 7]

The effect of yaw angle on stability can be seen in Figure 2.13. In this figure a vehicle is being driven at three different speeds into a corner. An identical steering input is then applied to each at the start of the curves.

Curve 1

The slowest vehicle follows a path that is an accurate reflection of the steering angle because the applied lateral forces are a small fraction of the potential tractive force available through the tyres, and very little slip results. The vehicle is well within the stable range with very little yaw angle and zero yaw rate.

Curve 2

The fastest vehicle starts to go out of control as soon as the steering input is applied. This is because the lateral forces needed to get the car around the corner are higher than one or more of the tyres can provide, the result in this case being significant over-steer. The resultant high levels of slip causes the vehicle to spin out of control with both large yaw angle and yaw rate.

Curve 3

The vehicle with moderate speed enters the corner at its traction limit and the induced lateral forces can just be met by the tyres. To do this the tyres must slip to a reasonable degree and as such the vehicle will not follow the steered course precisely. This incites a small yaw angle as well, but the vehicle remains in control and stable with a small yaw rate.

It can be seen that to remain stable none of the tyres on a vehicle must be allowed to slip excessively. The vehicle must also behave within the bounds of a small, predetermined yaw angle and have a yaw rate that operates within certain limits for stability. The allowable limits for both yaw angle and yaw rate will each vary with the prevailing vehicle dynamics, predominantly speed and road surface.

2.2.2. Performance Tests

There are a number of standard performance tests aimed at providing quantitative and qualitative comparisons between vehicles and vehicle control systems. Quantitative tests aim at removing the most subjective element of the driver / vehicle / road system, the driver, and replacing their inputs with various open-loop commands. These tests are incorporated into the ISO standards and include [1, 2]:

- Steady-state skid pad circulation
- Transition response
- Braking while cornering
- Sensitivity to crosswinds
- Straight running properties
- Power on / power off transitions

These open loop tests do not provide sufficient data to evaluate vehicle response completely. The subjective, closed loop, assessments made by experienced drivers remains an important tool in gathering data on general handling characteristics. To this end, a number of standard tests are carried to gauge vehicle stability, steering response, brake performance and handling at the limit, including the "elk" and the "split μ" tests.

2.2.2.1. Steady-State Skid Pad

During this test a vehicle is placed on a skid pad and driven around a circle at a number of defined speeds. This gives the maximum lateral acceleration that the test vehicle can reach under steady-state conditions and also provides data on the vehicle's dynamic handling transitions under a range of cornering forces.

2.2.2.2. Transition Response

Transition response tests aim at obtaining data on how the vehicle handles under a range of different driving manoeuvres. Such manoeuvres include selected steering inputs after driving in a straight line at speed, lane changing, counter-steering and evasive action.

2.2.2.3. Power On / Power Off Response

The various load shifts involved in power on and power off situations (such as braking during cornering) affect the vehicle's cornering attitude, and thus its stability. These tests are designed to characterise some of the most critical situations encountered in everyday driving and gauge the disposition of each vehicle under such conditions. As a result the vehicle's reaction to these manoeuvres must represent the optimal compromise between steering response, stability and braking efficiency.

2.2.2.4. Elk Test

The elk test, as described in Figure 2.14, is an evasive action test designed to permit drivers to make comparisons between the dynamic response and general handling of different vehicles and vehicle setups. The test mimics the conditions encountered when a vehicle has to make an evasive manoeuvre to avoid an obstacle, such as an elk. It enables an assessment of the overall dynamics of the vehicle system, including the driver, and provides realistic simulation of everyday traffic conditions but is very subjective and relies highly on the skills of the driver.

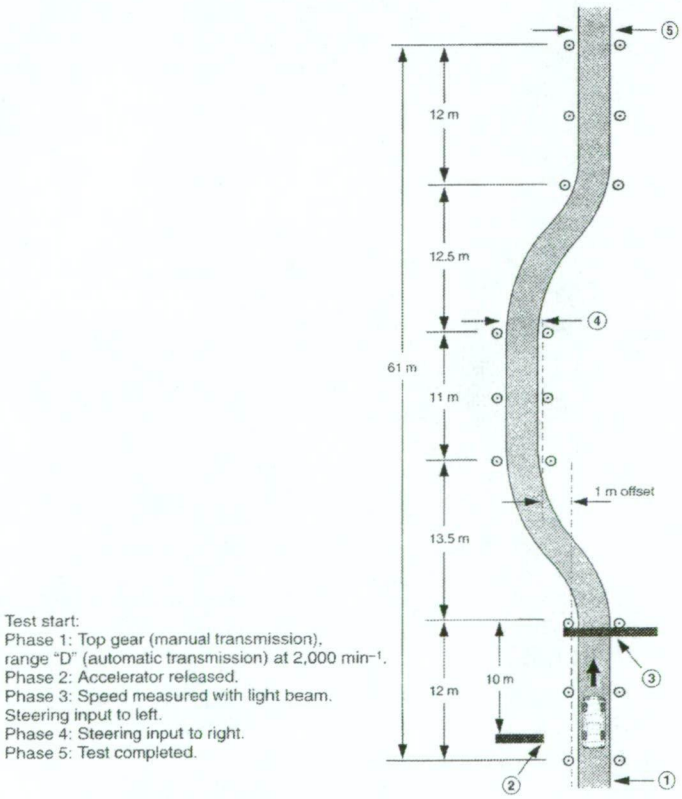

Figure 2.14: Elk test design [1, 2]

2.2.2.5. Split μ Test

The split μ test is designed to test the dynamics of a vehicle when it is driving on a road surface of high coefficient of friction on one side and low coefficient of friction on the other, as shown in Figure 2.15. The typical arrangement is to use a dry asphalt or concrete pavement on the high μ side and an ice or a grass surface on the other, on anything from a level surface to a steep incline. The test is primarily used as an indicator of the low speed ability of various active control systems to make best use of the traction available at each wheel [3, 5, 18].

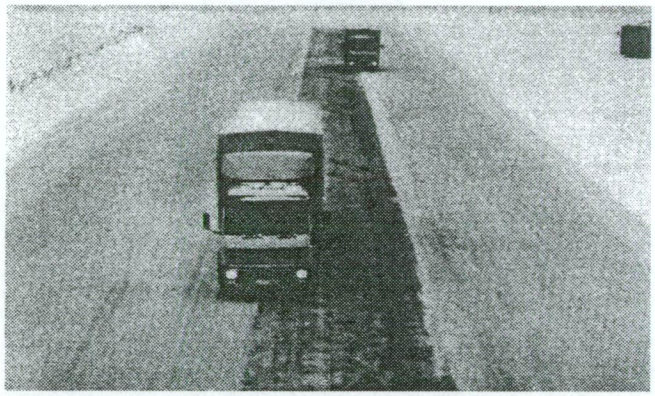

Figure 2.15: Split μ surface demonstrating the advantages of traction control [5]

2.3. Anti-lock Braking System

One of the first active safety systems to be installed on commercially available vehicles was ABS, which was introduced by Bosch in 1978. The system was designed to assist the driver in panic braking by preventing wheel 'lockup', thereby increasing vehicle stability and control. This section will introduce the principles behind ABS operation and highlight its functional benefits and limitations. It will also discuss hardware requirements and their effects in performance [19, 20].

2.3.1. ABS Operation

ABS works on the principle that during panic braking the driver will most likely be required to alter the vehicle's course, such as in the case of avoiding an unexpected obstacle or an oncoming vehicle. This means that the tyres must be held at a particular slip ratio that provides a reasonable proportion of lateral force while supplying sufficient longitudinal (braking) force. As discussed above, lateral force can only be achieved through the sacrifice of available longitudinal force, which results in an increased stopping distance. As such, Mathues [9] states that the required slip ratio at each wheel must reflect a compromise between manoeuvrability and stopping distance on a variety of road surfaces and environmental conditions. Figure 2.16 shows the general ABS control range [9].

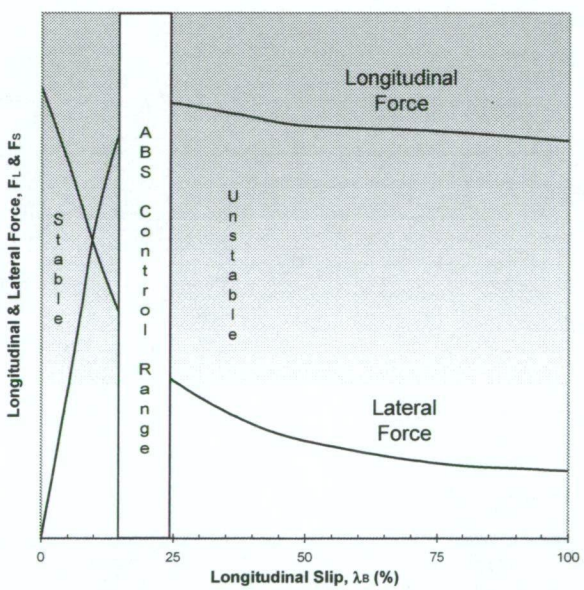

Figure 2.16: ABS slip control range [5, 23]

The techniques that different manufacturers use to achieve this result are varied, but all are based on the same general arrangement, which is depicted in Figure 2.17. A number of wheel speed sensors are installed on the vehicle which, as well as giving individual wheel speeds, can also be used to infer vehicle speed. With this estimate, the longitudinal slip ratios (λ_B) at each wheel can be calculated within the ABS Electronic Control Unit (ECU) and compared with the desired values. If the slip ratios are too high (inferring that a wheel has 'locked up' or is not providing enough lateral force) the ECU

will then reduce the brake pressure to the effected wheel(s) by a specified step. This results in an increase in wheel speed and a reduction in slip, which is then re-measured, completing the closed loop control function. By operating at a frequency of about 4 – 10 Hz this method provides a means of controlling wheel speeds accurately and within the necessary control range [1, 2].

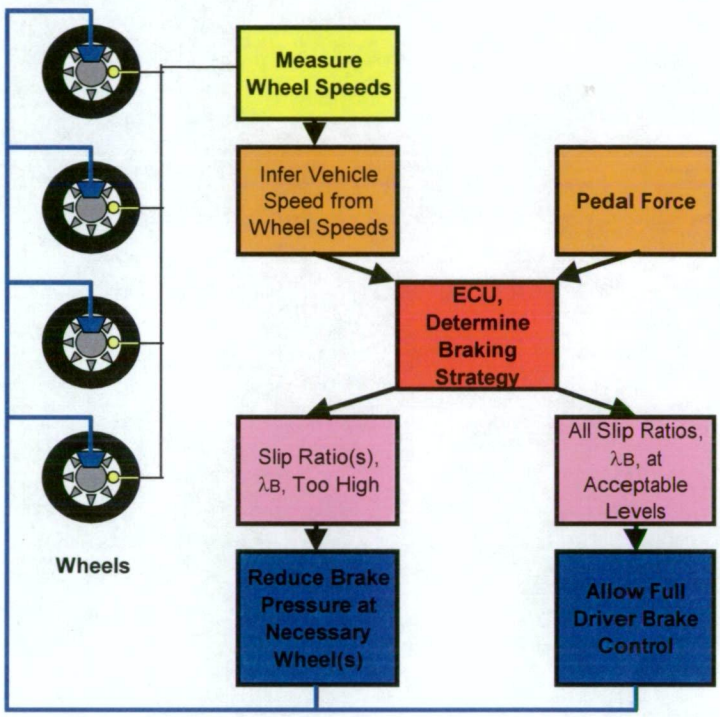

Figure 2.17: General operation of ABS (4 channels)

2.3.2. ABS Performance and Limitations

ABS has proved itself as an important safety tool by providing vehicle stability during panic braking. One study conducted by Evans et al. [6] finds that, overall, it has reduced crash risk by about 3% and has severely reduced the likelihood of many accident types. It also suggested that ABS was responsible for an accident risk reduction of:

- (13 ± 4)% on wet roads
- (13 ± 5)% when raining
- (34 ± 15)% of pedestrian crashes

However, the study also observed an ABS rollover risk increase of (44 ± 22)% and wildly varying effects in snow and ice conditions. The inference is that ABS does not so much prevent crashes, as to alter the type and severity of them. The four main reasons cited for this are increased travel speeds, driver experience, the effects of initial accident avoidance and inaccurate ABS control.

2.3.2.1. Increased Travel Speeds

Test track experiments have provided direct evidence that drivers of vehicles equipped with ABS choose slightly higher travel speeds. The perceived braking benefits of the system allow the driver to travel faster and brake later while remaining within what they regard as a safe environment. However, while the ABS can control most braking situations, the increased speed itself can give a dramatic rise to the probability of some accidents. The increase in rollover risk of ABS could be attributed to this since the likelihood of rollover is very sensitive to travel speed, while the overall risk of other speed-insensitive accidents is reduced.

2.3.2.2. Driver Experience

The main goal of active safety systems is to enable inexperienced drivers to control their vehicle better under panic situations. The systems effectively help inexperienced drivers emulate the driving style of experienced drivers. Therefore it is reasonable to state that an inexperienced driver will achieve more performance benefits from ABS than an experienced one will, because the margin for improvement is greater. In the case of snow and ice covered roads, geographic position can be the determining factor in the level of experience of the drivers who reside there. Drivers from such areas would encounter these conditions much more frequently than drivers from elsewhere and thus their driving skills in snow and ice would be superior. This would limit the effectiveness of ABS under those conditions in comparison to drivers from elsewhere.

systems that seek to balance cost and benefit for the specific ABS application. The complexity of the ECU, the number of wheel speed sensors used and the number of control channels provided by the vehicle's hydraulic modulation units are major factors in the cost and effectiveness of the complete system [22, 23].

2.3.3. ABS Electronic Control Unit

The ABS ECU is used to control the hydraulic pressure applied to the brakes of each wheel in the interests of maintaining vehicle stability under panic braking. Figure 2.18 shows the operation of a four channel ECU.

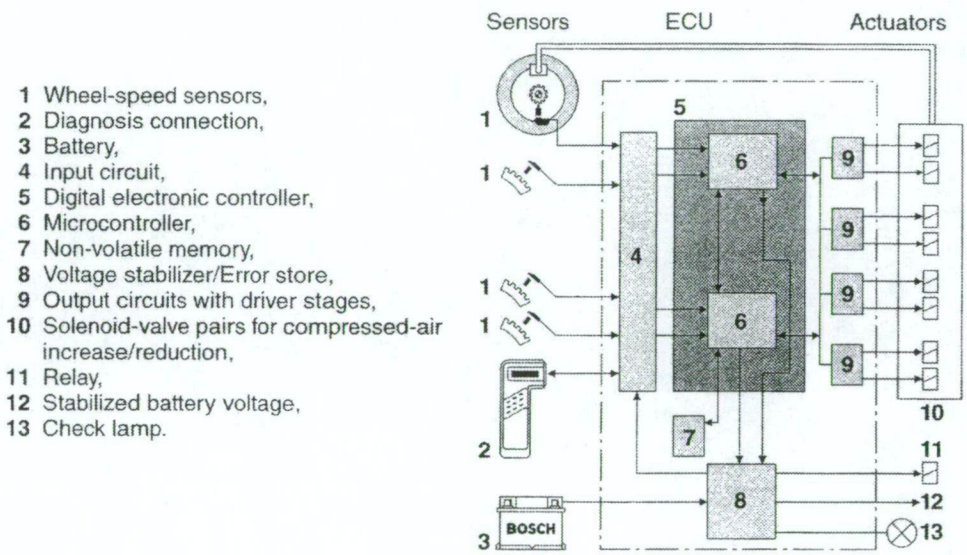

Figure 2.18: Operation of Bosch's 4 channel ECU [1, 2]

The ECU first receives, filters and amplifies the data from the wheel speed sensors (using the two microcontrollers for reliability), which it then uses to calculate peripheral wheel speeds and wheel acceleration or deceleration. This data then passes through a number of logical operations and complex controller logic to estimate vehicle speed and, thus, slip at each wheel in order to evaluate a control strategy to operate the hydraulic modulators. Wheels that are seen to be decelerating too fast to represent vehicle deceleration are assumed to be about to lock and control measures taken, while wheels that seem within their stable range are used to calculate vehicle speed [1, 2].

2.3.2.3. Initial Accident Avoidance

The finding that ABS equipped cars experience different types of accidents to non-ABS equipped cars may also be the result of the after effects of the ABS helping to avoid an accident. Consider a situation where a car has headed off the road and is heading for a tree. A car without ABS may not be able to manoeuvre around the tree and end up crashing into it, while the car with ABS may avoid the tree and continue on into the off-road terrain, with consequent risk of rollover. In this case the ABS equipped vehicle has avoided a serious accident, but by doing so may have converting this non-rollover accident into a rollover one.

2.3.2.4. Inaccurate ABS Control

Since ABS generally only measures the vehicle's wheels speeds, the information base it works from is somewhat limited. At low speeds Strickland et al. [37] found that it can even reduce deceleration when compared to the completely locked wheel scenario it is designed to avoid. Factors such as road surface, suspension travel, steering angle and vehicle yaw rate are not included in the control model and so ABS must make a number of control assumptions. These assumptions are based on 'normal' driving behaviour, with slip control in the vicinity of 5 to 15% [4]. Deviations from these conditions lead to less than optimum brake control as the control logic fails as stated by Scheider [21]. Driving on an unsealed road is a good example.

Referring to Figure 2.3 again and approximating an unsealed road to dense sandy soil we can see that the optimum slip for braking is at about 40% while the optimum slip for a wet road is at about 20%. Since the ABS has little idea of the road surface it may not allow the wheels to slip further than 20% when activated, which in this case reduces the braking force by about a half, increasing stopping distance dramatically. In this case the ABS has a negative effect on braking (while still providing stability however) and, as a reflection of this, many vehicles provide the facility to turn ABS off when driving in conditions that it operates poorly within.

Additionally, the cost of the installation of ABS into automobiles places some performance limitations on its operation, and as a result there are a large number of

2.3.4. Wheel Speed Sensors

ABS generally uses wheel speeds as the only measured variables for the control of the brake system. The speeds are normally measured using an inductive sensor that operates on a 'comb' made from steel as shown in Figure 2.19.

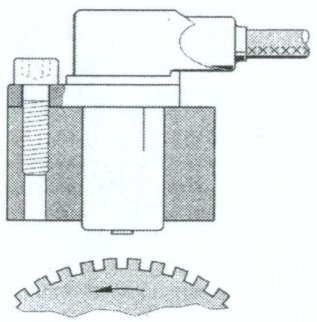

Figure 2.19: Inductive wheel speed sensor operation [1]

The comb is installed to fit onto a rotating part of the wheel assembly and the sensor is mounted to a fixed point in close proximity to it. As the wheel turns a magnetic field is induced in the sensor as each tooth of the comb passes it. This data can then be relayed back to the ECU to calculate rotational speed, which can then be used to calculate the peripheral speed of the tyre. These peripheral speeds can then be used to gain an estimate of the absolute vehicle speed, the accuracy of which depends on the application and the number of sensors installed. The number of sensors typically installed varies with respect to the desired level of performance and the overall cost of the system [1, 2, 22].

2.3.4.1. Two Wheel Speed Sensors

The use of wheel speed sensors on only the front two wheels has shown to have many disadvantages. The lack of data on rear wheel speed means that the system must make a number of control assumptions based on vehicle setup and 'normal' driving conditions. Any deviations from these assumptions, such as brake fade, different tyres front and rear and abnormal road conditions result in flawed ABS control. Under such conditions

and with no input of the rear wheel speeds, the ECU may allow the rear wheels to lock which will effect vehicle stability drastically since lateral control will be lost [23, 24].

2.3.4.2. Three Wheel Speed Sensors

The three sensor approach places wheel speed sensors on the front two wheels and onto the propeller shaft at the differential at the rear. The since the rear speed sensor works on the principle that the speed of the propeller shaft is proportional to the average speed of the two rear wheels, it can be used to evaluate whether or not a rear wheel is locked. It can also be used as an aid in determining vehicular speed. While providing a significant improvement over two channel systems, it still does not provide a complete representation of wheel slippage, and so prevents accurate ECU control under all conditions [1, 2, 24].

2.3.4.3. Four Wheel Speed Sensors

A wheel speed sensor mounted to each wheel is the most common approach in current ABS design. For a small cost increase it enables a reasonably accurate estimate of vehicle speed under most driving conditions and also provides the ECU with data on the slip rates at each wheel. With the data from these sensors the ECU can control brake pressure to prevent any wheel lockup, and also fine tune slip rates to gain high levels of braking stability and reduce braking distances. The installation of four wheel speed sensors is also required to accommodate the addition of TCS and VDC systems to the vehicle and, as such, is the most common arrangement on current automobiles [1, 2, 8, 24].

2.3.5. Hydraulic Modulators

The vehicle's hydraulic modulator provides the ECU with control of the braking system when needed and is the most expensive component of ABS. They come in two, three and four channel variations, where each channel controls the hydraulic pressure to a single brake line whenever the ECU sends it a signal to override the hydraulic pressure exerted by the driver through the brake pedal. The design of a single channel of a

hydraulic modulator is shown in Figure 2.20, which operates within three states of brake control as defined by the positions of the inlet and outlet solenoid valves [1, 2, 22].

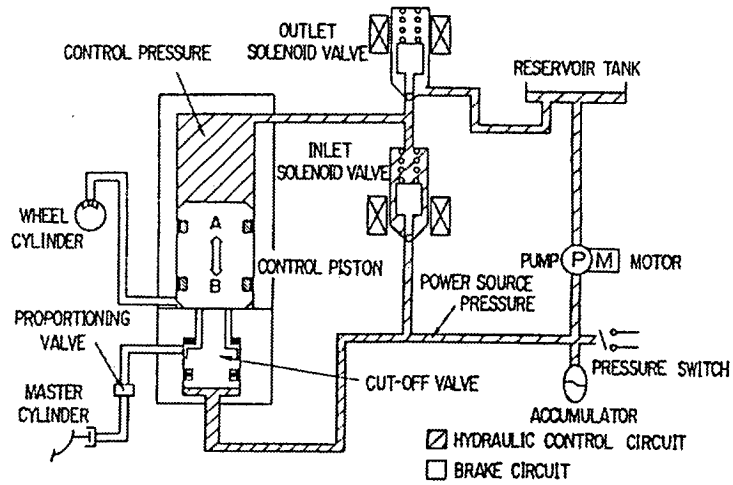

Figure 2.20: Layout of a single channel of Sumitomo Electric's hydraulic modulator [22]

2.3.5.1. Channel State 1 – Driver Controlled

In this state the ECU has not activated the ABS for this channel and the driver remains in control of the hydraulic pressure passing through the modulator. The two solenoid values in the modulator remain de-energised and closed which allow only direct pressure from the brake pedal master cylinder to pass through the control piston to the wheel brake cylinder. This is the only state where hydraulic pressure is allowed to increase.

2.3.5.2. Channel State 2 – Constant Pressure Intervention

When the ECU detects that ABS control is required through this channel it will decide to either reduce the pressure to the brakes or to hold it constant. To hold it constant it will energise the inlet solenoid valve and ensure that the re-circulation pump is running. This removes the control of the brakes from the driver and ensures the brake pressure will not be allowed to increase, which would result in further vehicle instability.

2.3.5.3. Channel State 3 – Reduced Pressure Intervention

If it becomes necessary to reduce the braking pressure within the hydraulic circuit through ABS control the ECU will activate the third state. This reduction in pressure is accomplished by energising, and thus opening, both solenoid valves while the re-circulation pump is running.

This simple solenoid operation means that increases or decreases of the braking pressure are not only continual, but can also be stepped by switched-mode operation at rate of between 4 to 10Hz so that moderate pressure increases or decreases can be achieved. The pressure fluctuations also provide the driver with a level of feedback through the pedal that ABS is active and also of how it is operating [1, 2, 22, 23].

2.3.5.4. Two Channel Systems

Two channel systems offer the cheapest form of ABS and generally operate using data from two or more wheel speed sensors. The system, as shown in Figure 2.21, uses each channel to regulate the brake pressure at each of the front wheels. The pressure to the diagonally opposite rear wheels are then regulated simultaneously with the front wheel, through a proportioning valve which reduces the rear braking pressure. It is this use of each channel to control two wheels that produce many performance drawbacks to this low cost approach. Firstly, the proportioning valves are generally at a fixed ratio which means that the front / rear braking bias will not work optimally under all conditions. On some surfaces it may be possible to lock the front wheels before the rear, and on others the rear wheel before the front. The effectiveness of the proportioning valve setting is also dependent on the loading of the vehicle.

This problem also gives rise to another major performance difficulty, that of stopping distance. In the interests of stability ABS must not allow any of the wheels to lock, and under this system if one wheel is about to lock it must reduce the brake pressure to two. If a front wheel locks, the ECU must reduce the braking pressure to it, but this will also reduce pressure to the rear brake, which still has more braking potential. The result will be a small increase in stopping distance. However, this effect has a much more pronounced effect on stopping distance if it is the rear wheel that has locked up. In this

case it is the front wheel that is not allowed to reach its full braking force and, since the majority of the braking is done through the front wheels, stopping distances can increase dramatically.

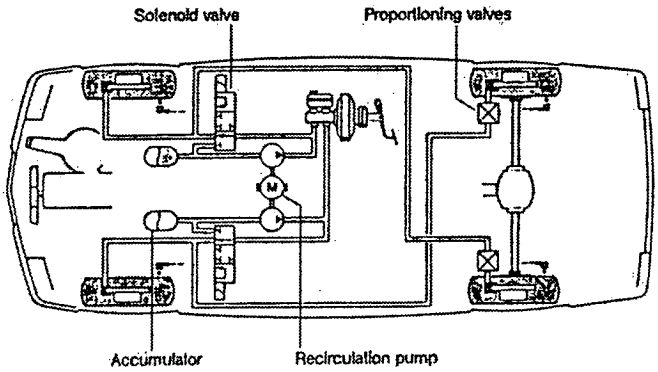

Figure 2.21: Bosch's two channel ABS [23]

The use of two channel ABS has proved limited in automobiles. This is because that while it provides the cheapest system and delivers reasonable stability under hard braking it can force very long stopping distances on some surfaces. It has been generally accepted by Demel et al. [23] that two channel ABS does not provide significant cost advantages in relation to its performance disadvantages in comparison to other systems.

2.3.5.5. Three Channel Systems

Three channel systems use a hydraulic channel for each of the front wheels and the remaining one to control the pair of rear wheels in arrangements similar to that shown in Figure 2.22. The result being that the rear brakes must operate at equal pressures.

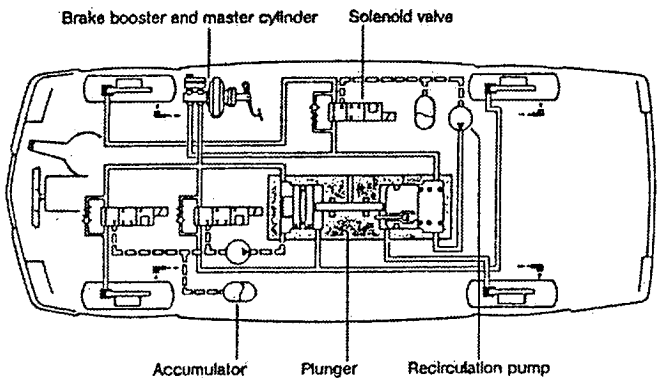

Figure 2.22: Bosch's three channel ABS

The system generally operates on the 'select low' principle which uses the rear wheel with the least amount of slip to control the joint brake pressure to both rear wheels. This is done by controlling only one of the rear wheels directly through the hydraulic modulator while a hydraulic plunger provides the separation of the brake circuits and transfers the pressure of the controlled rear wheel to the other rear wheel. This leads to the wheel with the higher rate of slip being slightly under-braked, increasing stopping distance a little but also increasing stability [23].

2.3.5.6. Four Channel Systems

Four channel systems also operate, in most cases, on the select low principle, but replace the need for the hydraulic plunger to govern rear wheel braking pressure with another hydraulic modulator channel. This presents the vehicle with one hydraulic modulation channel for each wheel, and so gives the ECU total control over the reduction of braking possible at each wheel, as shown in Figure 2.23.

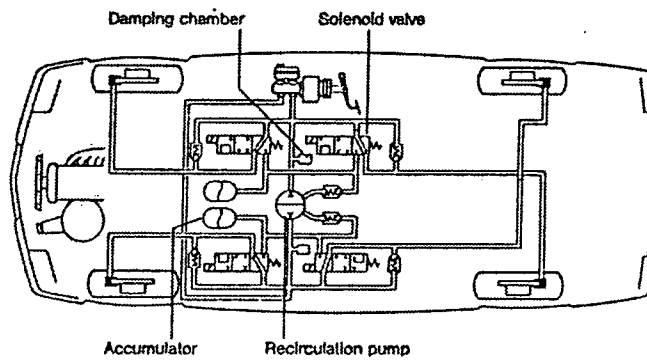

Figure 2.23: Bosch's four channel ABS

The use of the select low principle, however, means that the system works identically to the three channel system, except that it is often more costly. Improvements have recently been made that allow improved ABS performance using individual control of each wheel. This gives each wheel the ability to independently be controlled to provide the best possible contribution to the braking process and as such offers shorter stopping distances than the select low principle [1, 2, 23].

The most important advantage of four channel ABS over the three channel system that should be noted is that it can easily be integrated into other active safety systems. Much of the hardware between four channel ABS and current TCS and VDC designs are common, which then makes the addition of such systems to production vehicles easier and thus cheaper. As such four channel systems are becoming prevalent.

2.3.6. ABS with an Acceleration Sensor

A study conducted by Saito et al. [25] states that the inclusion of a longitudinally placed acceleration sensor can further increase ABS control by providing the ECU with data as to whether or not the wheel speed sensors are giving an accurate description of vehicle speed. This is because absolute vehicle speeds can be hard to obtain using just wheel speeds sensors alone. The slip at each tyre during braking means that the predicted vehicle speed will always be slightly lower than the actual speed. Also, when a wheel starts to lock it will further reduce the predicted speed until the system chooses to ignore it from the vehicle speed calculations. Furthermore, consider a four-wheel drive (4WD) travelling on an ice covered road. The front and rear axles are connected so the possibility of all four wheels slowing by equal amounts is much higher than in two wheel drives (2WD), resulting in highly erroneous vehicle speed estimates and thus slip ratios. The likelihood of simultaneously locking all four wheels is also high and both situations result in severely reduced ABS effectiveness, as shown in Figure 2.24. An acceleration sensor can aid in estimating vehicle speed, thus improving ABS performance.

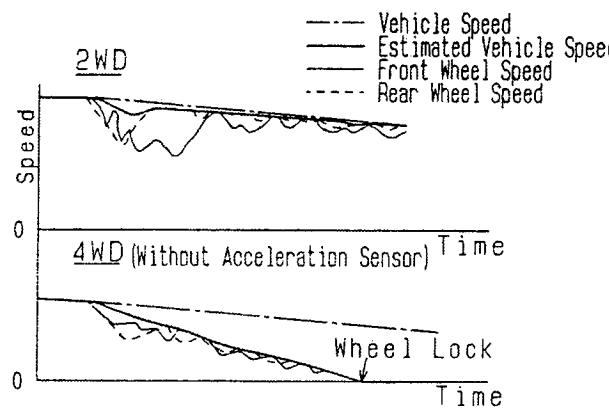

Figure 2.24: 2WD and 4WD ABS performance on an ice covered road [25]

The low cost, conventional approach to the addition of an acceleration sensor uses a switch that can differentiate between high (< 0.35G) and low (> 0.35G) deceleration. The estimated deceleration rate of the vehicle could then be correlated with this data, allowing the ECU to decided if the vehicle speed was travelling faster than the wheel measurements indicated. However, fully accurate vehicle speed could not be reliably estimated for a wider range of road surfaces, from ice and compressed snow to wet asphalt and unsealed roads.

An acceleration sensor that makes continuous measurements of vehicle deceleration can provide a more reliable solution. Figure 2.26 shows the block diagram of the ABS control with such a sensor, and enables vehicle speeds to be precisely estimated, even when braking on low μ roads. The acceleration sensor can give a vehicle deceleration description, which can be compared to the estimated vehicle deceleration derived from the wheel speed sensors. When the measured and derived decelerations show differences, the data from the acceleration sensor can then be used to calculate a much more accurate vehicle reference speed, which in turn gives more effective ABS control as shown in Figure 2.25 [25].

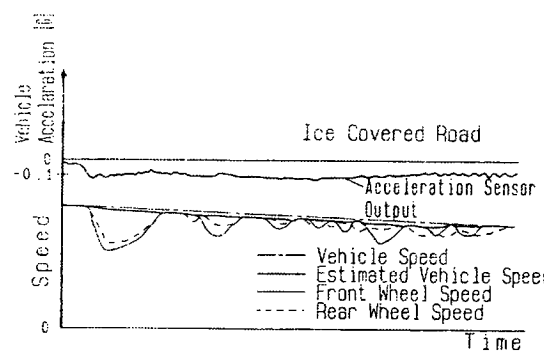

Figure 2.25: 4WD ABS performance on an ice covered road with acceleration sensor [25]

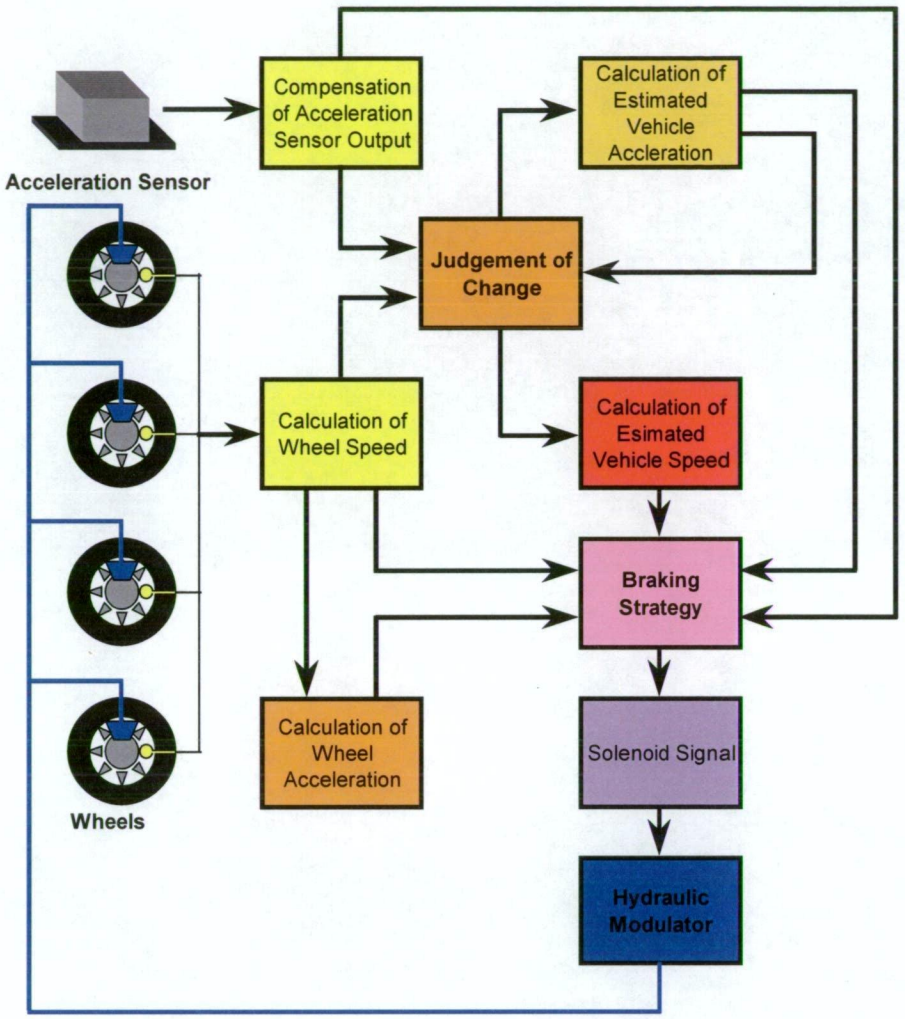

Figure 2.26: ABS control using an acceleration sensor [25]

2.3.7. ABS with Fuzzy Logic Control

The control algorithms for ABS controllers are predominantly mathematical model based. This means that the ECU design requires a mathematical model of the dynamics of the vehicle and knowledge of the control theory behind its operation. Areas of the model that are considered too difficult to simulate are often replaced with simpler rules that, while insuring operation, do not provide an accurate simulation of the vehicle dynamics in all conditions. This can manifest itself in erroneous control strategies when the vehicle is driven in abnormal conditions, such as is the case on low friction surfaces like ice covered roads and unsealed roads.

Fuzzy logic control offers an alternative to this situation. Fuzzy controllers do not require detailed mathematical models of the control system or control theory; instead

they encode heuristic knowledge. This means that they use a set of 'if –then' decision rules to control the system, often encoded in english language which can be easily understood and modified as needed.

One such problem of model based ABS is that the system has very little information on the type of road surface it is travelling on. Difficulties arise, in particular during braking on ice, where the activation of even a small portion of a high gain, dry road based command tends to result in the application of excessive braking force, leading to instability and increased stopping distance. A fuzzy logic controller can address this problem by the addition of a road condition identifier that is based on the comparison of brake pressure and detected slip ratio using existing sensor data, as shown in Figure 2.27 and presented by Mauer et al. [26]. If the slip ratio is larger than anticipated based on the current assumption of road conditions and current brake pressure, a new road condition state based on lower μ can be selected and ABS control altered accordingly.

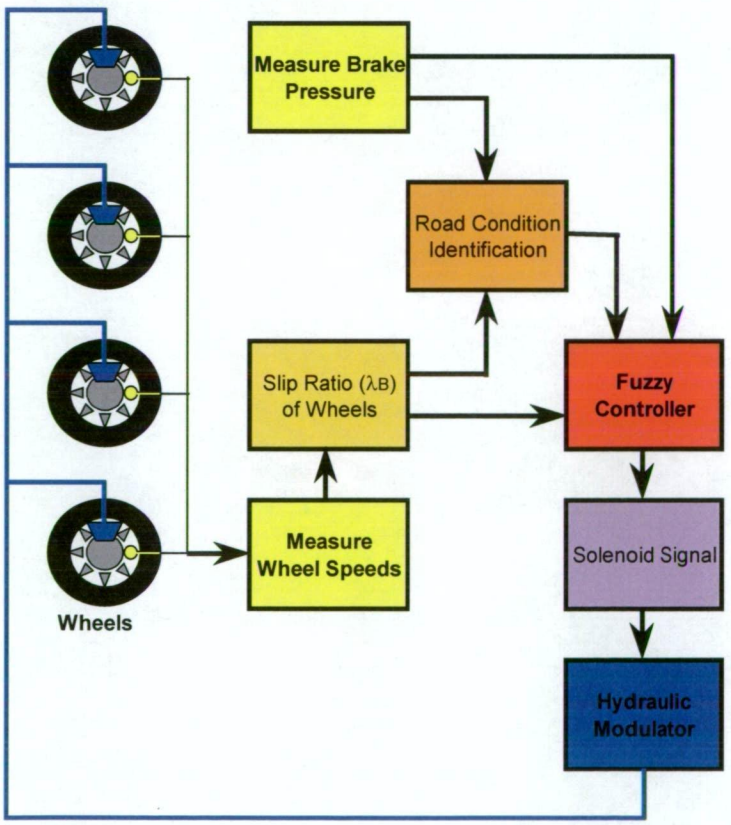

Figure 2.27: Fuzzy logic controller concept [26]

As depicted, the measured values in this system are the wheels speeds and the applied brake pressure. The wheel speeds are then used to gain an estimate of the wheel slip ratios and were used, in conjunction with brake pressure, to gain road condition identification. The resulting data could then be fed into the fuzzy controller which can then make control decisions based on its control logic.

2.3.7.1. Slip Ratio Prediction

The slip ratio can be computed using traditional techniques and from past records, it then can be made available to the road condition identifier and fuzzy controller. This introduces a PD element into the control process and can partially compensate for braking system delay. In the case of the application of this fuzzy controller, the braking system induces a delay of about 35ms while the controller samples at 5ms. In this case the slip ratio predictor can, for instance, re-initiate braking seven sampling periods before a stalled wheel is predicted to return to zero slippage.

2.3.7.2. Identification of Road Condition

The road condition identifier, used here, is capable of identifying four separate road conditions; dry, wet, ice covered or blocked wheel. The logic behind its operation is shown in Figure 2.28. Initially, a dry road condition is assumed. If the slip ratio exceeds a preset limit not encountered during normal operation (U=14% in this case) wheel blockage (lock) is assumed. A series of tests are then run though the identifier to try and gauge the road condition. Expected slip and actual slip are compared for a given brake pressure and then used to identify the road as icy or wet, or whether or not the road surface has returned to dry again. Only one of the four conditions can be true and once a decision is made it is then passed onto the fuzzy controller.

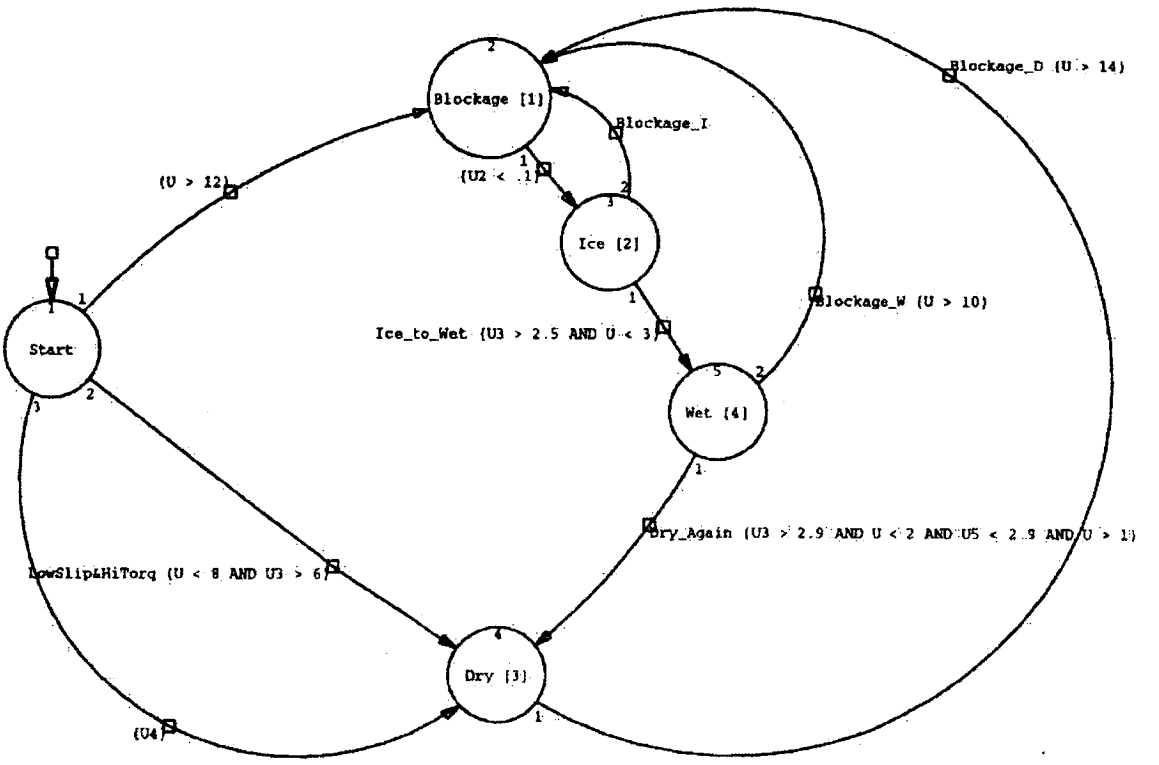

Figure 2.28: Road condition logic state diagram [26]

2.3.7.3. Fuzzy Logic Controller

The fuzzy logic controller processes the input from the road condition identifier of dry, wet, icy or blocked, as well as vehicle's slip ratios and brake pressure. The controller then evaluates a set of 11 braking rules; 4 governing dry roads, 3 governing icy surfaces, 2 governing wet pavement and one governing wheel blockage. The output from the road condition identifier ensures that only one set of rules is active at a time. An example of the rule base for quantising control of the hydraulic modulators on dry roads is shown below. It has inputs PREDICTED_SLIP, MEASURED_SLIP and MEASURED_BRAKE_PRESSURE, output CONTROLLED_BRAKE_PRESSURE and six fuzzy classes ranging from ZERO to VLARGE.

Rule DRY1;

If DRY is TRUE and;
PREDICTED_SLIP is not VLARGE;
Then CONTROLLED_BRAKE_PRESSURE is LARGE;
RULE_1;

Rule DRY2;

If DRY is TRUE and;
MEASURED_SLIP is LARGE and;
MEASURED_BRAKE_PRESSURE is LARGE;
Then CONTROLLED_BRAKE_PRESSURE is MEDIUM;
RULE_2;

Rule DRY3;

If DRY is TRUE and;
MEASURED_SLIP is SMALL and;
MEASURED_BRAKE_PRESSURE is LARGE and;
PREDICTED_SLIP is not VLARGE;
Then CONTROLLED_BRAKE_PRESSURE is LARGE;
RULE_3;

Rule DRY4;

If DRY is TRUE and;
MEASURED_SLIP is MEDIUM and;
MEASURED_BRAKE_PRESSURE is LARGE and;
PREDICTED_SLIP is not VLARGE;
Then CONTROLLED_BRAKE_PRESSURE is LARGE;
RULE_4;

2.3.7.4. Fuzzy ABS Operation

Figure 2.29 shows the simulated results of the Fuzzy ABS controller on an even road with varying surface conditions, where brake torque is the controlled variable. In this case the vehicle starts braking the moment the analysis starts and travels over dry road for the first 0.5 seconds. The road surface then experiences an immediate transition to icy conditions for the next 0.5 seconds, before reverting back to dry conditions thereafter.

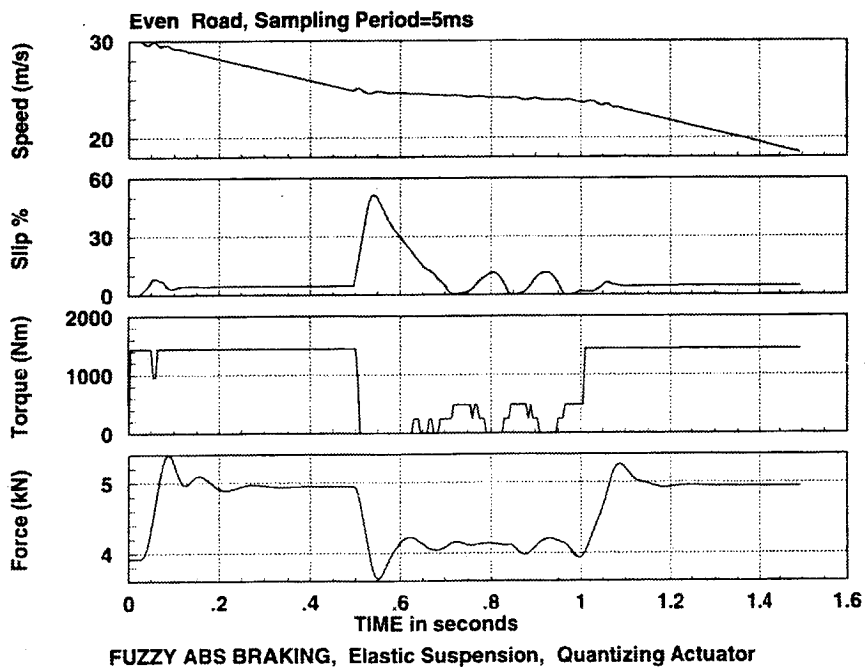

Figure 2.29: Simulation results of fuzzy ABS control [26]

The figure shows near-optimal braking after a small initial oscillation as the ABS first starts to operate on the dry surface. Upon the transition to the ice conditions the decision logic recognises the onset of blockage at once, and reduces braking force as quickly as the system allows. The wheel block is limited to only 50% at this moment which compares favourably to model based adaptive systems which can induce 100% wheel blockage before returning to normal operation. The fuzzy ABS then starts the process of identifying the road condition and adjusts the brake pressure to provide optimal slip ratios for the conditions. Because of the stepwise, quantising, operation of the controller the brake force is then allowed to oscillate marginally during the remainder of the braking process on the ice covered road. The vehicle then travels onto the dry surface again. It instantly recognises that the brake force to slip ratio has improved and the road condition identifier logic shows that the vehicle is travelling again on dry pavement. The braking strategy is then altered and normal ABS control resumes, after a small oscillation period [26].

This section, thus, shows that the addition of sensory data, or the use of existing data to establish additional vehicle dynamics parameters, can improve ABS operation. It can also be seen that the conventional use of just wheel speed sensors to gather vehicle dynamics information can result in flawed control when abnormal conditions are encountered.

2.4. Vehicle Dynamics Control

While ABS seeks to assist the driver during braking manoeuvres, "Vehicle Dynamics Control" (VDC) aims at helping the driver during steering manoeuvres. For ABS the wheel is the controlled element, with wheel acceleration controlled to keep the slip sufficiently small to preserve some amount of lateral force capability. For VDC, however, the vehicle is the controlled element, with vehicle motion controlled to keep any deviation from its nominal motion as small as possible and conform with the environment through the control of wheel slips to gain the required lateral and longitudinal forces. It does this by using the braking system and engine control to regulate the individual wheel torques, but also utilises additional data input from a

steering angle sensor, a yaw rate ($d\beta/dt$) sensor and a laterally placed accelerometer [1, 2]. This section will first investigate the need for these sensors and then give a brief outline of the control method. It will then display the functional principles of VDC through a number of operation examples, which also highlight its performance benefits.

2.4.1. VDC Additional Sensors

The effect of yaw rate on stability has been outlined above. An important observation is that the sensitivity of yaw moment on vehicle stability, with respect to changes in the steering angle, decreases rapidly as the slip angle of the vehicle increases. It seems important to control the yaw rate of the vehicle to correlate to the drive's desired path (determined from the steering angle). At large vehicle slip angles (where the μ_L-slip curve of the tyre is maximum) variations in the steering angle hardly change the yaw moment, while the absolute value of the yaw moment is almost zero. The result is that manoeuvrability is lost at vehicle slip angles larger than about 10° on dry surfaces, while it is lost at about 4° on packed snow [1, 2, 3, 7].

The addition of a yaw rate control does not, however, guarantee stability in all conditions. If the control is used on a slippery road the yaw rate of the vehicle may correspond to the driver's requested turning rate through the steering wheel, but the vehicle may just be spinning in oversteer, and not following the intended course. In this case, while the yaw rate is controlled correctly, the lateral (cornering) acceleration of the vehicle does not correlate to the driver's intended path, and it spins off the road. The addition of the lateral acceleration sensor to the yaw rate sensor eliminates this problem and forms the backbone of the VDC system, displayed in Figure 2.30 and shown conceptually in Figure 2.31.

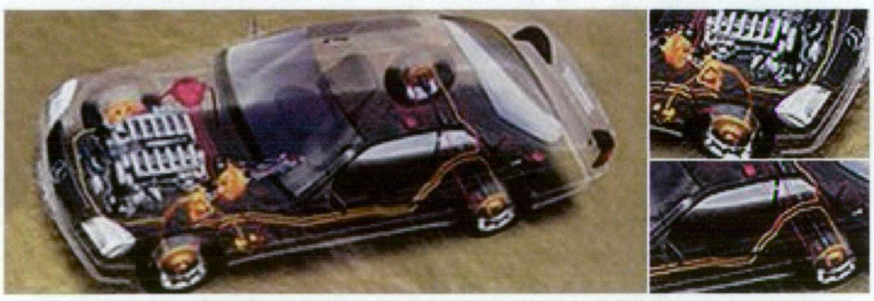

Figure 2.30: Mercedes-Benz ESP system

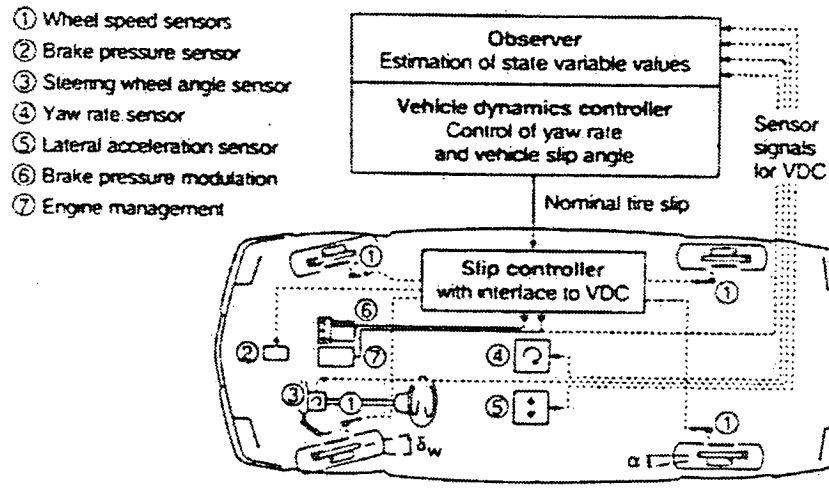

Figure 2.31: VDC system and control concept [38]

2.4.2. VDC Operation

The first task of the VDC controller is to determine the driver's desired (nominal) path. It does this from the data gathered from the onboard sensors, including driver inputs of steering wheel angle, throttle position and brake pressure, but must also account for unknown variables, such as coefficient of friction, which can affect driving attitude and behaviour. Steering wheel angle, vehicle velocity and yaw rate can be used to determine the nominal yaw rate during stationary turns of [3, 7]:

$$\dot{\beta}_{No} = \frac{v_x \cdot \delta_w}{(a+c)\left(1+\frac{v_x^{\,2}}{v_{CH}^{\,2}}\right)}$$

where: a = longitudinal distance from front wheels to centre of gravity of vehicle

c = longitudinal distance from rear wheels to centre of gravity of vehicle

v_x = longitudinal vehicle speed

v_{CH} = characteristic vehicle velocity

δ_w = angle of steered wheel

Eqn 2.10

Which is limited by the coefficient of friction of the road to:

$$\dot{\beta}_{No} \leq \mu_L \cdot \frac{g}{v_x} \qquad \textit{Eqn 2.11}$$

Once the nominal path is determined it then compares it with the actual path of the vehicle, as measured through the wheel speed, yaw rate and lateral acceleration sensors. Any deviations are then sent to the dynamics controller to either brake or accelerate the offending wheel(s), the dynamics of which are shown in Figure 2.32.

If the braking slip of the left front tyre is increased by a small amount $\Delta\lambda$ from an initial value λ_o and if tyre slip angle is α_o, then the yaw moment on the car is in a first approximation changed by the following amount:

$$\Delta M_{Yw} = -\frac{dF_S}{d\lambda}\cdot\Delta\lambda\left(a\cdot\cos\delta_w - b\cdot\sin\delta_w\right)+\frac{dF_B}{d\lambda}\cdot\Delta\lambda\left(a\cdot\sin\delta_w + b\cdot\cos\delta_w\right)$$

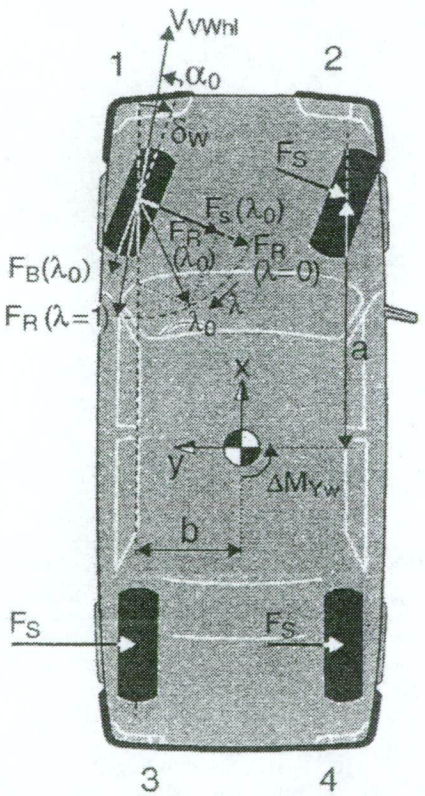

Here, changes in the tyre normal force as a result of a change in the tyre longitudinal of lateral force are neglected, as are the changes in the aligning torque on the tyre. Similarly, the lateral and longitudinal forces on the vehicle will be changed by the following amounts:

$$\Delta F_x = -\frac{dF_S}{d\lambda}\cdot\Delta\lambda\cdot\sin\delta_w - \frac{dF_B}{d\lambda}\cdot\Delta\lambda\cdot\cos\delta_w$$

$$\Delta F_y = -\frac{dF_S}{d\lambda}\cdot\Delta\lambda\cdot\cos\delta_w - \frac{dF_B}{d\lambda}\cdot\Delta\lambda\cdot\sin\delta_w$$

These relations which can be derived for each wheel of the vehicle are extremely non-linear, since the derivatives of the forces are highly dependent on the operating point (λ_o, α_o) of the tyre.

The effect of variation in the tyre slip may be explained best by using the figure. This illustration shows the forces F_R (λ=0), F_R (λ_o), F_B (λ_o) and F_S (λ_o). F_R is the resultant tyre force that is obtained by the vectorial sum of the longitudinal and lateral tyre forces. F_R (λ=0) is the resultant tyre force acting on the free-rolling tyre and is equal to the lateral force on the tyre that results from the slip angle α_o.

If the tyre slip is increased to the value λ_o, then the lateral force on the tyre is reduced to the value F_S (λ_o). At the same time a brake force F_B (λ_o) is generated. F_R (λ_o) is now the resultant tyre force. At the limit of adhesion between the tyre and the road the absolute values of F_R (λ=0) and F_R (λ_o) are approximately equal. Clearly, increasing the tyre slip then means rotating the resultant tyre force and therefore changing the yaw moment, the lateral force and the longitudinal force on the vehicle.

Figure 2.32: Control of slip angle with tyre slip [3, 7]

It can be seen that braking or accelerating a given tyre can be used to control the vehicle slip angle, effectively helping to 'steer' the automobile. This means that by controlling individual wheel slip values it is possible to significantly aid the driver during cornering manoeuvres. Unfortunately, this comes at a cost of unwanted deceleration or acceleration of the vehicle. It also can cause a lateral deviation from the nominal path, as the ability of the tyres to transmit lateral forces changes with the controlled longitudinal slip. The VDC system must control individual wheel slips to achieve a compromise between these effects, with the overall aims of:

- Keeping the driver in charge by providing vehicle response similar to normal driving conditions.
- Intervening on a 'smart' basis and only when needed.
- Emulating the expert driver to assist the average driver in realising the performance potential of the vehicle.

2.4.3. VDC Performance

The operation of VDC (which is similar in operation to the Electronic Stability Program – ESP) is best described through a number of different operating manoeuvres, as illustrated by Bauer et al. [1, 2] and depicted in the following sections.

2.4.3.1. Cornering at speed

Initially two vehicles (one with ESP, the other without) travel on a high μ road at speed and enter a tight corner, as shown in Figure 2.33. It can be seen that the vehicle without ESP soon becomes unstable (oversteer) and departs from its intended course. The driver then is forced to counter-steer to try and gain control of the vehicle, but the vehicle has become too unstable and quickly becomes uncontrollable. It can also be seen that the vehicle with ESP remains on its intended course by selectively braking individual wheels to increase yaw moment, and thus helping the car to steer through the corner.

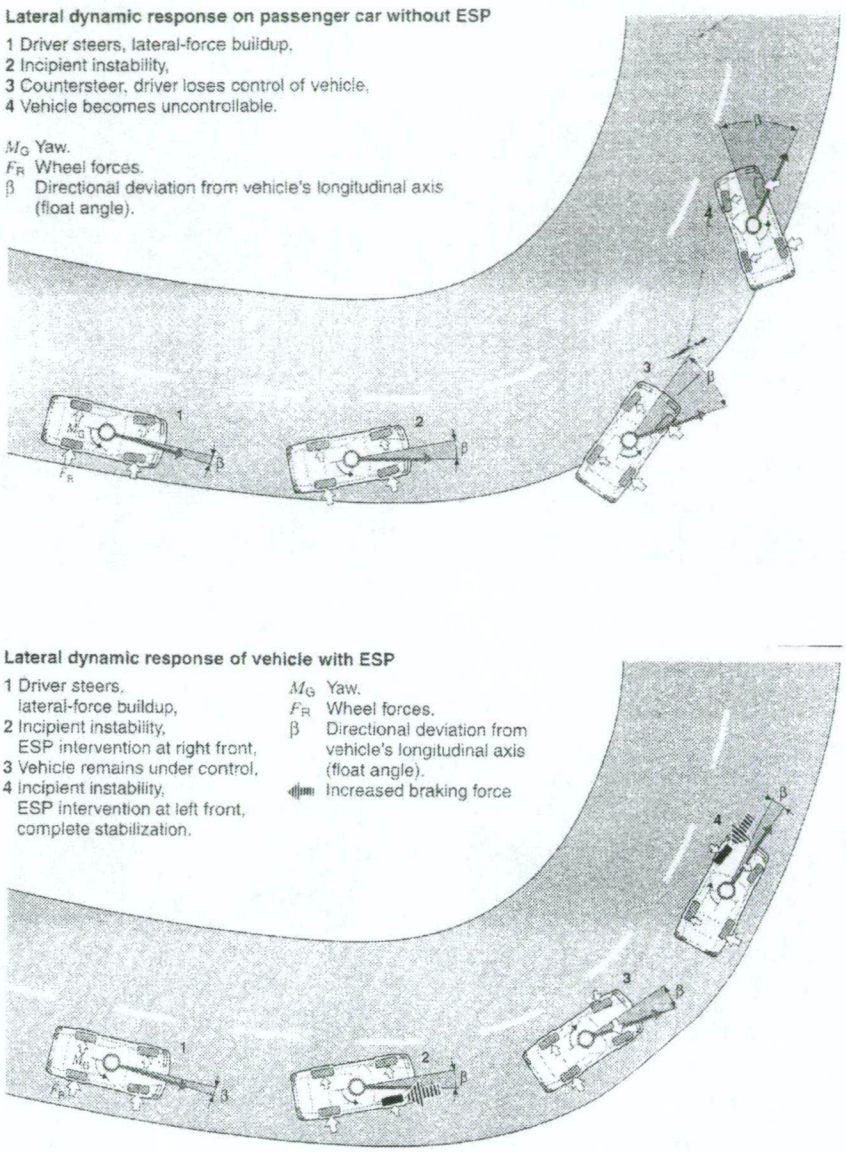

Figure 2.33: ESP operation on a tight corner [1, 2]

2.4.3.2. Steering and Counter-Steering (Slalom)

Figure 2.34 shows two vehicles travelling along a low μ (μ_{static} = 0.45) snow covered road at 72 km/hr. In this case the vehicles try to complete a constant velocity steering / counter steering manoeuvre with identical and progressively larger steering input angles, such as may be encountered on a series of S-bends or on a slalom course. The vehicle without ESP generates progressively greater wheel slip at the driven wheels as engine output is increased to maintain constant roadspeed. The steering / counter-steering manoeuvres then further increase the drive slip and the vehicle becomes

unstable, eventually braking into a slide, showing a obvious deviation in nominal lateral acceleration, yaw rate and yaw (float) angle. The vehicle with ESP follows its intended course by using brake interventions in the interests of controlling slip angle and yaw rate as far as possible as the environmental conditions allow.

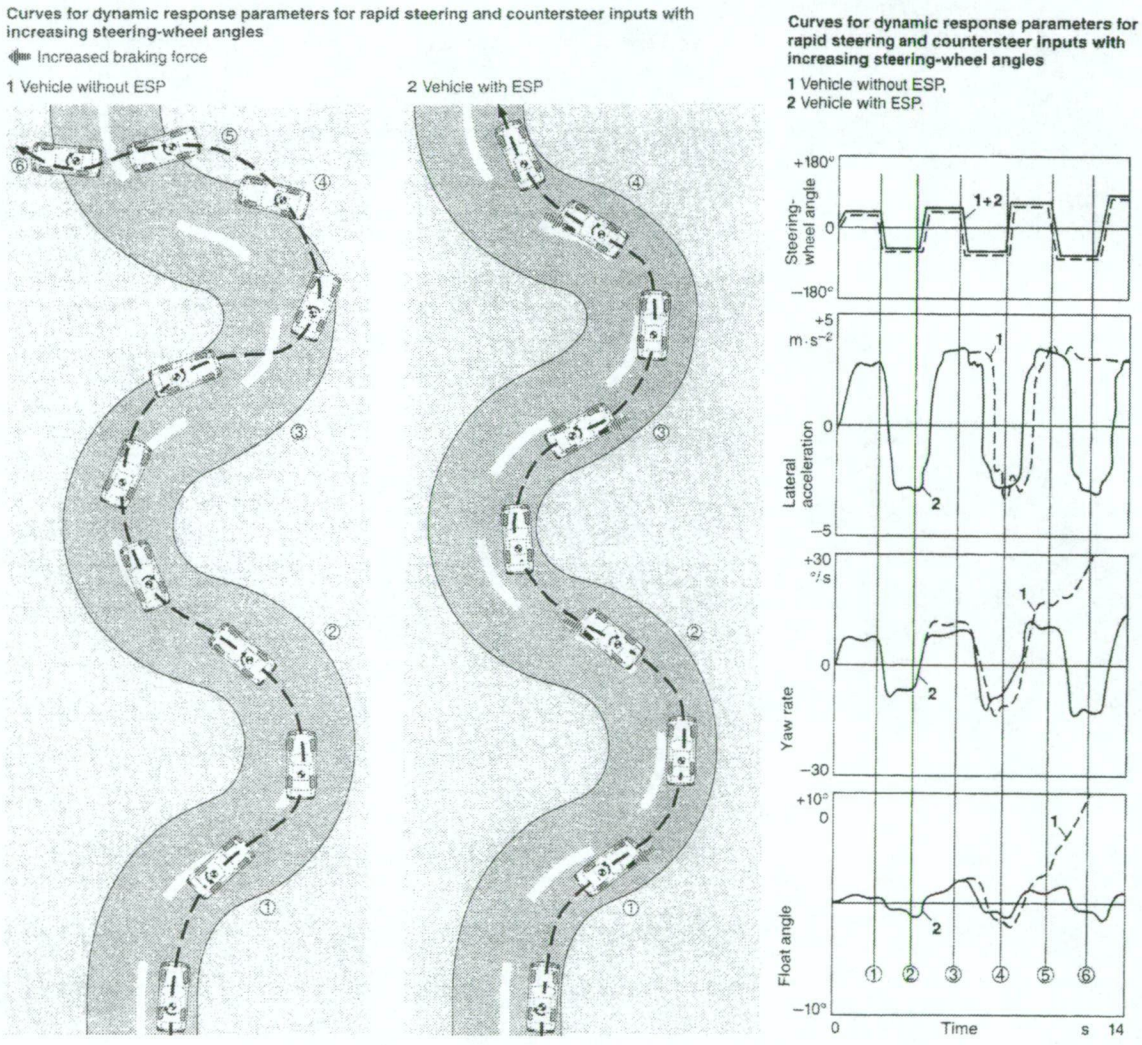

Figure 2.34: ESP operation on a slalom course [1, 2]

2.4.3.3. Panic Braking (Elk Test)

The abilities of ESP can also be shown during panic braking to avoid an obstacle. Figure 2.35 shows the dynamic behaviour of a vehicle with ABS and a vehicle with ESP in avoiding an accident and maintaining stability in such a case, with very low μ

(μ_{static} = 0.15) and initial speed of 50 km/hr. It can be seen that the vehicle with ABS, while completing the manoeuvre, becomes very unstable. As the driver steers around the obstacle the vehicle's slip angle and yaw rate increase to the point where the driver must counter-steer to avoid a spin. In doing so the driver creates excessive slip angle in the opposite direction and must counter-steer again to regain stability. On the other hand, the vehicle with ESP maintains stability at all times, reducing the demands placed on the driver and allowing them to devote full attention to keeping the vehicle on course.

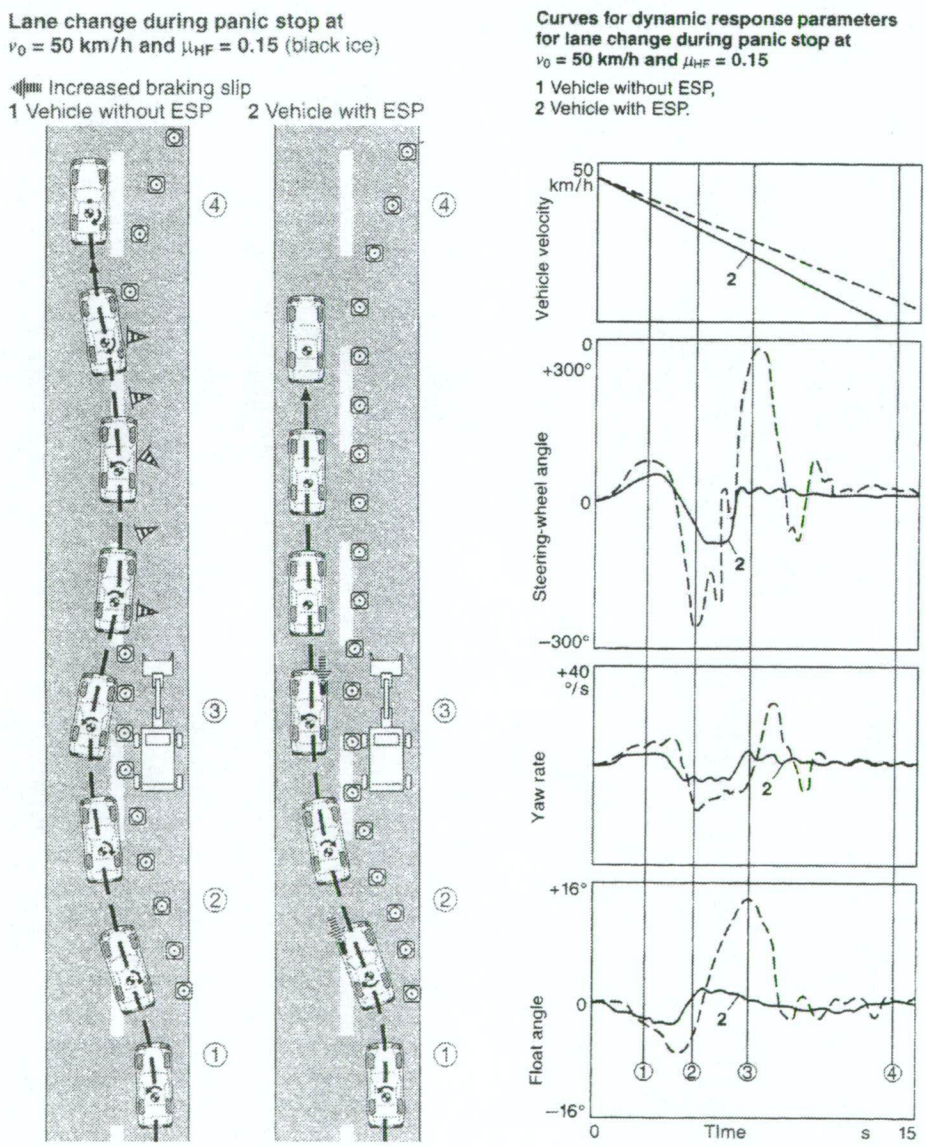

Figure 2.35: ESP operation during panic braking [1, 2, 3]

2.4.3.4. Accelerating While Cornering

Figure 2.36 shows the potential benefits of ESP when a vehicle is accelerating at its physical limit around a corner of constant radius. On a high μ (μ_{static} =1.0) surface and at a corner radius of 100m the vehicle without ESP reaches its stability limit at 95 km/hr. The result is significant understeer as the slip angle increases rapidly and the driver faces a very difficult job of keeping the vehicle on the course. As the vehicle speed increases further to 97 km/hr, the rear end brakes away and all stability is lost as the vehicle leaves the course. The vehicle with ESP also reaches its stability limit at 95 km/hr, but at this point the ESP reduces engine torque so the limit cannot be exceeded. It also controls wheel torques to help steer the vehicle through the corner, reducing the sensitivity of driver steering inputs. This control results in small deviations from the nominal path, but which can easily be corrected by the driver, who is still left with a major role to play in the closed loop control of the vehicle.

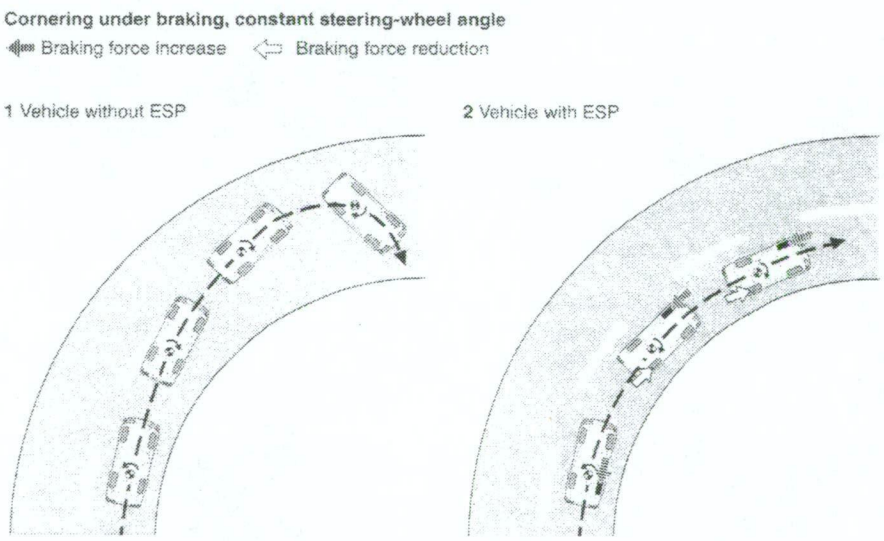

Figure 2.36: ESP operation when accelerating while cornering [1, 2]

It can be seen the VDC can significantly aid when driving at the vehicle's stability limit by controlling individual wheel torques. This section shows the advantages that can be accomplished in vehicle dynamics modelling over ABS by the addition of just three sensors (yaw rate, lateral acceleration and steering angle), and also represents the current state in commercially available active control systems.

2.5. Traction Control System

Traction control systems, as the focus of this study, were introduced in the interim between the development of ABS and VDC, to help control a vehicle during acceleration. The first system was launched in 1987 by Bosch in the interests of optimising both the available longitudinal and lateral forces generated by the vehicle's tyre, in a similar manner to the operation of ABS, except under acceleration and not braking [19, 20]. The potential benefits of TCS can be summarised as follows [5, 27]:

- Clearly enhanced driving in straight line running and cornering by maintaining the tyre forces within their optimum slip ranges.
- Higher traction forces can be transmitted to the road when moving off from stationary and when accelerating.
- Intervention to prevent departures from the desired course, and possible incident.
- Limited active braking by providing negative torque through the engine.
- Increased acceleration on split μ surfaces by utilising all available traction.
- Reduced tyre wear and noise from spinning wheels and engine overrevving.

This section will discuss, firstly, the potential benefits of traction control and its general operation, before examining the different systems available individually and demonstrating their effectiveness. It will also present research into the performance of unconventional control logic.

2.5.1. TCS Operation

Vehicle stability can be lost in a number of ways during an acceleration manoeuvre. If traction while accelerating is broken in front wheel drive (FWD) vehicles, the front tyres are no longer able to produce significant lateral force and the driver loses steering control. This manifests it self in vehicle under-steering. If traction while accelerating is broken in rear wheel drive (RWD) vehicles it is the rear tyres that cannot provide enough lateral force, giving the vehicle an over-steering attitude and the possibility of

spinout as yaw stability is lost, as shown in Figure 2.37. Also, the widespread use of 'open' differentials, which can only deliver equal amounts of torque to each driven wheel, has a negative effect on vehicle stability during acceleration on surfaces of varying levels of friction coefficient. If one wheel is travelling on a surface that offers limited traction and starts spinning excessively, the torque that can be transmitted through the other wheel is severely reduced regardless of the level of μ it is travelling on [3, 4, 28].

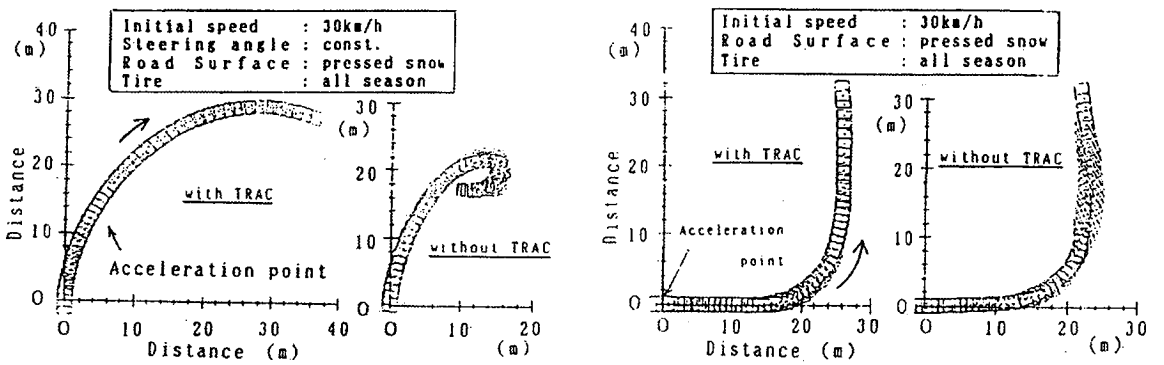

Figure 2.37: Benefits of the Toyota traction control system "TRAC", (a) under constant steering input & (b) at an intersection (sampling rate = 200ms) [18]

Just as with ABS, there is a clear need to precisely control wheel slip in the interests of maximising longitudinal and lateral tyre forces for a range of situations, and as such it also relies on data gathered from wheel speed sensors. Smooth and slippery roads on a gradient and cornering can create critical situations and place excessive demands on the driver, and incorrect reactions can result. TCS can intervene in such situations and optimise stability to an extent that is beyond the abilities of the driver, also shown in Figure 2.37. In most production vehicles it is this demand for stability that is the overriding function of TCS. Unlike ABS, for safety there is little need for high longitudinal acceleration. Lateral forces are more important and as a result the control range of TCS operation is at slightly lower slip values than for ABS as stated by Maisch et al. [45] and shown in Figure 2.38.

In any case, the application of TCS should utilise the following information for optimum operation in the interests of producing a control stately based on directional control, traction and steerability [17]:

- Vehicle Speed – to give traction priority at low speed and directional control priority at high speed.
- Cornering Manoeuvre (from non-driven wheel speed differences) – to give directional control priority during cornering.
- Vehicle Acceleration and Throttle Position – to identify situations where TCS operation is sensitive to small differences.

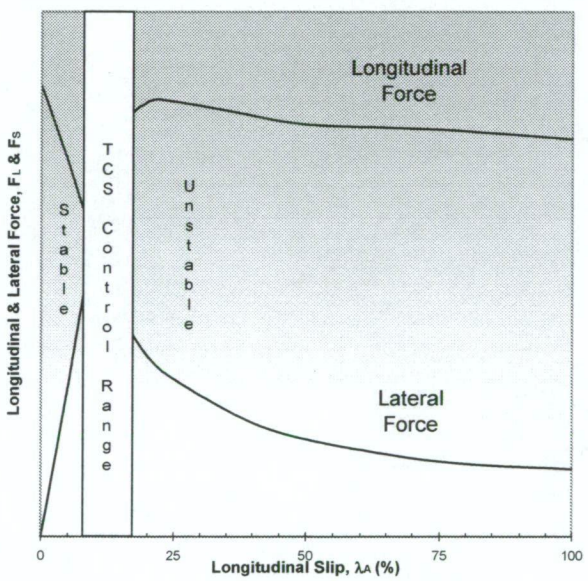

Figure 2.38: TCS slip control range [4, 18, 23, 33, 35]

Slip values can be kept within this range though a number of techniques. The simplest is the use of a limited slip differential (LSD), which offers passive control by proportioning driven wheel torque across the differential. Engine torque can also be limited through throttle valve intervention or by retarding or preventing combustion in specific cylinders using fuel injection and ignition control. And finally drive torque to the wheels can be offset though the use of the braking system. Each system can give reasonable results under specific conditions, but can be combined with other systems to provide comprehensive and comfortable control.

2.5.2. Differential Intervention

Most automobiles feature a differential unit at the drive axle, which offers almost loss free differences in wheel speed for cornering and provides uniform torque distribution at each of the drive wheels. Under normal conditions the application of this uniform torque inhibits vehicle yaw and provides favourable dynamic response. Unfortunately, when a situation arises when one of the driven wheels is on a surface that cannot offer as much tractive force as the other (slip μ), the differential can only transmit as much torque to both wheels as the wheel with the least traction will allow. This can pose significant limitations on acceleration and, if the coefficient of friction on the one wheel is close to zero (such as is the case on icy surfaces), can make the resulting total drive torque negligible. This problem experienced by open differentials can be overcome through the use of limited slip differentials [3, 18].

There are a number of different types of LSD, but all seek to improve traction by sending more torque to the wheel with high μ, with varying levels of success [17, 23, 28, 30].

2.5.2.1. Open Differential

As mentioned earlier, an open differential (Figure 2.39) can only transmit uniform torque to the drive wheels. This means that when it is used on a split μ surface it has a significant performance limitation. On such a surface the wheel on the low μ surface will not be able to transmit as much torque to the ground as the other wheel, and wheel spin will likely be induced. The general operational range of the open differential is shown in Figure 2.40 and depicts significant limitations as shown by Hosomi et al. [31].

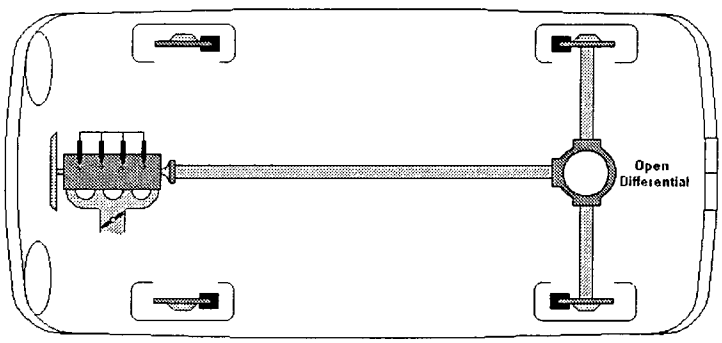

Figure 2.39: Open differential layout

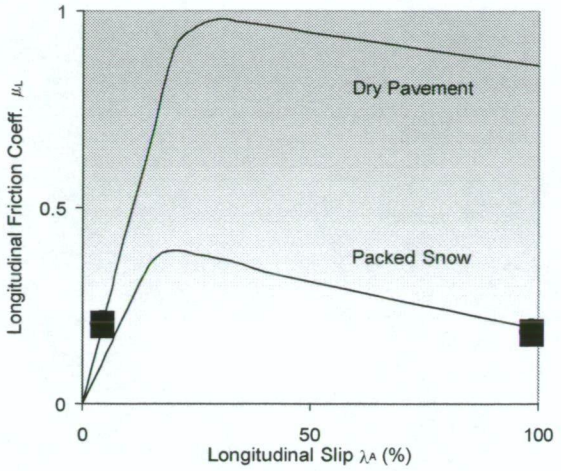

Figure 2.40: Operation of an open differential [28]

2.5.2.2. Limited Slip Differential

One way to improve the use of the available traction is to proportion it, sending more torque to the high μ wheel, which has more available traction. In this case drive torque still has the potential to exceed that available to the low μ wheel but, in general, it has the effect of increasing the tractive potential. LSDs operate on this principle, as stated by Jawad et al. [32], with the increase in performance shown in Figure 2.41 and layout shown in Figure 2.42.

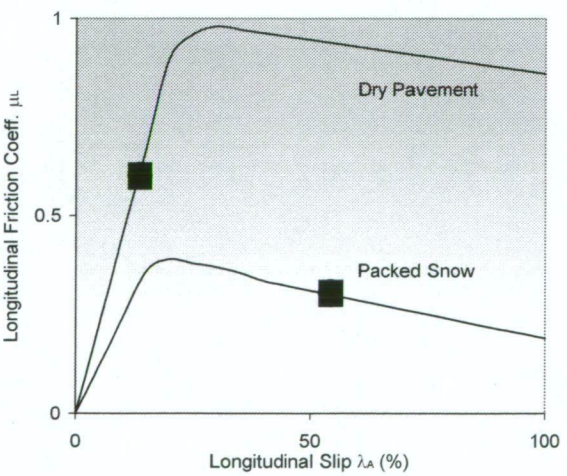

Figure 2.41: Operation of proportioning control [28]

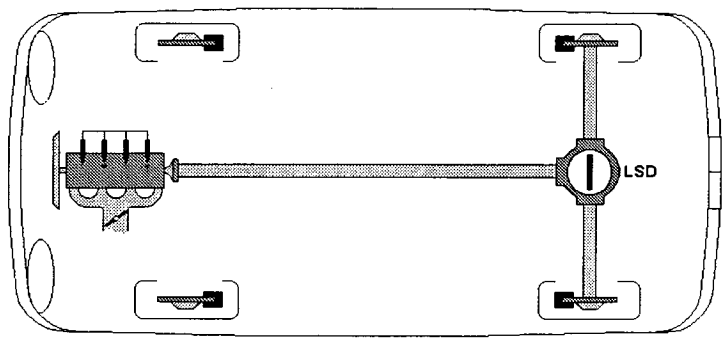

Figure 2.42: LSD layout

LDS's generally come in two types; torque-sensing and speed-sensing. Speed-sensing, viscous, differentials require a difference in wheel speeds to actuate, meaning that the low μ wheel must lose traction and spin up to a comparatively high speed in order to engage the proportional characteristics of the differential. Torque-sensing differentials, on the other hand, require torque differences to develop between the driven wheels. When a torque difference develops, the differential senses it and sends more torque to the wheel that needs it while reducing the torque to the wheel that is starting to spin. This mechanical action means that the torque-sensing differential can bias torque without wheel spin, which has many stability advantages [28, 55].

2.5.2.3. Differential Locks

Hydraulic differential locks can provide electronic control of the way torque is proportioned between the driven wheels. Using a similar hydraulic controller as used in ABS, hydraulic pressure can be applied to the differential locks. As the pressure increases the differential increasingly locks, providing effective control of the torque between the driven wheels. The nature of this system, of course, means that it must be actively controlled. It is not a passive system and so requires ECU control and data input from the wheel speed sensors around the vehicle, as shown in Figure 2.43.

By actively controlling the torque biasing of the differential the vehicle is able to both significantly improve traction on a split μ surface and also improve stability by minimising over-steering [3, 17].

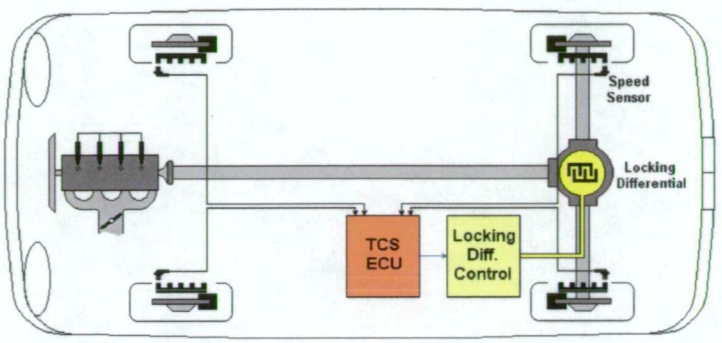

Figure 2.43: Locking differential TCS layout

2.5.3. Throttle Intervention

While limited slip differentials can proportion the torque developed by the engine between the driven wheels, it has one serious drawback. If the engine produces too much torque, or the surface is sufficiently slippery, both wheels may start to lose traction and spin. There is a clear need to be able to limit the torque delivered to the wheels. This means that wheel spin can be eliminated and slip can be optimised to provide the most traction by limiting engine torque. Using an open differential on a split μ surface means that this limiting approach will give the most available traction to the low μ wheel, but this will limit the torque delivered to the high μ wheel, as shown in Figure 2.44.

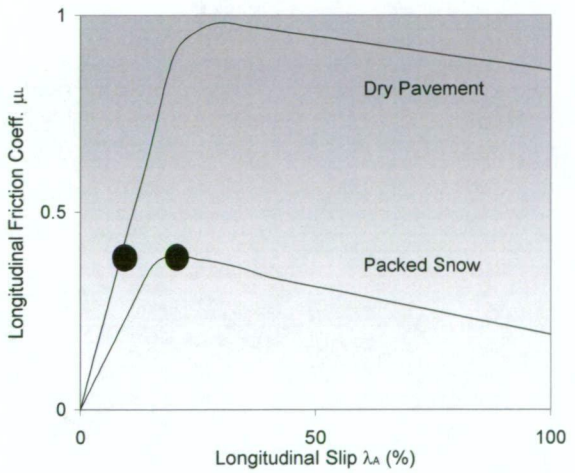

Figure 2.44: Operation of limiting control [28]

Ordinarily the driver reduces drive torque when needed by releasing the accelerator slightly. When and by how much will determine the vehicle's stability and acceleration. Inexperienced drives may 'spin out' in situations when more experience drivers could have controlled the vehicle. Clearly, TCS can be used to help the inexperienced driver control the accelerator to improve traction. To this end, wheel speed sensors are generally used to feed data to the ECU, which determines the slip at the driven wheels and evaluates a control strategy to improve stability and/or acceleration – in a similar manner to the operation of ABS. In the case of throttle TCS, the ECU controls the throttle butterfly valve position by overriding driver commands through the accelerator, as shown in Figure 2.45.

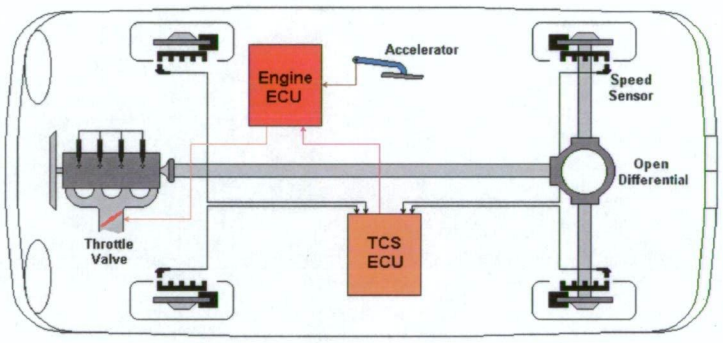

Figure 2.45: Throttle TCS layout

Throttle control can be achieved in two ways, fly-by-wire control or the addition of a second throttle valve. Fly-by-wire removes the standard cable link between the pedal and the butterfly valve, replacing it with a potentiometer at the pedal, which controls a servomotor at the butterfly valve [23]. This method enables the incorporation of the TCS ECU to control the throttle when needed though the engine ECU, but has the potential of failure resulting in an uncontrollable throttle, and so requires many safety considerations. The second throttle control places a secondary, electronically controlled, butterfly valve upstream of the valve controlled mechanically by the driver, as Asami et al. [33] shows. In this case, when the driver opens the throttle too much the second valve can close a little and limit the airflow to the engine, reducing its power. The advantage of this method is that failure of the system can at worst stall the engine, while also enabling the relatively simple addition of TCS to vehicles without an engine

ECU or fly-by-wire technology. Figure 2.46 shows the advantages throttle control TCS can have when hydroplaning by controlling the secondary throttle valve [3, 18, 28, 33, 34].

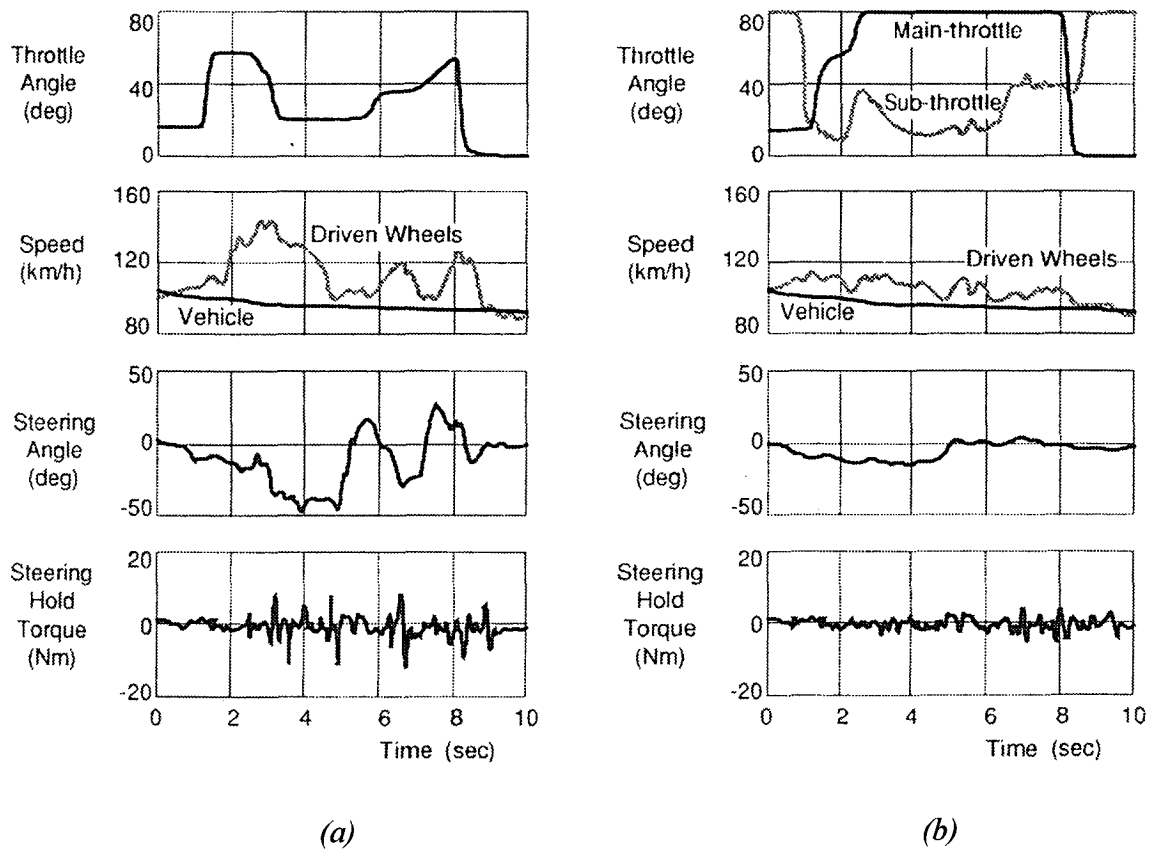

Figure 2.46: Effects of hydroplaning, (a) under driver control & (b) using secondary throttle valve intervention as a form of TCS [34]

2.5.3.1. Performance and Limitations

By limiting engine torque, and thus reducing wheel spin, throttle TCS improves stability considerably. It also has the advantage that steering control is not effected by the TCS operation, as it is under the operation of an LSD. Its operation is very smooth and as such makes the systems very driver friendly, inhibiting excessive noise and vibration which can distract the driver.

This operation comes at a significant cost however because, as the throttle only controls the airflow to the engine, there is a significant lag in engine control as the air fluctuates

in pressure. This slow response means that throttle TCS has difficulty in responding to the rapid changes in wheel slip and as such can have trouble providing accurate traction control [7, 34].

2.5.4. Ignition / Injection Intervention

The slow response of the use of the throttle to control engine power can be overcome by replacing the throttle control element with ignition / injection control. By progressively altering the way engine cylinders fire this system provides almost instantaneous command of reduction of engine power when the vehicle requires TCS intervention. The control system is shown in Figure 2.47.

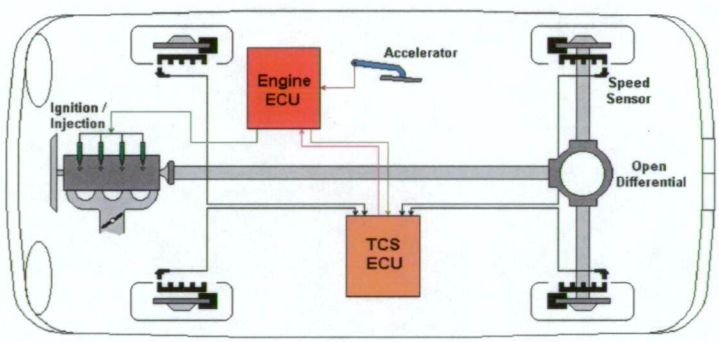

Figure 2.47: Ignition / Injection TCS layout

It can be seen that this form of engine control requires significant engine ECU control of the ignition and injection systems to limit power under the command of the TCS ECU. The fuel ratios and ignition timing must be precisely controlled to avoid damage to the engine and the catalytic converter. This combined with the inertia of the engine at different engine speed means that the TCS ECU must also gather data on the operating conditions of the engine, and not just from the wheel speed sensors as in previous situations. This bi-directional exchange of data between the engine and TCS ECUs is also shown in Figure 2.47. Using the engine speed, load parameters and appropriate time delay elements to account for engine dynamics, the engine torque at a given instant can be determined within the TCS ECU. The TCS ECU can then send a control signal to the engine ECU, that then directly controls each engine torque reduction stage using pre-programmed maps for each stage [17, 23].

2.5.4.1. Ignition Retard

Figure 2.48 shows the effect of varying ignition timing on combustion pressure (and thus power). It can be seen that engine power can be effectively limited by retarding the ignition timing, allowing unignited fuel to exit the combustion chamber though the exhaust port.

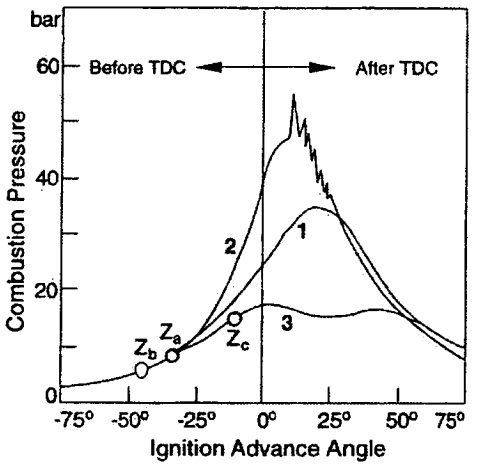

Curve 1 depicts correct ignition timing, Z_a, curve 2 excessive ignition advance Z_b and curve 3 excessive ignition retard. Z_c.

Figure 2.48: Effect of ignition timing on engine power [3]

This method can offer infinite stages of engine torque reduction from full combustion to zero combustion with high response and smooth operation. But, practically, this is not the case. Sending unignited fuel through the exhaust causes a significant temperature rise within the exhaust system as the fuel subsequently burns, which as well as having a detrimental effect on engine life, can destroy catalytic converters. In reality, it is only safe to operate ignition retard for short periods of time and over a small range of operation, and so is generally only used in conjunction with fuel injection suppression [3, 17, 23, 35, 36].

2.5.4.2. Fuel Injection Suppression

Engine power can also be reduced quickly by not allowing cylinders to fire. Shutting down cylinders progressively on a four-cylinder engine will reduce engine power by

about 30% for each cylinder, with most of the power of the last cylinder going into overcoming engine frictional forces, as suggested by Bonning et al. [352]. By suppressing the fuel delivery to specific cylinders, engine power can be effectively controlled within this range for each cycle (720° of crank rotation) of the engine's operation.

This method of control also has its problems. Firstly, fuel injection suppression operation can be very coarse because the number of torque reduction stages is very limited (Figure 2.49). Secondly, during injection suppression the liquid fuel film from port walls will evaporate quickly. This means that when injection resumes some of the fuel will go into reforming the film, and not into the cylinder where it is needed, resulting in abnormal combustion. Fuel maps within the engine ECU must take this into account and inject more full when injection resumes in reference to how long the cylinder was shut down for and engine speed [35, 36].

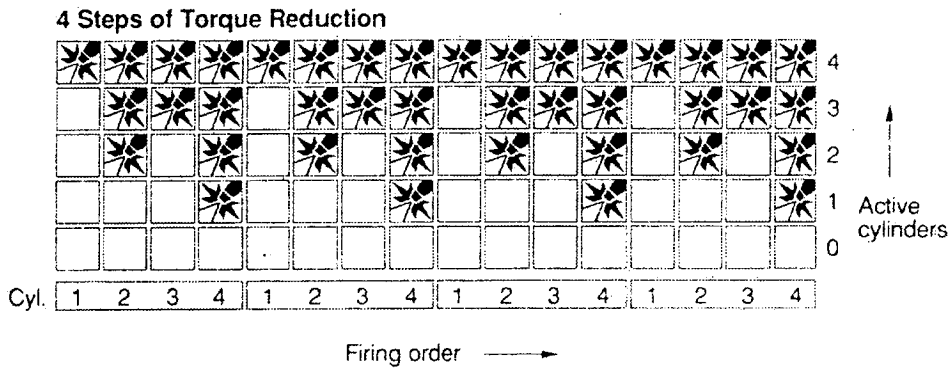

Figure 2.49: Torque reduction stages using fuel injection suppression for a 4cyl engine [35]

2.5.4.3. Alternating Fuel Injection Suppression

The effect of the problems with fuel injection suppression can be reduced using an alternating suppression scheme, as shown in Figure 2.50 and demonstrated in Figure 2.51. Using this method the torque reduction stages are increased over two engine cycles (1440°) instead of one. This meets a number of control goals:

- Single cylinders can be shut off for a single 1440° cycle.
- ½ cylinders can be shut off by suppressing injection on every 2nd 720° cycle.
- Shut off cylinders can be alternated to insure that no one cylinder is constantly off, reducing the evaporation of the fuel film and thus making fuel maps simpler.
- Shut off cylinders can be controlled to improve engine vibration, smoothness and crankshaft torsional stresses.

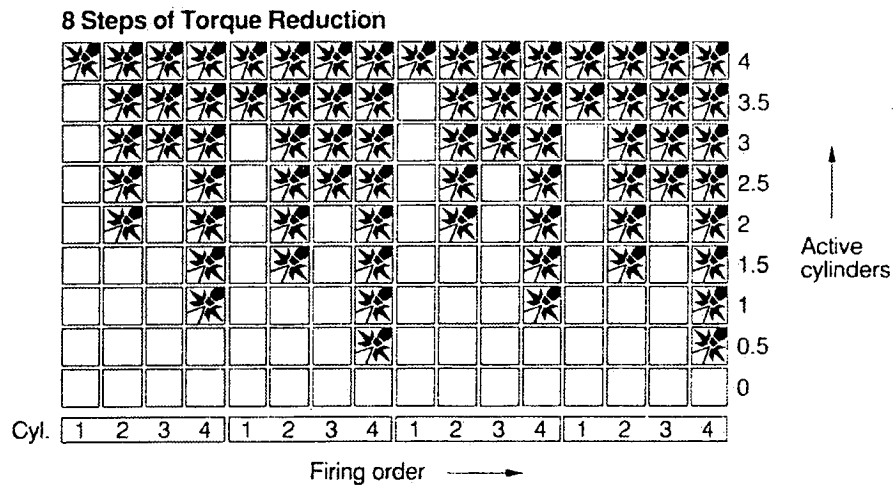

Figure 2.50: Torque reduction stages using alternating fuel injection suppression for a 4cyl engine [35]

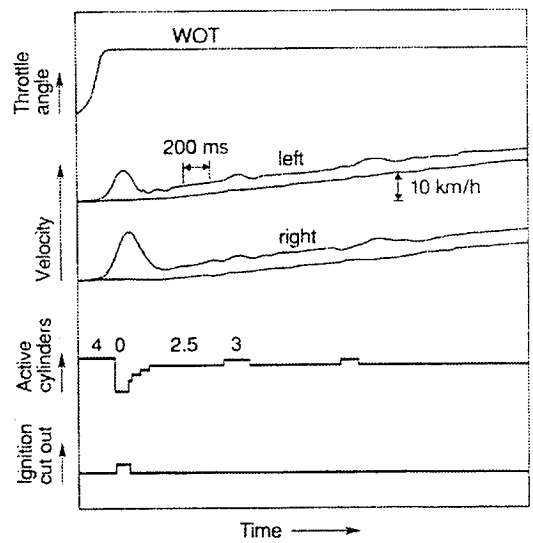

Figure 2.51: Operation of the alternating injection suppression method with ignition cut out for a FWD on packed snow travelling initially at 40 km/hr [35]

2.5.4.4. Performance and Limitations

Like throttle TCS, ignition / injection TCS aims at limiting engine torque only. Again it offers high stability and steering control, but has a very limited ability to improve traction. It does, however, differ from throttle TCS in a number of ways.

The direct nature of the ignition / injection TCS significantly improves the system's responsiveness and can offer extremely fast modulation of engine torque. This means that it can control wheel slip within much tighter bounds than throttle TCS, but also induces a reasonable amount of vibration through the vehicle – reducing comfort and drivability slightly. The coarseness of the system operation also means that it can have trouble operating on low μ surfaces and during engine warm-up [35].

2.5.5. Brake Intervention

Just as in ABS, wheel slip can be controlled using the braking system for TCS, as shown in Figure 2.52. Instead of optimising slip for all wheels under deceleration the TCS uses only the brakes on the driven wheels to control their slip under acceleration. In this way they can both limit the amount of torque transmitted to the road (by converting the torque supplied by the engine into heat) and proportion it between the wheels (by providing bias across the differential through the brake system). This is shown in Figure 2.53 and represents the ability of the driven wheels to provide the best tractive force available, while also providing stability. Operation of the system, however, requires a hydraulic pressure source in addition to the ABS hydraulic modulators to enable the system to increase braking force and well as reduce it, shown in Figure 2.54, [3, 7, 31].

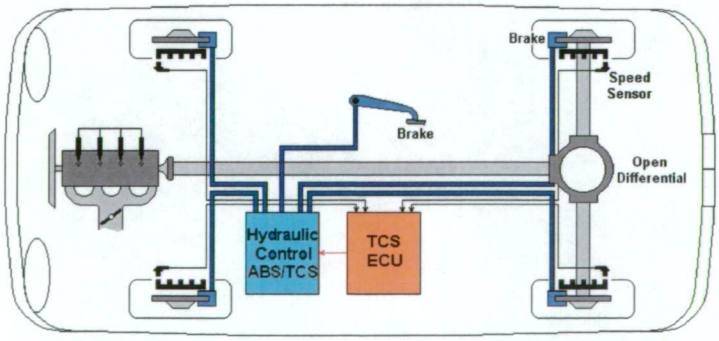

Figure 2.52: Brake TCS layout

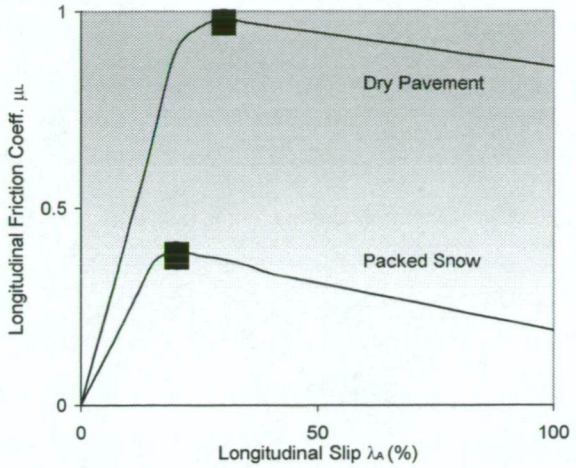

Figure 2.53: Operation of a proportioning and limiting control [28]

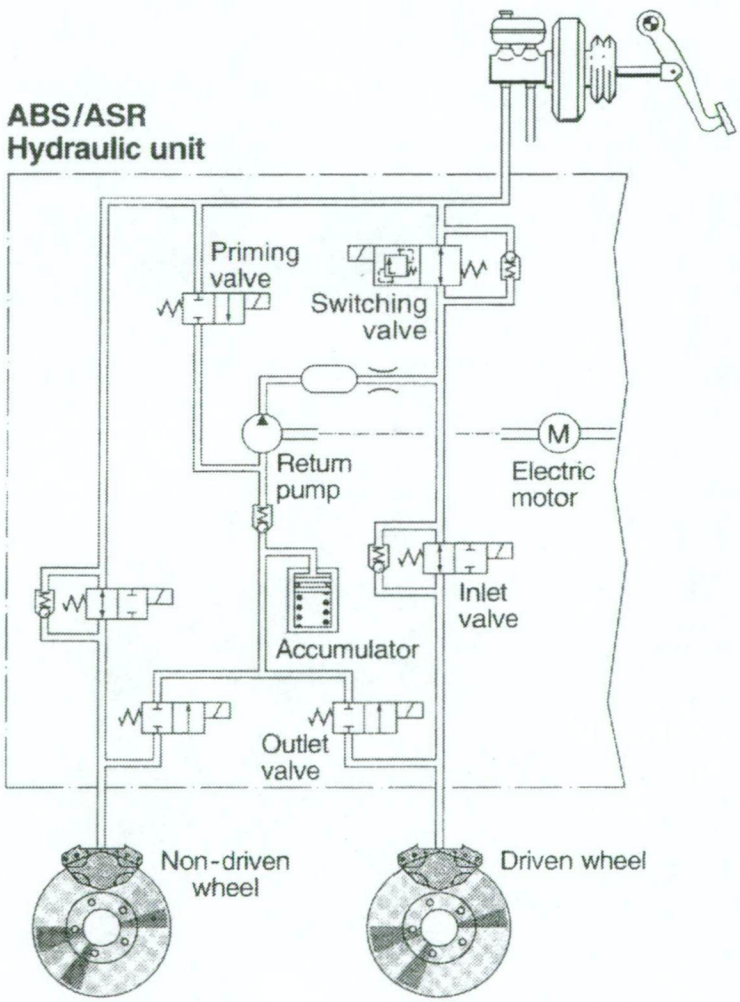

Figure 2.54: Bosch's ABS / TCS (ASR) hydraulic unit operation [29]

2.5.5.1. Performance and Limitations

This method would appear to provide a highly effective way of controlling traction and vehicle stability. It can use the same hydraulic modulators as ABS and the brakes can produce large negative torques to control wheel speeds with both speed and accuracy.

The main problem that arises with this system is the amount of heat generated within the brakes. The very high loads imposed by the engine can accumulate heat within the brakes quickly, as can the actuation of the brakes at high speed. Brake actuation must be limited to a time and speed range to avoid brake overheating and subsequent failure. High performance TCS, on the other hand, requires operation over unlimited time and speed for optimum operation. It also can adversely affect steering and vibration levels. As such, brake TCS has very limited application, restricted to only low speed, low load situations [34].

2.5.6. Combined Intervention

Because of the wide variety of TCS control strategies, each with their own specific benefits and drawbacks, it is often necessary to combine one of more systems to improve overall performance. This brings about increasing complexity into the design of the TCS ECU control algorithms and associated hardware, but the benefits to performance can be large, as shown in Figure 2.55 and Table 2.1.

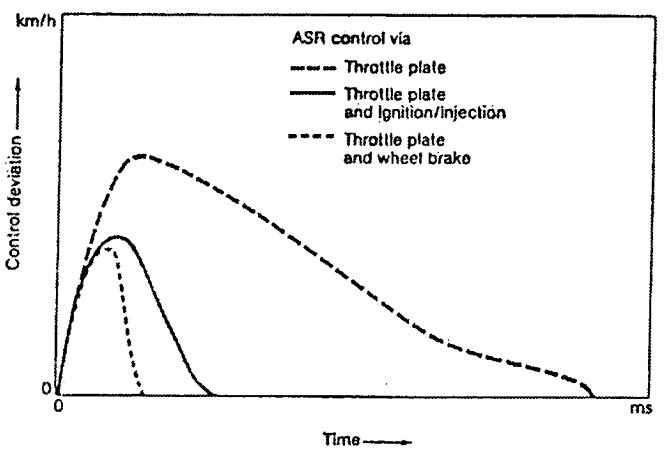

Figure 2.55: Control deviation using different TCS combinations [23]

	FWD Stability	RWD Stability	Traction (Split μ)	Comfort	Component Stress	System Complexity	Operational Time	Response
Open Differential	- -	- -	- -	+ +	+ +	+ +	+ +	- -
Limited Slip Differential	-	-	+	- -	-	+	+ +	-
Locking Differential	+	+	+ +	-	-	- -	-	+
Throttle Control	-	- -	-	+ +	+ +	+	+ +	- -
Ignition / Injection Control	+ +	+	0	0	0	+ +	-	+ +
Brake Control	+	+	+ +	- -	- -	-	- -	+
Throttle / Injection	+ +	+ +	0	+	+	+	+ +	+ +
Throttle / Brake	+ +	+ +	+ +	+	+	-	+	+ +
Throttle / Injection / Brake	+ +	+ +	+ +	+	+	- -	+	+ + +
Injection / LSD	+	+	+	-	+ +	+ +	+	+
Throttle / LSD	0	0	+	+	+ +	+ +	+ +	-
Throttle / Injection / LSD	+	+	+	0	+ +	+	+ +	+
Brake / LSD	+ +	+ +	+ +	0	-	-	0	+
Throttle / Injection / Locking Diff.	+ +	+ +	+ +	+	+	- - -	+ +	+ +

Table 2.1: TCS concept evaluation

2.5.6.1. Throttle and Injection

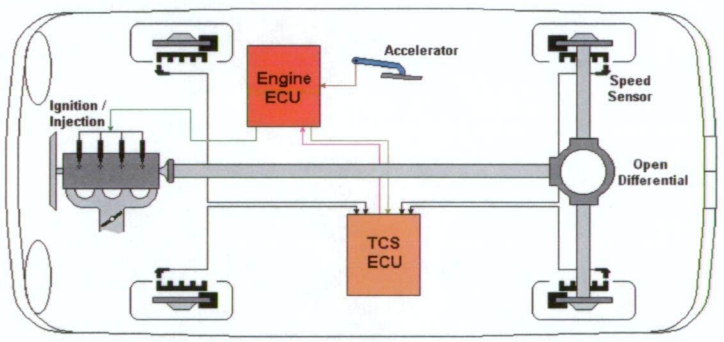

Figure 2.56: Throttle and injection TCS layout

Throttle and injection TCS, as shown in Figure 2.56, incorporates the best of the two systems. The injection control is able to implement high frequency control while the throttle control is able to improve comfort and operation time by limiting engine power less severely. If the amplitude of the control deviation and the wheel slips indicate that the throttle valve on its own is not sufficient for control, the TCS ECU will either retard the ignition for a limited time and/or start shutting cylinders down thought the injection

system. The result is a control system that ensures a high level of vehicle directional control and stability & comfort, but with limited traction ability [17, 23].

2.5.6.2. Throttle, Injection and Brake

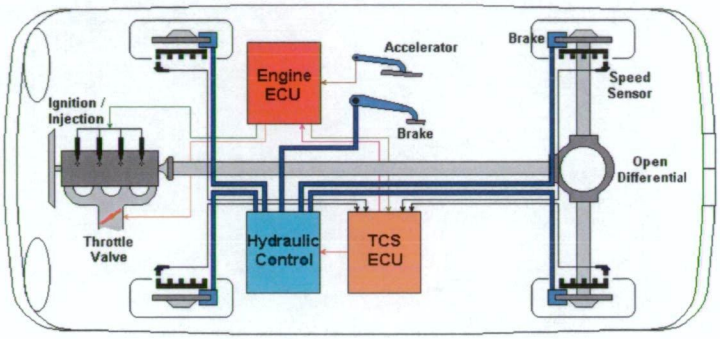

Figure 2.57: Throttle, injection and brake TCS layout

Incorporating the brake into the throttle and injection TCS further improves the system. The engine control can be used to limit the torque delivered to the wheels, while the brake system can provide optimum operation on mixed μ surfaces. Since the drive torque is limited to only what is required, the brakes do not have to work as hard as they have to when operating alone, increasing their available activation time. The system can thus meet almost any situation without reservation, providing excellent stability, directional control and traction while also maintaining comfortable operation, as depicted in Figure 2.58 [17, 23].

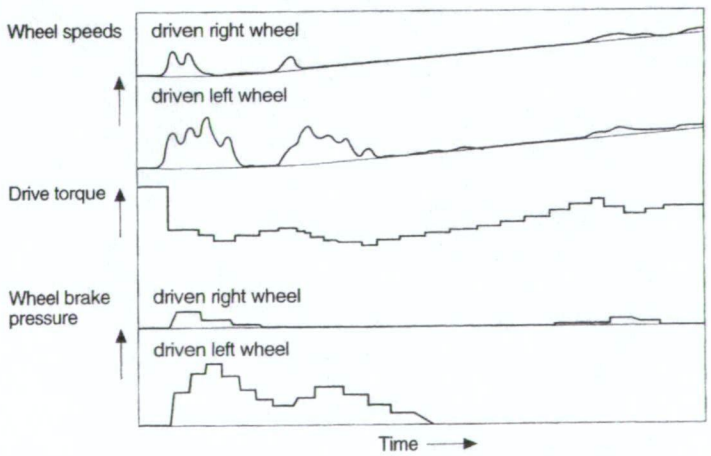

Figure 2.58: TCS operation using engine and brake intervention on a snowy road [3]

2.5.6.3. Throttle, Injection and Locking Differential

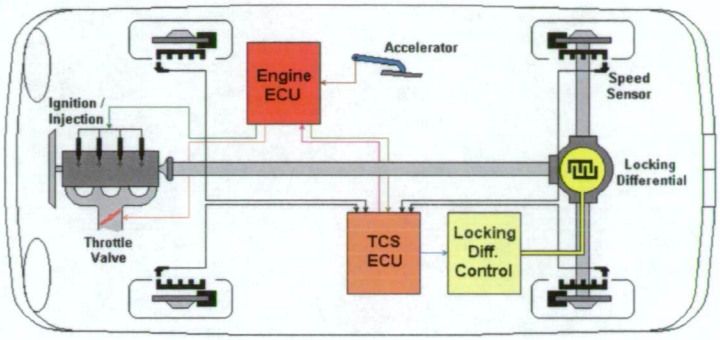

Figure 2.59: Throttle, injection and locking differential TCS layout

TCS with engine control and a locking differential operates in a similar way to systems with engine control and brake intervention. The differential provides TCS ECU control over the biasing of the torque to the driven wheels and, as such, incorporates increased tractive ability to the system. It provides increased traction on mixed μ roads, but cannot offer the quite same level of directional control that brake intervention can [17, 23].

2.5.6.4. Throttle and LSD

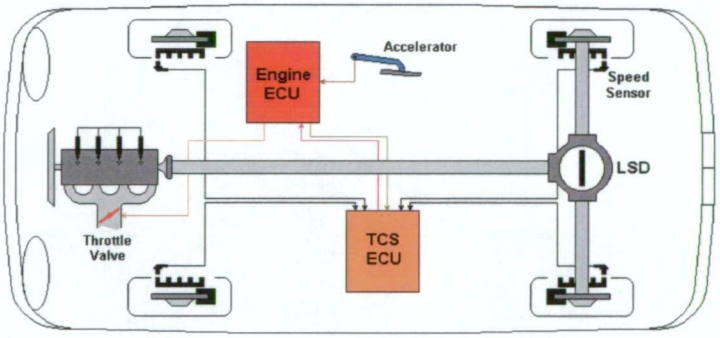

Figure 2.60: Throttle and LSD TCS layout

Since throttle control offers a limiting control and LSDs offer proportioning control this system can offer stability, directional control and traction. The use of an LSD significantly reduces the system complexity and provides reasonable all round response. Its overall ability depends on a few factors, such as throttle response and LSD type. A study conducted by Holzwarth et al. [28] (Figure 2.61) shows the operation of this TCS

using an open differential, a torque-sensing differential (TORSEN®), a speed-sensing differential (viscous) and the use of a viscous differential with no TCS (ETCS) operating, under the same driver inputs on a split μ surface.

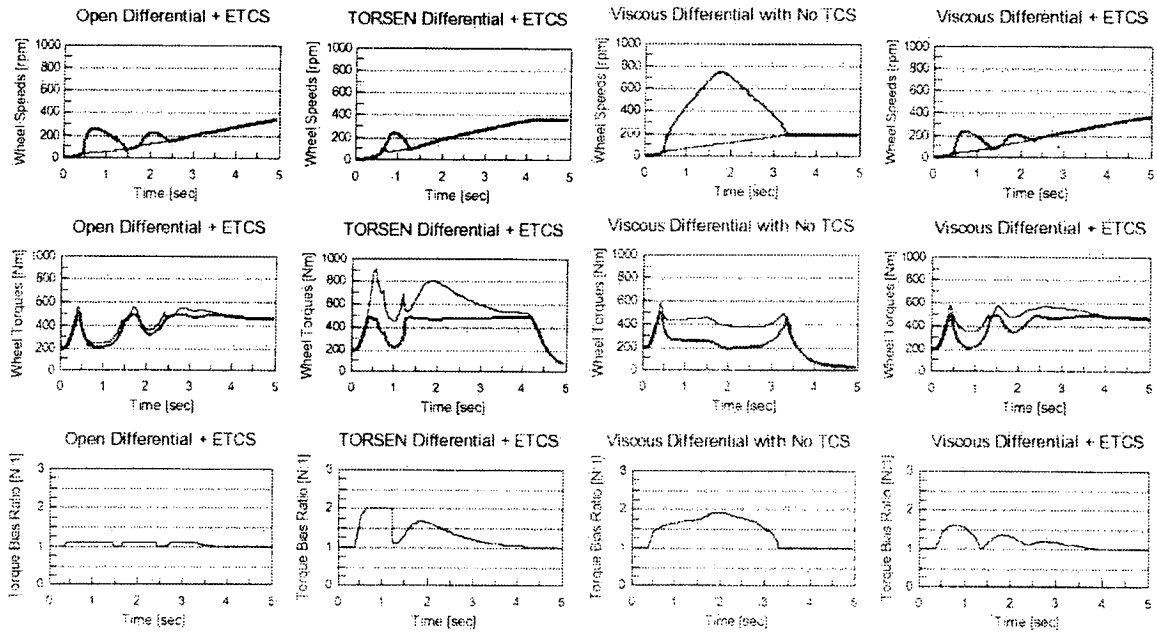

Figure 2.61: Comparison of LSDs with engine TCS (ETCS) on split μ surface [28]

It can be seen that the open differential gives very little torque biasing, which is reflected in the vehicle's acceleration. The TORSEN LSD starts biasing torque almost immediately, transferring more torque to the road and reducing the severity of the required engine torque reduction. The viscous LSD with no TCS develops significant wheel spin at one wheel and, as such, the differential biases torque to the high μ wheel throughout the simulation. And finally, the viscous LSD with TCS shows limited torque biasing because the TCS ensures that large driven wheel speed differences do not develop. This last case illustrates that the operational requirements of a speed sensing LSD is in direct conflict with the control parameters of the TCS – speed-sensing LSDs require wheel spin to activate, while TCS tries to minimise it. The only advantage, as Iwata et al. [30] points out, of the use of speed-sensing differentials over open is that they can increase vehicle stability during cornering manoeuvres because such manoeuvres produce large driven wheel speed differences without slip.

Figure 2.61 also illustrates the potential of LSDs to reduce the need for active TCS operation. Torque-sensing LSDs, in some circumstances, eliminate the need for TCS intervention completely, as well as reducing the severity and duration of activation [28].

2.5.6.5. Injection and LSD

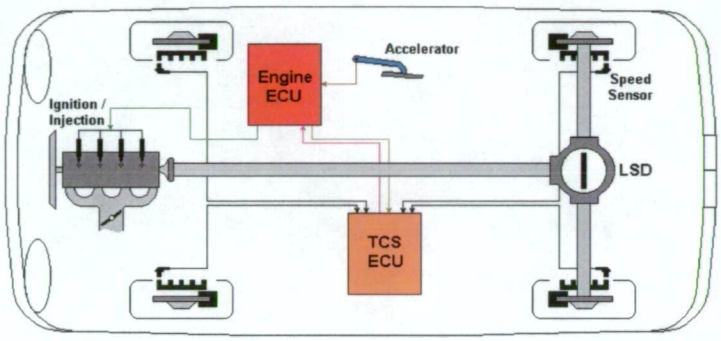

Figure 2.62: Injection and LSD TCS layout

Just as with throttle TCS with a LSD, this system offers a reasonable all round response to improve stability, directional control and traction. However, the use of ignition / injection control offers much faster response to wheel slip, increasing stability, but at the cost of comfort and duration of operation. Again, this operation can be improved with the addition of throttle control to the ignition / injection control to provide a system with good response and improved comfort and unlimited duration times.

2.5.6.6. Brake and LSD

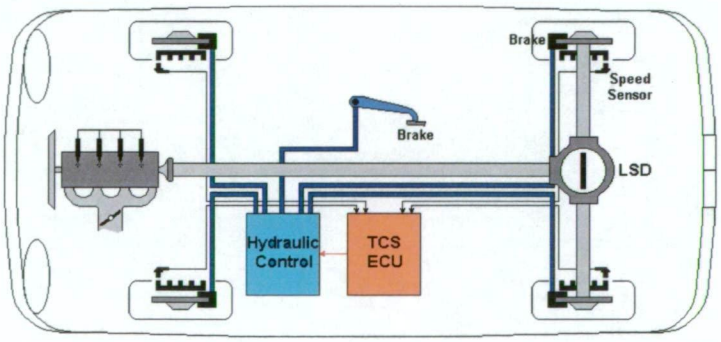

Figure 2.63: Brake and LSD TCS layout

The main problem with brake only TCS is that of brake over-heating. The installation of an LSD can reduce the necessary loading supplied by the brakes to proportion torque to the driven wheels, as shown by Holzwarth et al. [28] in Figure 2.64. In this way the period of time that the brake system can intervene can be substantially increased.

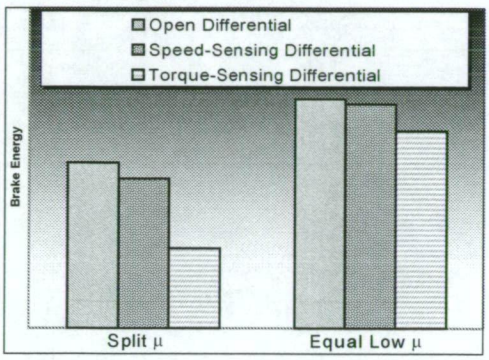

Figure 2.64: Brake energy absorbed by the most heavily braked wheel [28]

Another problem that brake only TSC can have is that of 'hunting'. Hunting is when the two brakes across the drive axle get out of phase with each other, and typically happens on equal μ surfaces. As one wheel begins to spin the brake system tries to slow it, sending increased torque to the other wheel. This then can make the other wheel start to spin as the first comes under control, repeating the cycle. LSD operation can reduce this effect because it has a lag in operation (wheel speeds and torques must reach a specific level before biasing will occur), as shown in Figure 2.65.

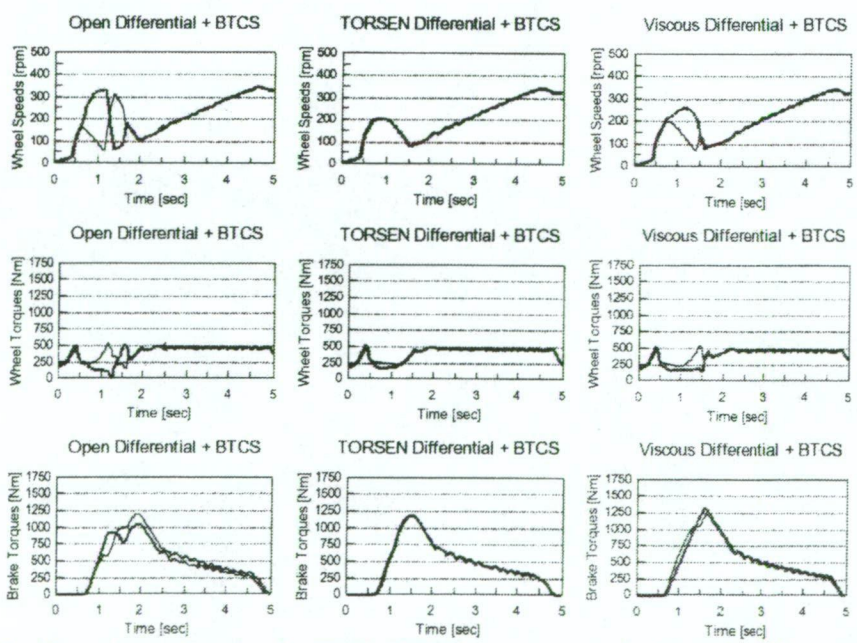

Figure 2.65: Hunting using brake TCS (BTCS) on wet asphalt with different LSDs [28]

2.5.7. TCS with Fuzzy Logic

As with the ABS fuzzy controller, TCS can benefit from fuzzy logic in the same way. By replacing complex mathematical models with heuristic decision rules, traction control strategies can be accomplished with limited understanding of the systems and less effort.

One such controller is presented by Cheok et al. [15]. In this situation fuzzy TCS was installed into a 4WD with throttle, brake and transmission intervention, as shown in Figure 2.66. Transmission intervention was included into the system to enable gear upshifts to reduce engine torque, while also controlling engine torque through throttle relaxation.

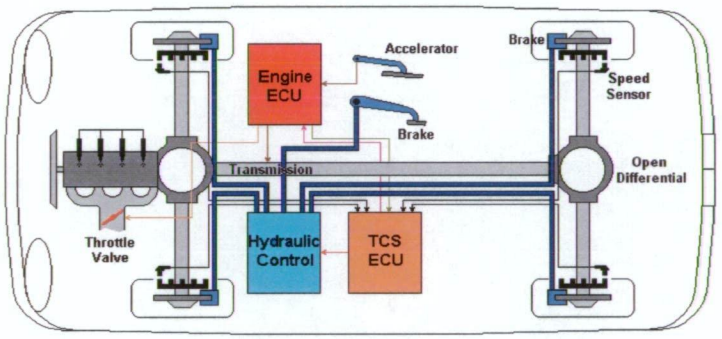

Figure 2.66: Layout of TCS for fuzzy controller

In this situation fuzzy logic controllers were first developed to control the brake pressure at each wheel. The variables that were identified to be the controlling values were transmission speed, throttle position and calculated slip at each wheel, and were designated quantities of either (L)arge or (S)mall. Since the hydraulic modulators fitted to the vehicle allowed only brake pressure levels of 0, 50 or 100% the control logic for the controllers used only S, M & L labels to represent these functions respectively.

The engine torque in this case was considered a secondary controlled variable, its activation was just to reduce the forces acting on the brakes to increase their operating time. As such, the only controlling variables for throttle and transmission control was the applied brake pressure to each wheel. In this case the control logic used S for small torque reduction and L for large, with the actuation signals of each determined by

experimentation. The overall fuzzy control logic is shown below in Table 2.2, with its yaw angle and yaw rate control abilities on a low μ surface shown in Figure 2.67.

Transmission Speed	Throttle Position	Wheel Slip	Brake Pressure
IN	IN	IN	OUT
L	L	L	L
L	L	S	S
L	S	L	L
L	S	S	S
S	L	L	L
S	L	S	S
S	S	L	M
S	S	S	S

Transmission Speed	Throttle Position	Wheel Slip	Brake Pressure
IN	IN	IN	OUT
L	L	L	L
L	L	S	S
L	S	L	L
L	S	S	S
S	L	L	L
S	L	S	S
S	S	L	M
S	S	S	S

Transmission Speed	Throttle Position	Wheel Slip	Brake Pressure
IN	IN	IN	OUT
L	L	L	L
L	L	S	S
L	S	L	L
L	S	S	S
S	L	L	L
S	L	S	S
S	S	L	M
S	S	S	S

Transmission Speed	Throttle Position	Wheel Slip	Brake Pressure
IN	IN	IN	OUT
L	L	L	L
L	L	S	S
L	S	L	L
L	S	S	S
S	L	L	L
S	L	S	S
S	S	L	M
S	S	S	S

Brake Pressure				Throttle	Upshift
FR	FL	RR	RL		
IN	IN	IN	IN	OUT	OUT
S	S	S	S	S	S
S	S	S	M	S	S
S	S	S	L	S	S
S	S	M	S	S	S
S	S	M	M	S	S
S	S	M	L	S	S
S	S	L	S	S	S
S	S	L	M	S	S
S	S	L	L	L	L
S	M	S	S	S	S
S	M	S	M	S	S
S	M	S	L	S	S
S	M	M	S	S	S
S	M	M	M	S	S
S	M	M	L	L	L
S	M	L	S	S	S
S	M	L	M	L	L
S	M	L	L	L	L
S	L	S	S	S	S
S	L	S	M	S	S
S	L	S	L	L	L
S	L	M	S	S	S
S	L	M	M	L	L
S	L	M	L	L	L
S	L	L	S	L	L
S	L	L	M	L	L
S	L	L	L	L	L
M	S	S	S	S	S
M	S	S	M	S	S
M	S	S	L	S	S
M	S	M	S	S	S
M	S	M	M	S	S
M	S	M	L	L	L
M	S	L	S	S	S
M	S	L	M	L	L
M	S	L	L	L	L
M	M	S	S	S	S
M	M	S	M	S	S
M	M	S	L	L	L
M	M	M	S	S	S
M	M	M	M	L	L
M	M	M	L	L	L
M	M	L	S	L	L

M	M	L	M	L	L
M	M	L	L	L	L
M	L	S	S	S	S
M	L	S	M	L	L
M	L	S	L	L	L
M	L	M	S	L	L
M	L	M	M	L	L
M	L	M	L	L	L
M	L	L	S	L	L
M	L	L	M	L	L
M	L	L	L	L	L
L	S	S	S	S	S
L	S	S	M	S	S
L	S	S	L	L	L
L	S	M	S	S	S
L	S	M	M	L	L
L	S	M	L	L	L
L	S	L	S	L	L
L	S	L	M	L	L
L	S	L	L	L	L
L	M	S	S	S	S
L	M	S	M	L	L
L	M	S	L	L	L
L	M	M	S	L	L
L	M	M	M	L	L
L	M	M	L	L	L
L	M	L	S	L	L
L	M	L	M	L	L
L	M	L	L	L	L
L	L	S	S	L	L
L	L	S	M	L	L
L	L	S	L	L	L
L	L	M	S	L	L
L	L	M	M	L	L
L	L	M	L	L	L
L	L	L	S	L	L
L	L	L	M	L	L
L	L	L	L	L	L

Table 2.2: Fuzzy TCS control logic [15]

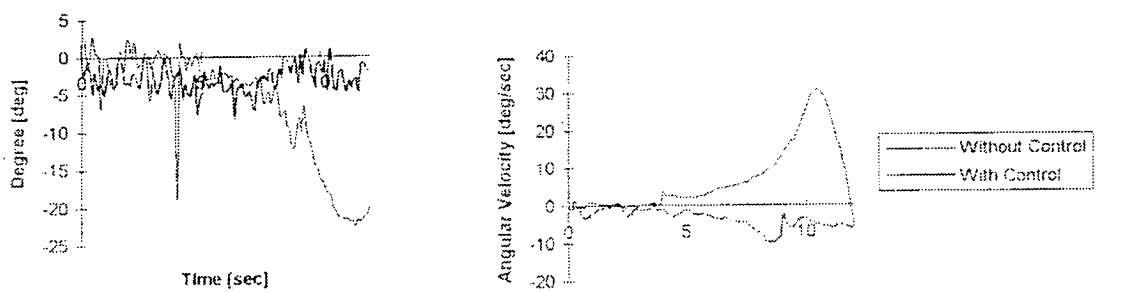

(a) *(b)*

Figure 2.67: Fuzzy TCS yaw stability on packed snow, (a) steering angle & (b) yaw rate [15]

It can be seen that unconventional approaches to traction control can provide control systems that are superior in some respects to conventional techniques. The ability to replace the complex mathematical models used in current systems with models based on observation can significantly reduce model complexity, allowing for the addition of extra sensory inputs. It is this ability to incorporate additional data into the control algorithm with minimal programming and computing resources that makes the use of these non-conventional techniques desirable.

2.6. Artificial Neural Networks

One such non-conventional technique that could be used in place of the traditional mathematical models exists in the form of artificial neural networks. ANNs offer an alternative to the complexities of modelling vehicle dynamics and control strategies using established TCS methods by providing a tool that both programs itself and learns on its own [39]. This section will introduce the reader to the concept of ANNs and their parallels to the operation of biological brains, before then explaining the basic operation of a single artificial neuron. The structures of various ANNs will also be discussed, and the performance benefits of each highlighted, followed by a description of the necessary 'training' techniques required to program ANNs. The section will then be concluded with the presentation of a number of examples of ANN applications in vehicle control.

2.6.1. Biological Neural Networks

Biological neural networks offer natural proof of the potential of ANNs. The neural structure of the brain provides an extremely powerful tool to recognise complex patterns and generalise those patterns of the past into actions of the future. It enables us to perform tasks such as recognising individual faces from different angles and provide accurate control of complex systems, such as an automobile. It also learns these patterns from experience.

The most basic element of the brain is the neuron, as shown in Figure 2.68. Based on our limited understanding of the operation of the brain, it is this cell that provides us

with our abilities to think, remember and apply previous experience in our actions. Its operation is largely unknown but, basically, it receives inputs from a number of other neurons, combines them in some way, performs a nonlinear operation to the result, and then outputs the final result to other neurons. The dendrites are hair-like extensions of the soma which receive electrochemical data through the synapse of other neurons and act as input channels. The soma then processes these signals over time and produces an output within the axon, which is subsequently sent to other neurons through the synapses.

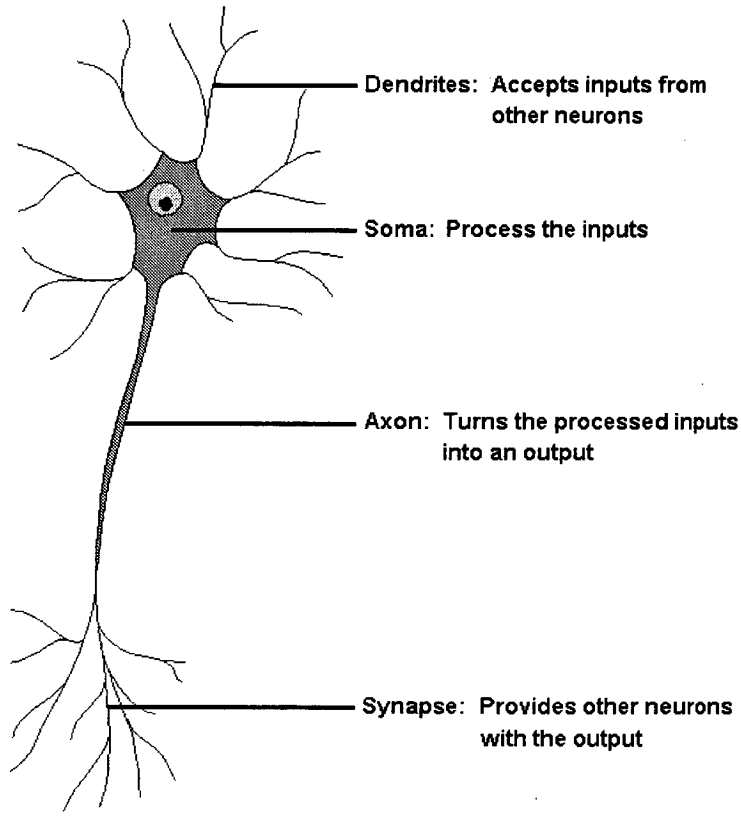

Figure 2.68: A simple biological neuron

In the human brain there are approximately 100 billion of these cells, each interconnected with anywhere up to 200,000 other neurons. The power of the human mind is thought to come from the sheer number of these components and the connections between them, including genetic programming and learning. Artificial neural network research seeks to harness this process to produce intensely parallel computer algorithms that act on past learning for pattern recognition and not on complex programming and modelling [39, 68, 69].

2.6.2. Artificial Neurons

The biological neuron is far more complex than depicted above, and there are many functions that it performs that are currently unknown. Current computing power cannot hope to emulate either these complex functions, or their vast numbers and interconnections. The simplified structure of an artificial neuron (Figure 2.69) reflects this. It can be seen that previous neuron outputs x_1, x_2 x_3 ...x_i provide data input to this neuron (neuron *j*) after being sufficiently weighted, simulating the role of the dendrites. The neuron then performs a summation function to gain a single value, which is then passed to the activation function. The activation function applies a nonlinear function to the result before passing it to the output function, which performs some form of signal conditioning. These three functions playing the role of the soma and axon. The output of the neuron is then made available for use by other neurons in a similar manner to the operation of the synapses [39, 40, 42].

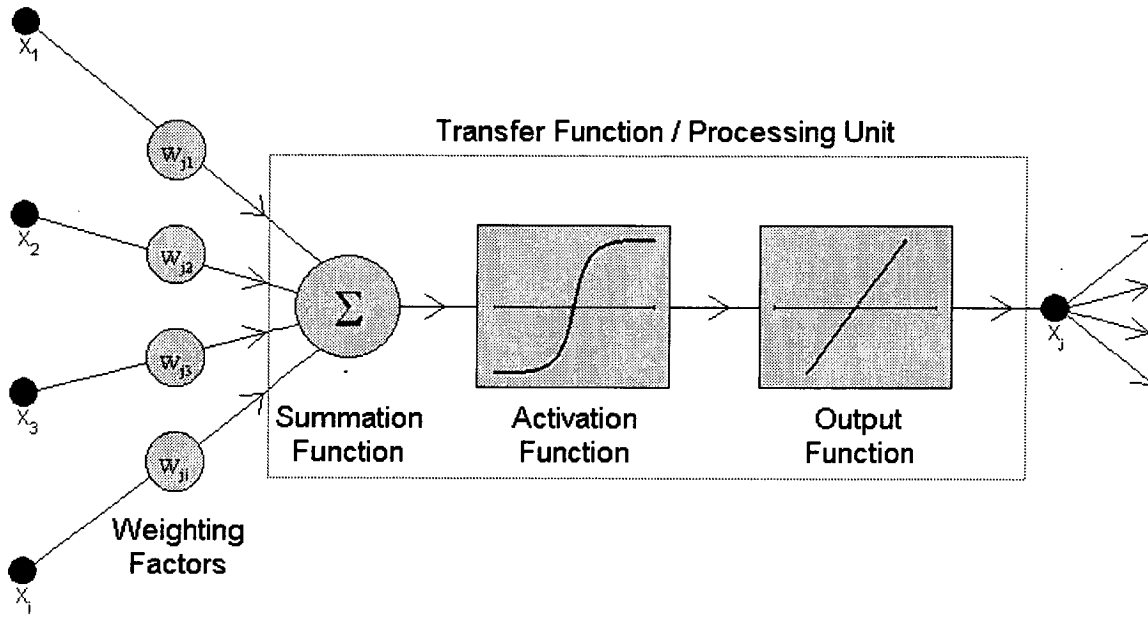

Figure 2.69: Structure of an artificial neuron

2.6.2.1. Weighting Factors

It is necessary to make some inputs more important than others so that they will have a greater effect on the response of the neuron. The use of weighting factors accomplishes

this by assigning each input with its own relative weight, giving it the required impact during the summation function.

Weighting factors are adaptive coefficients that determine the intensity of the input signals, the strengths of which are modified as the neuron 'learns' its role in the neural network.

2.6.2.2. Summation Function

The role of the summation function is to gather the weighted input data and turn it into a useful, single value. The most common method is the additive function, which obtains the summation result for the neuron by multiplying the proceeding neuron outputs with their individual weights and summing the result. For the neuron above, the result is:

$$net_j = \sum_i x_i w_{ji}$$

where: i = input neuron number in input layer i
j = neuron number in layer j
net_j = summation function result for neuron j
x_i = output from neuron i
w_{ji} = weighting factor of x_i to neuron j in layer j

Eqn 2.12

However, input and weighting factors can be combined in a number of different ways before passing the result on to the activation function, other than this simple product summing operation. Summation functions can include minimum and maximum operations as well as majority, product and normalising algorithms. The choice of defining which method to use depends on the network architecture and operating paradigm.

2.6.2.3. Activation Function

Once the result of the summation function is calculated, the single values, net_j, is passed on to the activation function, with the aim of comparing it with some threshold value and sending the result to the output function.

The transfer function could be something as simple as comparing net_j to a threshold value and generating an output signal if it is larger, and another if it is smaller. In such a case the output of the transfer function could be 0 or 1, 1 or –1, or some other numeric combination which produces a step function. Other functions used include ramping functions, logistic functions and hyperbolic tangent functions, all of which are shown in Figure 2.70.

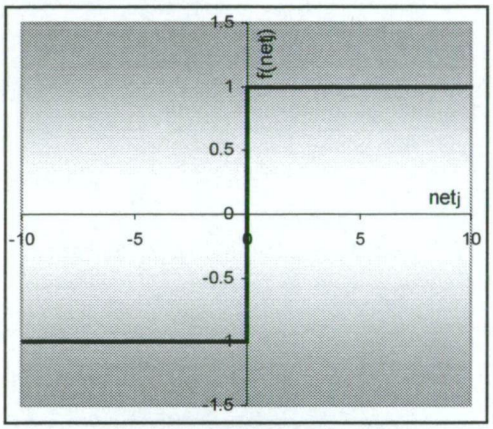

Step Function

$net_j > 0$, $f(net_j) = -1$

$net_j \geq 0$, $f(net_j) = 1$

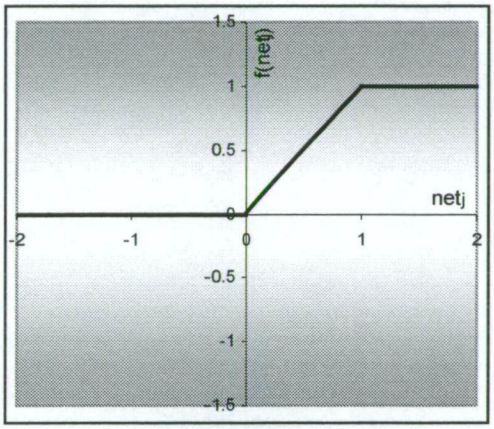

Ramping Function

$net_j < 0$, $f(net_j) = 0$

$0 \leq net_j \leq 1$, $f(net_j) = net_j$

$net_j > 1$, $f(net_j) = 1$

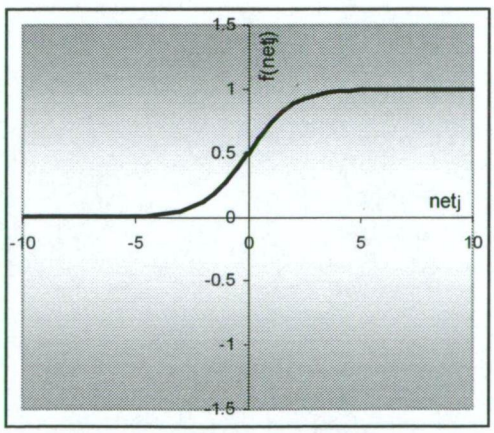

Logistic (Sigmoid) Function

$f(net_j) = 1/(1+e^{-net_j})$

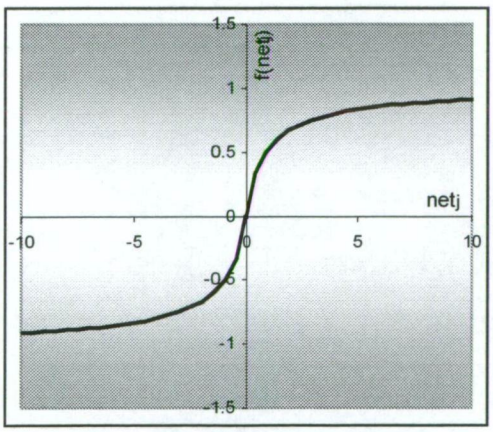

Hyperbolic Tangent Function

$net_j \geq 0$, $f(net_j) = 1 - 1/(1-net_j)$

$net_j \leq 0$, $f(net_j) = -(1 - 1/(1-net_j))$

Figure 2.70: Common activation functions [70]

Of these functions, the sigmoid function is the most common since it offers both a continuous curve and a derivative that is always positive, has a bounded range and can be easily computed.

2.6.2.4. Output Function

In most cases the output function simply outputs the value passed to it by the activation function to the surrounding neurons. However, in some models the output function is utilised to enable competition between neighbouring neurons, inhibiting output signals from other neuron unless they have great strength. This can then be used to determine which subsequent neurones in the network will be active and provides an output as well as determining which neurons will participate in the learning process of the ANN.

2.6.3. Artificial Neural Network Characteristics

An artificial neural network is produced by interconnecting the primitive functions performed by the artificial neurons in a specific manner, and adjusting each input weight to enable pattern recognition. The required weights for each ANN are trained into its structure, rather than programmed, allowing process modelling of systems that the programmer may not fully understand, nor be able to model mathematically. By doing so, they inherently associate items that they are taught, physically grouping similar items together within their structure. This enables the ANN to operate with incomplete, noisy or partially incorrect data, generalise results when presented with problems similar to its training and act at slowly degrading performance levels during system failure, but also comes at the cost of accuracy – with most ANNs being only approximately 90% accurate.

ANNs are often seen as a 'black box' with *n*-dimensional real inputs (x_1, x_2, ..., x_n) mapping to *m*-dimensional real outputs (y_1, y_2, ..., y_m). While it is desired that a certain input produces a particular output, how the network achieves the particular output is left to a self organising process. The accuracy with which is does this, though, depends on the structure of the network including:

- Network properties
  - network topology
  - types of connections
  - number of connections
  - weight range
- Neuron properties
  - summation function
  - activation function
  - output function
- System learning dynamics
  - weight initialisation scheme
  - activation error calculation formula
  - learning rule

Particularly, it is the arrangement of the neurons and their connections that define the network architecture. Neurons are usually arranged into layers – with neurons in each layer grouped together because they behave in a similar manner (defined by their activation function and pattern of weighted connections). This ensures that the way neurons send and receive data within each layer is the same.

Although there are useful networks that contain only one layer, or even one neuron, most applications require networks that contain at least three types of layers – input, hidden and output. The role of the input layer is to simply pass forward the presented input pattern to the neurons in the subsequent layer. It generally performs no computation on the data presented to it and is there simply to collect data from the outside world. Following the input layer are the hidden layers. There can be any number of hidden layers, although only one or two are normal, which perform the bulk of the ANN internal processing. The output layer neurons then correlate all of the data sent from the other neurons and send the result through the ANN output channels [39, 40].

2.6.3.1. Feedforward ANN

ANN structures can be broken down into two types – feedforward and recurrent. The structure of a feedforward is shown in Figure 2.71. Neurons in each layer only receive signals from the layer directly before it, forcing data flow in one direction – from the input layer, to the hidden layers and finally to the output layer [71].

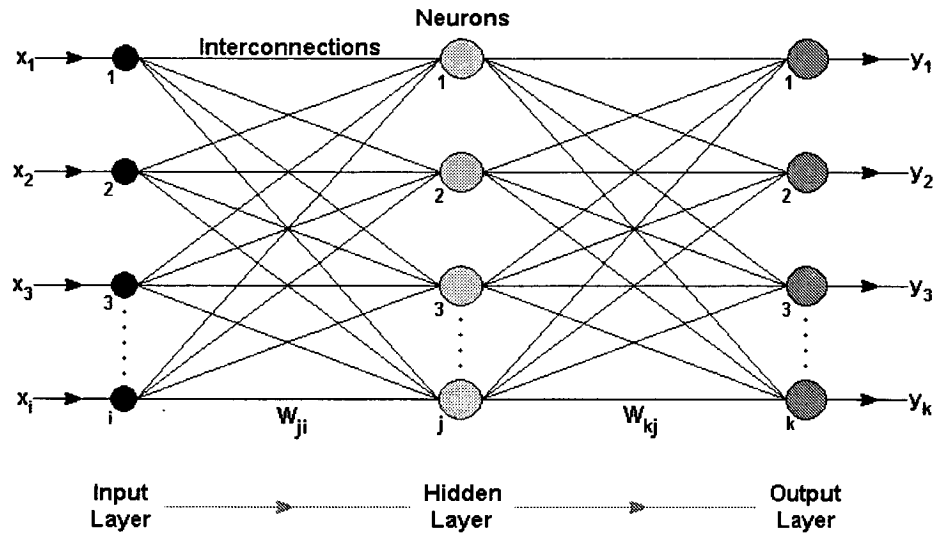

Figure 2.71: Basic structure of a multi-layer feedforward ANN [40]

2.6.3.2. Recurrent ANN

Recurrent networks do not follow the strict requirement of one-way information flow, incorporating at least one feedback loop. By feeding signals though a loop within the network, as shown in Figure 2.72, the ANN can exhibit dynamic behaviour by evolving from its initial state over time.

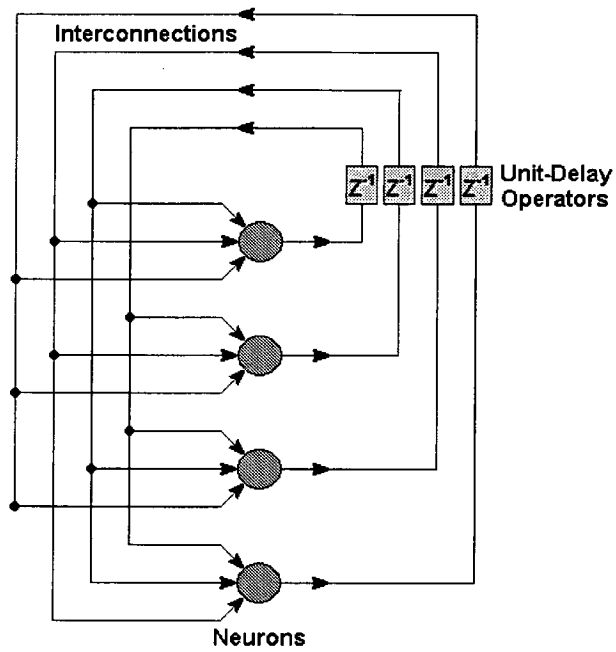

Figure 2.72: Recurrent ANN feedback loop [40]

2.6.3.3. Supervised Training

To successfully model a system, the correct weighting factors of each neuron in the ANN must be determined. This can be done using supervised or unsuppressed training. Supervised training provides the ANN with a set of input data and a set of corresponding output data. The network processes the inputs and compares its resulting outputs with the outputs provided in the training set, and then alters the individual neuron weighting factors to try and minimise the error. This process is repeated iteratively until the output error converges to the maximum accuracy obtainable with the training set and network architecture.

The ANN can also be trained under supervision using reinforcement learning. In this situation output values are not supplied, the network receives information only on whether or not its output is correct. However, this feedback is only evaluative and gives no hint of what the right answer should be, and thus can be very time consuming to train [39, 40].

2.6.3.4. Unsuppressed Training

Unsuppressed training uses a training set that contains only data inputs. The system must then decide how it will group the input data, so that similar inputs produce similar outputs. The input data is correlated into a number of different categories and then used to produces an output signal that corresponds to the input category. This means that the network must discover for itself any possibly existing patterns, regularities or separating properties within the input data and use it to discover the output, with no feedback as to whether or not it is correct [39, 40].

2.6.4. Network Training and Performance

An ANN can implement any transform between its inputs and outputs by varying the weighting factors at each neuron interconnection. The purpose of network training is to assign each of these weights with a unique real number to enable the network to perform the transform that yields the required outputs with maximum accuracy. This means that every ANN must be programmed with different weights for different applications, and, because it is impossible to compute the weights directly, the network must be 'trained'. This involves presenting the network with a set of data from the system it is to model, which it then uses to assign its own values to the weighting factors. The way it does this depends on the network type (feedforward or recurrent), the training set (supervised or unsuppressed) and the 'learning rules' it uses, but is always a repetitive and iterative processes that can be very time-consuming.

In order to receive optimum performance and a reasonable learning rate from the ANN there are a number of factors that need to be considered. The learning rules used can have a great effect in training time. The training data must offer an adequate representation of the system to be modelled by the network, as well as being presented to the network in a particular way. Network architecture is also an important consideration. The number of hidden layers, the number of neurons within them and the way they are interconnected greatly effects network performance [39, 40, 41].

2.6.4.1. Training Sets

It is important that training data sufficiently represents all aspects of the system. There are normally several input subgroups within the dynamics of a system that have their own tendency towards a particular output pattern. The dynamics of each subgroup must be adequately represented to the within the training set to enable ANN training of the complete system. Each subgroup must also contain enough data within it to include the effects of statistical variation of the data.

The general rule for the number of training patterns that need to be supplied is given by:

$$P = \frac{W}{e}$$

where: P = number or training patterns required
W = number of different weighting factors within the ANN
e = desired ANN accuracy classification

Eqn 2.13

In most cases the accuracy classification is chosen to be e = 0.1, meaning that the training data requires 10 times the number of training patterns than the number of weighting factors of the ANN.

It is also important to ensure that the order in which each subgroup is presented to the system is spread out. If the network is trained with just one example at a time, the weights set meticulously for one fact could by drastically altered in the learning of another. In short, it may forget things that it had previously learnt in learning something new. The training set should ensure that the ANN learns everything together so it assigns weights that suit the entire system.

2.6.4.2. Normalising Data

In addition to ensuring that the training data is sufficiently represented, network performance can usually be improved by normalising the training data, bounding all of the values between 0 and 1. The normalising function is given below in Eqn 2.14.

$$norm(x_i) = \frac{x_i - \min(X_j)}{\max(X_j) - \min(X_j)}$$

where: x_i = the *i*th value in a set of *j* values

X_j = the set of *j* values

norm (x_j) = normalised value for x_i

min (X_j) = original minimum value in the set of *j* values

max (X_j) = original maximum value in the set of *j* values

Eqn 2.14

This ensures that the network is not biased towards inputs that are of a higher magnitude than others in the training set and also helps remove insignificant characteristics within the data, such as the value of offsets and standard deviations.

Normalising the output is also an important step towards improving network performance, since most training algorithms attempt to minimise the total error of the outputs. Using data that is not normalised will cause the network to train the output with the largest magnitude (and thus statistically the largest error) to be as accurate as possible, to the exclusion of the accuracy of other, smaller, outputs.

2.6.4.3. Network Testing

Once a supervised network has been trained, with the weights adjusted to produce the most accurate outputs from the training data as the network permits, it is important to see how it performs with data it has not seen before. The network could have made a number of generalisations based on the test data that are not supported in reality. It is therefore important to gather a set of test data to be run through the ANN so that a comparison can be made between the desired output and the actual output. If the network cannot produce the desired accuracy it may have to be redesigned or the training set may need to be broadened.

2.6.4.4. Network Performance

There are a number of ways that an ANN can be improved. For feedforward neural networks these include changing the number of hidden layers within it, changing the number of hidden layer neurons and removing input neurons that provide repetitive or unimportant data.

In practice feedforward ANNs rarely require more than one hidden layer, but a second can be added for complex functions, and functions that contain discontinuities. It should be noted, however, that a second layer can potentially dramatically increase training times, make the network more unstable and introduce false minima into the training algorithm, into which it can get stuck. Generally, when training a network, it is recommended to use only one hidden layer - resorting to a second layer only if the network cannot perform as needed.

Before resorting to the second layer it is useful to experiment with the number of hidden neurons within the first. The goal is to select the least number of neurons that can be used without increasing the associated network error. It is important to choose the right amount - too few neurons will starve to network of the resources it needs, while too many will increase the training time and could cause overfitting. Overfitting can be a particular problem because it causes the network to memorise the test data, rather than generalise it, as shown below in Figure 2.73. In this case, the graph on the left shows a good generalised fit to the somewhat noisy training data, while the graph on the right has created a curve that fits all of the training data very well but does not reflect the true data relationship.

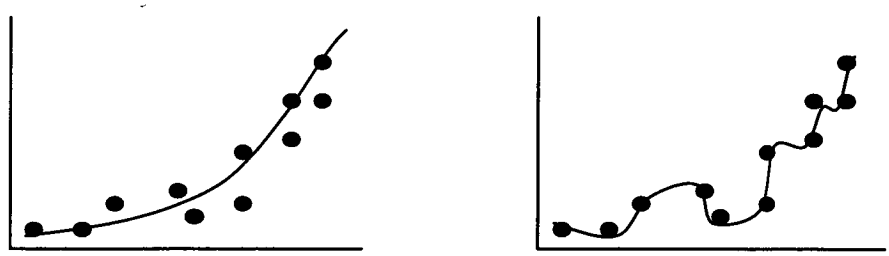

A good, generalised, fit to noisy data

Overfitting of the same data

Figure 2.73: Effect of overfitting [40]

The number of input layer neurons can also effect the accuracy of the network. The addition of input parameters that have little or no influence on the system outputs can significantly increase the network error. It is therefore important to identify the minimum number of inputs required to successfully model the system for optimum performance [40, 41].

To this end, input parameters can be graded in terms of their contribution to the model, and excluded if they are seen to have little or no effect. In this manner, the ANN itself can be used to decided which parameters require measuring to identify the data trends – providing an effective tool for data input decisions based on importance / cost.

2.6.5. Applications to Vehicle Control

Artificial neural networks have proven themselves as useful tools in a number of areas. Their ability to recognise complex patterns makes them especially powerful in [39]:

- Prediction
- Classification
- Data association
- Data conceptualisation
- Data filtering

As such, they are finding their place in numerous fields, including:

- Language processing
- Character recognition
- Image (data) compression
- Pattern recognition
- Signal processing
- Financial
- Systems control

While ANN applications expand into other areas, its use in controlling complicated system is one of the more promising areas of neural networks [39]. Recognition of this has spawned numerous attempts to use ANNs to model many facets of automotive control. Of particular interest has been the use of neural networks in engine control, including emissions prediction [43] and fuel injection control [44]. However, with this focus, there has been little published research into the use of neural networks in vehicle dynamic control.

This lack of research could be from applicable companies guarding their findings closely, but may also be because of the perceived difficulties in providing an ANN that can operate within acceptable error limits. It should be noted, also, that collection and correlation of the required data for ANN training can be a very expensive and time-consuming process, further restricting investigation.

2.6.5.1. Lane Changing

Because of these complications, much of the research previously conducted was done using ANNs to predict or control the operation of simplified computer models of various aspects of the vehicle dynamics. In 1987 Shepanski et al [45] introduced a model called "an automobile autopilot" based on a highly simplified computer simulation of traffic conditions. In this model it was assumed that when travelling on a wide shouldered two-lane freeway other vehicles would perform various pre-programmed manoeuvres, without consideration for the ANN controlled vehicle other than to avoid running into its rear end once passed. The model sort to decide on when the ANN driven vehicle should change lanes and then adjust vehicle speed and heading to perform the required manoeuvre based on the parameters below in Figure 2.74.

Two ANNs were then trained through back propagation to control the vehicle based on measured data during lane changes. A steering angle network was designed purely to keep the car within the lane it was travelling in, while another network was used to decide when to change lanes and to control vehicle speed, as shown in Figure 2.75.

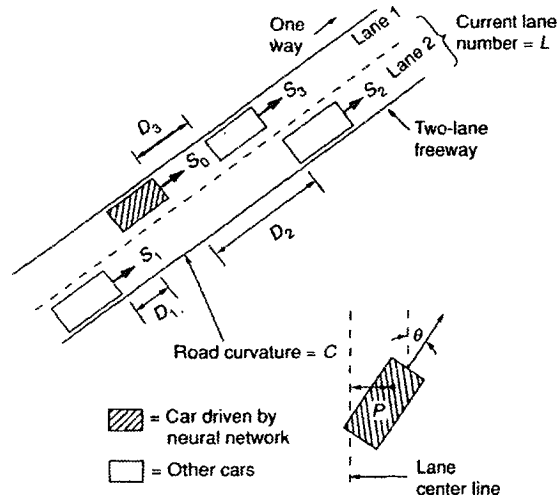

Where: D_1 = Distance from rear of the NN driven car to the front of the nearest car in the opposite lane and next to or behind it.

D_2 = Distance from front of the NN driven car to the rear of the nearest car in the opposite lane and in front of it.

D_3 = Distance from the front of the NN driven car to the rear of the nearest car in the same lane and in front of it.

S_0 = Speed of NN driven car.

S_1 = Speed of car in the opposite lane and next to or behind the NN driven car.

S_2 = Speed of car in the opposite lane and in front of the NN driven car.

S_3 = Speed of car in the same lane and in front of the NN driven car.

θ = Angle between the longitudinal axis of the NN driven car and the lane in which it is driving.

P = Distance laterally between the NN driven car centreline and the centreline of the lane it is travelling in.

L = Lane number the NN vehicle is travelling in (1 or 2)

C = Curvature of the road where the NN driven car is travelling.

Figure 2.74: ANN lane changing [45]

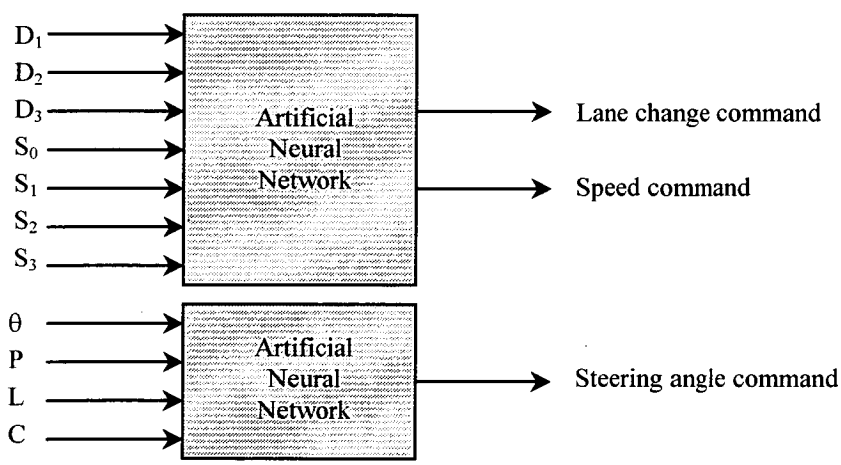

Figure 2.75: ANN models for vehicle control [45]

The networks demonstrated that, while the control model must operate within specific limits, it could provide intelligent control of the vehicle. It also showed that the driving style for the driver during the training stage was reflected in the control algorithm of the ANN.

2.6.5.2. Crisis Handling

Resent research conducted in 1999 by Jayakumar et al [46] chose to further investigate the use of ANNs in vehicle control. In this case the focus was on correcting driver mistakes when a crisis situation arises by overriding driver inputs and controlling throttle position, brake pedal position and steering angle in an effort to prevent road departures.

Again, the study used a simplified computer simulation of the vehicle dynamics to both train and test the control ANN. Training data sets from successfully corrected manually driven crisis scenarios within the computer simulation were then used to program the neural network. Interventions were then invoked with the sufficiently programmed ANN controller according to the driving conditions and driver inadequacies, such as a delay in human response or inappropriate control input. The study showed reasonable results but was, however, limited to a travel speed of only 20km/hr and simple curvature types to avoid tyre slip problems and other complex effects.

This section illustrates that ANNs have a number of performance benefits that show a potential in vehicle control methods. The abilities of neural networks to be trained, rather than programmed, were shown to provide an opportunity to model complex systems that would otherwise be extremely hard to model using conventional techniques. They have also been shown to provide model solutions with minimal computation, while also providing reasonable result accuracy as sensory inputs fail. Previous research has been shown to attempt to apply these benefits to various automotive applications to varying levels of ability. However, is seems that there is still a wide gap to fill between ANN models that can control simplified examples and models that can be used to control real life vehicle scenarios.

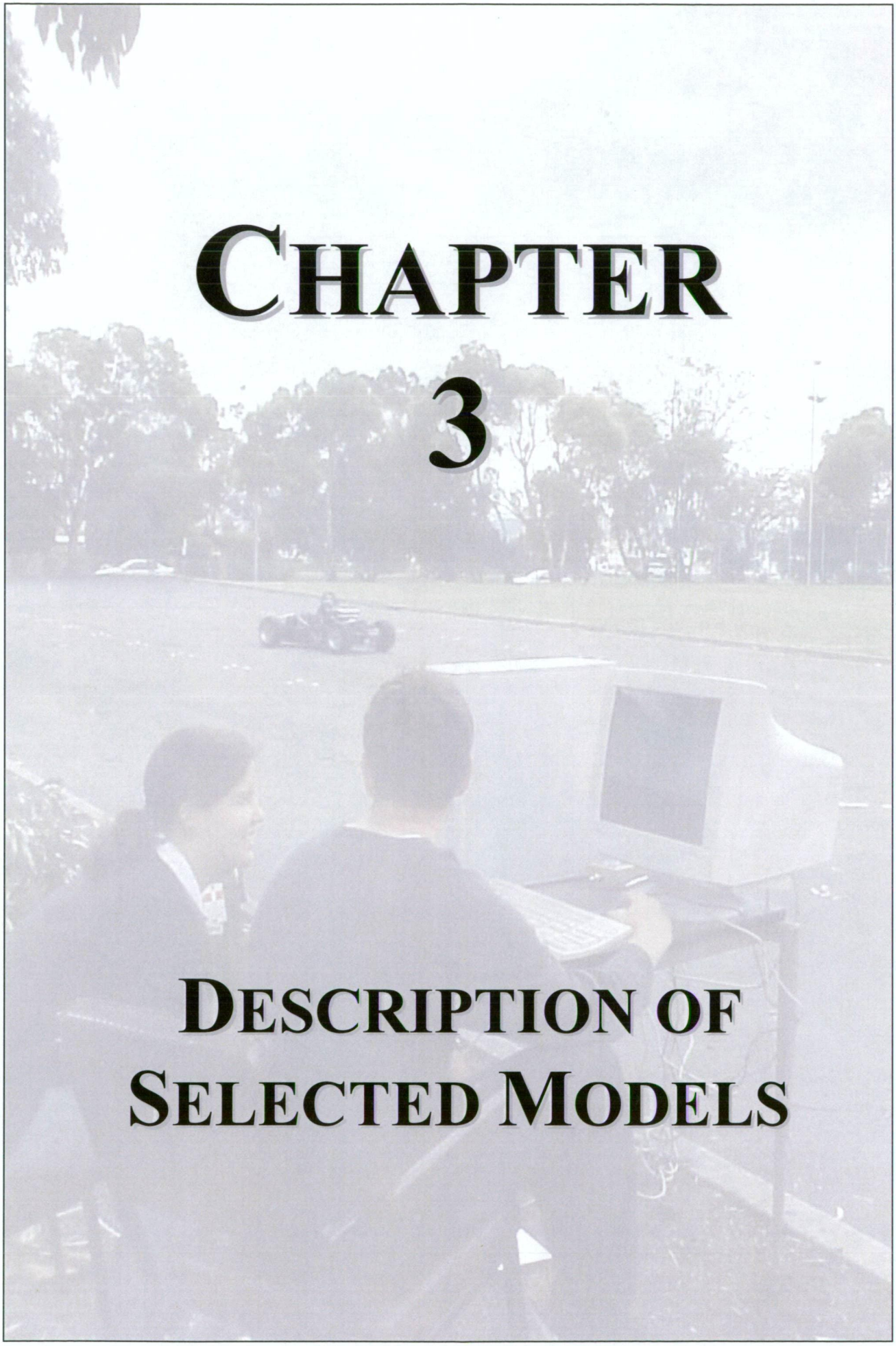

CHAPTER 3

DESCRIPTION OF SELECTED MODELS

There are numerous different artificial neural network models currently in use in wide ranging applications. In addition, new models are constantly under development. The choice as to which models will provide the best simulation of data depends on factors such as the network application, the desired computation / accuracy balance and the size and quality of the input data patterns. Furthermore, there is no exact way to chose the network model or its architecture, and so choice of the optimum network comes down to a trial and error procedure as different arrangements are tested. However, most models show ability in one or two specific areas, and so individual models can be selected or discarded based on selection criteria defined by the desired model properties. Some models may perform well with noisy data, others may have improved non-linear function prediction characteristics.

This chapter will discuss two such ANNs that have previously shown reliable results for complex system prediction in research conducted at the University of Tasmania and will be used in network development within this study. The two network models are backpropagation networks and general regression neural networks.

3.1. Backpropagation Networks

Feedforward, backpropagation (BP) ANNs were first developed in the early 1970's by several independent sources, and have since become the most widely used of the neural network paradigms. They are of particular use within the manufacturing domain for applications such as scheduling, monitoring, diagnosis and quality control because they provide effective and easy to use models for complex, non-linear, ill-defined systems.

Because they are feedforward networks, they are structured as shown in Figure 2.71. The input layer passes information to the hidden layer without performing any form of mathematical operation. The hidden and output layers then perform all of the network processing, before passing the final results through the output neurons. Information flow is always in one direction during normal operation. Backpropagation refers to the training method.

The backpropagation training procedure operates in two stages. The first presents the training inputs to the network, which then calculates the predicted outputs using its feedforward architecture and compares the result to the training outputs. The second uses the resultant error to modify the neuron interconnection weights by generating a flow of information from the output layer towards the input layer. The interconnection weights between the output and adjacent hidden layer are modified first, and then used to calculate the error value at the hidden layer. This error value is then used to adjust its interconnection weights with the layer above it, and so on until the input layer is reached.

Considering the most common neuron architecture used in backpropagation networks of:

$$Summation\ Function = net_j = \sum_i x_i w_{ji}$$

$$Sigmoid\ Activation\ Function = f(net_j) = \frac{1}{1+e^{(-net_j)}}$$

$$Output\ Function = Activation\ Function\ Result$$

Since the output function performs no mathematical operation within each neuron, the error values for the output layer neurons are given by:

$$\delta_k = (t_k - a_k) \cdot f'(net_k)$$

where: δ_k = error value for neuron *k*

t_k = target training value for neuron *k*

a_k = output value of neuron *k*

Eqn 3.1

With the sigmoid function derivative given by:

$$f'(net_j) = f(net_j) \cdot [1 - f(net_j)]$$

Eqn 3.2

Which has the form shown in Figure 3.1 below:

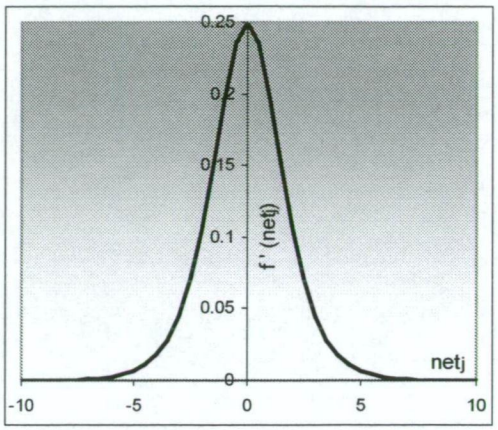

Figure 3.1: Logistic (sigmoid) function derivative [67]

These properties of the derivative provide advantageous tools for assessing error within the neuron. It can be seen that the total error between the predicted and training outputs is scaled by the derivative of the activation function. This scales the error term to be large when the summation result is close to zero, and small when the summation result has a large magnitude.

Since the hidden layer neurons have numerous, differently weighted, interconnections with the layers directly above and below them (as shown in Figure 3.2), their error values must incorporate this.

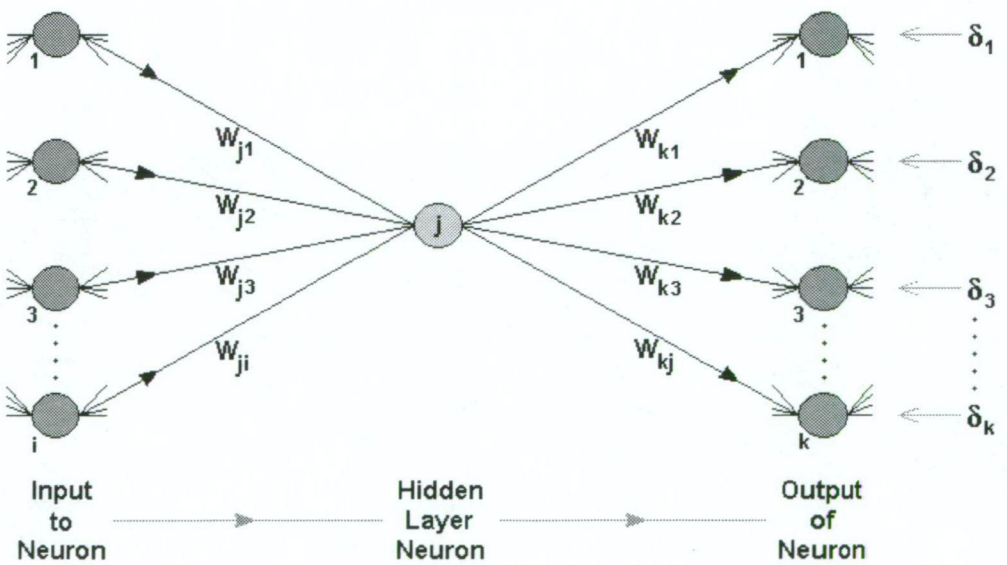

Figure 3.2: Interconnections for neuron j in the hidden layer

The error values for the hidden layer neurons are given by:

$$\delta_j = \left[\sum_k \delta_k W_{kj}\right] \cdot f'(net_j)$$

where: W_{kj} = interconnection weight to neuron k from neuron j

Eqn 3.3

The weight adjustments for the network interconnections can be calculated from these error values. Each interconnection weight is adjusted by considering the error value of the neuron that receives input from the interconnection, as shown below.

$$\Delta W_{ji} = \eta \cdot \delta_j \cdot a_i$$

where: ΔW_{ji} = weight adjustment

η = learning rate, $0<\eta<1$

Eqn 3.4

It can be seen that large error values and large output values result in a large adjustment to the interconnection weights, which is scaled with respect to the learning rate. Large adjustments can make the network learn faster but can lead to instability, while small adjustments can dramatically increase learning time but avoids instability. The value of η can be altered to scale the weight adjustment to achieve a compromise throughout the learning period.

In some cases, it may improve learning time and accuracy to vary the learning rate as the network trains itself. A popular way of doing this is by introducing a momentum term, which reduces oscillations in weight changes and improves convergence. In this case, the weight adjustment for each neuron is modified by an amount proportional to the weight adjustment from its previous iteration, as shown below.

$$\Delta W_{ji}^{\ h} = \eta \cdot \delta_j \cdot a_i + \alpha \cdot \Delta W_{ji}^{\ h-1}$$

where: α = momentum constant, $0<\alpha<1$

$\Delta W_{ji}^{\ h}$ = weight adjustment at iteration *h*

$\Delta W_{ji}^{\ h-1}$ = weight adjustment on previous iteration

Eqn 3.5

The resultant accuracy and training time of the network depends on the choice of η and α, as well as the initial values of the interconnection weights. If all of the interconnection weights are chosen to be the same value, the network will have problems during training because all of the output values will be identical to each other, resulting in weight changes within the network that are of equal magnitude. The network weights will never differ in this case. Thus, it is important to introduce a random element into the weight selection. To this end, a common procedure is to initialise weights with random values within a specified interval of -0.5 to 0.5 or of -1 to 1. This enables the network to assign a wide variety of weights to the neuron interconnects throughout the training procedure, allowing it to explore a number of possibilities within its structure and hopefully develop the most accurate one.

Once trained, the success of the network in learning its training data and simulating its test data can be quantitatively determined using its RMS error. This provides a useful measure of how well the network is predicting its target outputs, with a value of less than 10% generally indicating that the network has sufficiently learned its training set. The RMS error equation is shown below.

$$RMS\ error = \sqrt{\frac{\sum_p \sum_k (t_{kp} - a_{kp})^2}{n_p \cdot n_k}}$$

where: t_{kp} = target output of output neuron k after presentation of training data pattern p

a_{kp} = actual output value of output neuron k after presentation of training data pattern p

n_p = number of training data patterns

n_k = number of neurons in output layer

Eqn 3.6

3.2. General Regression Neural Networks

General regression neural networks (GRNN) were first developed in 1990 as memory based feedforward networks. They work as a function approximator system, and are useful for estimating values of continuous functions such as future position, future values and multi-variable interpolation, as well as performing well with noisy data. Nonetheless, the primary advantage of GRNNs is the speed at which the network can be trained. This is because the training of a GRNN is performed with one pass of the training data through the network, with the training data values copied to become the weight factors between layers, as specified by Frost et al. [40].

These advantages of fast training times, the ability to map both linear and non-linear data and the fact that overtraining is made less likely by the use of the smoothing parameter as the only adjustable variable, make GRNNs particularly useful in prediction, modelling, mapping, interpolation and as a controller for non-linear processes. This comes at a cost, however, since GRNNs demand many training samples to adequately span the variations in the data, and also require that all of the training samples be stored for future use. They also have trouble with irrelevant inputs and there is no intuitive method for selecting the optimal smoothing parameter

A basic GRNN, as shown in Figure 3.3, has four layers; the input layer, the pattern layer, the summation layer and the output layer, with *i* input neurons, *j* pattern neurons, *k+1* summation neurons and *k* output neurons. It also has weighted interconnections, w_{ji}, between the input and pattern layer and weighted interconnections, A_I & B_{si}, between the pattern and summation layers, where A and B refer to function numerator and denominator neuron inputs respectively.

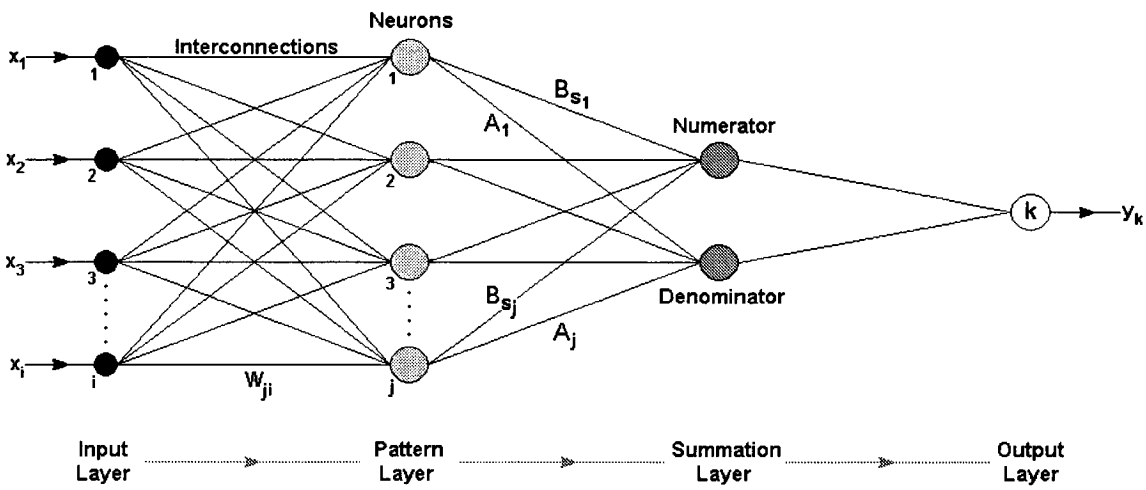

Figure 3.3: GRNN architecture

Again, the function of the input layer is to simply pass forward the input vector, and so the number of input neurons equals the number of input parameters. The neurons in the pattern layer then perform a non-linear transformation to the weighted values supplied by the input neurons. When a new vector, X, is entered into the network, it is subtracted from the stored weight vector representing each activity pattern. Either the squares or the absolute values of the differences are then summed and fed into the pattern layer activation functions, given below:

$$f(net_i) = e^{\left(\frac{-net_i}{\sigma}\right)}$$

where: net_i = sum of differences between input and weight vector pattern layer neuron *i*

$f(net_i)$ = output from pattern layer neuron *i*

σ = smoothing factor

Eqn 3.7

The resulting values within the pattern layer are then passed to the summation layer neurons. For a single output network, the summation layer consists of a denominator neuron and a numerator neuron, then for each additional network output another numerator neuron is added. Hence, the summation layer consists of a single denominator neuron and *n* numerator neurons, where *n* is the number of output neurons. The summation layer neurons perform a dot product between a weight vector and a vector composed of the pattern neuron signals.

For the denominator summation neuron, the weight vector is unity, so a simple sum is performed, as shown below:

$$den_{out} = \sum_j f(net_j) \cdot A_j$$

where: den_{out} = output from denominator summation neuron

A_j = interconnection weight between denominator neuron and all pattern layer neurons (= 1 for all A_j)

For the numerator summation neuron, its interconnection weight to each pattern layer neuron is equal to the value of the dependent variable for the training case of that pattern layer neuron. Hence, the numerator summation neuron performs a computation represented by the following equation:

$$num_{outs} = \sum_{j} f(net_j) \cdot B_{sj}$$

where: num_{outs}= output from numerator summation neuron s

B_{sj} = interconnection weight between numerator neuron s and all pattern layer neurons

Eqn 3.8

The outputs from the denominator summation neuron and all of the numerator summation neurons are then sent to the output layer neurons. The output neurons, again equal in number to the number of output parameters, then perform a division function between the output of their associated numerator summation neuron and the output of the denominator neuron.

Network training can then take place by assigning the values below and calculating the network error. These assigned values include:

- a smoothing parameter,σ, value
- pattern layer weights, w_{ji}, equal to the values of the independent variable in the training data set
- pattern to summation layer denominator weights, A_j, to one
- pattern to summation layer numerator weights, B_{sj}, equal to the values of the dependent variables in the training set

The performance of the GRNN is critically based on the optimisation of the smoothing parameter, σ, and so it is important to repeat the training process until a value of σ is found that produces the lowest error possible.

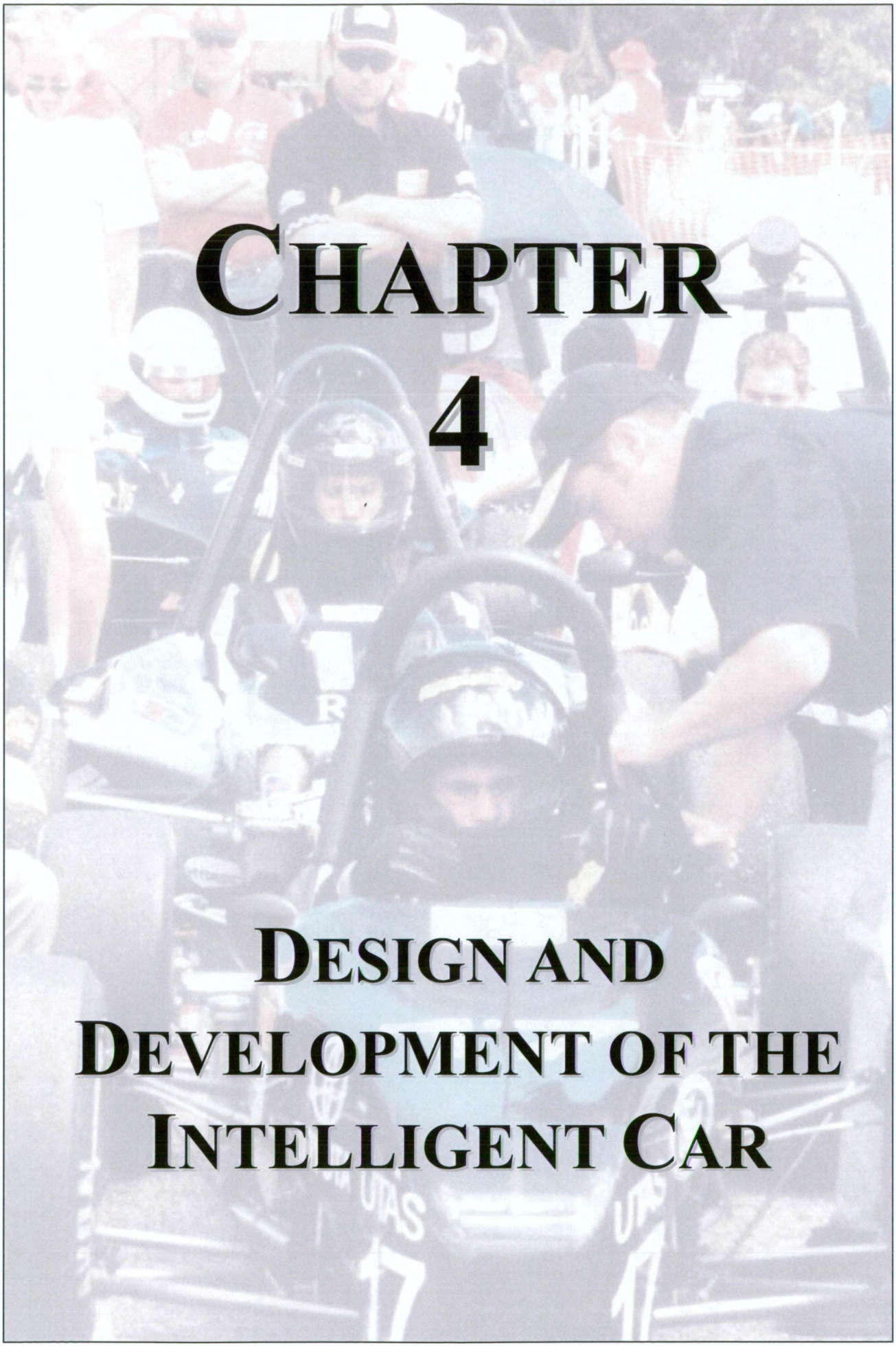

CHAPTER 4

DESIGN AND DEVELOPMENT OF THE INTELLIGENT CAR

A Formula SAE® (F-SAE) racecar was selected as the test vehicle for use in this project, photographed below in Figure 4.1. This international competition allows engineering students to conceive, design, fabricate and compete in small formula-style racing cars against other institutions under specific regulations [47]. The decision was made in favour of this type of vehicle because it presented the research team with a practical understanding of the complexities of automotive design and manufacture, enabled a greater pursuit of financial support and provided additional study opportunities for undergraduate students. Also, because the vehicle had to be completely designed and built by the research team, this choice permitted a design that placed the various sensors required for this study in their respective optimum positions.

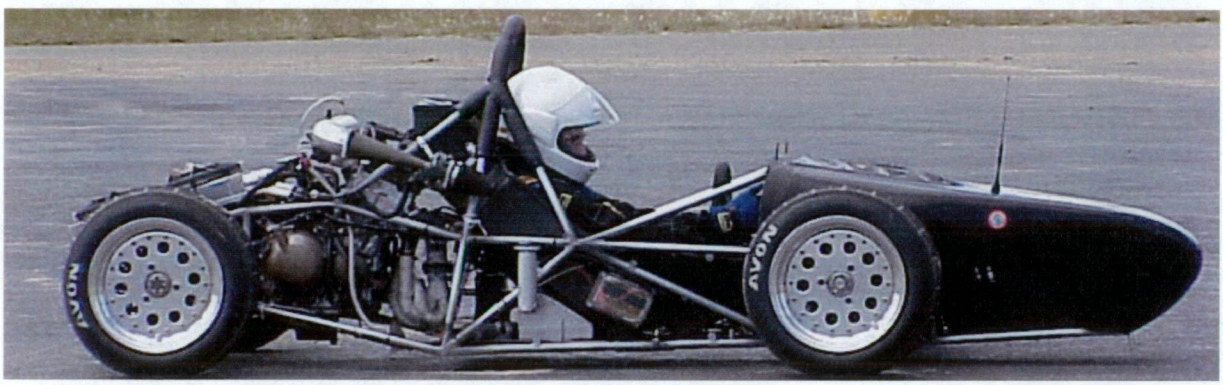

Figure 4.1: The F-SAE test vehicle

4.1. Design Considerations

The handling performance of any type of vehicle is influenced by an astoundingly large number of factors, which all must be considered during the design stage. Which parameters effect the vehicle the most depends to a great extent on vehicle type, but generally include:

- Weight distribution, centre of gravity and moments of inertia
- Wheelbase and track width
- Suspension and steering geometries
- Tyre choice and condition

- Available braking force
- Driver ergonomics
- Power delivery to the driven wheels

These factors had to be carefully considered and balanced in the design process, along with the design restrictions imposed by the F-SAE rules, to produce a vehicle that exhibited handling characteristics consistent with the racing category, shown in Figure 4.2. This lead to the identification of the design requirements as specified below.

F-SAE Rule Based Requirements:

- Open wheel and open cockpit type vehicle
- Wheel base of at least 1500mm
- Inclusion of front and rear suspension
- Engine size limit of 610cc
- Single seat design (no passengers)
- Front and rear roll over hoop positioning, dimensions and supports
- Side impact protection bar inclusions
- Bulkhead dimensions
- Crush zone dimensions
- Manufacturing materials (or demonstrated equivalence)

Performance Based Requirements:

- Must be as light as possible, while maintaining a long lifetime
- Must be reasonably simple and cheap to construct
- Must strive to make the car as compact as possible
- Must be reasonably ergonomic
- Must encourage component positioning to provide a low centre of gravity, and an optimum weight distribution between the front and rear wheels
- Must provided ample stiffness through the frame to encourage superior handling
- Must have minimum unsprung weight while also providing sufficient braking power

- Must provide optimum tyre contact with the road for common and critical, driving manoeuvres through the suspension geometry and steering angles
- Must produce high power while maintaining drivability and traction

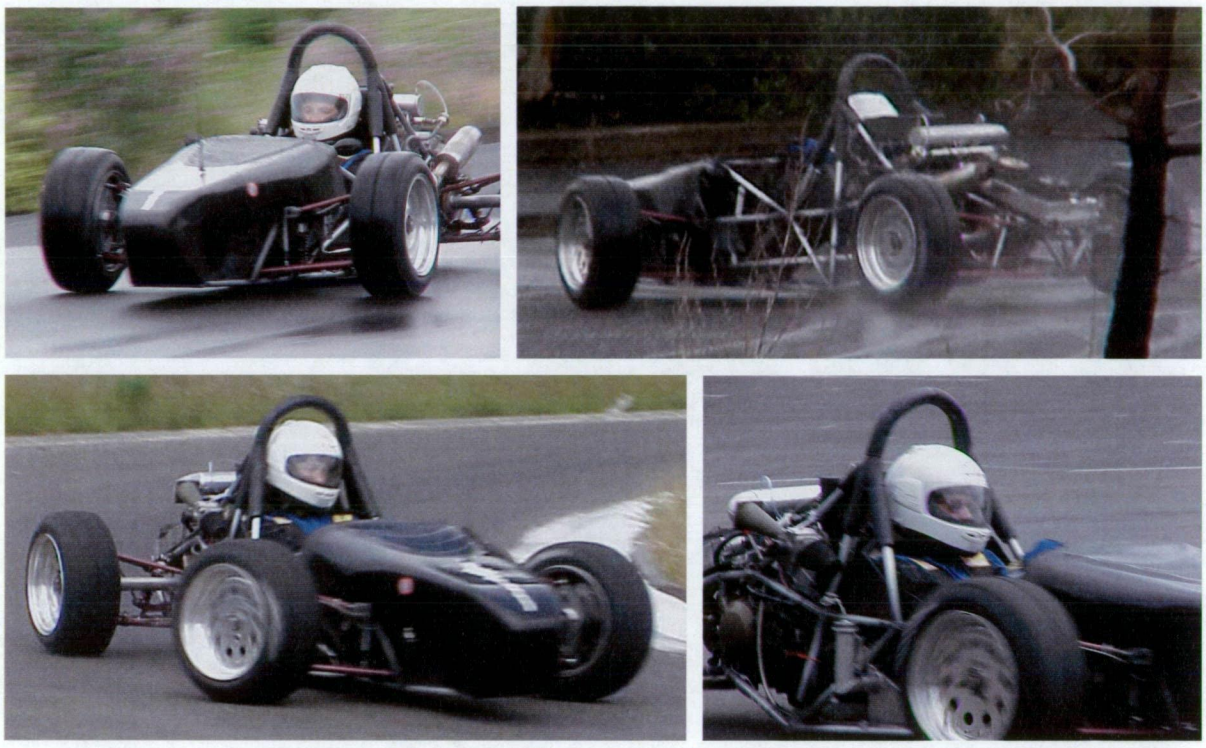

Figure 4.2: The F-SAE test vehicle during trials

Arguably the biggest factor in defining how well a vehicle will handle is how well the tyres grip to the road. The size and shape of the tyre contact patches as well as wheel loadings are important considerations, and while the contact patches are defined predominantly by the suspension and steering geometry, the wheel loadings are effected by the layout of the whole vehicle.

The weight distribution of a racecar refers predominantly to the wheel loading, with the static weight distribution defining the position of the centre of gravity in the horizontal plane. Of course, the weight distribution of a car is dynamic, acceleration in any direction, as well as any down-force experienced by the moving vehicle, will have an effect on the wheel loading. Thus, the position of the centre of gravity vertically has a large influence on the overall vehicle handling, as well as the weight transfer characteristics of the car dynamically. To

further complicate matters, the overall weight of the vehicle changes as the fuel load is burned and, if the fuel tank is not positioned at the centre of gravity, even the relative wheel static loadings can change.

Further consideration of the weight distribution of the vehicle shows that its moments of inertia can effect driving behaviour, particularly in yaw. Conceptually, this means that the driver of a vehicle with a high moment of inertia in yaw (with its main masses situated towards both ends of the chassis) will notice that it responds reluctantly to steering inputs. They will also notice that it is less likely to go into a spin during cornering manoeuvres, but will also be difficult to regain control of once spinning. Conversely, a vehicle with the main masses situated very near to its centre of gravity will have a low moment of inertia in yaw, and will respond quickly to steering inputs with 'twitchy' handling characteristics.

Because of the windy and slow nature of the F-SAE race track, the decision is normally made to make the polar moments of inertia as small as possible, by keeping as many of the components as close to the centre of the car as possible. This approach is also consistent with the desire to keep the car as compact and light as possible since wiring, plumbing and other connection lengths are minimised.

In the interest of these considerations the conventional F-SAE racecar layout places the driver in front of the mid-mounted engine, which sits just in front of the driven rear axle (Figure 4.3). A wheel base is also usually chosen to be in the vicinity of 1600 – 2000 mm to give a static weight distribution of between 40 / 60 and 55 / 45 (front / rear), depending on the desired handling characteristics. It also places all of the heavier components as low they can go without making contact with the road, in the interests of lowering the centre of gravity and minimising weight transfer under acceleration, braking and cornering. This leaves very little scope in the further placement of components in the interests of minimising the vehicle's moments of inertia further, other than to position the radiator, fuel tank and other moderately heavy components as close to the centre of gravity as possible. In practice however, other aspects of the general car design dictate its overall moment of inertia, resulting in the difference between a high moment of inertia and a low polar moment of inertia F-SAE car being very small. However, throughout the history of racing many credible drivers have

reported that they can "feel" small modifications to their cars which race engineers would say are immeasurable [48..56].

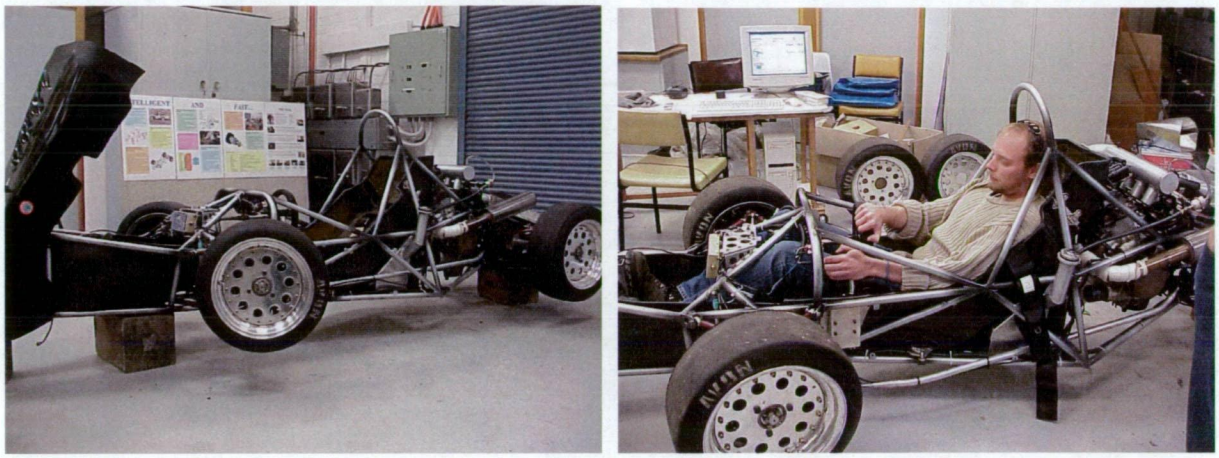

Figure 4.3: Mid-mounted engine layout of the F-SAE test vehicle with reclined driver position

4.2. Frame Development

The design of the frame, being the single largest component within the car, must consider every specification layed out within the rules, anticipate the requirements for the installation of each component and allow space for the addition of various sensors as they are called for. The overall design of the vehicle revolves around the shape of the frame (decided to be a tubular steel space frame of varying member diameters and wall thicknesses), and so its construction must consider all aspects of the intended design [53]. In the interests of high performance it is important to design to close tolerances, which entails strict identification of the various components available and their respective optimum positions, including the:

- Pedals
- Seat and harness
- Suspension wishbones, springs and pull rod pivots
- Steering components
- Gear changer mechanism

- Fuel Tank
- Engine and associated equipment
- Differential and drive shafts
- Radiator
- Bodywork
- Electrical equipment (engine management computer, data logger, etc)
- Assorted sensors

Upon the initial stages of the frame design it was evident that in order for the frame design to proceed, a general idea of what components were going to be used, and where they were going to be positioned was required. This mainly included the driver, suspension, drivetrain and engine positions, and initial designs centred on the respective positions of each of these. As the frame started to conceptually take shape, other components were included into the design to provide the close tolerances required and efficient load paths for minimum weight. This required the component selection process to proceed concurrently with the frame design, with the identification of appropriate parts often significantly altering the frame design

As such, many frame designs were made, and altered, to suit different component choices and positions, while also maintaining perceived structural integrity using the least members possible. As an aid to this process, an easily modifiable PVC piping mock frame was constructed, as shown in Figure 4.4. This enabled an iterative process that led to a stage where the correct parts could be ordered for later addition to the frame, and a frame design that met the spatial requirements of the overall vehicle design and component positioning.

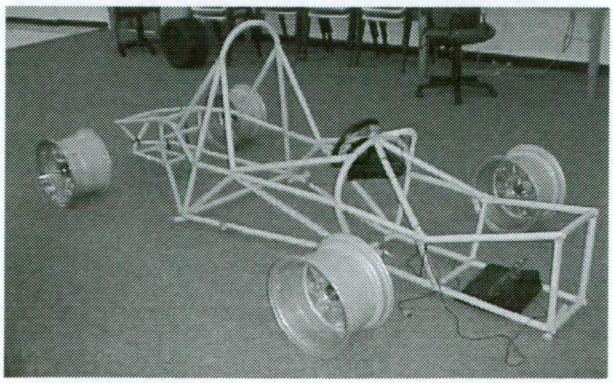

Figure 4.4: PVC mock frame

4.2.1. Finite Element Analysis

Once the frame was designed to meet the component positioning requirements, its structural integrity and load paths had to be tested in the interests of assessing its strength, rigidity and overall weight. Being a very complex system it was decided the easiest and most time effective way to do this was through finite element analysis (FEA). However, at this stage only a very vague idea of expected driving conditions was known. Vehicle mass and mass distribution were not known, either were the maximum accelerations from throttle, braking and cornering. Excessive values were assumed for these, that were not expected to be reached in even extreme driving conditions. This effectively introduced a safety factor into the modelling process, avoiding the need to apply it elsewhere. These values were:

Acceleration due to Throttle	$= 15ms^{-2}$	$= 1.5G$
Acceleration due to Braking	$= 3ms^{-2}$	$= 3G$
Acceleration due to Cornering	$= 2.5ms^{-2}$	$= 2.5G$
Acceleration due to Gravity	$= 10ms^{-2}$	$= 1G$
Vehicle Mass (wet, with driver)	= 360 kg	
Front / Rear Mass Distribution	= 49 / 51	

The model was then created in Strand7 [57], using only beam elements. This simplified the model construction and also made the results simple to understand. Material restrictions and availability were also taken into account and, as a result, only 25mm OD mild steel tubing of wall thicknesses 2.6mm and 1.6mm were chosen for the construction of the frame.

In an attempt to make the loading on the frame as accurate as possible a number of measures were taken, and are depicted in Figure 4.5. Firstly, a suspension system was included in the model, the dimensions of which had been under development concurrently with the frame. This included wishbones that were allowed to freely pivot on the frame (simulating rod ends) and a pull rod type suspension spring arrangement. The wishbone ends were then fixed in space to simulate the reactive forces of the wheels. Secondly, masses were applied to the frame to simulate component masses, such as the engine and driver. The masses were applied as 10kg 'blocks', each attached to member intersections distributed throughout the frame, in an attempt to gain the car's estimated weight distribution and centre of gravity. Thirdly, the frame was artificially stiffened around the engine mounts with additional members. This was

done because the frame design around that area relies on the engine to act as a sub-member, increasing stiffness but receiving minimal loads.

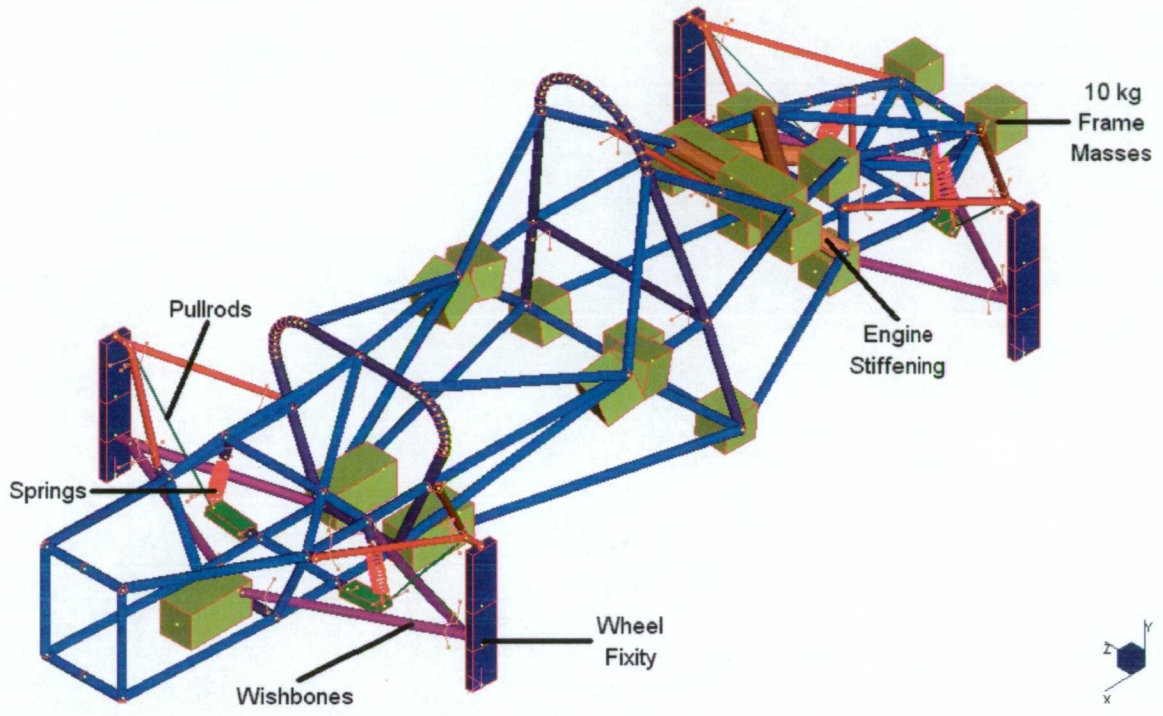

Figure 4.5: FEA frame model

By altering suspension restraint conditions a number of loading cases were created, each case using the applicable acceleration combinations above. The cases were:

- Normal driving
- Hard throttle
- Hard braking
- Hard cornering
- Cornering under throttle
- Cornering under brakes (Figure 4. 6)
- Torsional stiffness (Figure 4. 7)

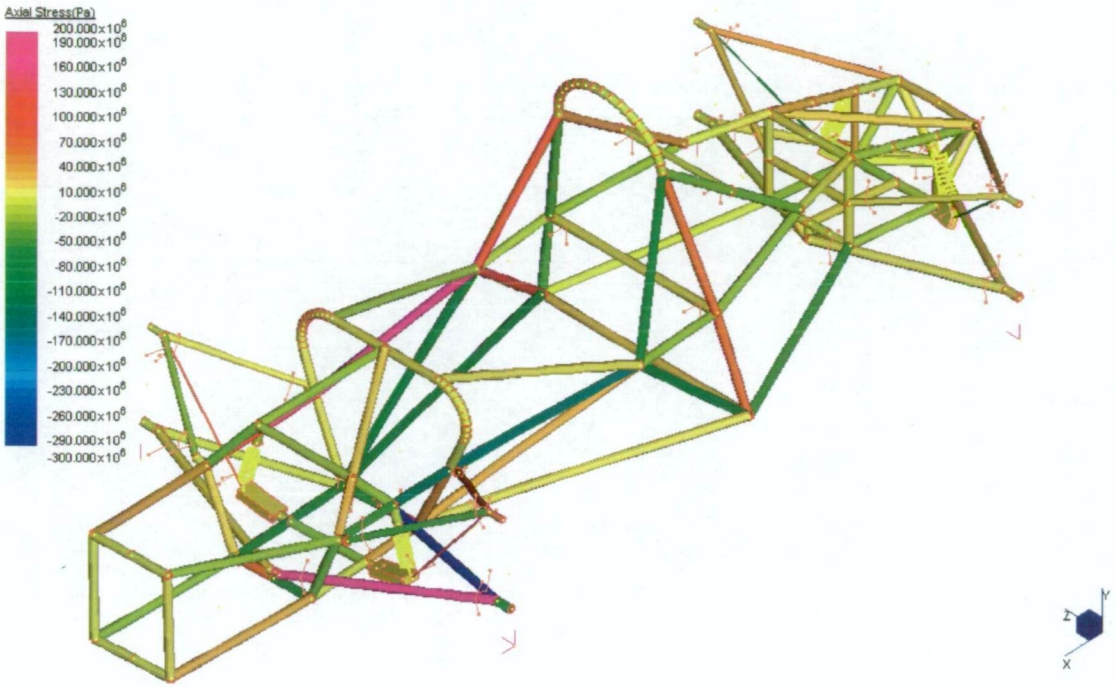

Figure 4.6: FEA results for cornering under brakes

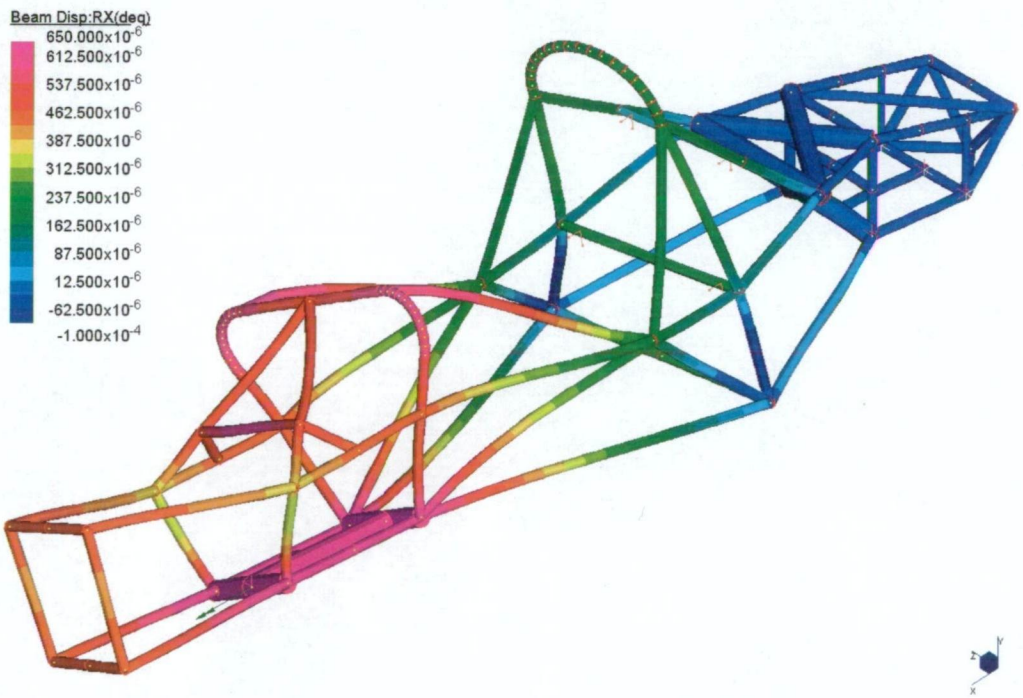

Figure 4.7: FEA torsional results under 1 Nm

These loading cases gave FEA results for member loadings and member deflections, as shown in "Appendix A", allowing for easy identification of severely loaded or deflected members, or the detection of superfluous ones. As such, the frame again went through a number of design iterations as efforts were made to decrease its weight while maintaining stiffness and strength. The end result being a frame model that was well below its strength limit and had a FEA torsional stiffness of 0.6° per 1kNm load between front and rear suspension points.

4.2.2. Computer Aided Design

Once frame dimensions and member sizes were defined using FEA the last requirement before construction could take place was to have CAD drawings ready. This was primarily to enable full dimensioning of the frame so member lengths and positions could be found for its construction, a feature that Strand7 lacked. To this end, a wire frame model of member centre lines was exported from the FEA package into the three-dimensional drawing package, CADKey [58]. It was then converted into a 'solid' model with complete member diameters and wall thicknesses (Figure 4.8) and later dimensioned for use in the frame construction. The frame dimensions are supplied in "Appendix A".

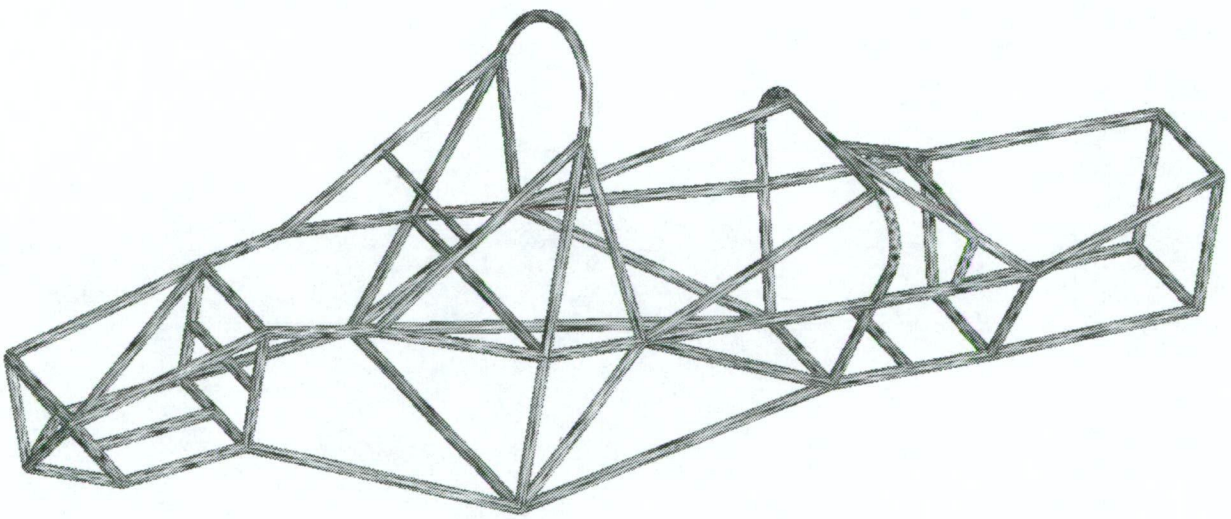

Figure 4.8: CAD drawing of the frame

4.2.3. Frame Construction

Frame construction proceeded in a number of steps. It was decided from the outset that the frame was going to be MIG welded due to workshop limitations and that it was going to be welded using a jig. The form that the jig took was as a steel table from which many of the members were lightly welded (tacked) into place in their correct positions. This provided an excellent baseline to work from as well as reducing the amount that the frame distorted due to residual welding stresses once it was removed from the jig.

Construction followed a logical sequence. The front and rear roll over hoops were first bent into shape and construction between them began. Members were cut to the correct lengths and their ends tapered to ensure a good fit to at the joints, which were subsequently welded. The front bulkhead was constructed next, followed by the engine bay and finally the rear most section, ensuring that a sequence of welding was maintained to minimise buckling due to welding stresses. The frame was then removed from the jig and all of the final welding was completed with minimal frame distortion. The complete frame is shown in Figure 4.9.

The 140 or so mountings for the various components such as the suspension system, the engine, the differential and the seat and seat belt were then designed, constructed and welded to the frame as required. With all of the mountings completed, the frame was painted using automotive acrylic paint, and subsequently the assembly began.

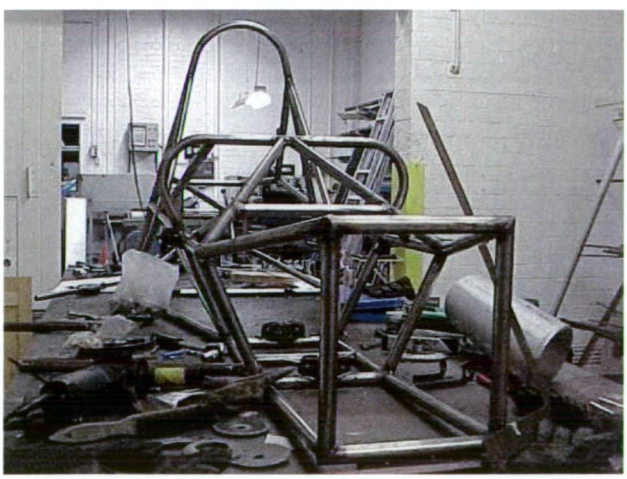

Figure 4.9: Mild steel frame

4.3. Suspension Development

The rules and nature of F-SAE directly specify many of the constraints on the vehicle's suspension design. On top of this, the competition course dictates how the suspension will be required to operate if the vehicle is to take full advantage of the level of grip available from the tyres during common and critical manoeuvres. This is dependent on the type of corners within the course, as well as the general track layout and its specified surface. Simply put, the purpose of a suspension system is to maximise the amount of contact between the racecar's tyres and the road surface when needed, and in a way that provides the required levels of traction as situations dictate. This is a difficult task, with extensive research into finding the optimum arrangements conducted throughout automotive history, seeking to balance the effect of the dynamic nature of suspension and tyres with respect to weight distribution and inertial forces of the vehicle under various driving conditions [50, 51, 52]. Taking this into account as much as possible with limited resources, the suspension was designed and constructed to:

- Conform to F-SAE rules, specifying the minimum allowable travel of all four wheels and general suspension system requirements
- Minimise the forces experienced by the frame since all major frame loads are induced by the suspension
- Conform to the chosen optimal suspension geometry and an appropriate level of strength and serviceability
- Minimise the overall size (especially the frontal area) and weight of the suspension system.
- Facilitate easy geometric changes, part replacement and tuning
- Use as few parts as possible
- Share as many common parts between wheels as possible
- Provide stable mounting points for the required sensors

4.3.1. Wheelbase

One of the first decisions made was to estimate a suitable wheelbase. The chosen wheelbase of a vehicle has a major effect on the weight transfer characteristics of the chassis and will also influence the polar moment of inertia about yaw, high-speed stability and the turning radius. The choice of wheelbase, in this case, stemmed from the key design motif of keeping the vehicle as compact as practical and its intended use on the tight, windy circuits of a F-SAE autocross track depicted in Figure 4.10. This also coincided with our decided driver and engine positions in order to maintain our goal of a near 50 / 50 static weight distribution.

Figure 4.10: F-SAE autocross style track (2001 Australasia competition)

Firstly, the rear wheel placement was decided on. With the driver reclined and the engine located midship, minimum practical clearances were allowed between the back of the gearbox and the differential spur gear to position the rear differential as far forward as practical (Figure 4.11). Since the drive axels were to be aligned with the differential (see the "Drivetrain Development" section), the position of the rear wheels relative to the driver could then be estimated readily.

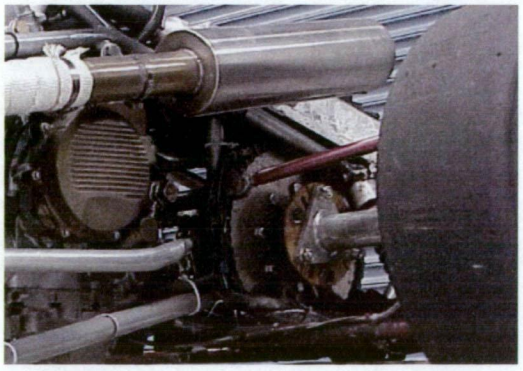

Figure 4.11: Location of rear axle, showing the clearance between gearbox and final drive.

The wheelbase was then defined by placing the front wheels at a distance to give the desired 50 / 50 weight distribution using estimates of the relative weights of the components in their tentative locations. Since this process was integral to the frame design, it also went through numerous design iterations as various components were juggled to find the most practical solution. The final result gave a wheelbase of 1835mm and a weight distribution of 49 / 51.

4.3.2. Track width

The next suspension design decision faced before kinematic analysis of the suspension system could begin was the determination of front and rear track widths, defined here as the distance between the centrelines of the front wheels and the rear wheels respectively.

The decision regarding track widths is critical. During cornering the lateral acceleration causes an overturning moment corresponding to the height of the centre of gravity from the road surface, the magnitude of the lateral acceleration and the mass of the vehicle. The front and rear track widths then directly determine the magnitude of the resisting force through the tyres required to overcome this moment, and do not necessarily need to be equal. In other words, defining the track widths is one way in which a vehicle designer can directly control the extent of lateral weight transfer.

For this reason the track widths were not as simply arrived at as the wheelbase. Locating the wheels as close as possible to the chassis significantly reduces frontal area (drag) and enables the vehicle to 'cut corners' to a great extent, but in this case would result in such a narrow vehicle that spinout or overturning would be probable during normal driving. Conversely, a wide vehicle handles cornering exceptionally well, but carries the disadvantages of increased weight and increased frontal area, as well has having to take corners at larger radii. A compromise needs to be found that places the wheels at a narrow enough track width to minimise frontal area and enable moderate corner cutting, while also ensuring stability.

4.3.2.1. Track Widths, Corner Speed and Lap Times

The track width compromise depends primarily on the use of the vehicle. To identify the optimum width, knowledge of the track type and performance necessities must be employed. In this case, the F-SAE racecar track widths were optimised for the slalom part of the

autocross track layed out in the rules, which was reasonably consistent with other sections of the course.

Firstly, it was identified that in order to improve lap times (directly dependant on velocity) we need to corner at the maximum possible lateral acceleration and choose the straightest racing lines around the course. This is obvious, but poor choice of vehicle track widths can prevent the vehicle from physically reaching these limits. Thus, we need to maximise lateral acceleration according to the relationship:

$$a = \frac{v^2}{r}$$

where: a = lateral acceleration
v = forward velocity of vehicle
r = radius of corner

Eqn 4.1

In this situation it was decided to consider two physical limits to the maximum lateral acceleration experienced by the simplified vehicle model; overturning and the amount of lateral grip which can be provided by the tyres.

During cornering there is an overturning moment caused by the vertical distance between the centre of gravity (C of G) of the vehicle and the ground, as well as the cornering force acting at the tyres. The horizontal distance between the C of G and the tyre contact patch, and the weight of the vehicle counteracts this moment. Thus, it can be simply assumed that near the limit of cornering the inside wheels have zero load. This gives:

$$a \cdot g \cdot m \cdot h = m \cdot g \cdot \frac{1}{2} \cdot trackwidth$$

$$a = \frac{1}{2 \cdot h} \cdot trackwidth$$

where: g = acceleration due to gravity
h = height of C of G
= about 0.4m for the test vehicle

Eqn 4.2

The amount of lateral grip provided by the tyres provides the other limiting factor for lateral acceleration. Given that there is no downforce, the maximum lateral acceleration obtainable from current F-SAE vehicles is around 1.3G, based on skidpan results from some of the top teams. This gives a baseline to compare track widths with respect to corner radius and cornering speed within these limits.

Observation shows that wide vehicles have to travel a greater distance around corners (and thus complete circuits) than narrower competitors. This is best illustrated on a slalom or chicane but is true for any corner at all.

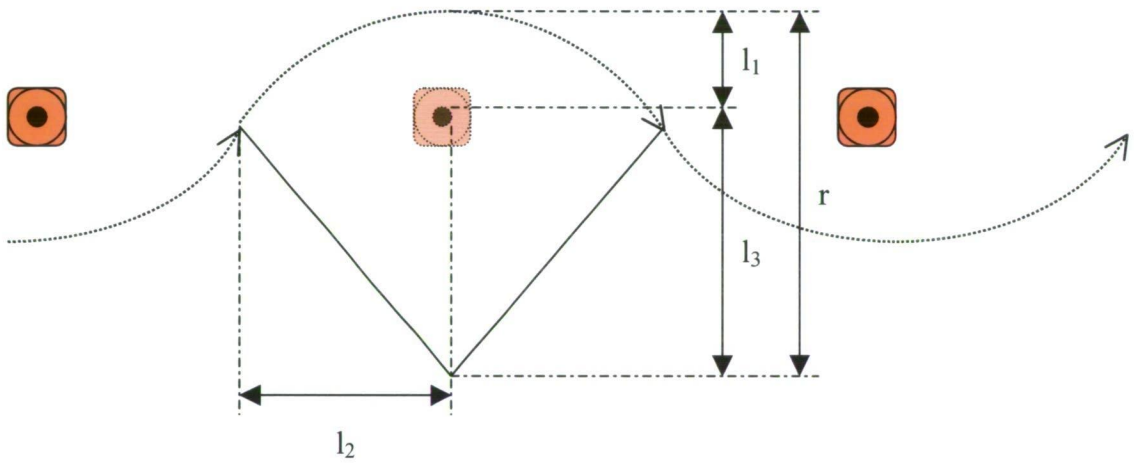

Figure 4.12: A typical path taken on a slalom course

In the slalom course in Figure 4.12 above the car is assumed to follow the ideal path, that is a set of perfect arcs where the maximum lateral acceleration is held for the duration of the slalom, changing sign as each cone is rounded. The dimensions of the path of the vehicle is given by:

$$l_1 + l_3 = r \qquad \textit{Eqn 4.3}$$

$$l_3^{\,2} + l_2^{\,2} = r^2 \qquad \textit{Eqn 4.4}$$

Substituting Eqn 4.3 into Eqn 4.4

$$(r - l_1)^2 + l_2^{\,2} = r^2 \qquad \textit{Eqn 4.5}$$

$$r = \frac{\left(l_1^{\,2} + l_2^{\,2}\right)}{2 \cdot l_1} \qquad \textit{Eqn 4.6}$$

And $$Arc\ length = \theta \cdot r \qquad Eqn\ 4.7$$

With $$\theta = 2 \cdot sin^{-1}\left(\frac{l_2}{r}\right) \qquad Eqn\ 4.8$$

This gives the basis for the calculation of the best time an F-SAE vehicle can achieve during a slalom course with respect to its track width, and allows the comparison of a variety of track widths as shown in Table 4.1, with an example calculation supplied in "Appendix B". It can be seen from the results that the fastest time corresponds to the vehicle that simultaneously reaches its rollover threshold and the maximum grip from the tyres. The vehicle that gives this has a track width of about 1.0m, and shows a 25% time improvement over a 2.0m track width. In this case, in the interests of maintaining a safety margin due to the large number of assumptions within this analysis, a track width of 1.1m was chosen as the basis for further analysis. Ultimately, the decision as to when further decreases in track width will produce unacceptable risk of rollover or skid for the marginal increases in lap time must be made by the designer for the vehicle's specific applications.

Track Width (m)	Lateral Acceleration (G)			Corresponding Velocity (km/hr)	Total Distance Traveled (m)	Total Time (s)
	Limited by Tyre Skid	Limited by Rollover	Maximum Value			
2.00	1.30	2.50	1.30	44.37	103.20	8.37
1.90	1.30	2.35	1.30	45.33	102.91	8.17
1.80	1.30	2.25	1.30	46.35	102.65	7.97
1.70	1.30	2.13	1.30	47.47	102.39	7.76
1.60	1.30	2.00	1.30	48.68	102.15	7.55
1.50	1.30	1.88	1.30	50.01	101.92	7.34
1.40	1.30	1.75	1.30	51.46	101.70	7.11
1.30	1.30	1.63	1.30	53.07	101.49	6.88
1.25	1.30	1.56	1.30	53.94	101.40	6.77
1.20	1.30	1.50	1.30	54.86	101.30	6.65
1.15	1.30	1.44	1.30	55.83	101.21	6.53
1.10	1.30	1.38	1.30	56.85	101.12	6.40
1.05	1.30	1.31	1.30	57.94	101.04	6.28
1.00	**1.30**	**1.25**	**1.25**	**57.95**	**100.96**	**6.27**
0.90	1.30	1.13	1.13	57.36	100.80	6.33
0.80	1.30	1.00	1.00	56.66	100.67	6.40

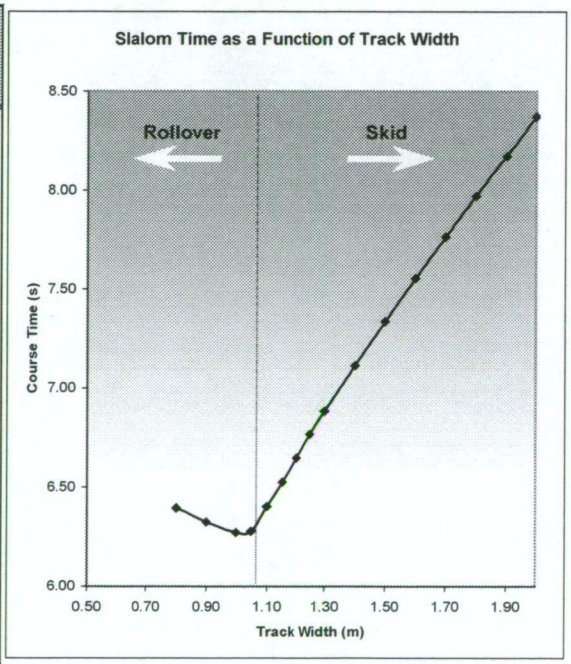

Table 4.1: Track width analysis for a slalom course of 10 cones spaced at 10m apart

4.3.2.2. Optimisation of Front Track Width

Closer investigation of the dynamics of cornering shows that the vehicle's front wheels do not follow the same arcs as the rear wheels do. It can be seen that when a vehicle with equal front and rear track widths turns, it is the inside rear wheel that limits the approach to the inside of the corner, as illustrated in Figure 4.13, assuming minimal lateral tyre slip. It is therefore evident that the front track width can be increased within bounds to provide improved cornering stability, without forcing the vehicle to travel along the larger cornering arcs as discussed above.

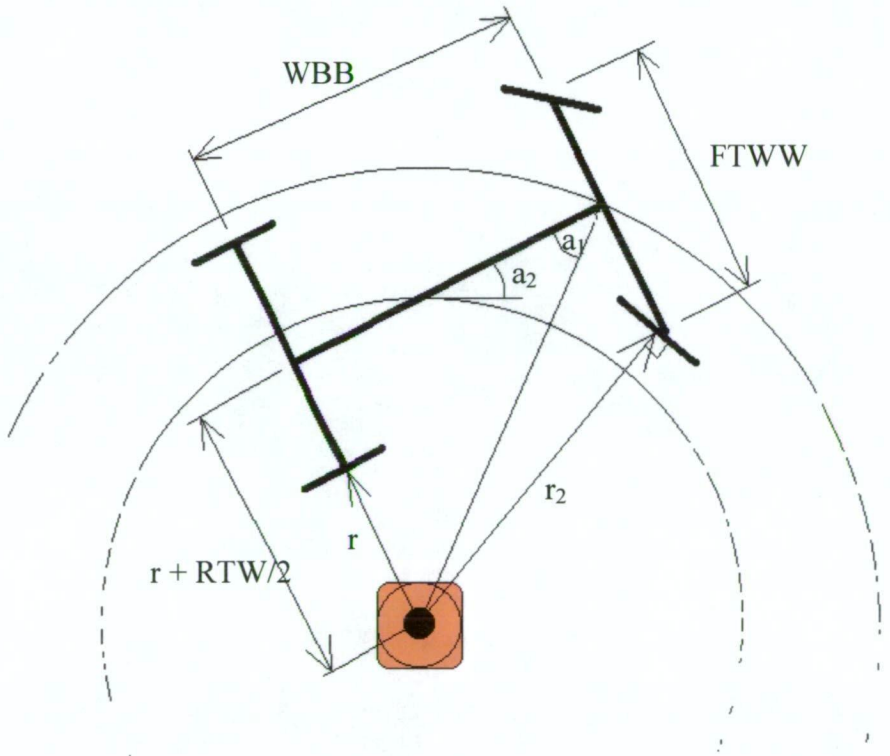

Figure 4.13: Geometry of turning vehicle

Inspection of the diagram above can then lead to the derivation of the radius of the inner front wheel arc:

$$r_2^{\,2} = \left(\tfrac{FTW}{2}\right)^2 + \left[\sqrt{\left(r + \tfrac{RTW}{2}\right)^2 + WB^2}\right]^2 - 2 \cdot \tfrac{FTW}{2} \cdot \left[\sqrt{\left(r + \tfrac{RTW}{2}\right)^2 + WB^2}\right] \cdot \cos\left[\tfrac{\pi}{2} - \tan^{-1}\left(\frac{r + \frac{RTW}{2}}{WB}\right)\right]$$

where:

r_2 = Radius tracked by the inner front wheel

r = Radius tracked by inner rear wheel

FTW = Front track width

RTW = Rear track width

WB = Wheel Base

Eqn 4.9

Thus, from the dimensions of the car (FTW, RTW and WB) and a given corner radius (r) we can determine the radius scribed by the front wheels. Our purpose for this equation, however, is to determine the maximum amount that we can increase the front track width before the front inner wheel begins to limit our approach to corners. To do this, the equation was solved iteratively according to the following steps:

1. Selection of an appropriate minimum radius for which the vehicle will be turning, factoring in the effects of corner apexing, etc. This becomes the value for r.
2. Calculation of the optimum wheelbase (WB) and rear track width (RTW).
3. Estimation of an initial value for the front track width (FTW).
4. Calculation of the arc radius scribed by the inner front wheel, r_2.
5. Reducing FTW if r_2 is smaller than r, or increasing FTW if r_2 is larger than r.
6. Repetition of steps 4-6 until r_2 converges to the chosen r.

This lead to the conservative selection of a 1.2m front track width, which is perhaps not taking full advantage of the possible gains in stability. This was done partly to avoid too radical geometry and keep frontal area reasonably small, and also done partly due to the break down of this simple analysis once the vehicle begins sliding.

Once this analysis was completed, the dimensions of 1.8m wheelbase, 1.1m rear track width and 1.2m front track width were selected as the final design goals. While it was observed that further work could be done in optimising these values to achieve marginal performance gains, it was decided to use these approximate values in the final design, shown in Figure 4.14, and focus further efforts into other critical areas, such a suspension geometry.

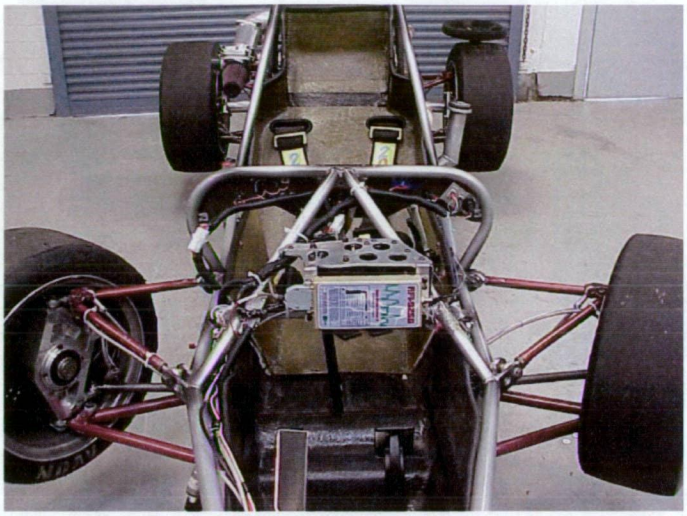

Figure 4.14: Track widths and wheelbase

4.3.3. Wishbone Geometry

Suspension design is always a compromise. Different suspension systems offer different advantages and disadvantages over others. Since the vehicle was to be built from scratch without any testing data it was decided that whatever type of suspension was used would require maximum adjustability for tuning out any inadequacies which may surface. This was coupled with a general desire to create a system that could be accurately modelled before manufacturing and was easy to produce. These desired properties lead to the decision to use the conventional independent four wheel double wishbone suspension system used throughout F-SAE.

The chosen geometry used in the suspension system was found to significantly effect the way in which the vehicle would react to different situations. Different suspension geometries can provide ideal bump but poor roll characteristics, ideal roll but poor bump, or a compromise somewhere in between. The best combination to choose depends on the performance characteristics most appropriate to the intended course. The F-SAE autocross course makes careful use of chicanes, tight corners and hairpins so that the racecars rarely reach speeds of over 120 km/hr, with an average speed of approximately 60 km/hr, which indicates a very tight track with a high emphasise on cornering ability. For this reason, it was decided that whatever suspension geometry was adopted, its focus should be on traction while cornering. To this end, it was required to keep the outside wheels as close to vertical as possible while

cornering throughout the range of movement of the suspension, since keeping the loaded wheel entire tyre width on the road is absolutely vital for maintaining corner speed.

To achieve vertical outside wheels under maximum expected roll the camber change properties under centripetal induced deflection needed to be carefully considered. Of note is that when using a double wishbone suspension system the wheels can never remain vertical under roll through their whole range of motion, but for small levels of roll (<5°) this can be controlled by using longer bottom and shorter top suspension arms. A traditional rule of thumb is that the top suspension arm should be about 2/3 the length of the lower arm. This is a figure arrived at as it gives a good compromise between these desired roll characteristics and also maintaining acceptable geometry in squat/dive under longitudinal acceleration.

Empirical figures such as this, arrived at through years of racing successes, offered valuable starting points for the suspension design, however finding an optimum geometry took place through the use of CAD modelling. To minimise the overall width of the frame (and hence the frontal area) and still have the necessary length difference between upper and lover wishbones, the lower wishbones were chosen to meet in the centre of the vehicle.

This design decision produced many significant packaging problems but was decided as core to the vehicle design and was not compromised. The upper wishbones could then be conventionally mounted to the side of the frame, which were spaced to suit with special consideration to driver ergonomics and engine/drive-train mounting.

The heights of the front and rear roll centres (the points in the transverse plane above the wheel contact patches, about which the sprung mass of the car will rotate under any disturbing force) were chosen to correspond to the expected mass distribution of the vehicle. The positioning of the roll centres is not an exact science, but a matter of opinion since it effects the extent of vehicle roll. The front roll centre was chosen at ground level based upon roll centre positions of successful international F-SAE cars and suggestions offered in race car design literature and by local racing engineers. The rear roll centre was then initially placed at 50mm above ground level. Similarly, appropriate values for the effective swing arm length were decided on, at between 100% and 150% of the track width using 6.5/19.5-13" and 7.2/20.0-13" Avon racing slick tyres for the front and rear respectively.

The final suspension layout, given in "Appendix B", was then achieved iteratively, with the final dimensions evolving with the selection of appropriate major component mounting arrangements and driver ergonomics. The resulting arrangement (illustrated below in Table 4.2) was shown to achieve camber change properties of approximately 1/2° on the outside wheels under full roll, which was deemed appropriate.

Front roll centre height	8 mm
Rear roll centre height	49 mm
Front effective swing arm length	1564 mm
Rear effective swing arm length	1114 mm
Front upper/lower wishbone length ratio	0.56
Rear upper/lower wishbone length ratio	0.71

Table 4.2: Wishbone design parameters

The loadings placed on the wishbones were then found from the FEA conducted on the frame. From this data, high strength chrome moly tubing of size 3/4" diameter and 1.47mm wall thickness was selected for the top wishbone construction with 1" diameter and 2.1mm wall thickness chrome moly tubing selected for the bottom. 7/16" high capacity chrome moly, Teflon lined rod ends where also chosen to connect the wishbones to the frame and to the wheels, shown in Figure 4.15, all in an effort to reduce suspension unsprung weight.

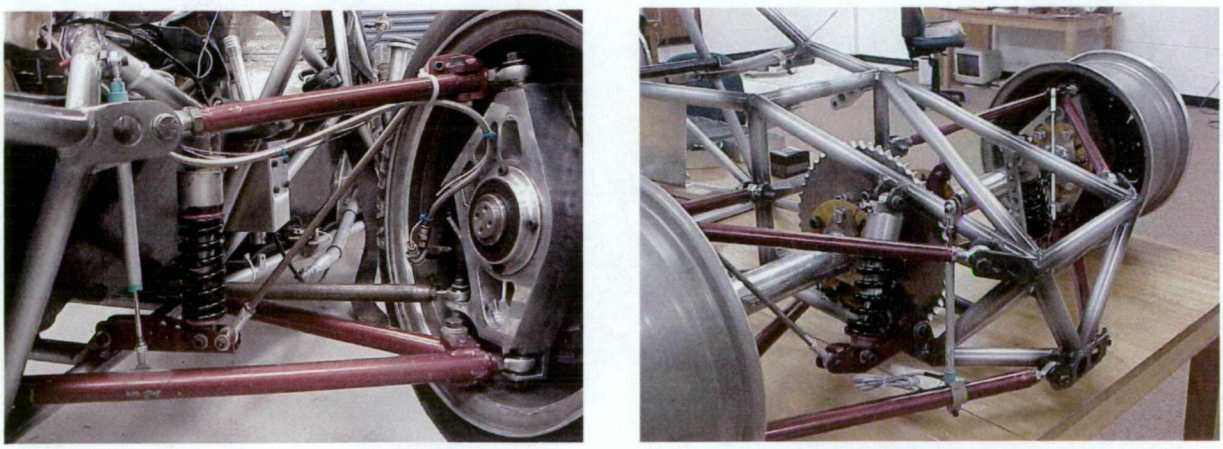

(a) *(b)*

Figure 4.15: Suspension geometry (a) front and (b) rear

Further weight reduction was achieved through the use of a pull-rod system incorporating an inboard coil over shock spring arrangement and 1/4" aircraft grade female rod ends, as can also be seen in Figure 4.15, with all rod end properties supplied in "Appendix B". The pull-rod suspension also provides progressive spring rates, which themselves can be adjusted through positioning on the rocking supports, while the springs used (RST 58 mountain bike rear shocks with stiffness 850 lbs/inch, as shown in "Appendix B") provide adjustable spring preload and damping in bound and rebound. The system also incorporates relatively simple alterations in ride height when called for.

4.3.4. Steering Design

The choice of placing the bottom wishbones pivots along the centreline of chassis produced a problem with the placement of the steering system. In order to avoid significant bump steer (undesired steering operation produced by the movement of the suspension) the steering linkages had to be either placed exceptionally close together under the driver's legs, or mounted normally within the cockpit below the level of the top wishbones. Inspection showed that the second option was not possible because of driver positioning, and so was discarded.

Two options were identified to provide a solution to the problem of mounting under the driver. The first was to modify or construct a rack and pinion steering box so that it provided a single mount to control the movement of the left and right steering linkages. The second was to use a worm and sector steering box that provided steering similar to a go-kart arrangement by rotating the mount, except geared to provide superior control. In the end, it was decided to use the worm and sector steering box (sourced from drag racing components) since it eliminated the need for universal joints and, with a few modifications, provided simple adjustment of both steering wheel position and steering rate, as shown below in Figure 4.16.

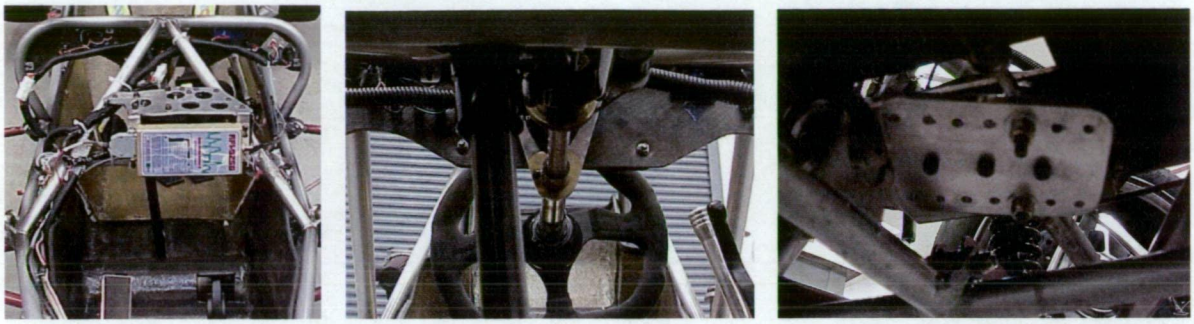

(a) *(b)* *(c)*

Figure 4.16: Steering system (a) placement, (b) worm and sector box & (c) sensitivity adjustment under seat

Ackerman steering was also included into the design of the suspension. This enables the inside steered wheel to turn to a greater extent than the outside one, allowing it to roll freely without slippage as it scribes its smaller radius arc. The philosophy used within this vehicle, however, went one step further, giving it 120% Ackerman, as shown in Figure 4.17. This means that the inside wheel turns slightly too much, forcing it to slip around the corner, slightly slowing the vehicle. However, the direction of the slip potentially produces a larger lateral force in the direction of the corner than 100% Ackerman produces, further helping the front wheels to steer the vehicle thought the bend.

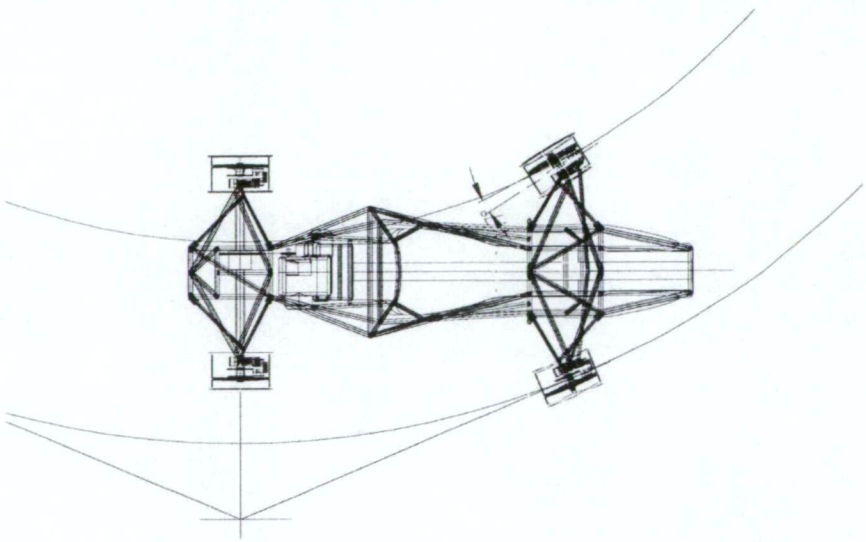

Figure 4.17: Ackerman steering geometry

4.3.5. Suspension Tuning

During the design process, numerous additional parameters effecting the performance of the suspension and steering systems were investigated. In particular, the effects of steering scrub radius (the distance from the wheel centreline to the steering axis of the wheel) and king pin angle (the angle of the steering axis from vertical) were explored in vehicle design literature. They were then assigned with their suggested dimensions and formed part of the design criteria for the wheel assembly, as described in the following sections.

Once the vehicle was constructed, further investigation was carried out to improve the suspension operation. Numerous suspension setups of camber and caster angles and tyre pressures were explored during driving trails to find their optimum arrangements. Efforts were made to keep the camber angles as small as possible to maintain high levels of traction during longitudinal acceleration without 'scrubbing out' the insides of the tyres during cornering manoeuvres. Camber angles were kept reasonably small to enable adequately free steering wheel movement, while also promoting self-aligning properties for high-speed stability. This iterative process highlighted the importance of selecting the correct setup, with the initial arrangement wearing out a set of tyres within a few kilometres, compared to the 500km tyre life that was later achieved. The end result showed excellent performance in both straight-line acceleration and braking, as well as during cornering, but suffered in the area of driver ergonomics – with the steering being relatively heavy at low speeds on tight corners. The final suspension design properties and adjustments are shown below in Table 4.3 with their performance depicted in Figure 4.18.

Scrub radius (fixed – front and rear)	57 mm
King pin inclination angle (fixed – front and rear)	4.2°
Front camber angle	0°
Rear camber angle	0°
Front caster angle	6°
Rear caster angle	0°
Front tyre pressure	16 psi
Rear tyre pressure	14 psi
Minium turning circle diameter	5 m

Table 4.3: Suspension setup parameters

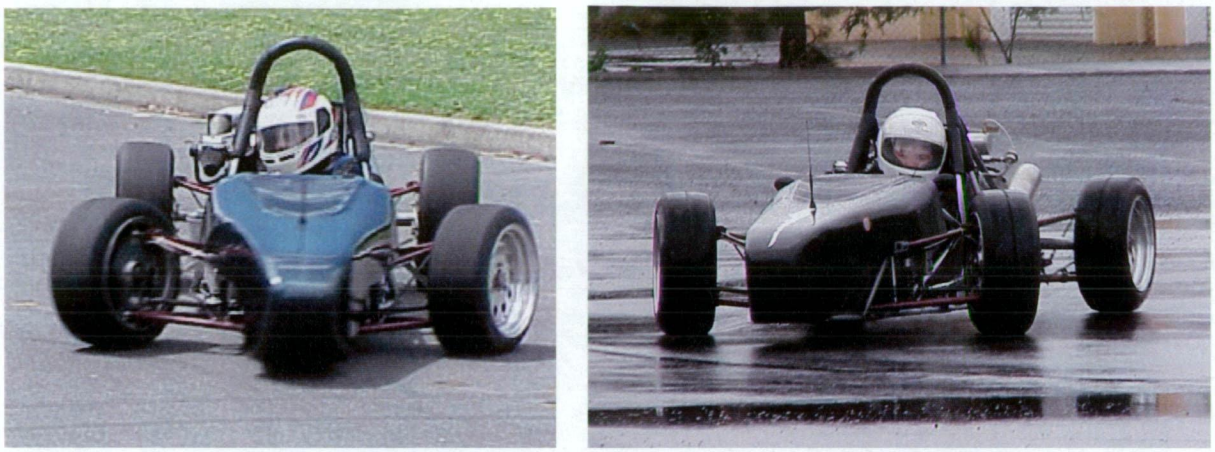

Figure 4.18: Suspension performance during tight cornering

4.4. Wheel Assembly Development

The wheel assembly is defined here as the set of components that link the suspension wishbones to the road. This includes the wheel rims and tyres, as well as the brake system, hubs, stub axles, uprights and bearings, and is shown in Figure 4.19. The design and integration of these components had to address the following criteria:

- Be simple and relatively cheap to fabricate
- Be as light as possible without compromising strength or lifetime
- Must house the largest brakes possible
- Must not interfere with rim rotation
- Must mount to the wishbones while ensuring adequate suspension and steering movement
- Must have a mount for steering linkages
- Must house a wheel speed sensor
- Must allow attachment to the drive axle for the rear wheels
- Must give the desired scrub radius and king pin angle
- Should allow significant adjustment in parameters such as camber and caster angles to enhance drivability

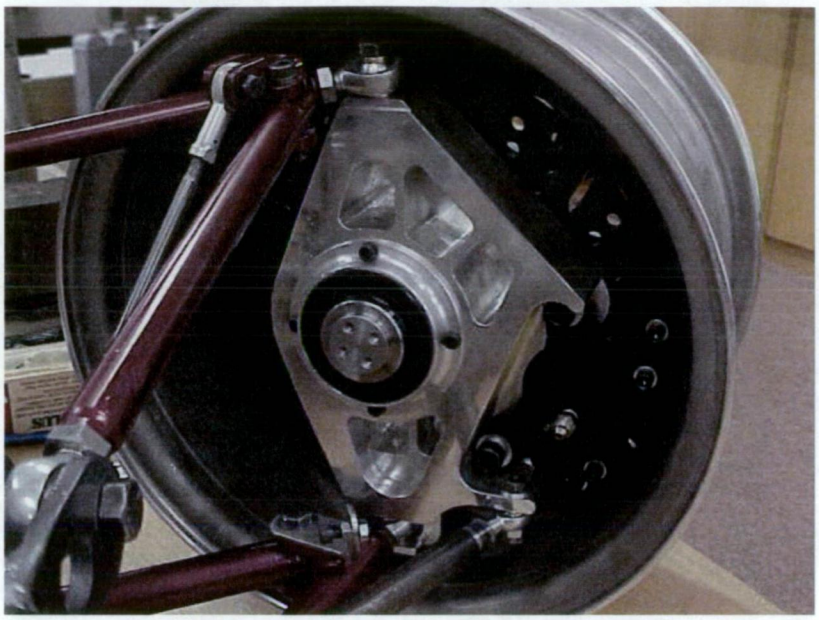

Figure 4.19: Wheel assembly

The same design for the front and rear wheels was also used. The argument for this addressed a number of points, firstly a common design would enable cheaper and easier fabrication. Also, the design requirements between the front and rear wheels where similar. The required mountings for the wishbones were the same front and rear, identical brakes where going to be used on all four wheels, all of the rims were matching and wheel loadings were similar. Conversely however, the front wheels needed to be steered while the rear ones did not, and the rear wheels needed to be driven while the front ones did not. It was decided that a design that allowed the wheels to be driven and steered would be best in this situation because, while it increased the assembly mass, it allowed reduced design and fabrication labour and allowed greater interchangeability of parts. The final wheel assembly dimensions are given in "Appendix C".

4.4.1. Rims and Tyres

The selection of rim size is critical to determine the overall design of the wheel assembly. F-SAE racecar teams typically select either 10" or 13" rims depending on what their specific requirements are. The selection of 10" rims makes the wheel assembly very light. The size of the tyre is reduced to a great extent and some of the bending moments within the assembly are diminished, resulting in a reduced need for strength. However, the size of the rim also

determines the size of the brake discs (rotors). Investigation showed that F-SAE cars running on 10" rims often have problems with ineffective braking and rotors that frequently over-heat. They also require rotors that are exceptionally difficult to find commercially, and thus would call for specialised fabrication. It was also found that within Australia, sourcing of 10" rims and tyres was extremely limited in both range and quality.

13" rims on the other hand typically add up to 15kg of weight to the car, but allow significant room for brakes. This allows for rotor selection from existing commercial sources, which also provide significant stopping performance without overheating problems. It also enables the choice of a wide variety of rim and tyre selections, which were considered essential in order to match the wheel characteristics to the desired performance parameters of the vehicle. It was decided that the weight compromise was acceptable and 13" aluminium rims were chosen, as illustrated in Figure 4.20. The rims were custom made to suit our required dimensions of 7" width, 144mm backspace offset and 152mm internal diameter needed to fit the wheel assembly components in. Tyre selection, as mentioned above, was chosen to be 6.5/19.5-13" and 7.2/20.0-13" Avon racing slick tyres for the front and rear respectively. The choice in sizes was made on the principle that it was best to 'stretch' the tyres onto the front rims to minimise sidewall deflection, and to make the rear tyres 'balloon' on their rims to allow them to act as energy absorbers, to aid acceleration.

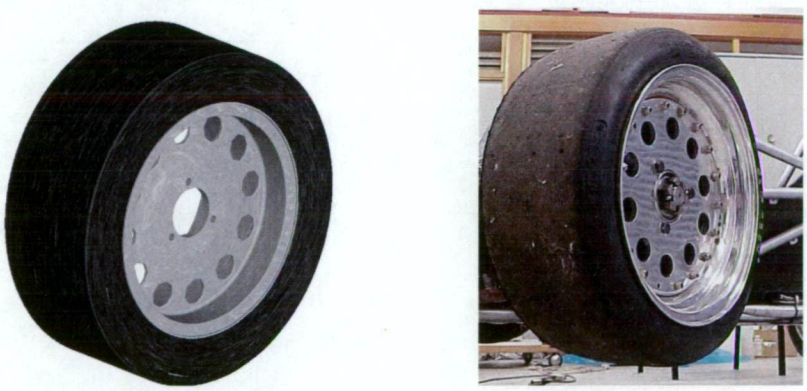

Figure 4.20: Tyre and rim

Competition rules also specified that during wet track conditions DOT 3 approved tyres must be used, and since tyre-changing facilities were limited during racing it was necessary to purchase a second set of rims. However, since a number of problems where encountered with

the quality of the inners supplied on the first set it was decided to CNC mill our own, as shown below in Figure 4.21.

Figure 4.21: CNC milled rim inners

4.4.2. Brake System

The choice of the disc brake system not only had a large impact on the racerar's braking performance, but also on the design of the wheel assembly. Rotor diameter and type, caliper profile and caliper width all define the dimensions of various components within the wheel. Because the brakes were going to be purchased, rather than manufactured, it was important to choose the correct system before further work on the wheel assembly design could proceed. Research showed that the possibility of using components from passenger cars, assorted racing cars, motorcycles and go-karts all existed, however finding a design that worked well proved difficult. Car brakes were very heavy but would simplify the design, motorcycle brakes were light and had excellent calipers but finding some to fit in a 13" rim proved fruitless, go-kart brakes were extremely light but their strength was in question and racing car brakes looked perfect but were expensive. The choice came down to if it was more important that the brakes were cheap or light. The decision was made in favour of light in this case, and racing components were used.

Research into racing brake systems to fit 13" rims showed that there was limited choice. Many manufactures made components that were too large, while others made components that were still too heavy. The selection of rotors and calipers supplied from Wilwood High Performance Disc Brakes proved to be the best choice in this case. 10.2" diameter 3 pin

mounted aluminium rotors were purchased in conjunction with aluminium billet dynalite single calipers, the specifications of which are given in "Appendix C" and are depicted in Figure 4.22. This provided a brake system that fits within the rims with only 4mm of clearance, maximising brake size, and weighing only 1.3kg at each wheel. The decision was also made to use the same brake components for the front and rear wheels. This was done to aid in brake force comparisons during testing and also because smaller brakes for the rear wheels would have reduced the front/rear interchangeability while only saving a small amount of weight and money.

Figure 4.22: Brake rotor and caliper

4.4.3. Stub Axle and Bearings

Passenger vehicles traditionally place the bearings for driven wheels about the vertical centre-line of the rims. While this practice has many benefits such as reduced bearing and stub axle loading it can also increase the complexity of design. This complication comes about because rim construction and brake caliper clearance generally require the brake rotor to also be positioned close to the rim centre-line. This gives two components that require positioning about the same point within the wheel. The most common solution to this problem is to move the brake rotor mounting to the hub of the wheel, thereby creating the traditional 'hat' design. The rotor, therefore, remains in its optimum position and a significant clearance is left for the bearings to be placed about the rim centre-line. This design, however, requires extra material to construct the hat, which increases the wheel's mass and rotating inertia. It also complicates the design of the bearing housing within the upright, which must protrude into the hat [48..62].

Conversely, the bearings can be placed off-centre. This avoids the need for a brake hat because the rotor can then be attached directly to the stub axle. It also avoids the need for the bearing housings within the upright to protrude. This solution generally reduces the cost for one-off construction as well as reducing the rotating inertia of the wheel but with the drawback of magnified bearing loading, which increases the stub axle and bearing sizes [57].

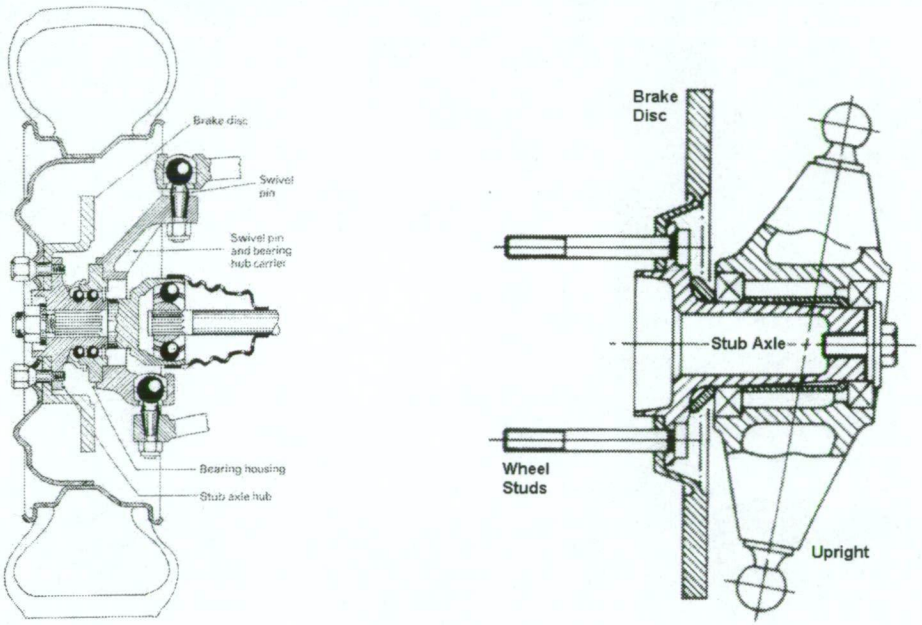

(a) *(b)*

Figure 4.23: Bearing placement, (a) on centre [48] & (b) off centre [50]

The choice of which design (depicted in Figure 4.23) was best came down to which choice best suited the design criteria of the F-SAE racecar. The hat design is almost universally used in the production of passenger vehicles for a number of reasons. It is economical to manufacture for large scale production, is easy to construct (using cast materials), is long lived and is less likely to fail under unexpected driving conditions. However, the car being built is nor a passenger car, its a racecar. It must be light, must have high acceleration and deceleration, must have good handling characteristics and be economical to manufacture in short production runs, in accordance with F-SAE rules. The centred and the off-centred bearing designs must be appraised against these criteria and not on those of commercially available vehicles.

Finite element analysis was introduced in order to facilitate this design choice. FEA was chosen because it has the advantage of being able to accommodate quite complex loading and design characteristics, while also being able to display the results in a clear and useful manner. Also, since the models were created suitably, they could easily be altered to account for small design changes as the results demanded.

Models of the centred and off centre bearing cases were created to allow comparison. Each model initially used 30mm diameter stub axles, used a set of identical single row tapered roller bearings spaced at the same interval and used matching common parts (such as the brakes and rims). This ensured that the two models were operating from the same initial baseline and allowed simple comparisons. The models were created using 'plate' elements for the wheel components and 'brick' elements for the axle and bearings. This was done to make the models easier to both structure and modify, while preserving accuracy at the axle, where it was required. The plate element properties and thicknesses were chosen as per our own initial design and a pressure of 20psi was applied to the tyre walls and rim to gain a more accurate simulation. The two models are shown in Figure 4.24 below.

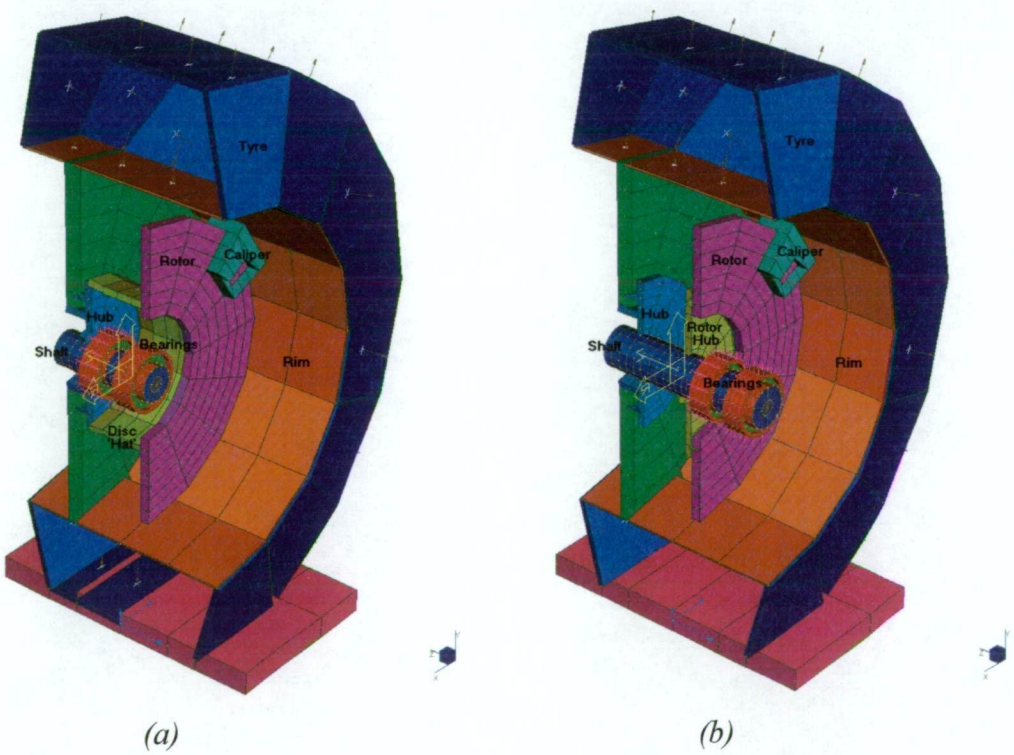

(a) *(b)*

Figure 4.24: FEA wheel model cross sections, (a) centred bearings, & (b) off centre bearings

The models were created in Strand7 [57] and assumed to be stationary (non-rotating), with the bearings fixed in an X arrangement in space but free to rotate. The brake caliper was represented by a fixity condition at a node restricting rotation only and a point load was applied at the bottom of the tyre through a plate representing the ground. The magnitude of the point load was chosen to represent the worst case scenario for this F-SAE racecar, deceleration of $10m/s^2$ (1G) in braking and centrifugal acceleration of $20m/s^2$ (2G) in cornering. Under these accelerations the FEA completed within the "Frame Development" section gave loading conditions of 1.6kN vertically, 4.6kN in the direction of braking (along the length if the car) and 4.9kN from cornering (along the width of the car).

The results, given in "Appendix C", showed that a 35mm diameter stub axle in the off centre bearing case gave the same internal stresses as the 30mm diameter axle in the centred case. It was these two cases of similar load to yield that was the basis of further comparison, the results shown in Table 4.4 [63, 64, 65]:

	Centred Bearings	**Off-Centre Bearings**
Bearing Loads		
F_{radial}	23.1 kN	33.1 kN
F_{axial}	4.9 kN	4.9 kN
Bearing Parameters		
C_{req} (10^8 rev)	43.9 kN	62.9 kN
Internal Dia.	30 mm	35 mm
Bearing Choice	FAG 32206A	FAG 32207A
External Dia	62 mm	72 mm
Axle, Bearing & Brake Hat Weight		
$W_{assembly}$	2.0 kg	2.2 kg
Moment of Inertia of Axle & Brake Hat		
$I_{assembly}$	$0.31x10^{-3}$ kgm^2	$0.19x10^{-3}$ kgm^2
Stub Axle Deflection	0.1 mm	0.5 mm

Table 4.4: Wheel bearing selection

In comparison of the two models it was important to note that the bearing positions would significantly effect the design of surrounding components. The design of the upright particularly was subject to change since it must house the bearings in their different respective

positions. In the case of the F-SAE racecar, it was found through a short investigation that the upright weights for both cases would be similar, but remained very design dependent. A deviation in the above assembly masses of 200g, while not negligible, can seem less important when considering the design of the upright as well. A simple calculation considering a 330kg racecar accelerating at $10m/s^2$ showed that this increase in weight reduces acceleration by $0.02m/s^2$ while the increase in moments of inertia account for a completely negligible reduction of $0.0002m/s^2$.

The last comparison that could significantly affect the wheel assembly performance was the stub axle deflection. The axle in the off-centre case obviously deflected more than in the centred case because much more of it was subjected to the maximum stress, and therefore strain. This small amount of deflection was not a significant problem in the case of this racecar. It can be shown that the resulting wheel misalignment (0.4° from vertical) is small when compared to wheel misalignment resulting from car roll and pitch when cornering and braking.

Budgetary constrains also had to be considered. The difference in the cost of production of the wheel assembly essentially fell to the cost of the upright. This was because all the other components within each of the assemblies could be made using very similar methods. The most cost-effective method of producing a lightweight upright for the very limited number of units required was to machine it out of an aluminium block. In the case of centred-bearings this would require a very thick and expensive plate to machine, while the off-centred bearings will require a plate only about half as thick and much cheaper. Machining the uprights for the off-centred bearings in this case also requires far less material removal resulting in cheaper production costs.

In summary, the centred bearing design proved slightly lighter, showed marginal increases in handling characteristics and also probably has a longer lifetime due to its added ability to cope with unexpected driving conditions. Conversely, the off-centre design revealed itself to be cheaper to construct in 'one off' production, but at a cost of slightly lower performance and life. The decision was made in favour of the off centre case, using a 35mm stub axle and 35mm ID and 72mm OD single row tapered roller bearings because of the perceived

difficulties in fabrication for marginal performance increases using the centred bearing design [66].

The stub axles (show below in Figure 4.25 were made on a CNC lathe using free machining 709M steel. A thread was also placed on one end of each to allow for the addition of a castellated nut to hold the entire assembly together, as well as provide bearing pre-loads. The stub axles were then moved to a mill where a hole for the castle nut cotter pin was drilled and a grove for the keyway was cut.

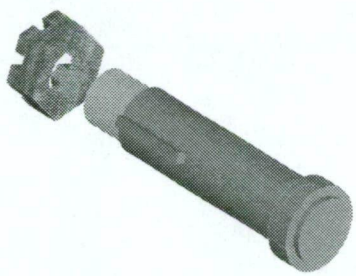

Figure 4.25: Stub axle

Finally a modification was made to the stub axles of the driven wheels to allow the installation of the 'composite disc' CV joint replacements detailed in the "Drivetrain Development" section. These discs transmitted the drive torque and had to be mounted onto the stub axle via a triangular plate with a bolthole at each corner. The mild steel plates were stick welded, using a special heat treatment process, to the stub axles which also had journals included in their common design to facilitate centering and alignment of the plates.

4.4.4. Oil Seals

One of the disadvantages of using single row tapered roller bearings is that they cannot be purchased in a sealed condition. As such, the design required that a pair of oil seals be used to hold the lubricating grease within the bearing pairs, which were housed within the upright. Oils seals of 40mm ID and 72mm OD were purchased to run on the bearing journal of the stub axle on the suspension side of the upright and on the wheel / brake hub on the other. These seals, however, had to be mounted onto the upright in some fashion, since its design did

not enable direct mounting. This was due to increased machining complexity and material cost incurred by including the oil seal mounts into the upright construction.

Oil seal mounts were designed to be interchangeable on either side of the upright. This required them to be as compact as possible since to distance between the upright and the wheel / brake hub was already small. Furthermore, positioning the seals near to the bearings results in the requirement of less grease, reducing weight. This resulted in the CNC construction of 8 aluminium oils seals of a 'bolt on' design shown in Figure 4. 26 below, with the bolt holes drilled at even intervals, using the mill dividing head, to ensure interchangeability and correct alignment.

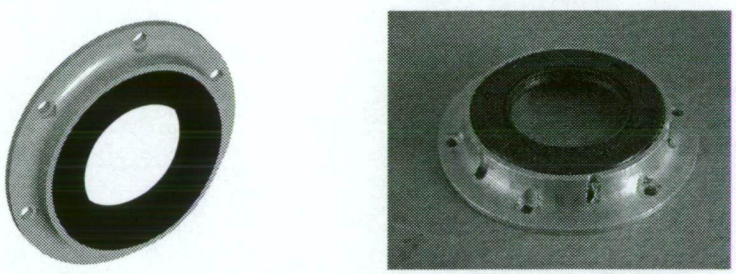

Figure 4.26: Oil seal

4.4.5. Wheel / Brake Hub

The wheel / brake hub must serve a number of functions. First and foremost it must provide an attachment for the wheel and the brake rotor to each other, and to the stub axle. It must also provide a means to allow driven wheel torque to be transferred from the stub axle to the wheel as well as provide a system to facilitate bearing pre-loading. Furthermore, a general design had already been established above of a wheel hub plate and a brake hub plate attached to a shaft. There were also the requirements of the inclusion of the oil seal running surface and a keyway to the stub axle.

In addition to these requirement, the dimensions were also defined through the overall assembly design. The position and diameters of wheel mounting was known, as was the details for the brake mounting. The oil seal journal also needed to be a specific size and the diameter of the sleeve to fit the stub axle was also defined. The design of this component was

simply focused at producing a component to these very specific requirements that was both cheap and easy to manufacture, while being as light as possible. The result being a 2kg mild steel hub manufactured on the a CNC lathe with the keyway cut with a broach and the bolt holes drilled in a mill with a dividing head, as shown below in Figure 4.27.

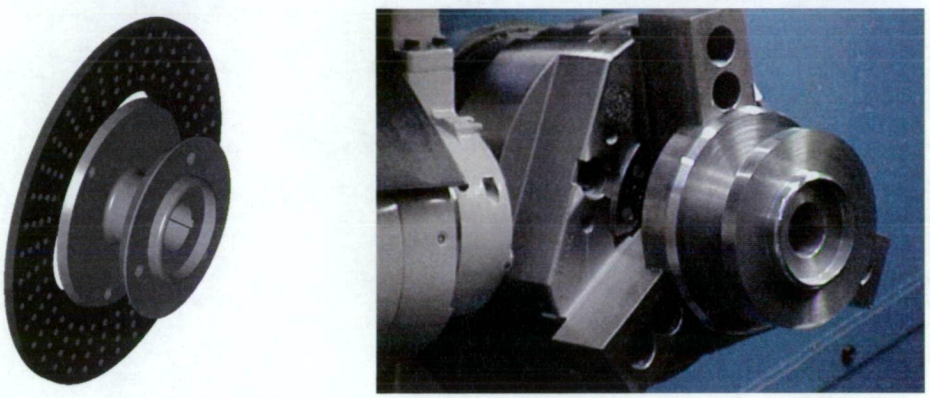

Figure 4.27: Wheel / brake hub

4.4.6. Upright

The design of the upright had many conflicting requirements, and as such was difficult to gain an optimum solution. The decision to use common steered and driven wheel designs also made the design more complex.

The first consideration was the bearings and bearing spacing. The selection of a small bearing spacing allowed for the choice of a relatively thin upright (50mm), but the increased loading resulted in large bearings that forced the upright to be quite wide about its centre.

Suspension mounts where another big consideration. The suspension design called for the placement of the bottom wishbone to be a low as possible, and the placement of the top to be spaced at the same distance from the stub axle centre line. When considering the placement of the wishbones at varying suspension travel positions, the different suspension geometries front and rear and the clearances during turning, the problem becomes very complex. Factors such as king pin angle (chosen as 4.2°), and caster and camber adjustments also had to be taken into account. In addition it was also decided that, since the forces on the bottom mount were much higher than at the top, the bottom mount would be designed for double shear while the top for single shear only.

The placement of the brake caliper and steering mount were also integral to the design. The brake caliper radial positioning was defined exclusively by the brake rotor diameter, however it could be placed anywhere on that radius, within reason. The best design, though, favours the placement of the caliper as low as possible. This lowers the centre of gravity, reduces the 'back flow' of hydraulic fluid that results from caliper positioning higher than the master cylinder and provides extra strength within the upright in its lower portion, which is subject to large loads. Further investigation into the design of the caliper mounting also showed a small alteration would also allow the integration of the steering mounting into the design with little effort.

Once all of the individual design requirements had been identified a final design for the upright was produced. Factors such as milling limitations, weight reduction and appearance where taken as priorities in the design, which also met all other requirements suitably.

The aluminium uprights were manufactured in a number of steps. The bearing journals were first lathed out to a J6 clearance, with the upright subsequently CNC machined to shape. The suspension joint, steering tie rod joint and brake caliper mounting bolt holes were then manually drilled and taped followed but the drilling of the bolt holes for the oil sealed in the mill dividing head. The resulting product is illustrated in Figure 4.28.

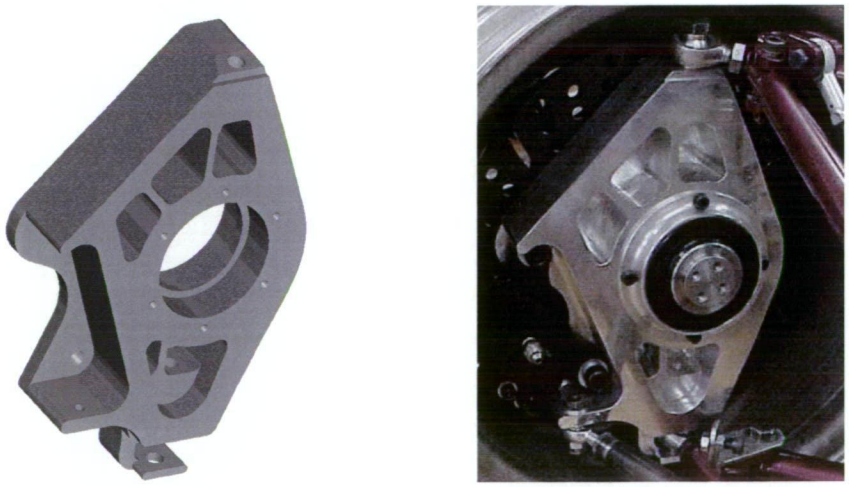

Figure 4.28: Upright

4.4.7. Assembly

Due to the small clearances within each wheel assembly, they must be assembled in a specific manner. Figure 4.29 shows the exploded and cut-away views of each wheel assembly, which are put together in the following manner:

1) Press the oil seals into their mountings,
2) Grease the tapered roller bearings,
3) Press and Loctite® the bearing outers into the upright,
4) Slide one of the oil seals along the stub axle to the non threaded end,
5) Press the first bearing inner onto the stub axle and slide it to the journal,
6) Slide the upright over the bearing and bolt and Loctite® the oil seal in place,
7) Press the remaining bearing inner onto the stub axle and bolt and Loctite® the other oil seal in place,
8) Bolt and lock nut the brake rotor to the hub and slide both onto the shaft with the keyway key installed,
9) Place the washer and castellated nut onto the tread end of the stub axle,
10) Bolt and Loctite® the bake caliper into place on the upright,
11) Bolt the rim and tyre to the hub,
12) Tighten the castellated nut to pretension the bearings so that the wheel freely rotates no more than one turn when spun by hand,
13) Insert the cotter pin to stop the castellated nut from loosening,
14) Bolt and Loctite® the suspension and steering rod ends to the upright utilising the brass spacers to ensure full movement,
15) Bolt the rim to the wheel / brake hub.

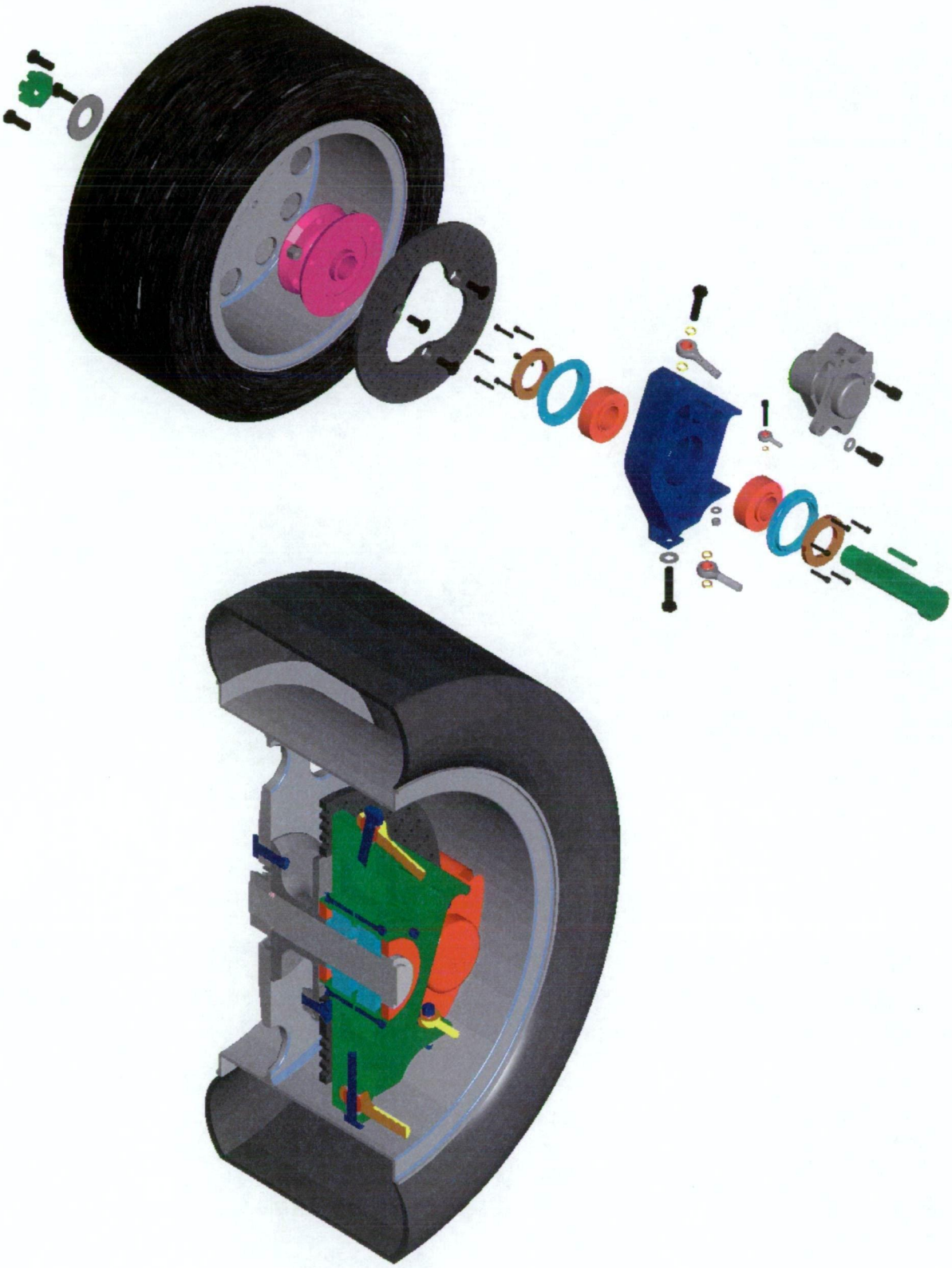

Figure 4.29: Wheel assembly CAD drawings

4.5. Cockpit Development

Since the driver was identified as the most crucial element in vehicle performance, the need for ergonomic and efficient design was highlighted at an early stage. F-SAE also highlighted a number of different design requirements in the interests of driver safety, which also had to be met. This resulted in a list of design considerations of:

- Adequate visibility, while wearing a full faced helmet
- Reasonably comfortable seat design for 15 minute track runs
- Fast (high ratio) steering
- Easy throttle and brake control
- Fast clutch control to take advantage of the sequential gearbox
- Efficient placement of the gear shifter
- Total driver closeout forward of the front roll hoop
- Use of a 5 or 6 point restraint harness
- Use of arm restraints
- Fire protection
- Maximum driver egress of 5 seconds

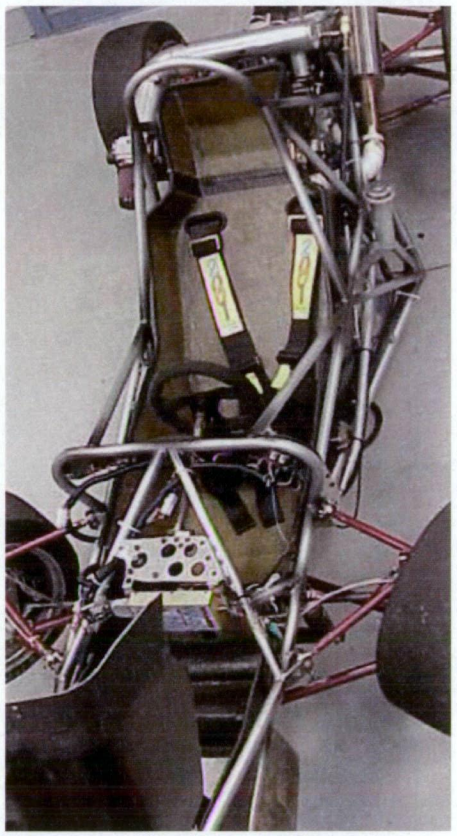

Figure 4.30: Driver cockpit

4.5.1. Seat, Nose and Driver Closeout

The requirements for the positioning of driver closeout, seat and nose are shown in Figure 4.31. It can be seen that design of the seat revolved around the reclined driver position. Thus, in the interests of minimising vehicle weight and making the car as compact as possible, the seat was constructed from composite materials, as were the nose and the majority of the floor closeout as shown in Figure 4.32.

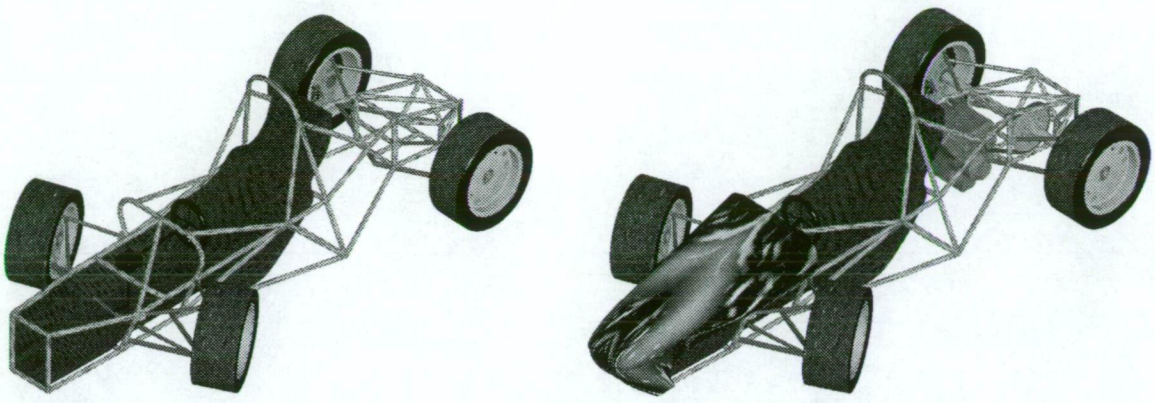

Figure 4.31: CAD drawings of the vehicle, highlighting seat, floor and nose closeout

The moulded carbon fibre – foam – carbon fibre / kevlar layered construction of the seat meant that its shape could take full advantage of the driver space within the frame. It also meant that it could provide all of the required firewall shielding from the engine, could protect the driver from track debris and allow the simple connection of the 6 point restraint harness to the frame. Its female moulded construction also allowed the seat to be constructed to be a snug fit around all of our drivers to minimise excessive movement during the high accelerations and cornering forces during driving, while being reasonable comfortable over the short times required. This design to close tolerances, however, produced problems in the installation of the seat and access to the engine. Since the engine and two removable members must be dismantled in order to install the seat, it was decided to minimise the need for its subsequent removal. This was done by cutting its head rest section from the seat to improve engine access and clipping it on instead.

Since the seat only extended to the front roll hoop, further closeout was required to protect the driver. To this end, the floor closeout section near the driver's legs and feet was also constructed using a female mould, into which a single layer of carbon fibre was layed. This section also made best use of the available space within the frame and also restricted the number of suspension and steering components that intruded into the driver space.

Lastly, a nose cone was shaped to complete the closeout requirements, with aerodynamics not considered in detail due to the slow nature of the F-SAE course. The nose was shaped using a male mould (plug) which was painted to achieve a smooth finish. A female mould was then

layed over the plug using fibreglass, from which the final carbon fire nose could then be layed.

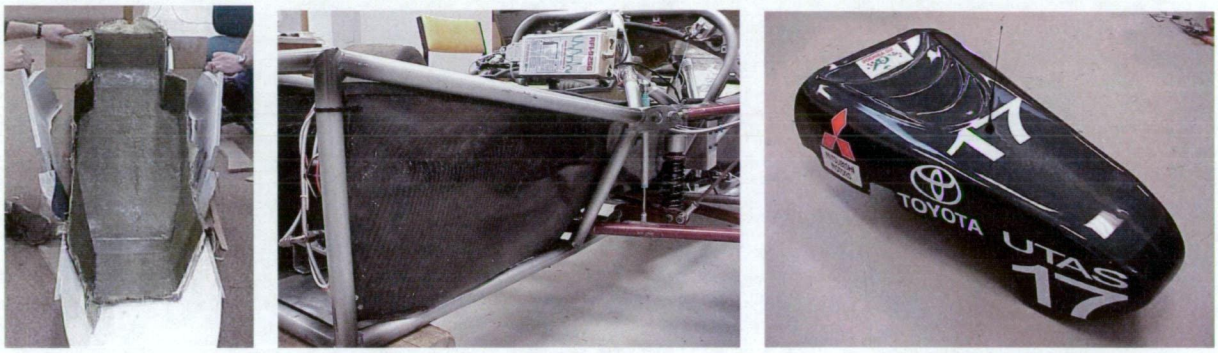

(a) *(b)* *(c)*

Figure 4.32: Closeout components, (a) seat, (b) floor & (c) nose

4.5.2. Steering Wheel

The F-SAE rules specify that the steering wheel must be a circular type of a minium diameter of 250 mm, and must incorporate a quick release mechanism to aid in driver egress. Such a steering wheel was installed into the vehicle, just out of the driver's view, as shown in Figure 4.33. However, the tight conditions within the cockpit limited arm movement significantly, so a high ratio steering setup was selected, with one full turn of the steering wheel going from full lock in one direction to full lock in the other. The incorporation of the adjustable steering wheel position was also used to make the system as comfortable as possible for the vehicle's range of drivers.

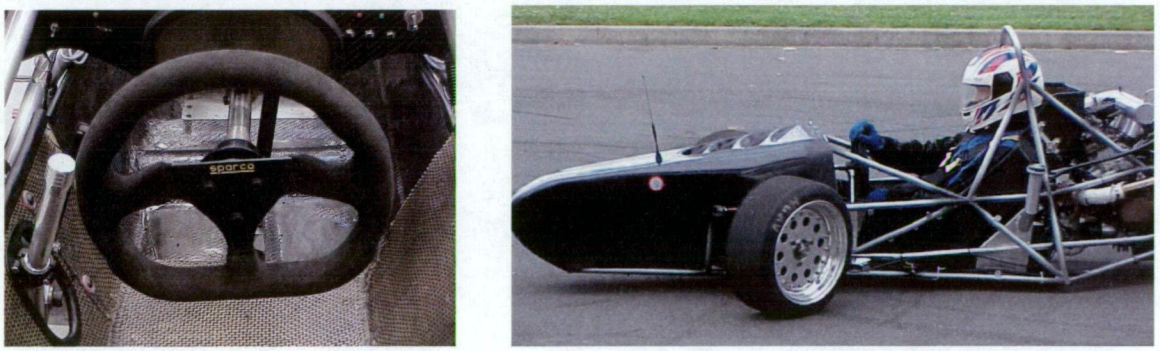

(a) *(b)*

Figure 4.33: Steering wheel, (a) position & (b) high ratio steering movement

4.5.3. Gear Shifter and Clutch

Since the gearbox installed within the vehicle utilises a sequential gearbox as discussed in the "Engine Systems Development" section, the only movement required to change gears is either forwards (up through gears) of backwards (down through gears). This means that the gear shifter could be constructed on the simple principle of a lever running to the gearbox by means of a linkage, depicted in Figure 4.34. The lever was also installed closely to the steering wheel to provide the driver with ease of movement between the two, and allowed simple adjustment of the lever position in accordance with driver requirements and steering wheel position.

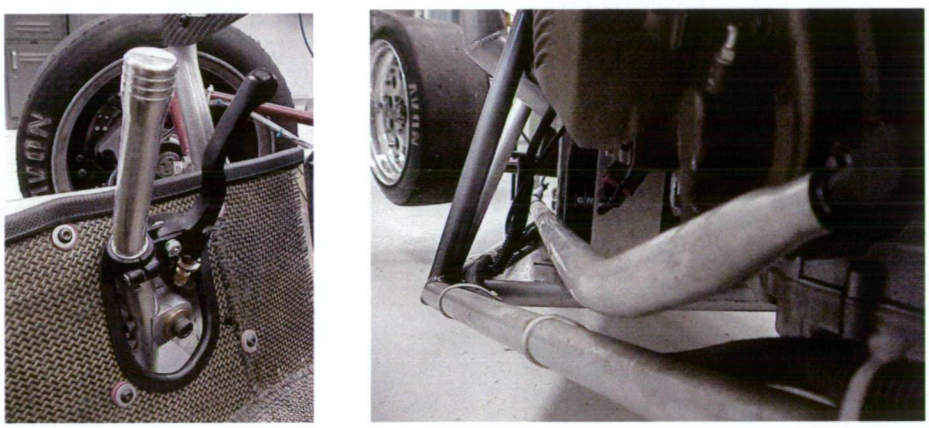

(a) *(b)*

Figure 4.34: Gear shifter, (a) lever and clutch & (b) linkage to the gearbox

In an effort to further increase gear change speeds, it was decided to move the clutch mounting position from the pedal assembly, as is standard in automotive design, to the gear shifter lever, to be used only when changing down gears. Early conceptual designs (Figure 4.35) for this arrangement tried to include the automatic operation of the clutch through a lever system when changing gears, but resulted in systems that required careful tuning and were slightly unreliable.

As a result, the simple addition of a motorcycle clutch to the gear shifter, as depicted previously in Figure 4.34, was chosen as the preferred option. This system proved to be easy to use and completely reliable, while also provided extremely fast gear changes and total control of the clutch.

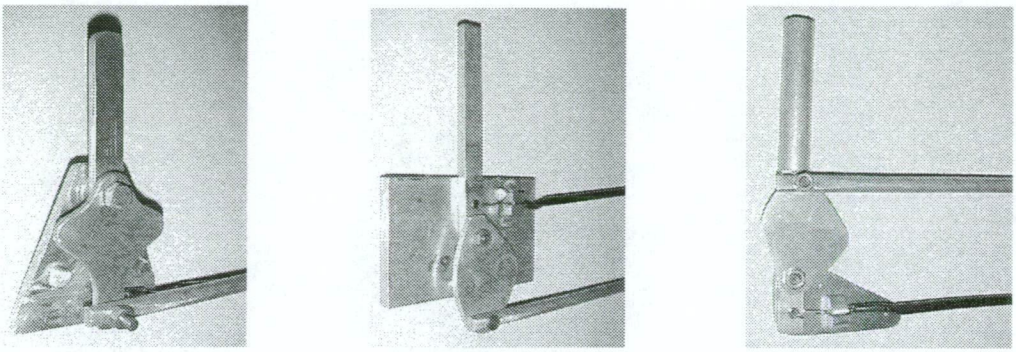

Figure 4.35: Automatic clutch early conceptual designs

4.5.4. Brake and Throttle Pedals

With the clutch designed for hand operation, the pedal arrangement required only the incorporation of the accelerator and brake pedals. This allowed for pedal operation using only one foot exclusively for each, similar to a go-kart style, allowing for much faster transition between accelerating and braking manoeuvres. Also, due to the non-adjustable nature of the seat design, it was decided to make the position of both these pedals modifiable. To this end, the two pedals were placed on an aluminium plate that could be bolted to the floor in a number of positions, as shown in Figure 4.36. This also meant that all of the connections to the pedals had to be flexible.

The throttle pedal was constructed out of aluminium plate and pivoted at its base, with the throttle cable connected to it to enable adjustment while minimising tight cable corners over the range of adjustment positions, which could effect throttle feel and possibly cause the throttle to stick open. The brake system was supplied by Wilwood® and includes twin composite master cylinders that control individual front and rear brake circuits that are proportioned by means of a balance bar incorporated into the aluminium brake pedal, as shown in "Appendix D". A brake over travel switch was also included into the brake system to cut power to the vehicle in the case of simultaneous hydraulic circuit failure, as was a microswitch to control the brake light.

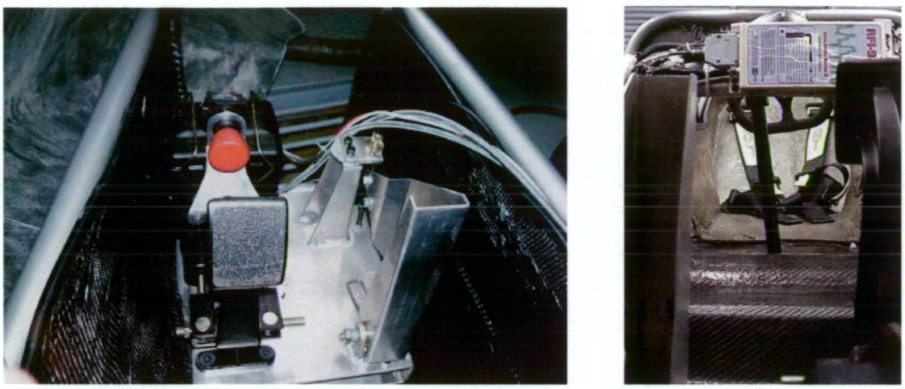

Figure 4.36: Brake and accelerator pedal positions

4.6. Engine Systems Development

The use of a motorcycle engine as the power plant for a F-SAE race car is more-or-less a standard choice. The 610cc displacement limit imposed by the rules [47] significantly reduces the possible sources from which an engine can be obtained, and motorcycle engines offer exceptional performance benefits. They are generally highly tuned and lightweight, and, coupled with the almost universal inclusion of a sequential gearbox, provide significant power within a compact unit. Most manufactures make a number of such 600cc engines of varying levels of performance and reliability depending on their application. In this case it was decided to focus on the high performance end of the market, and a 2000 model Kawasaki Ninja ZX6 engine was chosen, as shown below in Figure 4.37. This high revving in-line 4 cylinder, 4-stroke, water cooled super-bike engine with double overhead cam offered a compression ratio of 12.8:1 with large low RPM torque and high power within a 55kg (dry) unit with 6 gears. The engine also offered a deep oil sump (which is needed to ensure oil flow during high lateral accelerations) and an oil cooler that is integral to the water cooling system, reducing weight. The engine specifications are given in "Appendix E".

(a) *(b)*

Figure 4.37: 2000 model Kawasaki Ninja ZX6, (a) motorcycle & (b) separate engine

4.6.1. Fuel Injection System

The Kawasaki Ninja engine typically operates with a carburetted air intake system, with separate CV carburettors for each cylinder running from a single air box that receives ram air. This system offers efficient and lightweight fuel control under normal operation, but F-SAE specifications enforce two major limitations. Firstly, all intake air must pass through a 20mm diameter air restrictor, and secondly, the throttle body must be located upstream of the restriction. This, coupled with the fact that the motorcycle carburettors operate with degraded performance under high lateral accelerations and are inherently difficult to tune, lead to the choice of the addition of a fuel injection system.

This option was not without its difficulties either, the addition of a multi-point fuel injection system required the design and construction of many associated components and extensive tuning. The general schematics of the required injection and ignition systems are shown below in Figure 4.38 and Figure 4.39.

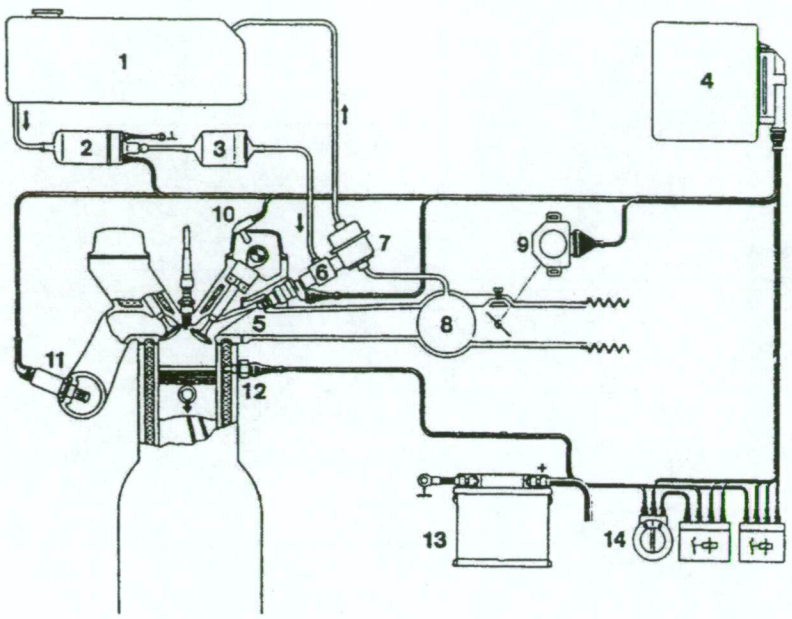

(1) Fuel tank, (2) electronic fuel pump, (3) fuel filter, (4) engine ECU, (5) fuel injector, (6) fuel distributor, (7) fuel pressure regulator, (8) intake plenum, (9) throttle position sensor, (10) cam angle sensor, (11) lambda sensor, (12) water temperature sensor, (13) battery & (14) ignition switch

Figure 4.38: Schematic of the pulsed fuel injection system

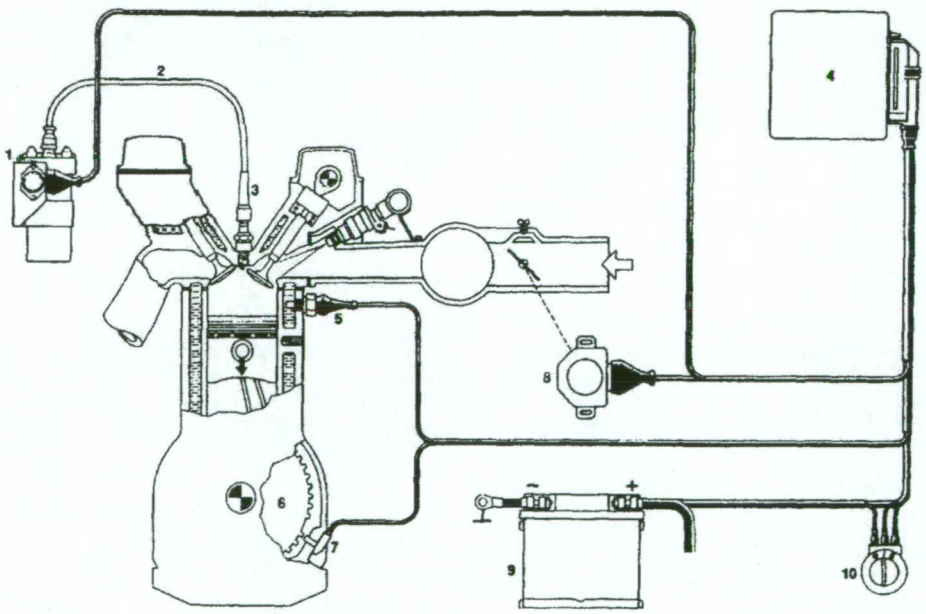

(1) Ignition coil, (2) high voltage lead, (3) spark plug, (4) engine ECU, (5) water temperature sensor, (6) crankshaft hall effect sensor wheel, (7) engine speed and crankshaft reference sensor, (8) throttle position sensor, (9) battery & (10) ignition switch

Figure 4.39: Schematic of the electronic ignition system

4.6.1.1. Air Intake Manifold

A well designed air intake manifold is of great importance in optimising the airflow to the engine. The design should avoid separation and extended boundary layers along with excessive turbulent eddies to provide efficient air delivery to the engine. A single plane induction manifold with all intake runners extending from a common plenum was chosen as the design basis, as depicted in Figure 4.40. This was chosen over a dual plane manifold option because the open plenum smooths out the induction pulses as cylinders periodically 'suck' in air more effectively, and can give better power in the high rev range.

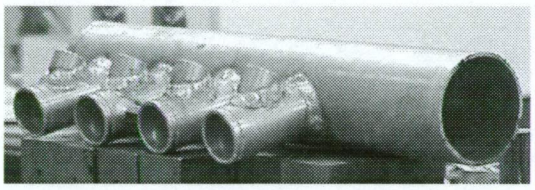

Figure 4.40: Single plane induction manifold

Intake Runner Diameter

The intake runners supply each cylinder with the air they require, and the way they do it can significantly alter engine performance. The first consideration is the runner diameter, which defines the speed at which the air must travel though it and the resulting pressure losses. Various texts specify that the air should not be allowed to travel at more than 60 m/s within each runner at maximum revs and, in this case, the runner diameter of 40mm defined by their mounts to the engine proved adequate.

Effective Intake Runner Length

The induction pulses generated as the cylinder valves open and close to allow air in (and air inertia) produce both high and low pressure waves along the intake plenum. These pulses can significantly effect the delivery of air to each cylinder and so can have large effects on engine performance. The goal of the design of the intake runners is to ensure that a high-pressure wave approaches the cylinder air intake valve as it opens, with the resultant high pressure forcing slightly more air through it.

Inspection shows that this sort of tuning will only work for specific rev ranges. As engine speeds alter, so does the size and timing of the induction pulses. For this reason the intake runners must be optimised for rev ranges where power is needed using the first (or second) set of pressure waves to increase air induction. An investigation into the operation of Ninja engine showed that at 12 000rpm (1 500rpm below red line) the effective runner length for the second set of pressure waves was approximately 42mm. It should be noted, however, that this theoretical calculation was an estimate only due to the complexities of the pressure wave dynamics. The only way to fully tune the runner length to specific rev ranges is through experimental analysis, observing the torque and power on a dynamometer or, better still, by track testing with an experienced driver. The problem is made increasingly complex since varying lengths may increase peak power but lower average power and torque. A balance needs to be found, which can only be identified through extensive experimentation, requiring large resources and time that were both unavailable. The limited investigation carried out, however, produced an intake runner length that proved to be very efficient, providing comparatively large torque and power throughout the rev range.

Plenum Volume

The appropriate size for the plenum depends on a number of complex factors. However, a general rule exists to construct the plenum to a volume of at least 50% of total engine displacement. To this end, it was decided to not go into the complexity of optimum design, and a plenum of volume 1.7 litres was built.

4.6.1.2. Air Restrictor

The purpose of the 20mm diameter air restrictor layed out in the F-SAE rules is to reduce engine power for safety and competitive reasons. All air that is used in combustion must pass through this 20mm orifice, which produces a significant pressure reduction in the plenum at high revs, thus restricting air flow and associated engine power and torque. The restriction imposed by this component can be extremely severe, and so must be designed for optimum performance.

From basic computational flow theory the best application here to maximise airflow is the use of a converging diverging nozzle. The contraction ratio was defined by the surrounding

components to be 57/20 at each end of the nozzle, and so the design criteria became the exit flow uniformity and boundary layer thickness, separation, choking and space the physical space and cost of the component.

Calculations were made on a number of different nozzle designs, but manufacturablity imposed a number of limitations. The idea matching cubic curve converging section of the nozzle was abandoned for this reason and replaced with a simple radius converging section. This was followed by a short 7° diverging section to meet the plenum diameter to reduce boundary layer sizes, as shown in Figure 4.41.

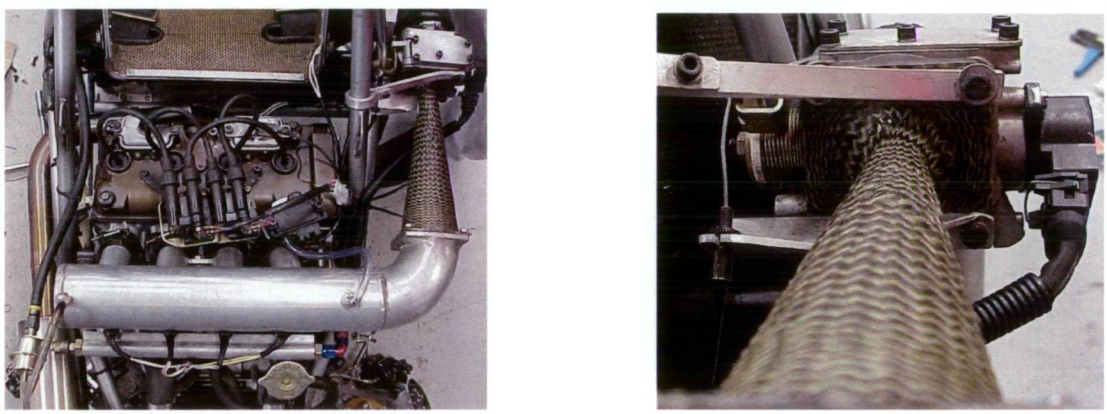

(a) *(b)*

Figure 4.41: (a) Intake system & (b) restrictor

4.6.1.3. Throttle Body and Air Cleaner

A throttle body was selected with a butterfly valve diameter of 57 mm to enable efficient air flow but maintain throttle responsiveness. The unit was also chosen because it provided a throttle position potentiometer, which is required for the fuel injection control, and mounted a cone shaped K&N air filter that provided reduced airflow restrictions and enabled ram air effects.

4.6.1.4. Fuel System

In the design of the fuel system, the first consideration was to calculate the maximum fuel flow rate required for the choice of fuel pump and injectors. The maximum required fuel flow

for each cylinder at maximum revs and maximum power was considered as follows (for unknown volumetric efficiency):

Air used at 12,500 RPM	= 9,000,000 cc/min
	= 2.2 kg/min
Required fuel flow	= 0.000166 kg/min
	= 221 cc/min

This means that for the four cylinders of the engine, the peak fuel flow will be almost 900 cc/min. However, due to F-SAE rules which state that a threaded or OEM type connection is required throughout the fuel system, a fuel pump could not be sourced that delivered this comparatively small amount of fuel at the high pressure required by the fuel injectors. As such, a much larger fuel pump was selected than necessary, with a 2.5 bar regulator mounted at the end of the fuel rail to recirculate unused fuel back to the fuel tank, depicted below in Figure 4.42. This provided a constant fuel pressure to the injectors, and considering a maximum cylinder fuel flow of 221cc/min, enabled the correct choice of injectors. This was important because injectors that have a pulse width that is too large do not allow the engine to idle well because their minimum injection time cannot restrict fuel flow enough, while too small injectors cannot provide enough fuel at high revs.

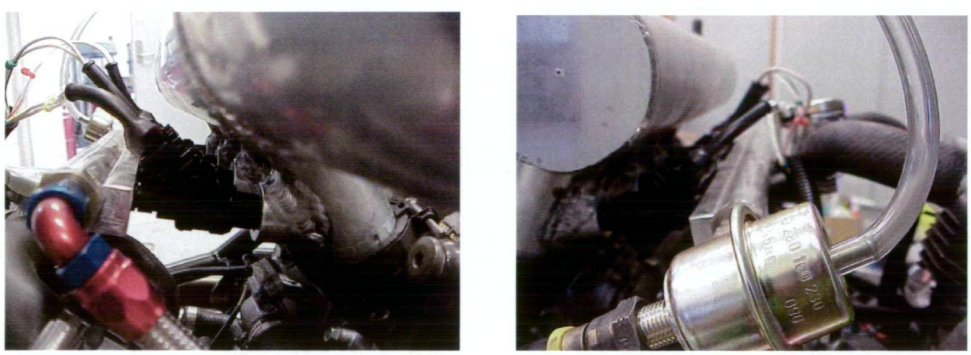

(a) *(b)*

Figure 4.42: Fuel injection system, (a) injectors & (b) fuel regulator

4.6.1.5. Engine Management System

Extensive research and management system comparisons were conducted into engine electronic control units (ECU) and the MoTeC M4-Pro system shown in Figure 4.43 was

found to best suit our purposes. The system provided sequential injection that was desired for fuel efficiency and optimum fuel injection timing, but required the installation of a Hall effect sensor on the camshaft in addition to the factory crank angle sensor. This system also provided 3D-map programming of the engine parameters and had the option of closed or open loop operation from an exhaust oxygen (Lambda) sensor for improved fuel economy or performance control. It also included oil pressure and water temperature sensor inputs, as well as the facility to include engine based traction control within its operation from wheel speed measurements.

The system was installed according to the wiring diagram given in "Appendix E" to use either the throttle position sensor (located on the throttle body) or the manifold air pressure (MAP) sensor located on the plenum as the controlling variable. After extensive tuning with both sensors it was found that the throttle position sensor provided better engine response, and so was chosen as the driver's controlling variable over the engine management system. Other data inputs to the ECU that were provided were water and air temperatures, which were included to enable cold start enrichment at low temperatures and fuel mixture adjustments depending on air density respectively.

The engine was then tuned using a combination of dynamometer and track testing for a Lambda reading of 0.89, which equates to an air/fuel ratio of 13.8:1. This provided a balance between the stoichiometric value of 14.7:1 for fuel economy and approximately 13:1 for maximum power.

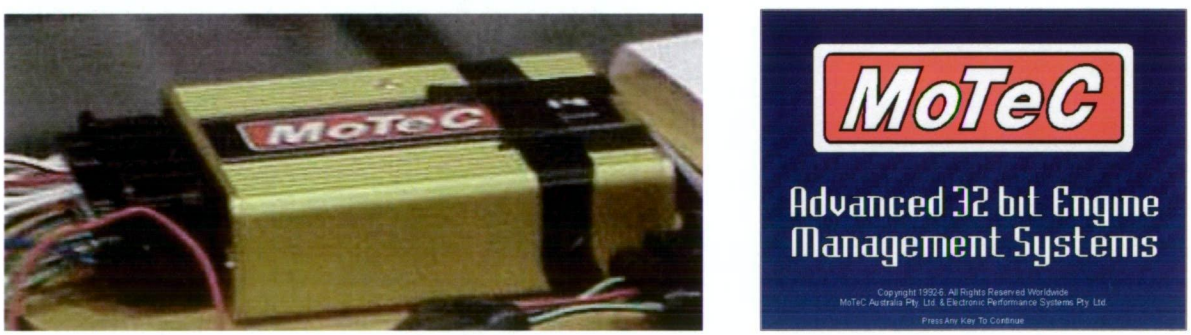

(a) *(b)*

Figure 4.43: ECU, (a) computer & (b) tuning software

4.6.2. Exhaust

The exhaust system was designed originally to accommodate the addition of a turbocharger. However, due to a number of factors including exceptionally long delivery times, the restrictions imposed by the F-SAE rules, and the expected marginal increases in performance it was decided that the addition of the turbocharger was not a worthwhile pursuit. The four into one exhaust system, illustrated in Figure 4.44 was constructed in two pieces, with a mounting flange connecting the two where the turbo was supposed to be positioned.

The outlet ports of the engine defined the diameter of the extractors of 25.4mm, which were constructed from a number of stainless stain mandrel bends that lead to the 4:1 junction. A 50.8mm diameter stainless steel pipe then lead from the junction, to a muffler constructed as an integral piece. The muffler was designed as a 'straight through' type, constructed by surrounding a perforated pipe with fibreglass, and tuned in length to reduce the noise in the higher rev ranges. A Lambda sensor was also installed at the 4:1 junction.

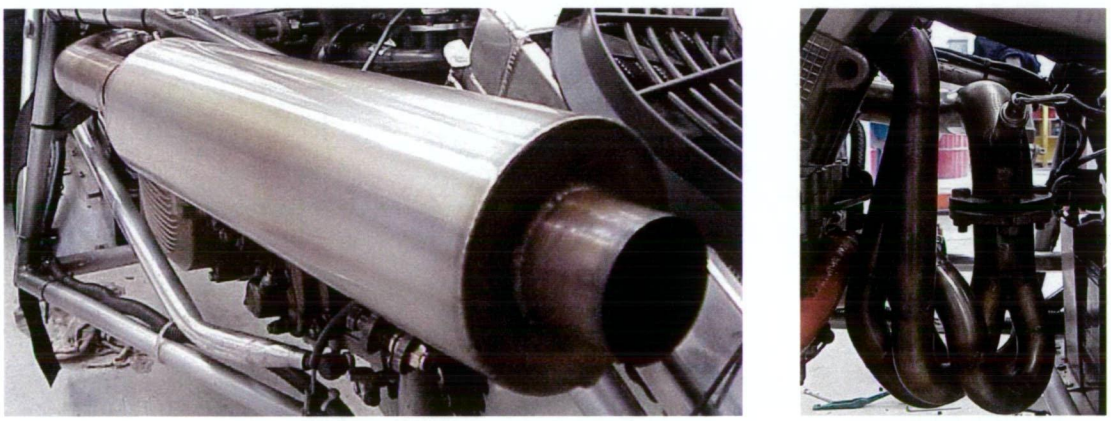

(a) *(b)*

Figure 4.44: Exhaust system, (a) muffler & (b) extractors with Lambda sensor installed

4.6.3. Radiator

The placement of the radiator into 'side pods' on the racecar was decided against after much deliberation. It was observed that, while the increased airflow within the side pods would ensure more effective cooling, the pods and required hose lengths would increase vehicle weight and drag. Coupled with the low speed nature of F-SAE racing it was decided that the

cooling requirements could be met with a radiator placed at the rear of the vehicle with twin thermo-fans, as shown in Figure 4.45, and a separate high flow rate electric water pump.

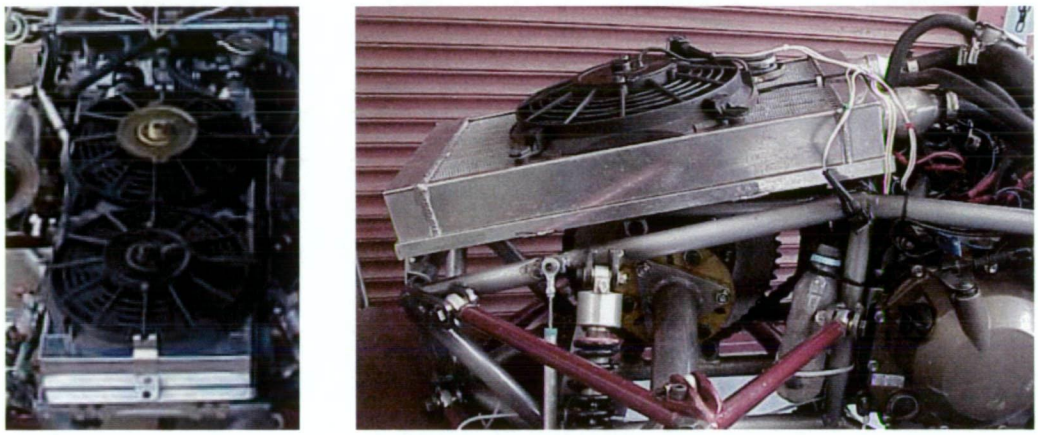

Figure 4.45: Radiator positioning

4.6.4. Fuel Tank

The F-SAE rules specify that the fuel system must have a volume of less than 7.5 litres and also state that the maximum distance raced during competition is 22 km. Since it is desirable to carry the least fuel load that is possible, the fuel tank must be designed to allow scavenging of as much fuel as feasible, without fuel surge as the liquid moves during cornering and acceleration. To this end, and after some experimentation, it was decided to build a fuel tank of just 5 litres to be placed under the seat, as shown in Figure 4.46. Since the placement of the tank required it to be long and shallow, special care was taken to avoid surge by installing foam and including a small, baffled, chamber at the fuel pump pickup.

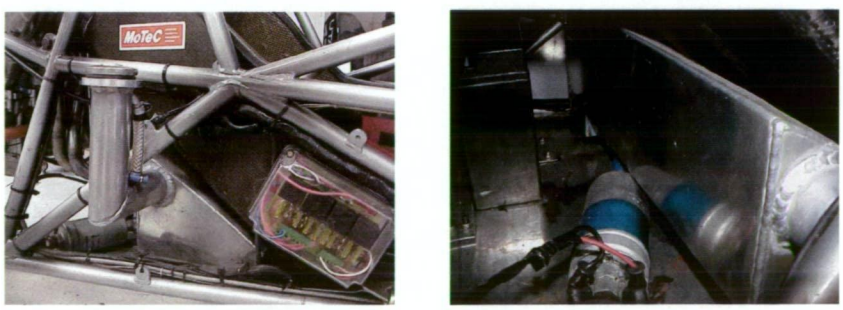

Figure 4.46: Fuel tank

4.7. Drivetrain Development

The engine gearbox and clutch specifications are given in "Appendix F". As described above, the use of a motorcycle engine is very common within F-SAE. However, this produces the unique problem of converting the engine chain drive output to provide sufficient torque to the driven wheels, while ensuring cornering ability and low power losses with minimal weight.

4.7.1. Differential Selection

The use of a differential is almost universal in F-SAE. The tight turns that the vehicle experiences, coupled with the suspension requirements within the rules, make the use of a differential a necessity for efficient cornering. Investigation showed that the use of a front wheel drive differential also provided a solution to the problem of making use of the chain drive. By mounting the differential bearings to the frame, a sprocket can be bolted onto its circumference so that engine torque can be delivered to it, and thus to the driven wheels. This use of sprockets also enables relatively simple adjustments to the final drive ratios to be made in accordance with the track requirements.

Extensive searches were conducted and it was found that Quaife® made a differential specially modified for the competition, as illustrated in "Appendix F". Their fully sealed, automatic torque biasing (ATB) limited slip differential was purchased, and proved effective in testing as the smallest and lightest automatic torque biasing differential available in maintaining maximum traction during acceleration and cornering, and is shown in Figure 4.47. It also allowed the simple addition of a blank motorcycle sprocket that was machined to fit, but required the additional construction of splined inserts to the drive shafts.

(a) (b) (c)

Figure 4.47: Differential, (a) with bearings fitted, (b) mounting position & (c) spline milling

4.7.2. Chain Tensioner

Because both the engine and the differential were designed to be fixed in place on the frame, a facility to tension the drive chain need to be included. This was accomplished by the addition of a chain tensioning gear near the smaller, drive sprocket. The gear was designed to be mounted from the frame in a manner that allowed it to pivot and thus apply tension to the chain. An adjustment bolt mounted directly to the engine then supported the chain tensioner, as depicted below in Figure 4. 48.

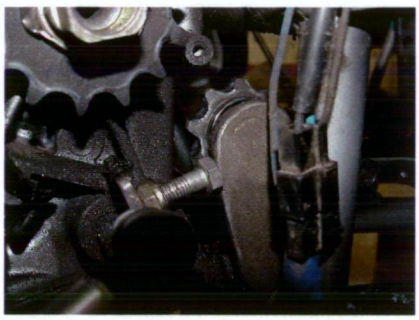

Figure 4.48: Chain tensioner (without chain installed)

4.7.3. Composite Discs

The common method of providing torque from the differential to the driven wheels is through drive shafts, hinged with either universal or CV joints. However, since the required suspension travel was small (25mm in jounce and in rebound), an unconventional approach was taken, incorporating kevlar composite discs, supplied by GKN Motorsport®, into the design to replace the joints, shown in Figure 4.49 and dimensioned in "Appendix F".

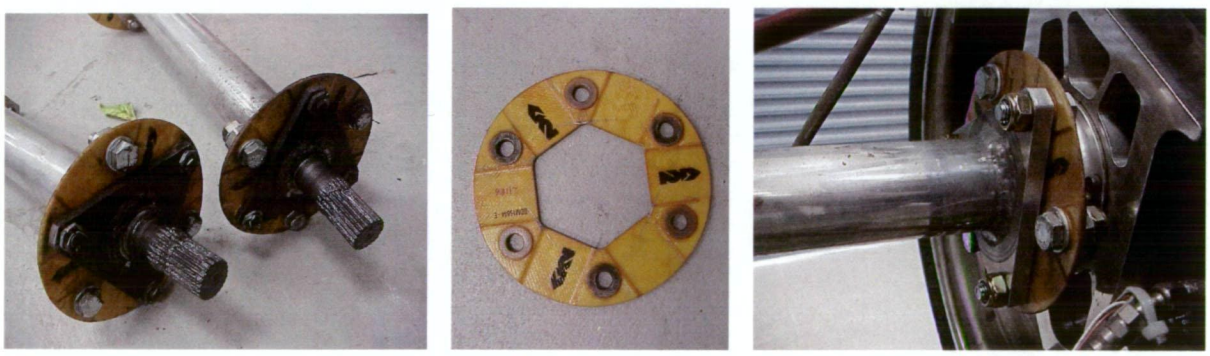

Figure 4.49: Kevlar composite discs

The composite discs themselves are made form laminated unidirectional kevlar fibre and weigh only 55g each (compared to 1.5kg CV joints), despite having a transmission of torque rating of over 1000Nm. However, they operate by flexing between the two shafts connected to them, and so are restricted to only 3° deflection for continuous running and 6° instantaneously, imposing significant limitations on the placement of the differential. This amount of deflection was within what was expected during driving, and had the side benefit of providing power transmission efficiency close to that of a solid shaft because of the required near perfect operating alignment. Additionally, the plunge required for their operation was supplied by the splined inserts to the differential.

4.7.4. Drive Shafts

Another benefit from the use of the composite discs was the easy addition of large diameter aluminium-alloy tubes that were both stiffer and lighter than the traditional solid steel, as shown in Figure 4.50. This unconventional approach was achievable since the drive shafts could to be flanged and bolted directly to the composite discs, a feature that normal CV joints make very difficult.

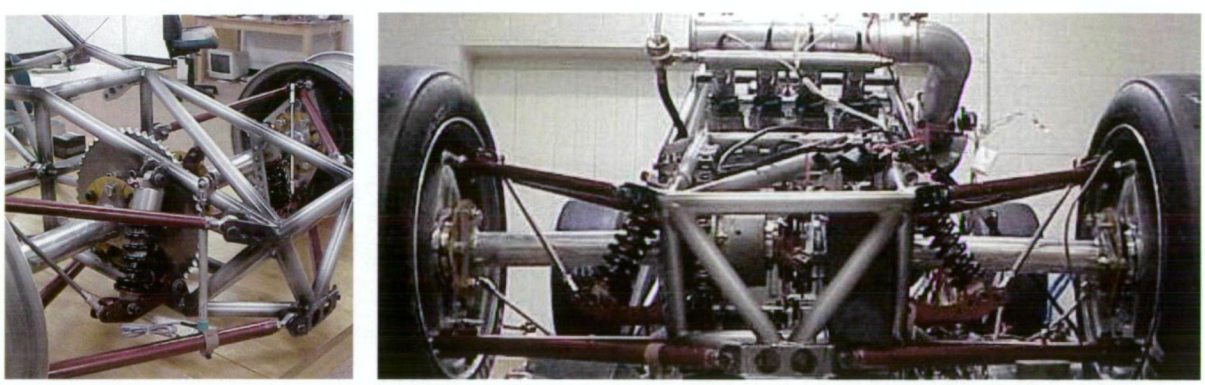

Figure 4.50: Large diameter aluminium drive shafts (note also the near perfect alignment required by the composite discs)

The aluminium drive shafts were designed to exceed the strength and stiffness offered by a traditional 22mm steel drive shaft, which are commonly used in racing applications of this nature. Various aluminium sections were analysed using FEA techniques to investigate torque ratings (yield torque) and torsional deflections for each possibility, as depicted in

Figure 4.51. The result was the choice of a 6mm wall, 50mm OD aluminium section that proved much lighter and many times stiffer than the steel option.

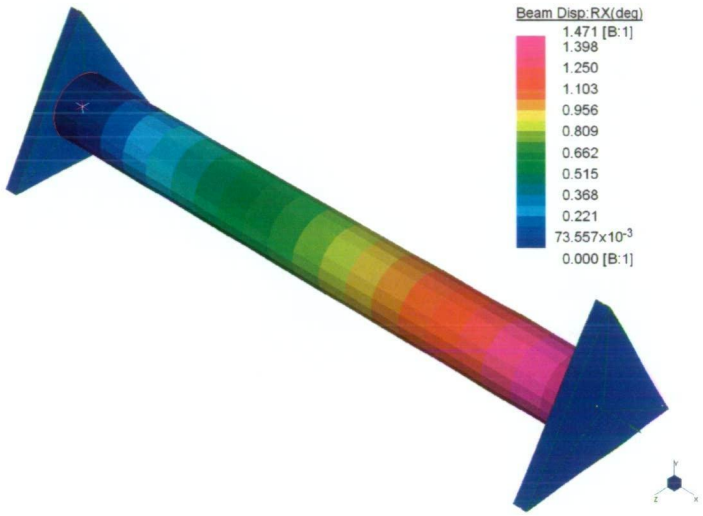

Figure 4.51: Drive shaft FEA defection under 500Nm (not including end plate effects)

4.8. Electrical Systems Development

In developing a working electrical system for use in the intelligent car project the following objectives were identified as essential:

- Simplicity - this includes things like minimising the number of wires, using common parts where feasible and designing straight runs between common points.
- Ease of fault finding – creating fault finding access locations, common locations of like components and using fully colour-coded looms.
- Minimal maintenance requirements – the system developed must be robust and require little maintenance.
- Neat and aesthetically neutral/appealing.
- Open architecture and expansion capability – for further development of on board electrical systems.

4.8.1. Wiring Loom Design

The wiring loom was designed to fit neatly away from the major moving parts of the car most likely to cause damage. For this reason the engine electronic control unit (ECU) was located well away from the engine, and positioned under the seat with the ignition module bolted to the floor. Further protection of the ECU was not deemed necessary since it was designed to be waterproof. The wiring loom from the ECU was then positioned to run down the right hand side of the driver to the fuse box located on the side of the seat. The bulk of the remaining loom then continues along this line to a junction with the wiring from the battery, located near the starter motor and alternator on the left hand side of the vehicle.

4.8.1.1. Wire Specification

The wire utilised in this design was chosen to withstand the foreseeable harsh driving conditions. Standard automotive wire has been specifically developed to withstand bombardment with dirt, oil, heat water and low temperatures and hence was specified for all wiring connections. Wiring sizes were taken from the largest likely current rating of each individual component they served. For instance, the fan wiring could expect a continuous operational current of between 2 and 3 Amp with a stall or start up current in the vicinity of 7 Amp. In this case the wire chosen was rated at 10 Amp. The trade off in weight for this type of decision was deemed necessary for the absolute reliability required of the electrical system.

Additionally, to ensure easy removal of all components and improved signal to noise ratios in respect to the senor wiring, all wires were crimped, and not soldered. Also, where possible, large multiple connectors were used to eliminate the possibility of misconnection upon re-installation of components.

4.8.1.2. Wire Protection

For reliability during testing it is imperative that the complete wiring loom be dependable in all weather conditions. The major concern in this case was rain and contact with water and mud under wet track conditions. The insulated cables within the wiring loom were further insulated by comprehensive wrapping in electrical tape in all areas exposed to the elements. Care was also taken to ensure that the wiring was positioned as far as practical from hot

objects, especially from around the exhaust system. All other exposed wires were then wrapped tightly and neatly by hand and covered where possible with conduit for reasons of aesthetics and extra durability.

4.8.2. Fuse Box

The most vulnerable components of the wiring system were identified as the system of relays and fuses that allow the MoTeC system to control the higher currents of the engine control system. In order to protect these components it was decided to place them into a sealed, yet easily accessible, fuse box located on the side of the seat to minimise wiring length, and is shown in Figure 4.52 and detailed in "Appendix G".

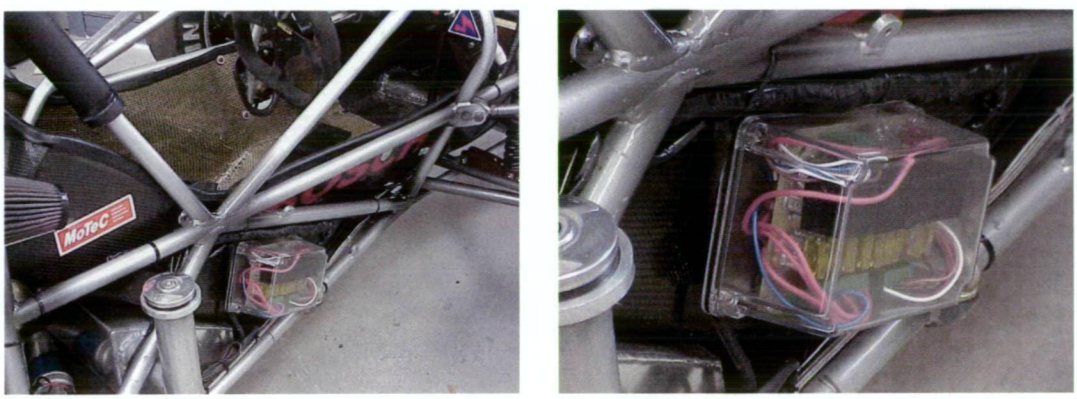

Figure 4.52: Fuse box

4.8.2.1. Physical Considerations

In fitting with the major objectives of the electrical system, the original loom design with in line fuses and multiple bulky relay mountings was re-designed to incorporate a single fuse and relay box. The box itself is made of clear material for reasons of fast identification of loose connections or burnt out fuses and relays, as well as aesthetics. The wires are grommeted and fed in groups through the back of the box to allow removal of the box without the loom and vice versa, while maintaining waterproofing. The cover is then screwed onto the aluminium backing plate that is mounted to the frame.

4.8.2.2. Circuit Design

The circuit for the fuse box was taken almost directly from the MoTeC ECU wiring diagrams. Major alterations involved the removal of a relay that was redundant in this particular application and the unification of relay types used throughout the vehicle. For instance, a diode activated relay was replaced with an in line diode and a standard relay to fulfil informality. Extra fuses were also included for each of the major components, allowing for very simple component fault finding.

One of the major objectives of the fuse box was to find a neat and effective way to mount all the required relays and fuses in one place where they could be easily accessible to check and change. The ideal situation was chosen to be a set of closely located relay and fuse sockets on a printed circuit board, which was consequently layered with solder tracks to increase the current rated capacity to in excess of 12 Amps.

4.8.2.3. Fuse Specification

Load ratings of fuses were selected according to the components they served. In general, fuses will withstand up to their rated current plus 200% for 2 minutes. The majority of components have around 7-8 Amp start up current with a continuous 2-3 Amp while running, so 10 amp fuses are most common within the electrical system. Automotive fuses were specified for their compactness, physical durability (plastic cases) and ease of mounting.

4.8.3. Dashboard

The dashboard is the driver's control panel, as shown in Figure 4.53. It was constructed from a composite sandwich of carbon fibre and foam constructed using vacuum bagging techniques, with the fibre set up on sheets of window glass to ensure a good finish. Profile cutting, drilling and finishing were all performed after the bonding process, and the dash attached to the frame through bolts and welded tabs.

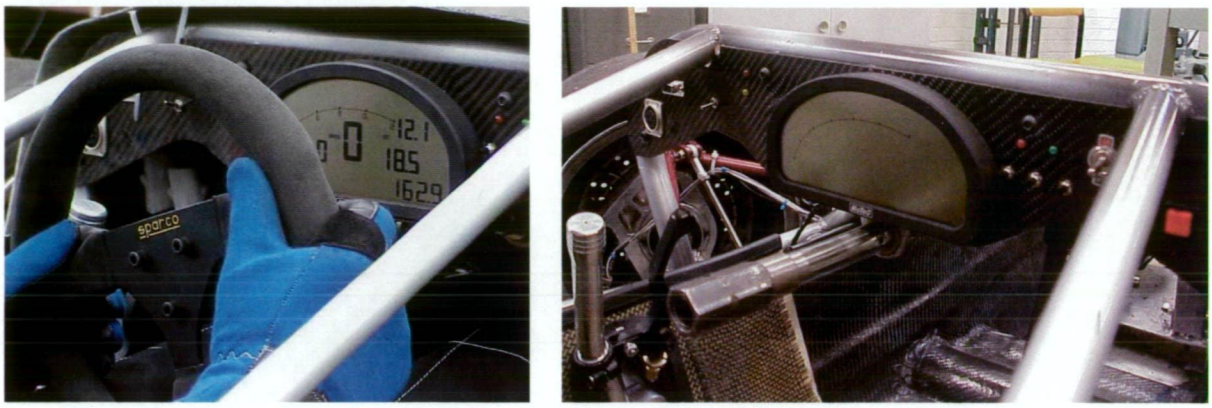

Figure 4.53: Dashboard layout

The dash contains:

- The Advanced Dash Logger (ADL), providing a programmable, digital display of many driving parameters, with 3 control buttons
- Gear change LEDs
- Neutral indicator and oil pressure warning LEDs
- 3 power switches for the ECU, ADL and the entire electrical system
- A starter motor button
- 2 computer COM ports for the ECU and ADL

The COM ports featured in the dash are used to facilitate fast and easy connection of the on-board computer systems to an external computer for information retrieval and further programming. The COM ports are installed in the dash with another set of plugs connected to them behind the dash to which the ECU and ADL are connected, facilitating easy removal of individual units. Further consideration was also made to allow the removal of the dash by placing all further connections within two main connectors. The detail of the wiring can be seen in Figure 4.54.

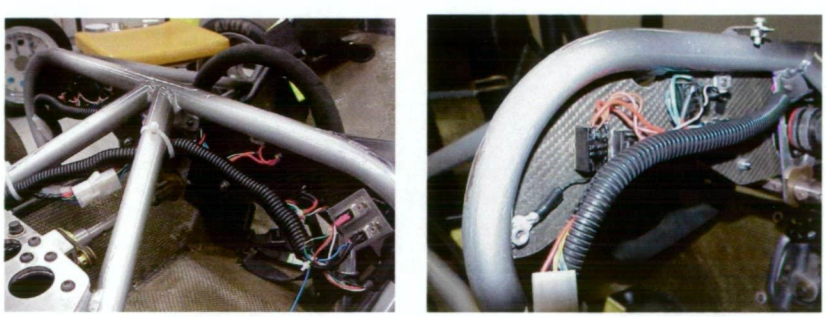

Figure 4.54: Dashboard wiring

4.8.4. Kill switches

Power for the entire car may be instantly cut using any one of three kill switches, depicted in Figure 4.55, which are placed by the engine, on the dashboard and as a brake over travel switch (all imposed be F-SAE rules). The brake over travel switch is located behind the brake pedal and is designed to activate only if the brake is depressed when there is a simultaneous failure of both independent braking systems (front and rear).

Cutting any one of these switches will deactivate the switch line to the main relay, which sources all power to components within the vehicle. Both human operated kill switches are clearly labelled with the international electrical symbol of a red spark on a white-edged blue triangle.

(a) *(b)* *(c)*

Figure 4.55: Kill switches (a) on dash, (b) at engine & (c) on brake

4.8.5. Brake Light

A brake light of 15 watt or equivalent is required within F-SAE rules, and is required to be mounted centrally between the wheel centres and the driver's shoulder height, at the rear of the vehicle. For aesthetic reasons a high intensity LED arrangement was selected with the LEDs mounted in parallel to prevent failure of the complete brake light in the event of single LED failure.

4.8.6. Engine Cam Sensor Circuit

The engine cam angle sensor is used by the ECU to determine the location of the pistons for fuel injection timing, as described in the "Engine Systems Development" section. The sensor

is a small hall effect type, similar in appearance to a transistor, and reads the rotation of a small permanent magnet mounted in the cam sprocket. The pulse from the sensor must be amplified to be read by the ECU input, which is done using a simple MOSFET amplification circuit. The circuit was built on printed track circuit board and mounted in a box on the outside of the engine, using kevlar insulated wiring to protect the system from the high engine temperatures.

4.9. Performance Characteristics

While the sections above give a brief description of the design and manufacturing processes used throughout the construction of the test vehicle, it is the interplay between components that dictate the vehicle performance on a whole. It is possible to derive huge amounts of power from an engine, but this power becomes void if the wheel arrangement does not allow power transfer to the road through the drivetrain. Similarly, the benefits from well-designed suspension geometries can be cancelled out if the spring rates are not of correct magnitude. It becomes necessary to consider all of the effects between the various aspects of the vehicle in order to prevent excessive design of components that will have little effect on performance, and to marry components together so that they compliment each other in operation. Simply stated, vehicle performance is defined primarily by the arrangement and effectiveness of components with respect to the entire vehicle, and not by individual elements. To this end, the overall specifications and performance characteristics of the vehicle are supplied in Table 4.5, with the measured acceleration field under a number of driving trials given in Figure 4.58.

To date, the vehicle has performed exceedingly well. In the seven months that the vehicle has been running it has driven approximately 1000km at a number of sites within Tasmania and Victoria, Australia, including racetracks, go-kart tracks, skid pads, airports and carparks, with some shown in Figure 4.56. In that period, it has travelled in wet and raining conditions without incident, as well as being involved in a number of small collisions due to driver inexperience, with the resulting damage limited to inexpensive and easily available parts. The majority of the testing was completed at Baskerville racecourse, where the vehicle has proven to perform better than the most of the racecars in the area. The test vehicle has shown consistently faster times than Formula V racecars on the track and posted a fastest time just

seven seconds above the track record of 53s. This is all despite the exclusive use of student drivers, all of whom are inexperienced to race driving, and the fact that the vehicle reaches its top speed (chosen for safety at 150km/hr) in three position on the track, often sitting on it for up to 9 seconds per lap.

Figure 4.56: Testing grounds used within Tasmania, Australia, (a) Baskerville raceway, (b) Baskerville pit area, (c) University carpark, (d) Derwent Entrainment Centre go-kart track.

The vehicle has also competed in the international Formula SAE competition, held in Melbourne during December 2001, depicted in Figure 4.57. The Australasian based event attracted entries from 14 Australian university and/or TAFE team combinations and the 4 leading international teams from the US and UK competitions. At the competition the test vehicle performed consistently well in all of the four dynamic events, posting competitive times for each. It particularly went well in the acceleration event, covering

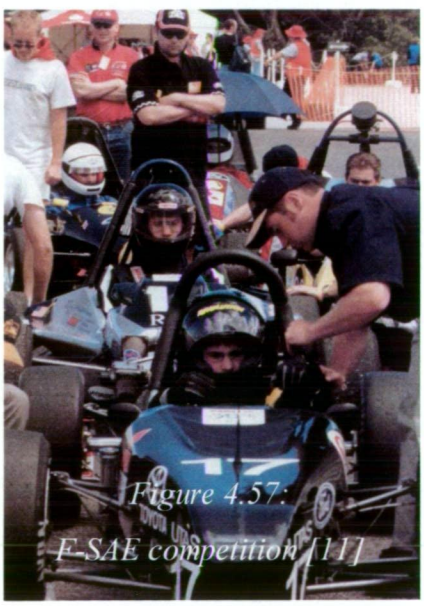

Figure 4.57: F-SAE competition [11]

75m in 4.32s, besting all of the Australian teams and coming second by only 0.06s to Rochester Institute of Technology, who is placed as one of the top international teams of the 150 strong international field. The final overall F-SAE result posted was third within Australasia and sixth internationally, with an additional award gained for vehicle testing.

Dimensions:	
Wheelbase	1830 mm
Overall length	2810 mm
Rear track width	1100 mm
Front track width	1200 mm
Overall width	1380 mm
Ground clearance	30 mm
Overall height	925 mm
Dry mass	255 kg
Wet mass	270 kg
Fuel tank capacity	5.0 L
Front/ ear weight distribution (77 kg driver)	49 / 51
Minimum turning radius	5.0 m
Frame:	
Type	Mild steel tubular space frame
Total weight	35 kg
Front tyres	Avon 6.5/19.5-13" racing slicks
Rear tyres	Avon 7.2/20.0-13" racing slicks
Suspension type	Double wishbone with pull rod
Maximum wheel travel	25 mm
Brakes	Four wheel aluminium rotors and calipers
Steering	Worm and sector, with adjustable rates
Engine:	
Capacity	599 ml
Bore and stroke	66 x 43.8 mm
Compression ratio	12.8
Injection system	MoTeC / Bosch custom multi-point
Water pump	Electric

Radiator	Custom built, with two thermo-fans
Maximum power (measured at wheels)	72 HP
Drivetrain:	
Clutch	Wet, multi disc
Transmission	6 speed, constant mesh
Final drive type	Chain
Final drive reduction ratio	3.786 (53 / 14)
Differential	Quaife automatic torque biasing LSD
Drive shafts	Aluminium tubing
Drive shaft joints	GKN composite discs
Performance:	
Maximum speed	150 km/hr
Maximum braking deceleration	1.4G (wet weather tyres on dry asphalt)
Maximum acceleration	1.3G (wet weather tyres on dry asphalt)
Maximum lateral acceleration	1.5G (wet weather tyres on dry asphalt)
Acceleration time over 75m (to 109 km/hr)	4.32 s (slick tyres on dry asphalt)

Table 4.5: General vehicle specifications

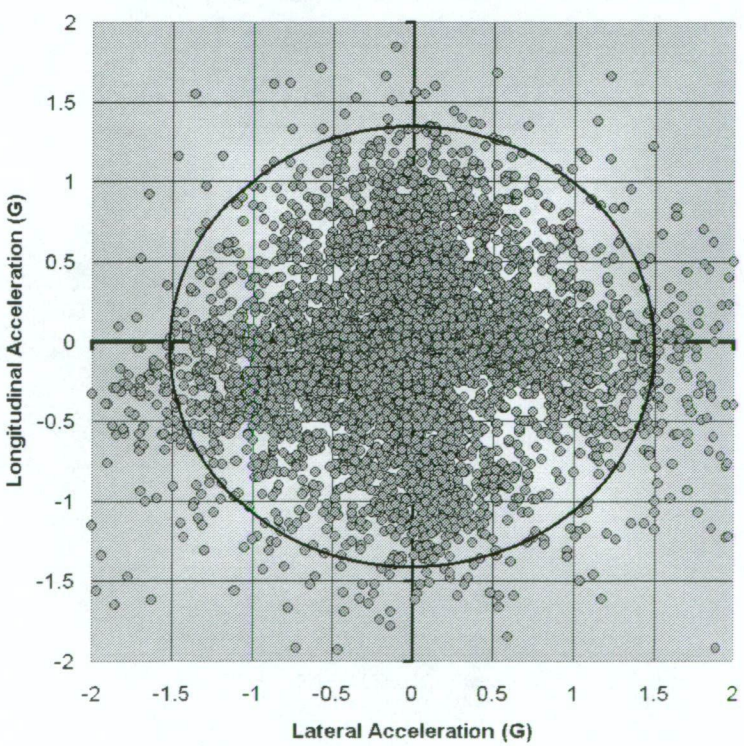

Figure 4.58: Test vehicle acceleration field (on wet weather tyres on dry asphalt)

CHAPTER 5

OVERVIEW OF EXPERIMENTAL INVESTIGATION AND SET UP

As mentioned in "Chapter 1", the philosophy behind this study was to measure as many vehicle parameters as possible that may have an effect on TCS operation, and to discard the ones that were shown to have little impact in the artificial neural network models predictions. To this end 40 parameters were dynamically measured, including 19 chassis based parameters, 4 engine based parameters and 17 calculated values, to cover most aspects of the vehicle dynamics system. These parameters are given below and the associated sensor locations depicted in Figure 5.1.

Chassis Parameters

- Time
- Four individual wheel speeds
- Four individual suspension positions
- Steering wheel angle
- Brake hydraulic pressure in the front and rear circuits
- Dynamic acceleration in three axes
- Yaw angular rate
- Yaw, pitch and roll angles (referenced from magnetic north)

Engine Parameters

- Engine RPM
- Throttle position
- Lambda value
- Efficiency point

Calculated Parameters

- Gear (calculated from RPM and drive speed)
- Pitch and roll angular rate (differentiated pitch and roll angles)
- Ground speed (averaged front wheel speed)
- Distance (ground speed integration)
- Drive speed (averaged rear wheel speed)
- Driven wheel slip (from rear wheel speed and ground speed)
- Drive slip (calculated from drive speed and ground speed)
- Individual wheel accelerations (differentiated wheel speeds)
- Individual suspension velocities (differentiated suspension positions)

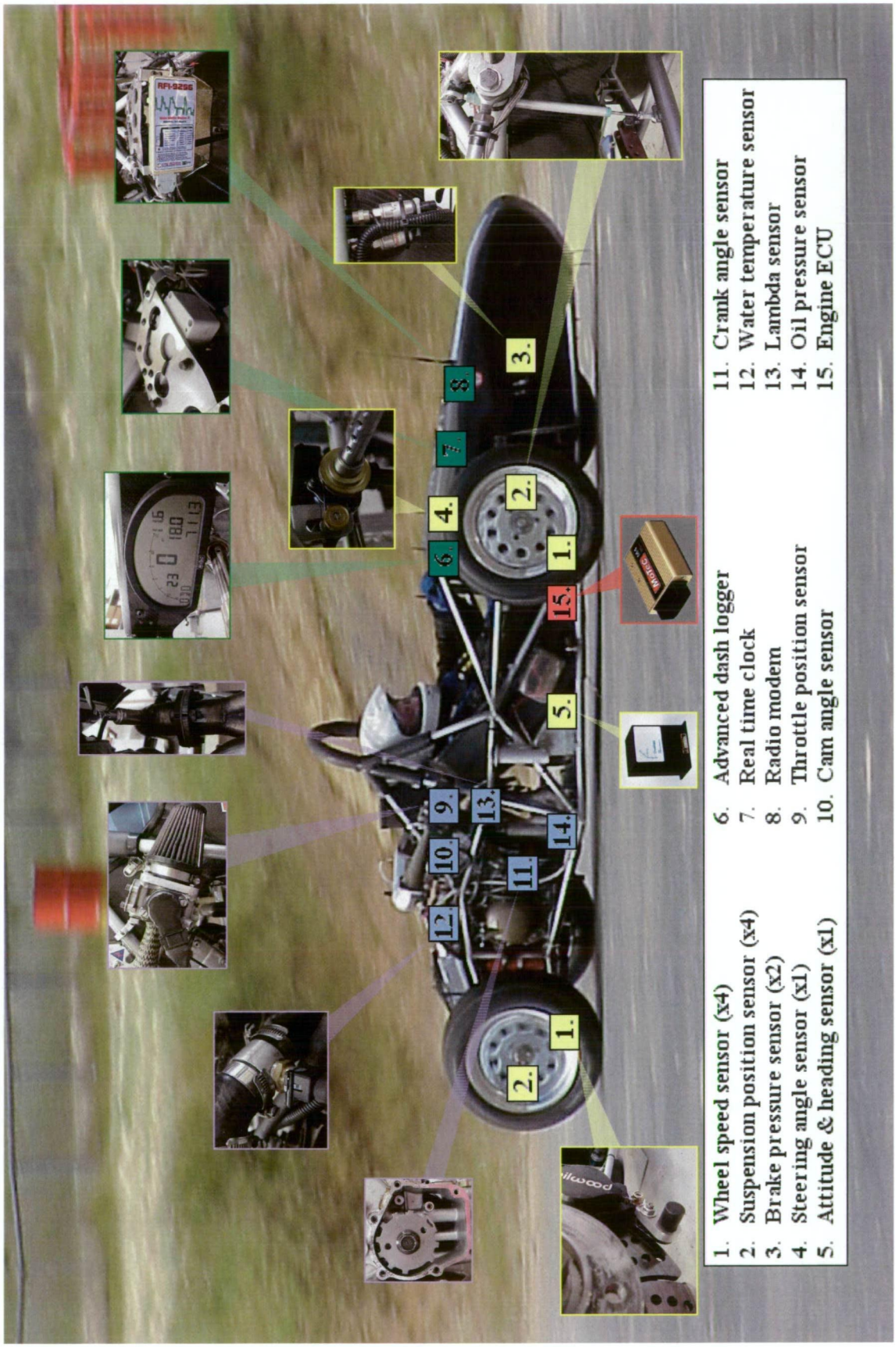

Figure 5.1: Sensor locations

It can be seen that a number of the engine parameters to be logged are recorded by the engine ECU, as discussed in "Chapter 4". As such, their operation will not be discussed further, other than to note that a number of these parameters have been omitted from sensory inputs due to data logging limitations and their perceived negligible effects on vehicle dynamics and traction control.

The remainder of this chapter will briefly discuss the operational principles behind the chassis sensors and data acquisition system used, while also giving an overview of the installation and calibration techniques adopted. It should be noted at this stage that much of the sensor calibration was covered in a previous study conducted by Neben [75] and as such will not be covered in detail here.

5.1. Data Logging

Data logging is achieved through the use of MoTeC's Advanced Dash Logger (ADL), the company's purpose-designed automobile testing data acquisition system (DAS). The unit, shown in Figure 5.2 and "Appendix H", is a compact data acquisition system suitable to control the on-board acquisition of data from the automobile sensors and the engine ECU. The layout of the complete DAS is also shown in Figure 5.3

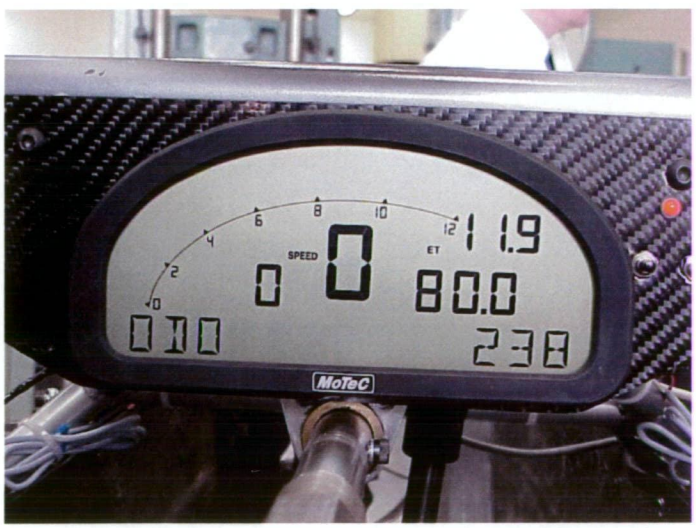

Figure 5.2: Advanced dash logger

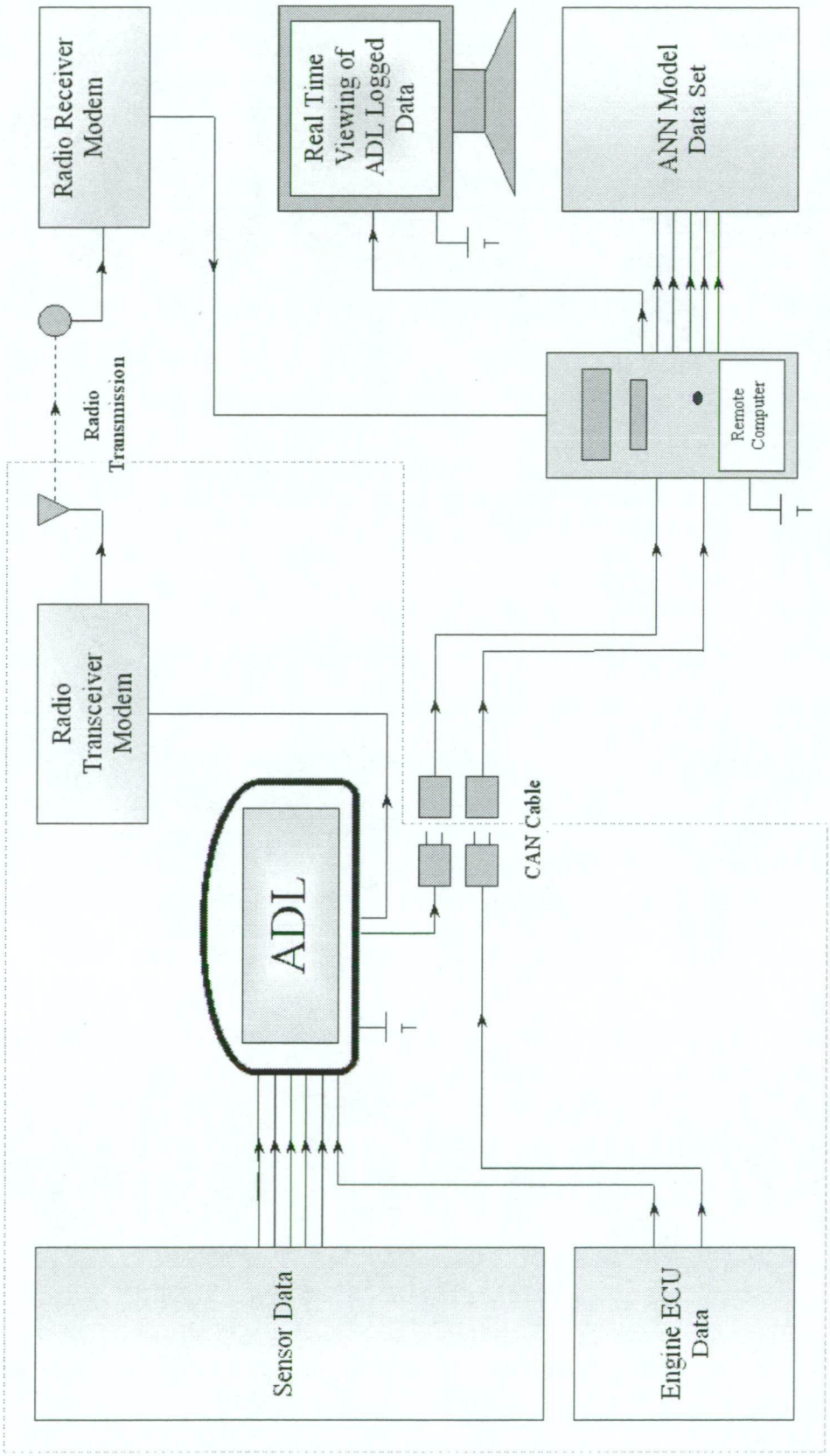

Figure 5.3: Data acquisition system layout

The ADL also serves as a programmable dash display unit for the test vehicle and supports 14 analog inputs, 10 digital inputs, one RS232 serial input and 4 auxiliary outputs in its current configuration. The ADL incorporates a high speed 32-bit microprocessor and also has 1Mb of memory, which enables up to 30 minutes of data acquisition (depending on input sensor arrangements) before the ADL data memory bank becomes full. Acquired data can them be downloaded to a PC parallel port through the use of a high speed CAN communication cable for later analysis at a rate of up to 19 sec/MB.

The ADL package also comes with two windows based programs. Dash Manager (Figure 5.4) serves as the configuration program for the ADL, and also provides to means to retrieve the logged data the ADL and engine ECU. From this program the sensor channel properties can be altered, calibration curves can be constructed, mathematical functions can be performed on the data sets and the digital display can be reprogrammed.

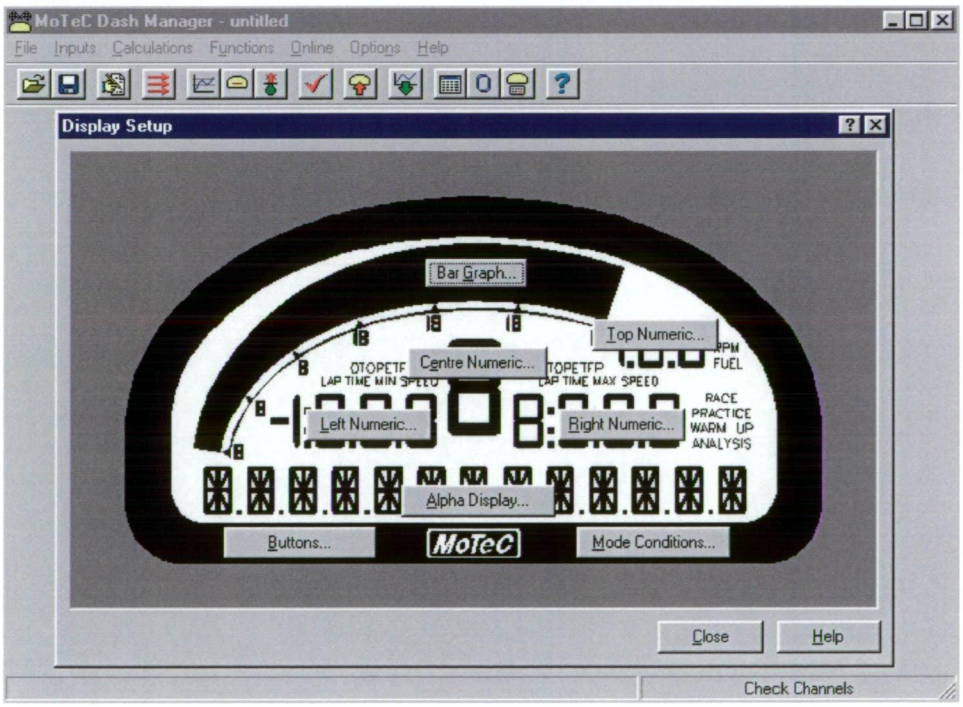

Figure 5.4: Dash manager software

Interpreter, as shown in Figure 5.5, serves as the MoTeC data analysis package. This program allows the graphical representation of the collected data, can supply statistical information and provides additional mathematical functions. It is also through this program that the data files supplied from the ADL and engine ECU can be exported into a Microsoft Excel, using a comma separated (*.csv), format.

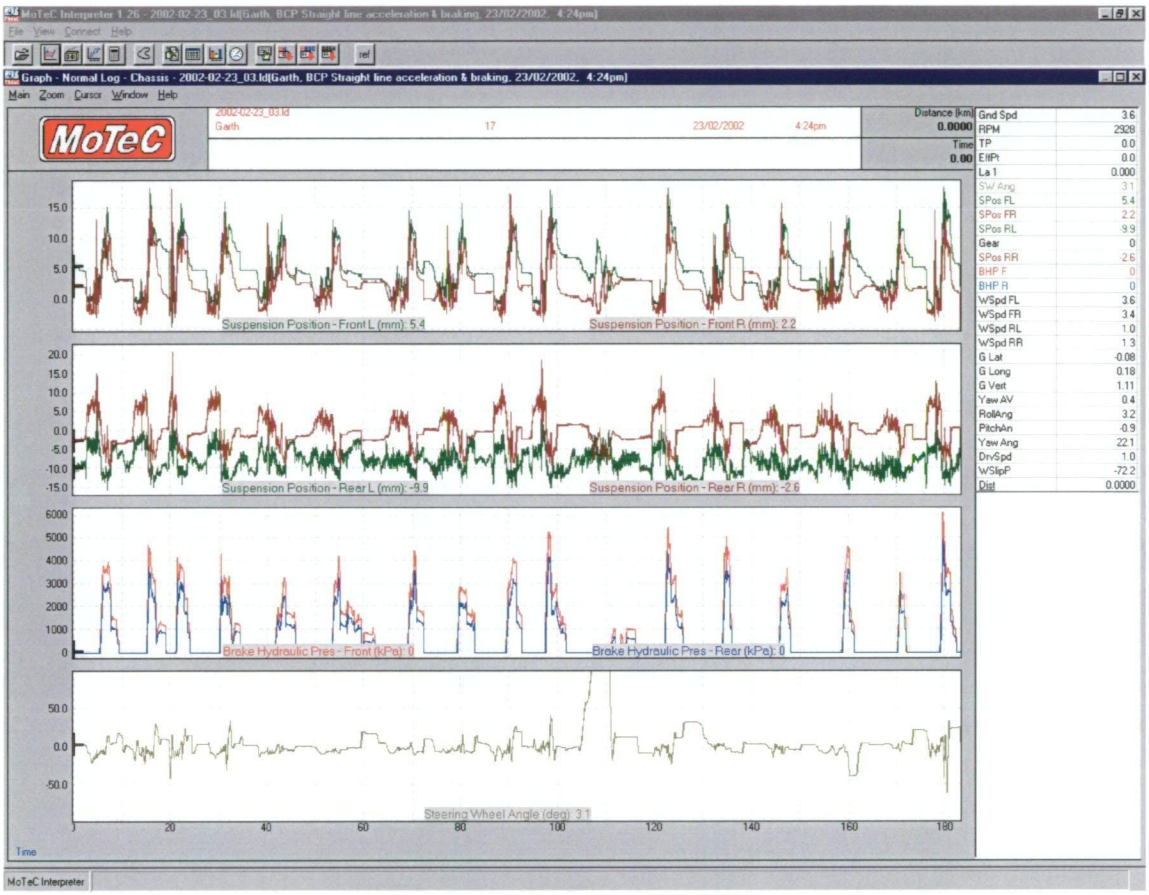

Figure 5.5: Interpreter software

5.1.1. ADL Installation

The ADL was installed into the centre of the dash to provide adequate driver visibility, with the CAN cable connection also included into the dash to allow simple data transfer. All sensor inputs were also appropriately connected the ADL wiring loom to their corresponding input channels and an additional 12V battery was included to isolate the system from the majority of interference from the vehicle's other electrical systems.

5.1.2. Time Stamping

Time and date stamping of the data collected through the ADL was achieved through the incorporation of a real time clock, as shown in Figure 5.6. This unit, installed at the steering box assembly, provides a time value to all data samples, enabling the automatic inclusion of running time and sample rate into the collected data. The unit also provides an additional RS232 communications port from the ADL.

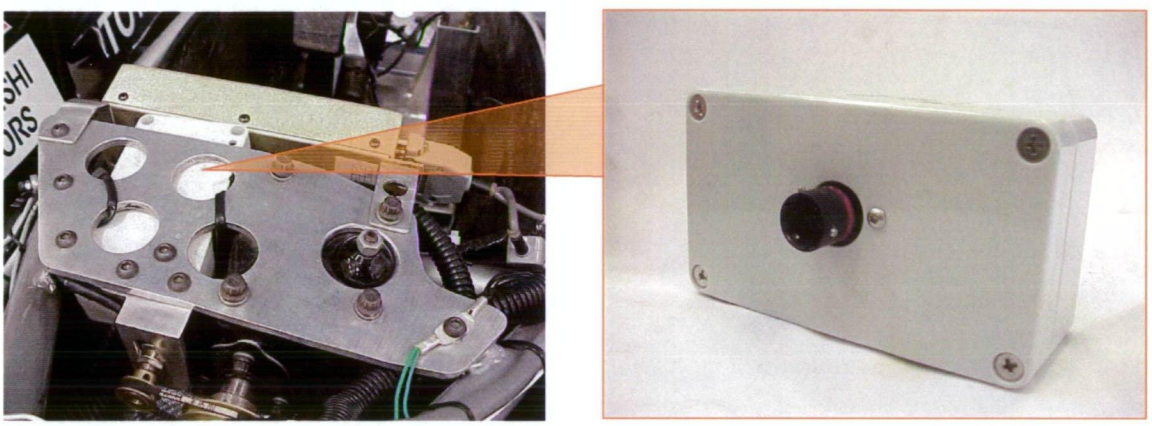

Figure 5.6: Real time clock

5.2. Remote Logging

In addition to the on board logging supplied by the ADL, the test vehicle is also fitted with the facility for remote logging. This means that some of the ADL and engine ECU measured parameters can be viewed and recorded in real time by a track-side computer, via a telemetry link. The system also has the potential to be upgraded to provide two-way communication, allowing the track-side computer to also alter ADL and engine ECU parameters in real time.

The remote logging is achieved through the use of a pair of RFI-9256 Data Strike Series 3 Spread Spectrum Radio Modems operating at 900MHz, one being a transceiver, the other a receiver. Their specifications are given in "Appendix H". The transceiver modem was installed onto the steering assembly of the test vehicle and its antenna installed onto the outside of the carbon fibre nose cone to prevent interference, as shown in Figure 5.7. It is also connected to the ADL through a switch input to turn it on and

an additional RS232 ADL output wire, acquired through MoTeC's telemetry upgrade package, to provide it with the output data from the ADL and the engine ECU.

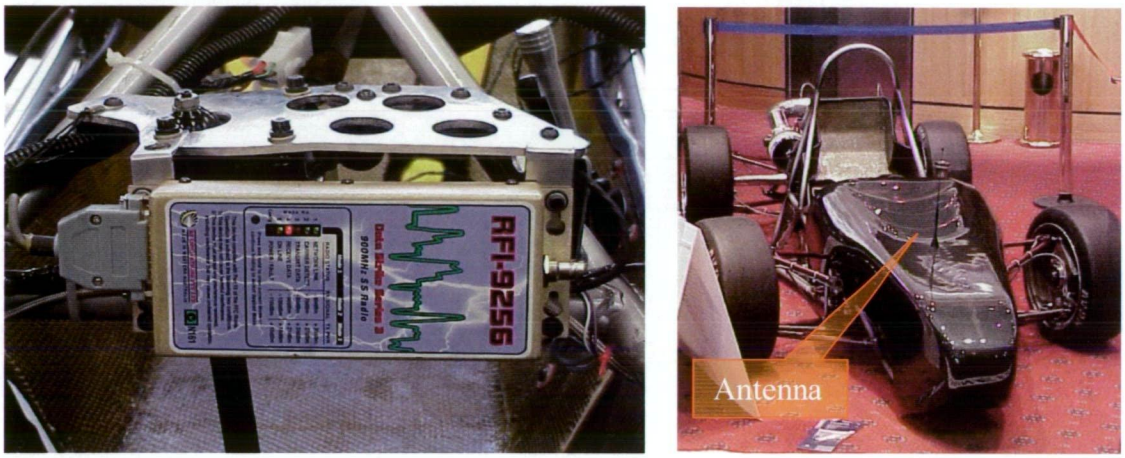

Figure 5.7: Transceiver radio modem

The receiver modem operates through the track-side computer's com port 2 and is used to receive the telemetry data, as well as synchronising communication between the modems. The remotely logged data can them be displayed via the Interpreter Virtual Dash software, as can be seen in Figure 5.8.

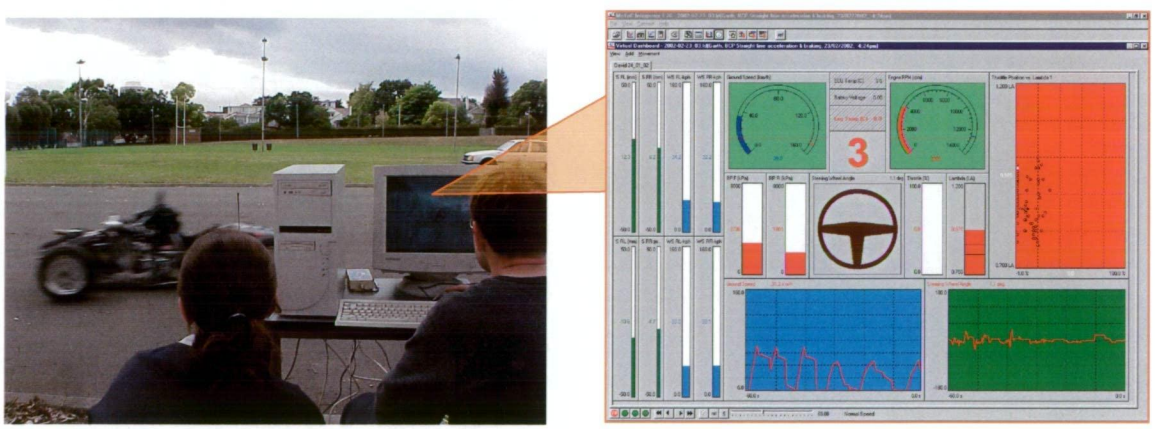

Figure 5.8: Remote data logging via a track-side computer

5.3. Wheel Speed Sensors

The test vehicle independent wheel speeds were measured through the use of four digital output Hall effect sensors. The sensors operate on the principle, discovered by Dr E. Hall in 1879, that when a current carrying conductor is placed into a magnetic field, a voltage will be generated perpendicular to both the current and the field. When a current is flowing perpendicular to a magnetic field, the Hall effect is observed as a potential difference or voltage developed across the material, with a value proportional to the current and the magnetic field intensity. Further, if there is no magnetic field present, the system will not induce any Hall effect voltage. This means that the Hall effect can be integrated into a digital sensor that measures whether of not a ferrous material is in close proximity to it. By combining this property with a ferrous gear tooth arrangement, as shown in Figure 5.9, the sensor can be used to measure rotational speeds for many different applications. As such, Hall effect sensors have become widely used within the automotive industry, with common applications including measurement of camshaft and crankshaft speed and position, as well being used for wheel and transmission speed measurement.

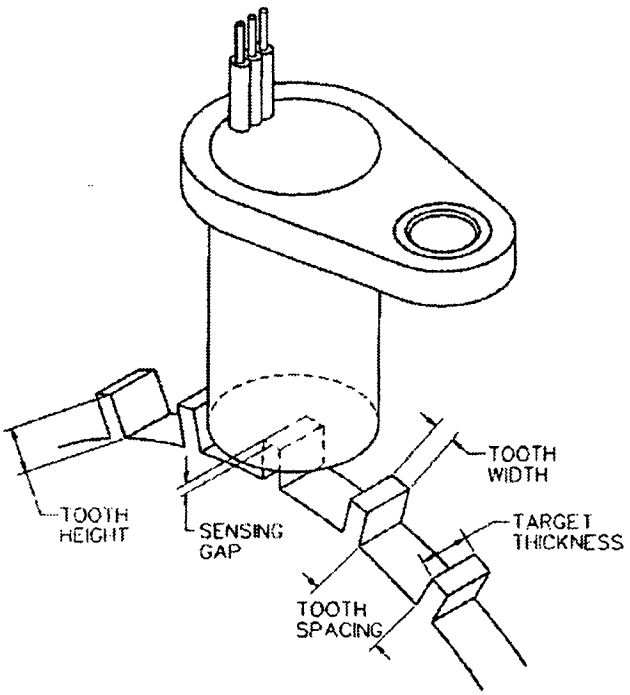

Figure 5.9: Gear tooth Hall effect sensor [74]

The wheel speed sensors used throughout the test vehicle were manufactured by Honeywell (GT1 series) and supplied through MoTeC. The sensors operate with a maximum switching time of 15μsec on and 1.0μsec off, with further specifications given in "Appendix H". The sensor is composed of an integrated circuit that is made up of discrete capacitors and a bias magnet, as can be seen in Figure 5.10. It is also sealed in a probe type, non-magnetic plastic package for physical protection and cost effective installation.

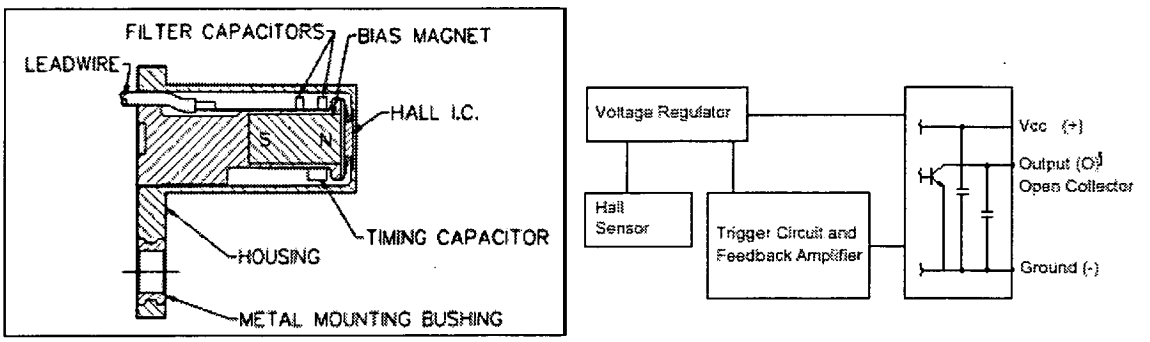

Figure 5.10: Honeywell Hall effect sensor configuration [74]

It can be seen that the Hall effect sensor incorporates three wires. One wire supplies the sensor with a power source, the second with a ground and the third is the signal wire that provides the sensor measurement value. As each gear tooth passes, the sensor detects the change in magnetic flux level away from its in-built bias magnet, as depicted in Figure 5.11, and digitises the result. This creates a stepped output within the signal wire, with the digital output switching between the supply voltage when it passes a gap in the gear and the saturation voltage (0.4 V) when it passes a tooth.

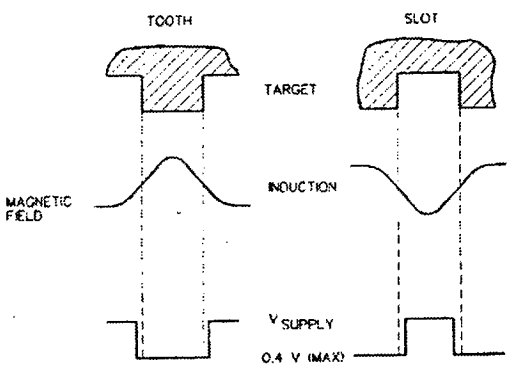

Figure 5.11: Hall effect signal voltage [74]

5.3.1. Sensor Installation and Calibration

The performance and accuracy of the Hall effect sensors are dependent mainly on the way they are positioned in relation to the target material, and also on its magnetic characteristics. The shape and number of teeth on the gear tooth wheel can significantly effect the accuracy of the results, as can sensor clearance with the teeth and sensor vibration.

The installation of the gear tooth wheel, potentially a large component within the wheel rim, had to conform to the design philosophy of the vehicle. As such it was decided that a solid steel plate with teeth cut into it would be too heavy and awkward to be included in the final design. Instead, it was decided to adopt a reasonably unconventional approach. As mentioned previously, the test vehicle was designed to use custom three-piece aluminium rims, which are bolted together using high tensile bolts. Since aluminium is non-magnetic and the bolts are, the rim itself can be used as the gear tooth wheel, with the bolts acting a teeth and the rim acting as the gaps. The operation of the Hall effect sensor with this arrangement is shown in Figure 5.12. This arrangement gives a total of 18 teeth on each wheel for speed measurement, which is well within the operating range of the sensors, but also provides a significantly high sampling period for accurate measurement.

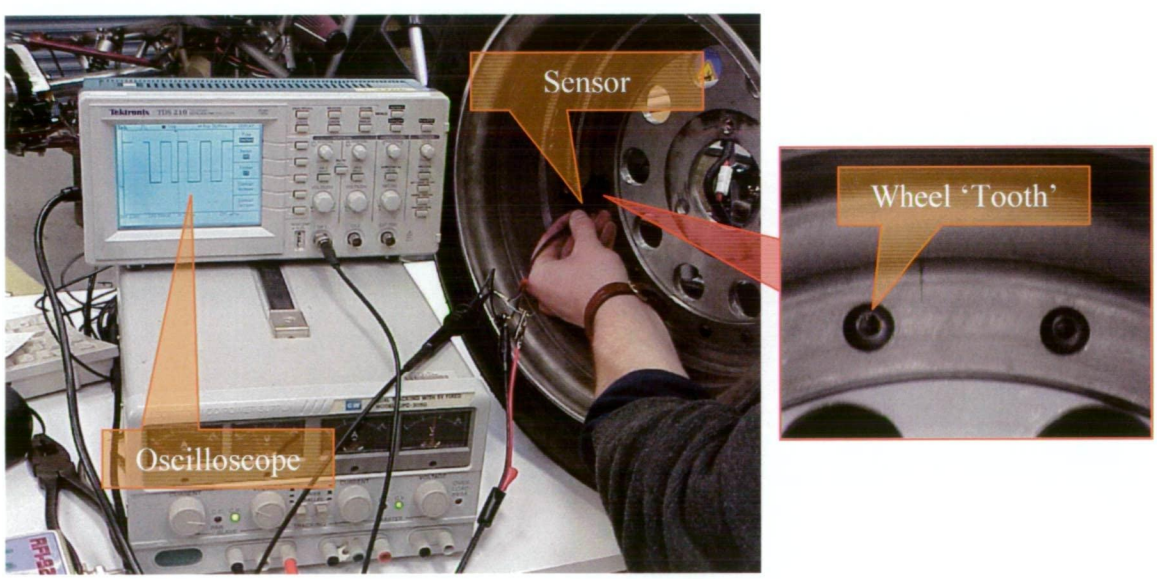

Figure 5.12: Hall effect sensor operation (output shown on oscilloscope)

The Hall effect sensor mounts, thus, required positioning in close proximity to this region of the rim. It can be seen in Figure 5.13 that the brake caliper provided an ideal mount, with the simple addition of a mounting bracket the only required modification. The mount was constructed to allow simple alignment with the wheel bolts, while also restraining the sensor from excessive vibration that had been shown to produce unreliable results and occasional breakages.

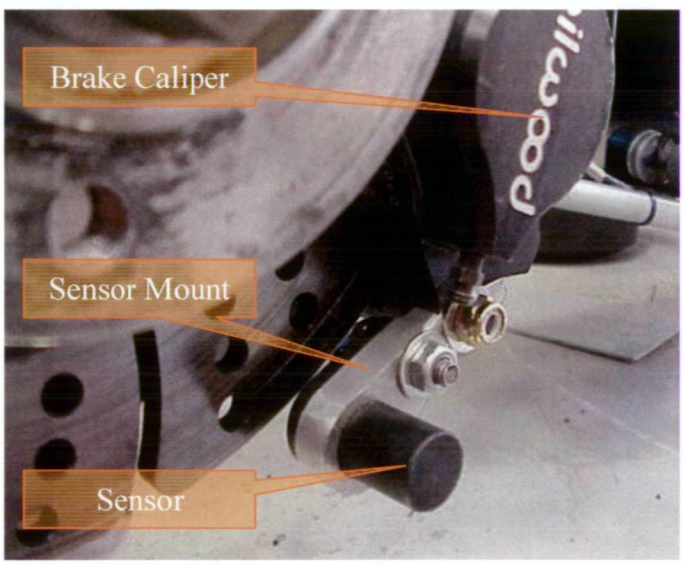

Figure 5.13: Hall effect sensor mounting

Once the Hall effect sensors were wired into the ADL wiring loom, the calibration function of the Dash Manager software was used to convert the digital output signal of the Hall effect sensors into wheel velocities. Since one wheel revolution is equivalent to 18 Hall effect pulses, wheel speed calibration was achieved by specifying this value within the software and including measurements of the circumference of the individual wheels, as shown in Figure 5.14.

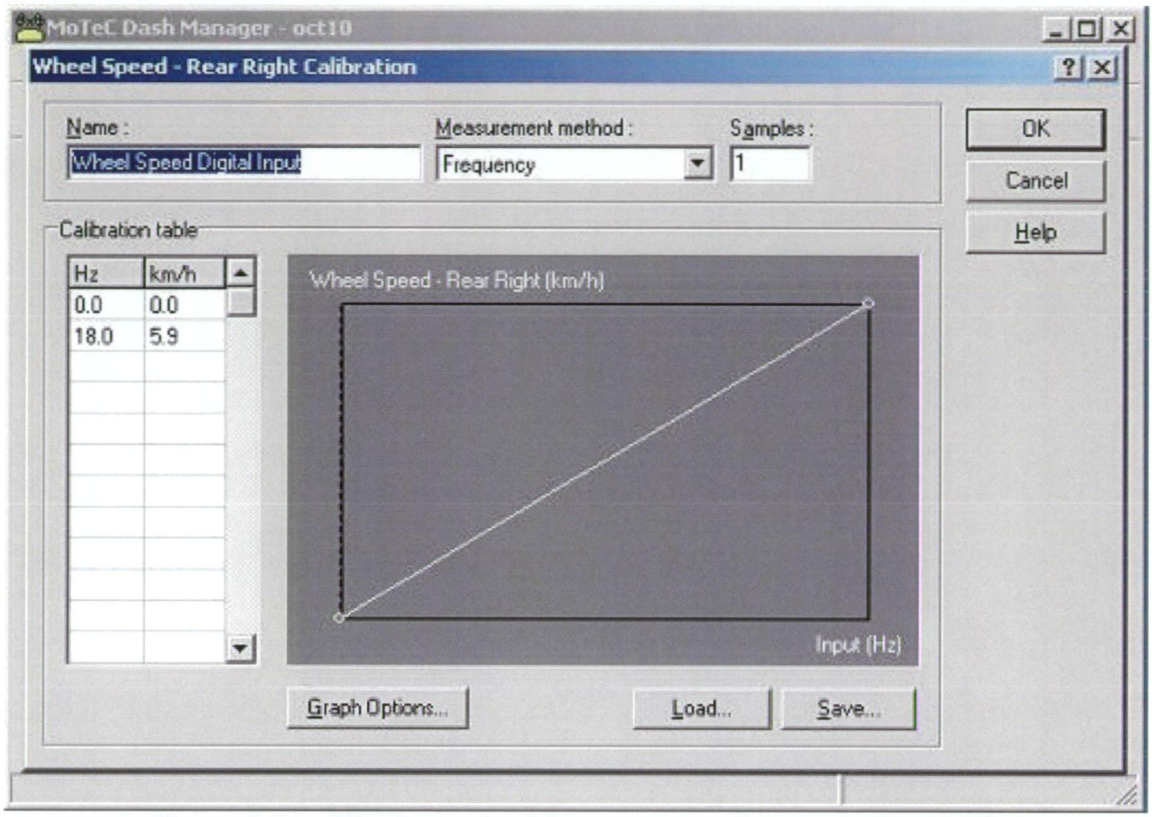

Figure 5.14: Wheel speed calibration curve (for rear right wheel)

5.4. Suspension Position Sensors

The four-wheel independent suspension positions were measured using linear potentiometers installed on the suspension wishbones at each wheel. A potentiometer, as an analog sensor, operates on the basis that electrical resistance is proportional to resistance length and that voltage is proportional to resistance. They generally consist of a moveable component that makes contact with an internal resistor, with the contact motion normally being either in translation or rotation. When a resistance element has a voltage applied to it (as shown in Figure 5.15) the motion of the moveable contact results in a change in output voltage across the sensor that is linearly proportional to the contact position.

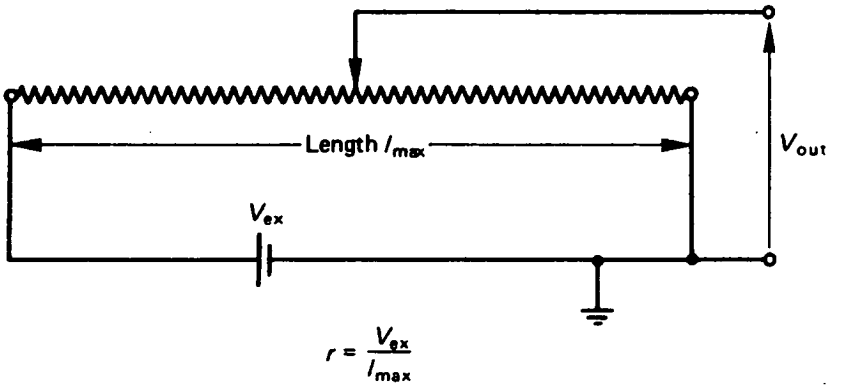

Figure 5.15: Potentiometer operation [72]

The potentiometers used in this case were chosen to be the 100mm stroke length linear potentiometers supplied by Gefran (model PZ12A). Theses sensors, as specified in "Appendix H" consists of an anodised aluminium cylinder case with an internal moveable control rod made from stainless steel, and has an extension capacity of 100 mm. At the end of the moveable rod and the bottom of the sensor there are two M5 self-aligning rod ends used for mounting purposes. Each sensor has a linearity accuracy of 0.05% and infinite resolution.

The electrical configuration of the sensor is depicted in Figure 5.16. It can be seen that it also incorporates three wires, one wire as a power source, the second wire as the ground and the third as the signal wire.

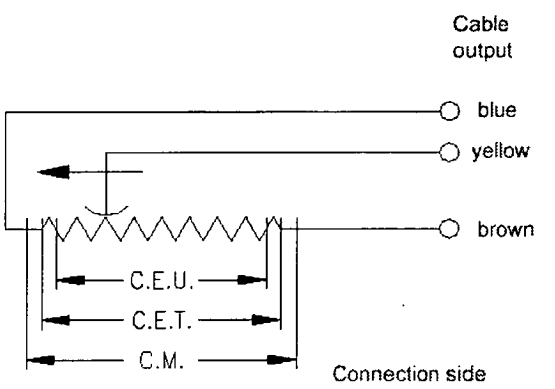

Figure 5.16: Gefran linear potentiometer configuration [72]

5.4.1. Sensor Installation and Calibration

Two methods were investigated to measure the suspension deflection at the wheels of the test vehicle. The first method involved mounting the linear potentiometers at a known installation position relative to the wheels of the vehicle. The deflection at the wheels could then be mathematically calculated using the geometry of the sensor installation directly from the sensor reading in its installed position. This approach, however, required the sensor to be orientated perfectly upright to simplify the wheel deflection calculations. Unfortunately, this approach would have severity limited both the installation options for the sensors and the total sensor deflection under normal driving, as so was discarded for a second option. This method used a calibration technique that eliminated the need for the sensors to be aligned and orientated with exact precision and accuracy in relation to the wheels, with the resulting installation shown in Figure 5.17. By applying a known deflection at each individual wheel of the vehicle, the calibration function in the Dash Manager software could then be used to gain the suspension deflection as a function of sensor output.

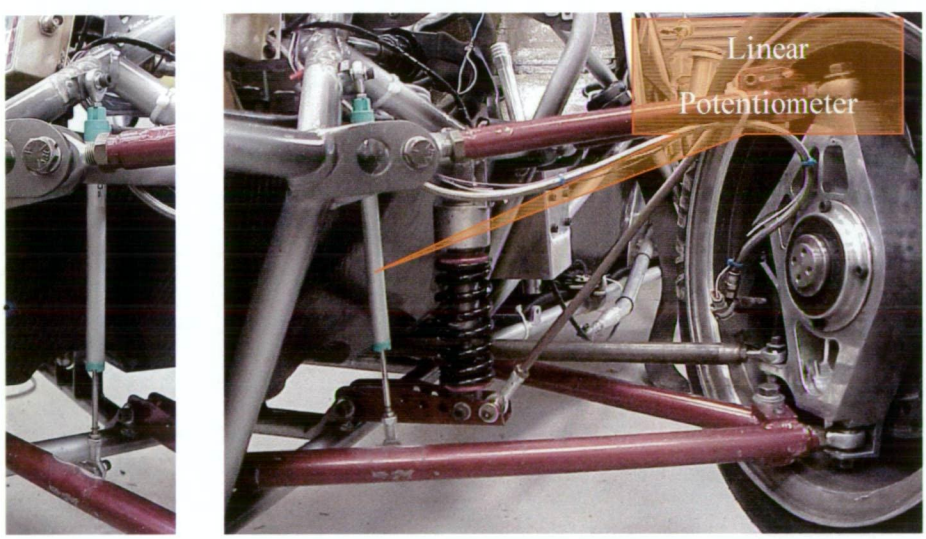

Figure 5.17: Linear potentiometer mounting (front left wheel)

The first stage in the calibration process involved the zeroing of the linear potentiometer readings in relation to normal driving conditions. To this end, the sensor zero voltage for each sensor was established when the vehicle was positioned on a level floor, with an average sized driver (77kg) sitting very still in the cockpit. During this process the

car was moved up and down a number of times to find the resting zero voltage position and minimise the effect of the small amounts of binding within the suspension system. A number of zero voltage readings were then recorded for each potentiometer and the recorded values averaged to obtain a single zero voltage reading.

The next stage in the calibration procedure involved lifting the four wheels of the test vehicle off the ground, and resting it level on its frame. The potentiometers were then calibrated individually for their range of movement about their zero position. This was done by disconnecting the suspension pull rod and measuring the suspension position and potentiometer relationship for a number of different wheel heights. Wheel height measurement (measured at the stub-axle castle nut) was accomplished through the use of a dial height gauge as shown in Figure 5.18.

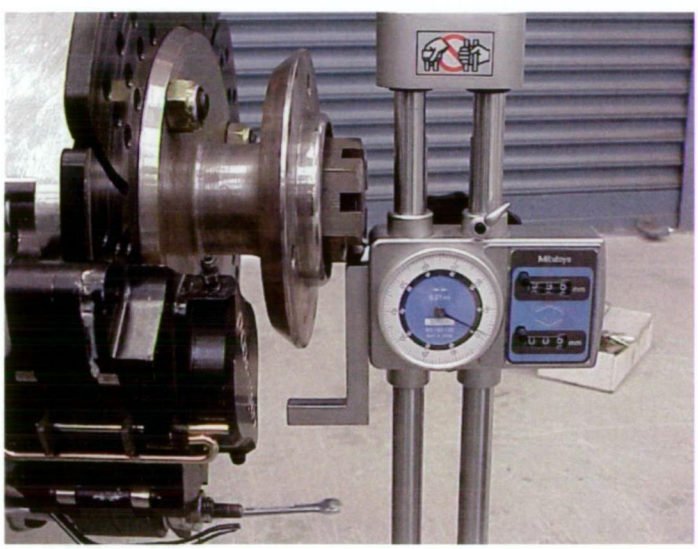

Figure 5.18: Linear potentiometer position calibration

Finally, the applied wheel assembly deflection value was then input into Dash Manager and compared to the recorded analog sensor voltage output in order to gain a calibration curve, as can be seen in Figure 5.19. The software assigned positive deflection readings for sensor compression and negative readings for sensor extension.

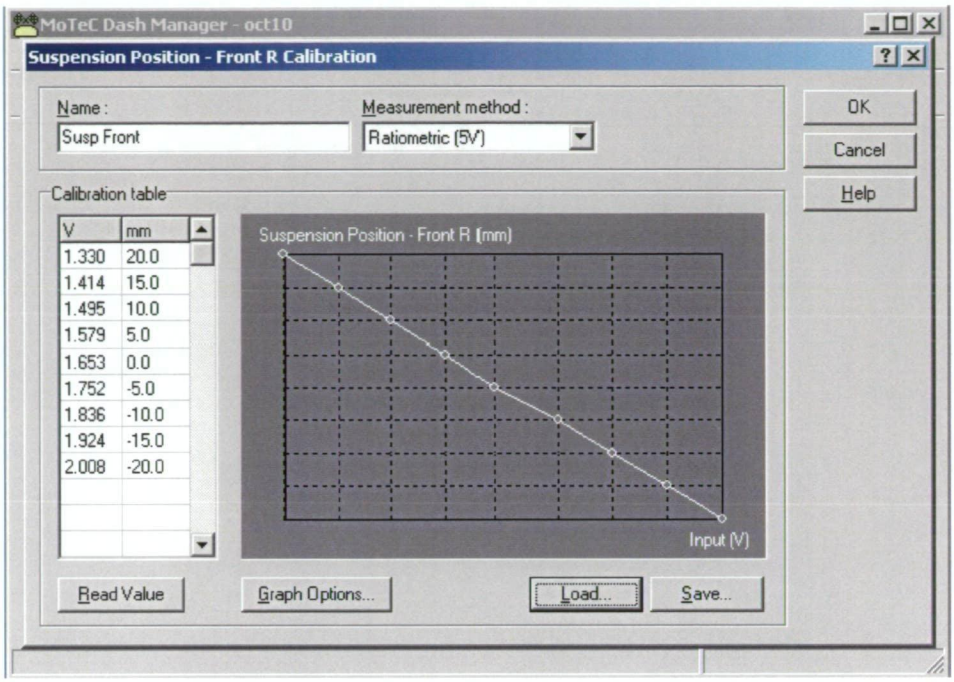

Figure 5.19: Suspension position calibration curve (front right wheel)

5.5. Steering Angle Sensor

The steering wheel angle of the test vehicle was measured through the use of a rotary potentiometer acting on a pulley system, as shown in Figure 5.20 and "Appendix H".

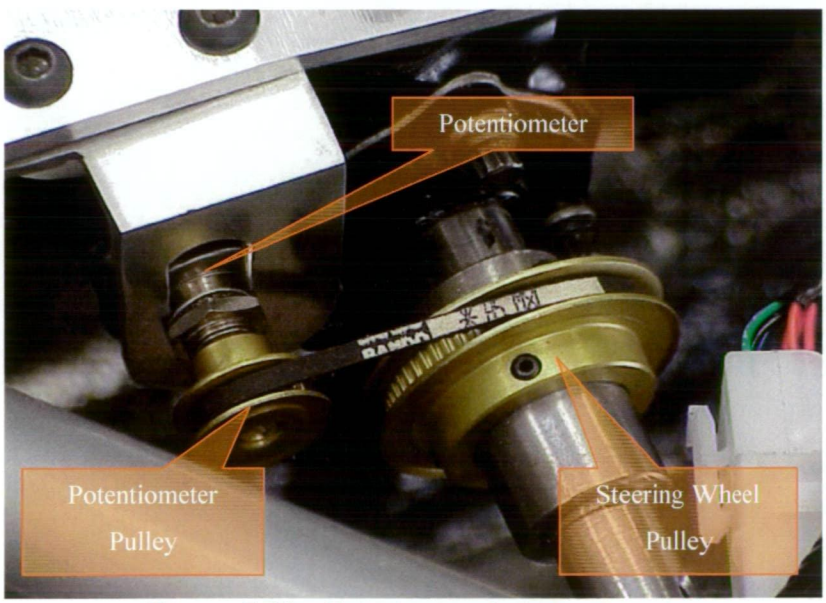

Figure 5.20: Steering angle potentiometer

5.5.1. Sensor Installation and Calibration

The installation of the sensor simply required the larger pulley to be attached to the steering shaft, the inclusion of a facility to allow tension adjustment of the pulley belt and connection to the ADL wiring loom.

The steering angle sensor could be calibrated to measure steering wheel angle (driver input) or steered wheel angle (at the tyres). In the case of this project, the system was calibrated for the former option since this eliminated the need for re--calibration every time alterations were made to the suspension and steering geometries. Calibration was thus achieved by turning the wheel through a known angle of rotation and then reading the voltage output from the sensor to develop a calibration curve within Dash Manager. To this end, a protractor was temporarily installed onto the steering wheel with a reference pointer to enable angle measurement, as depicted in Figure 5.21.

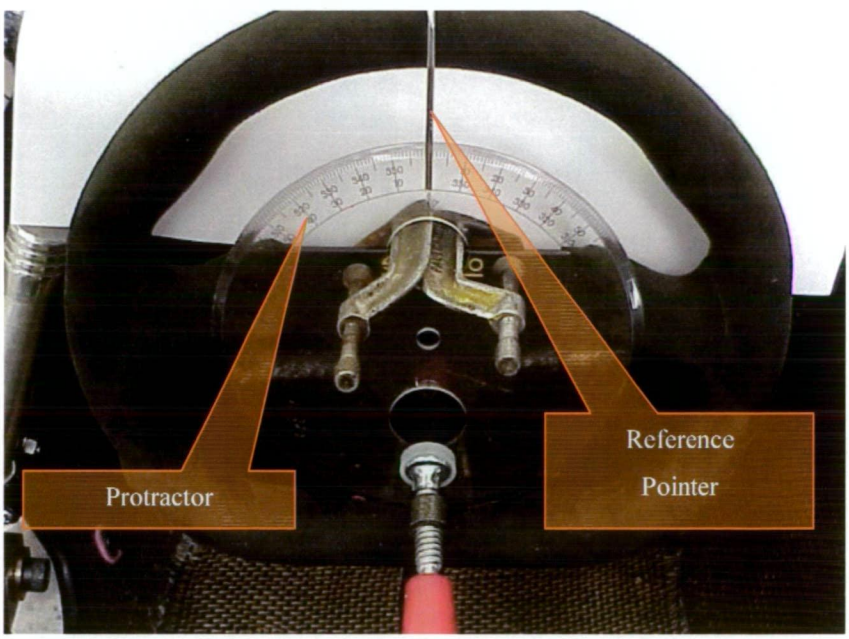

Figure 5.21: Steering wheel calibration

The steering wheel was then turned through increments of thirty degrees up to one hundred and fifty degrees, in both a clockwise and anti clockwise direction. Using the calibration function in Dash Manager software the sensor voltage output was then input at each thirty-degree rotation increment of the wheel. The corresponding actual steering

angle position, determined from the pointer position with respect to the protractor, was then assigned to the sensor voltage signal for the development of a calibration curve. During the procedure it was found that the steering system had 1° of free-play.

5.6. Brake Pressure Sensors

Since the braking system is separated into two independent circuits (one for the front wheels and one for the rear) two pressure transducers were installed to measure the braking pressure within each brake line. The pressure transducers provided an analog measurement of the brake fluid dynamic pressure using the piezoelectric effect. This effect occurs when an external force strains a crystalline substance, such as quartz, resulting in a measurable charge accumulation on the crystal surface as its ions are displaced. The electrical voltage that develops across the crystal due to mechanical displacement is also proportional to the input pressure that causes the deformation of the crystal, and forms the basis of pressure transducer operation.

The pressure transducers chosen for use in the project were Honeywell's 2000psi Eclipse OEM transducers which operate with up to ±4% total full-scale error, with full specification supplied in "Appendix H". They also incorporate preloaded quartz crystals to provide stable, repeatable operation and high result linearity, as shown in Figure 5.22. When the crystals are stressed, due to the fluid pressure applied through the connector, a high impedance output voltage is detected. This induced voltage then undergoes signal conditioning and amplification to convert the high impedance voltage to a useable low impedance signal output before being sent through the sensor output.

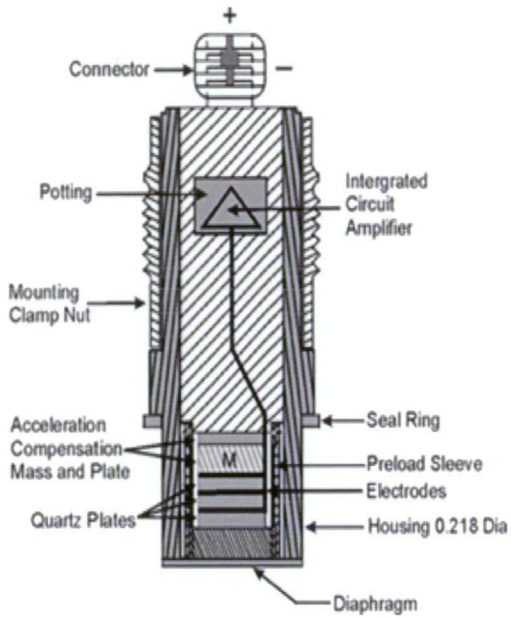

Figure 5.22: Pressure transducer cross-section [74]

5.6.1. Sensor Installation and Calibration

The two pressure transducers were installed onto each of the brake lines through the simple use of hydraulic T-junctions to the nose of the test vehicle, as shown in Figure 5.23. They were placed here, particularly, to enable easy access after some initial installation problems and also to keep the driver cockpit area as free from unnecessary components as much as possible. They were then wired to the ADL wiring loom. Calibration was also a simple affair, with the calibration files for this particular sensor supplied with the Dash Manager software.

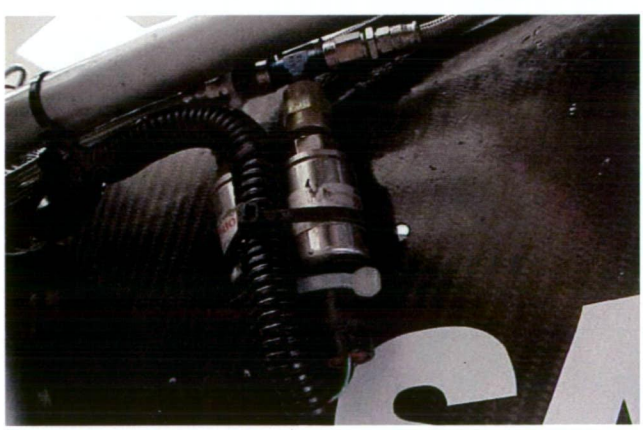

Figure 5.23: Pressure transducer installation

5.7. Attitude & Heading Reference Sensor

The measurement of vehicle acceleration and dynamic angles must be made at the centre of gravity of the test vehicle. This is because misalignment of the measured coordinate system with respect to the established coordinate system of the test vehicle can lead to significant error within the results. This can lead to crucial problems, particularly since the vehicle must be designed to allow sensor positioning at the centre of gravity and also that the sensor array for measurement of longitudinal, lateral and vertical acceleration and roll, pitch and yaw angles and angular rates must have identical reference positions. Because these problems highlighted the need for a single, yet sufficiently small, sensor to measure all of these parameters Crossbow's DMU AHRS400CA-200 was selected for use within the vehicle, and is photographed in Figure 5.24. This sensor eliminated the problems involved with the installation of multiple sensors, such as individual positioning, separate calibration and installation errors, and also provided an extremely compact unit that could be easily installed at the vehicle centre of gravity. The unit's full specifications are given in "Appendix H".

Figure 5.24: Attitude and heading reference sensor supplied by Crossbow (DMU model 400CA-200)

This attitude and heading reference sensor (AHRS) is a clustered measurement system, designed to measure nine parameters, including:

- dynamic acceleration on three axes (± 0.012G bias, 1% non linearity),
- stabilised roll, pitch and yaw angular rates (± 1.0° bias, 0.3% non-linearity),
- roll, pitch an yaw angles (± 2.5° dynamic accuracy with reference to magnetic north)

The AHRS measures these variables by using a combination of micro-machined silicon three-axis accelerometers, three-axis rotational rate sensors and three-axis magnetometers and can output the results in an analog for through nine channels or through a single RS232 digital output. Figure 5.25 depicts the block diagram of the DMU AHRS cluster measuring system and reference axes.

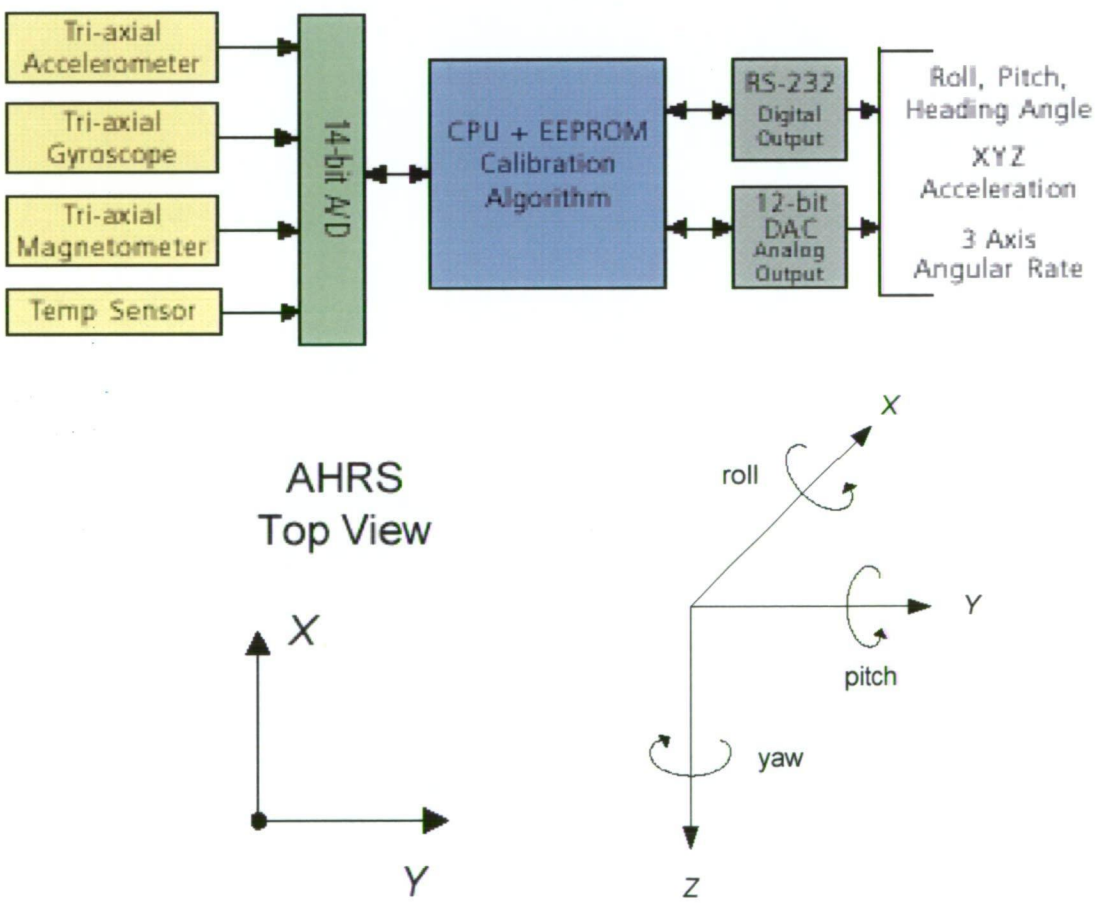

Figure 5.25: AHRS operation and reference axes [73]

5.7.1. Accelerometer Operation

All accelerometers can be thought of as measuring the relative displacement of a spring mass system to measure acceleration. The three micro-machined silicon micro electrical mechanical system (MEMS) accelerometers used in this sensor are no different, using differential capacitance to sense acceleration. Capacitive accelerometers operate by sensing a change in electrical capacitance with respect to an applied acceleration though the use of a distorting diaphragm sandwiched between two plates. The two plates form the capacitor unit and detect changes as they are separated due to the movement of the diaphragm due to acceleration in one a single plane. However, since capacitance is inversely proportional to the distance between the two plates and the diaphragm displacement is a non-linear function, the resulting capacitance differentials are not a linear function with applied acceleration. To this end, the AHRS performs some signal conditioning to the results to achieve linearisation.

5.7.2. Gyroscope Sensor Operation

The three angular rate gyroscopic sensors are made up of a number of vibrating ceramic plates that use a silicon MEMS structure to measure the Coriolis force ($F=2m\omega V\sin(\phi)$, where ω=angular velocity of the axis, V=relative velocity and ϕ=angle between vectors ω and ϕ) induced by the dynamic movement of the test apparatus. This data can then be used to gain the rotation rate around the given axis. The advantage of this approach is that the output angular rate is independent of the acceleration output. One problem that arises, nonetheless, is that a change in the direction around one axis of a driving transducer induces a vibration in the detection transducer on another axis. To overcome this problem an oscillator circuit is used to control the vibration, however, during testing it was observed that when supply power became sufficiently low (about 11V) this oscillator circuit began to fail and as such the angular rates were the first parameters to lose accuracy.

5.7.3. Magnetometer Operation

The three magnetometers within the AHRS are constructed as miniature fluxgate sensors and are used to provide the AHRS heading angles with respect to the Earth's

magnetic field. However, these values are only used for reference, with the angular rate integrals and gravity angle use to stabilise the results, as depicted in Figure 5.26. Unfortunately, this signal conditioning also introduced result errors into the angle measurement due to the effects of the erroneous angular rate conditioning inputs at low supply voltages.

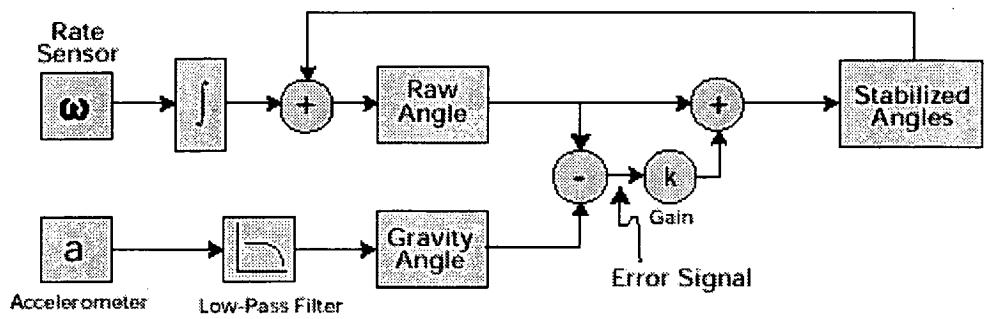

Figure 5.26: Angle value signal conditioning block diagram [73]

5.7.4. Sensor Installation and Calibration

The centre of gravity of the test vehicle was determined to be just behind the driver's lower back longitudinally and in the centre of the car laterally. This was found initially through the finite element analysis conducted above during the design stage, and was later verified through the measurement of the vehicle's weight distribution at each wheel. However, the vertical position of the centre of gravity could not be determined as easily and so with limited installation options, other than placing the sensor within the driver, it was decided that installation of the sensor on the floor was a sufficiently close approximation.

The sensor was then installed into the car, paying particular attention to the requirement of minimal ferrous materials around it, which can effect the magnetometer accuracy. Installation also required the specialised construction of the fuel tank to fit around its mounting position and the connection to the ADL's separate power supply. Mounting

was accomplished through the use of some foam for vibration isolation and Velcro to eliminate the need for bolts and to provide further insulation.

Installation and calibration with the ADL encountered a number of problems. Initially it was decided to use the RS232 capability of the AHRS as an input to the ADL, requiring only one digital input channel. However, since MoTeC had never supplied one of these sensors within Australia they did not have the necessary template software required to run it in this way. This meant that the nine analog channels had to be used instead, requiring two ADL upgrades. The cost was prohibitive in this instance and only one upgrade was bought, providing enough analog channels to measure only seven parameters from the AHRS. To this end, the roll and pitch rate measurements were omitted from the data acquisition, since they were considered the least important parameters to measure.

These sensors, together with the engine ECU sensors described in "Chapter 4", form the basis for the data collection necessary for the comprehensive measurement of the vehicle dynamics. While they do not cover every aspect of the vehicle system, such as dynamic tyre pressure as an example, it was felt that the measurement and computation of these 40 parameters would provide ample data for ANN modelling.

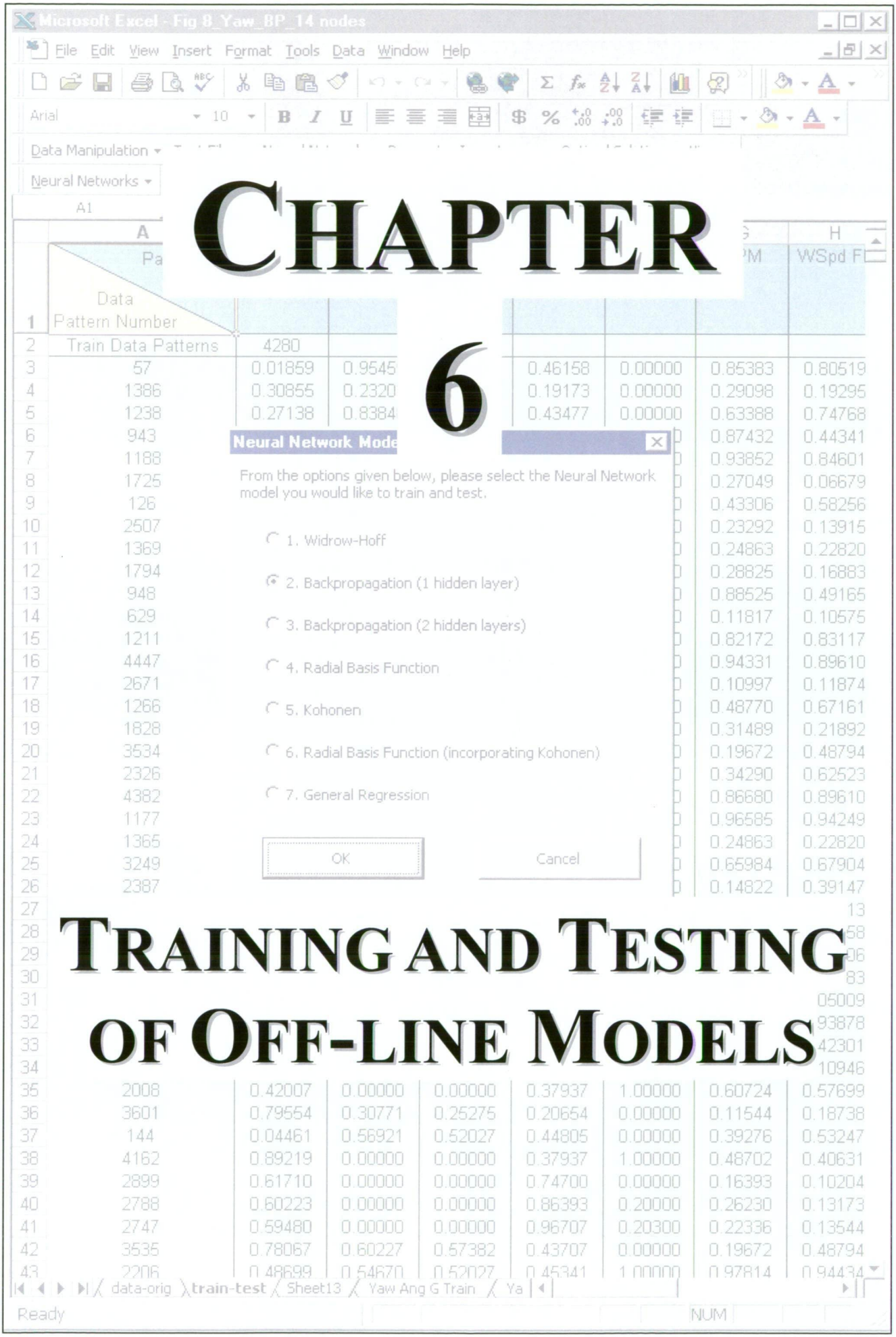

CHAPTER 6

TRAINING AND TESTING OF OFF-LINE MODELS

6.1. Strategy for Prediction

The aim of this study is to test the effectiveness of artificial neural networks in vehicle parameter prediction, using a variety of sensor data and ANN architectures, in order to determine its practicality for use in various controllers – particularly in traction control. This means that the parameters for prediction necessary for a traction controller need to be determined. It also means that the testing conditions that are representative of significant driving conditions must also be selected.

Since the goal here is to perform a reasonably fast identification of different ANN performance, training convergence speed is an important issue. The number of parameters input into the network, as well as the number of data samples, needs to be limited to a workable amount while maintaining a minimal sacrifice in accuracy.

6.1.1. Predicted Parameters

As shown in "Chapter 2", the most current vehicle dynamics controllers attempt to keep yaw, lateral acceleration and, sometimes, longitudinal acceleration within reasonable bounds to ensure stability. With this in mind, as well as their obvious effects on vehicle performance, it was decided to attempt to predict these parameters with the ANN models. If the predictions were accurate enough they could then be integrated into a controller, at a later date, which could control parameters such as brake force and engine power to ensure these predicted values remained within a safe region.

6.1.2. Input Parameters

For the purposes of this study it was decided that the inclusion of the 40 measured parameters into the ANN model would introduce significant architecture and training complexity that was beyond the scope of this initial investigation. Not only would the inclusion of so many parameters dramatically increase network size and associated training time, but many would most likely have little or negligible effects on performance. As a result, 14 input parameters were selected from the 40 parameters

that were dynamically measured during vehicle testing based on initial importance investigations, detailed by Neben [75], and a number of observational conclusions.

The criteria used for parameter selection were based on three simple qualitative observations, namely; presumed ANN importance, raw data quality and induced calculation error. As stated throughout this study, the optimisation of the networks and the identification of the most appropriate combination of input variables is left as a major goal for future work. As such this qualitative method provided a fast and convincing preliminary study.

The process is probably best described considering a number of examples of parameters that were excluded from the model. For example, while roll angle could be considered an important input variable for vehicle dynamics modelling, it was not included as an input value for the ANN. This was because the data quality derived from the AHRS for this parameter was believed to be of a lower quality than that of many other measured parameters. On the other hand, the measured data for the exhaust lambda value seemed to be of a quite high quality, but when trying to relate it to vehicle dynamics it was believed that there were too many degrees of separation for it to have more than a negligible effect. Lastly, although different types of slip were considered as an input to the model, slip calculation requires knowledge of the vehicle's absolute ground speed and tyre deformation, which we did not have other than through approximation. Inclusion of these parameters would have not only initiated unneeded error, but also introduced the parameters that were the goal of the study to avoid.

The chosen parameters are detailed below and can be generalised into three subsets; driver inputs, engine condition and vehicle attitude.

- Hydraulic brake pressure (front)
- Hydraulic brake pressure (rear)
- Steering wheel angle
- Throttle position

Driver inputs

- Engine speed (RPM)

Engine condition

- Distance
- Wheel speed (front left)
- Wheel speed (front right)
- Wheel speed (rear left)
- Wheel speed (rear right)
- Suspension position (front left)
- Suspension position (front right)
- Suspension position (rear left)
- Suspension position (rear right)

Vehicle attitude

It can be seen that all of these values (except distance) are measured directly through the ADL, with no calculations performed other than through calibration. This decision to avoid using data gathered through further data conditioning, such as differentiating wheel speed to get wheel acceleration, was made to avoid additional error sources and test the effectiveness of the ANNs using just directly measured values.

6.1.3. Parameter Conditioning

Reducing the number of inputs goes part of the way in reducing the size of the training data set. In addition to this, the number of measured samples can be lessened to improve the training speed of the ANN. This means, of course, that the total sampled time must be limited to a value that reflects this. The sample set must encompass as much relevant data as practical, while maintaining a small size. As a result, the chosen sampling rate must represent a compromise between that required to gain an accurate estimate of the vehicle's dynamics and the total sampling time available. Many of the parameters have widely varying suggested sampling rates (e.g. suspension should be measured at 200Hz, while wheel speed should be at 20Hz), but the component with the

highest rate determines the total size of the ANN data set, with the other values simply repeated in between readings. A decision had to be made on what could be the lowest practical sampling rate while maintaining accuracy. To this end, data was collected at two different sampling rates, one at 200Hz with all of the sensors operating at their suggested optimal rates, and the other with all of the sensors operating at 100Hz. The second option essentially doubled the total training data time-span from 20 seconds to 40 while maintaining the selected sample limit of approximately 4000 data samples.

In addition to reducing the sample size, further parameter conditioning was conducted on the measured longitudinal and lateral acceleration values used in the training process. The first was to multiple the values by a scaling factor of 100. This was done because the values were otherwise operating in a range close to zero, which can give very exaggerated %RMS errors making optimum model selection difficult.

The second was to remove the noise from the acceleration data. Vibrations within the frame and insufficient isolation induced severe oscillation within the sensor, making the result trends hard to identify in some cases. While the noisy data was used to train the network models, some conditioning was conducted to enable the comparisons of the ANN outputs with the actual, noiseless, vehicle accelerations. In this case, the noise was removed by averaging the measured results over the preceding 25 and subsequent 24 samples, creating a running average function which eliminated the majority of the noise but conserved trend accuracy within acceptable limits.

6.1.4. Course Types

To further simplify the prediction models, testing was conducted on a flat, uniform asphalt surface using just two different course types. This was done particularly to prevent problems with the identification of varying surface friction coefficients and other pavement surface effects, as well as providing a baseline to allow for simplified comparison of results in the interests of identifying sensor faults and other problems. With this in mind, the first course was selected as a straight line, testing primarily under longitudinal acceleration. In this case the vehicle was placed on the surface, and from a standing start accelerated up to between 30 and 70 km/hr before braking and coming to

a complete stop. After each run the vehicle was turned around and ran in the opposite direction. Testing was conducted for a variety of maximum speeds and brake pressures until it was felt that testing data had been gathered of sufficient quality to enable network training.

The second course was designed to test the effectiveness of ANNs under combined longitudinal and lateral accelerations. To meet this objective the course was selected as a figure of eight type, with different radius turns at each end. The test vehicle was then driven around this course at varying levels of aggression to gain data for a number of stability states.

The two courses were laid out at the testing grounds at the University of Tasmania, as shown in Figure 6.1, and ran over two days. On both occasions similar fine weather conditions were encountered and track conditions remained comparable. Also, in the interests of avoiding unnecessary complications, the vehicle was equipped with its wet weather tyres – which are far less prone to characteristic changes in response to temperature increases and wear than the racing slicks.

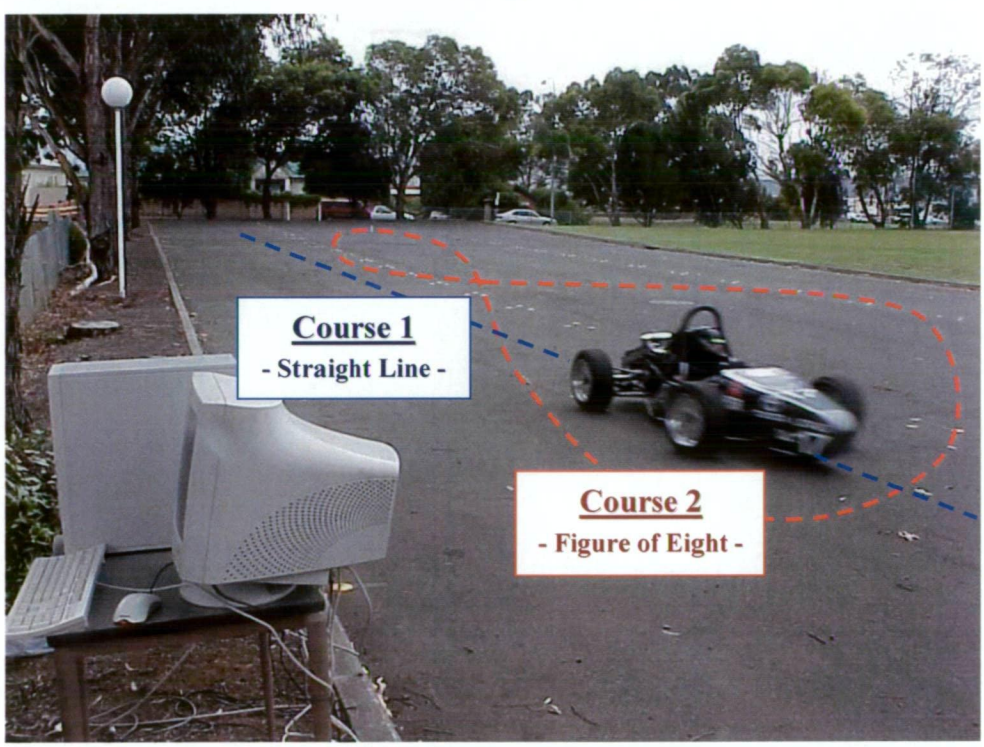

Figure 6.1: Course layout at the University of Tasmania carpark

6.2. Network Training

Once the testing data was logged for a number of different driving conditions on the two courses it could then be used for network training and testing. Since the network training data set time-span was limited to 20 to 40 seconds it was important to select the driving conditions that provided both reliable sensor results and broad representation of the vehicle dynamics.

In the case of the straight line course (course 1), where logging was conducted at 200Hz, this meant 'cut and pasting' representative runs and excluding repetitive or poor quality ones. With the 20 second limit imposed by the data size requirements this meant a total of four runs could be included into the model, with the logged results shown in "Appendix I". In the case of the figure of eight course (course 2), where logging was conducted at 100Hz, a total of 40 seconds could be logged, which equated to two complete laps. This meant that the two consecutive laps that showed maximum driving condition representation could be selected for the model, thus avoiding the need to 'cut and paste' relevant sections as was necessary for course 1. The figure of eight logged results are also given in "Appendix I".

With the ANN data set alterations completed, network training of the model shown in Figure 6.2 could begin. As discussed in "Chapter 3" two models were to be used to allow performance comparisons; back propagation networks and general regression neural networks. For simplified results and improved accuracy it was decided to use only single output ANNs, meaning that for each case and network type separate networks needed to be trained for longitudinal acceleration, lateral acceleration and yaw angle prediction.

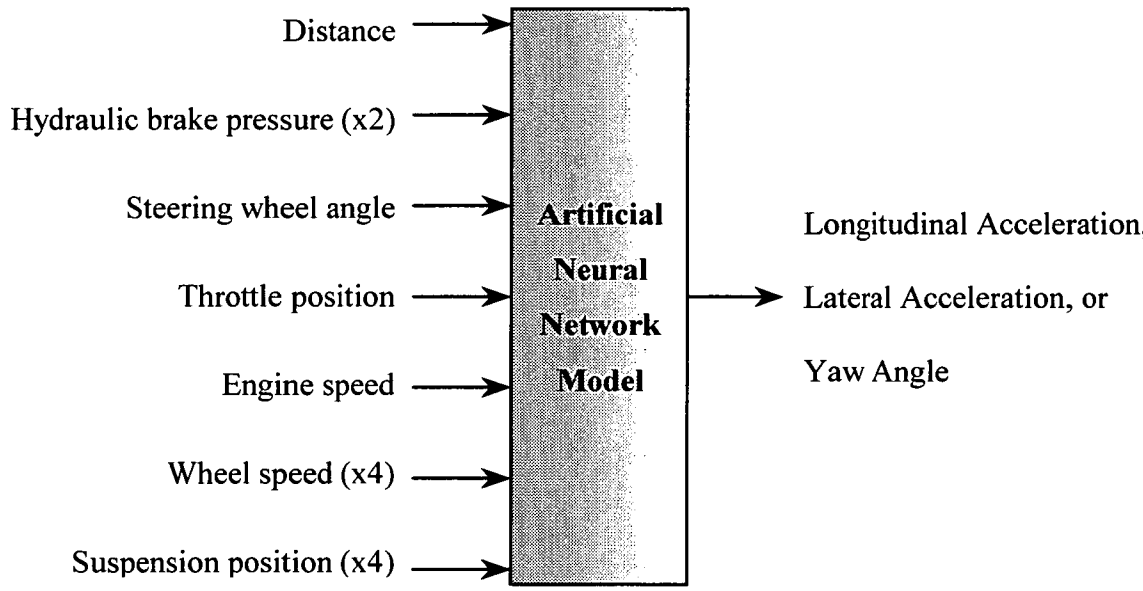

Figure 6.2: Artificial neural network model for parameter prediction

The University of Tasmania has been developing Microsoft® Excel based software to train and test these selected ANNs (and others) over a number of years with a focus in manufacturing applications, as covered in [40], and was also used for this study. As a result its operation will not be discussed in detail here, but in very vague terms the software works by first inserting the properly formatted data into an Excel sheet and normalising the values. The program then presents a number of training options - such as network type, transfer function, number of neurons (nodes), number of iterations and smoothing factor values. Training then commences until the network converges, after which a number of functions are available such as testing the network with new data, plotting graphs to compare network accuracy with testing data, evaluating RMS error and conducting input importance analysis.

Network training was conducted using the software for the BP and GRNN models for both course types, altering the architectures of each iteratively to gain an approximation of optimum network architecture for each case. It should be noted, however, that the choice of the optimum network architecture remains a complex task and the method used here could be significantly improved upon in later investigation.

The BP network results are shown and discussed below, while the GRNN results are given in "Appendix J". Each of the longitudinal and lateral acceleration graphs include both the data used for network training, the same data with the noise removed and the network predicted results. The absolute error graphs are also supplied, with the error calculated from a comparison between the network results and the measured data with the noise removed. The same is true for the yaw angle graphs, except that the measured values can be seen to display very little noise and, as such, conditioning to remove noise was deemed unnecessary.

6.3. BP Network Model - Course 1

6.3.1. Longitudinal Acceleration Prediction

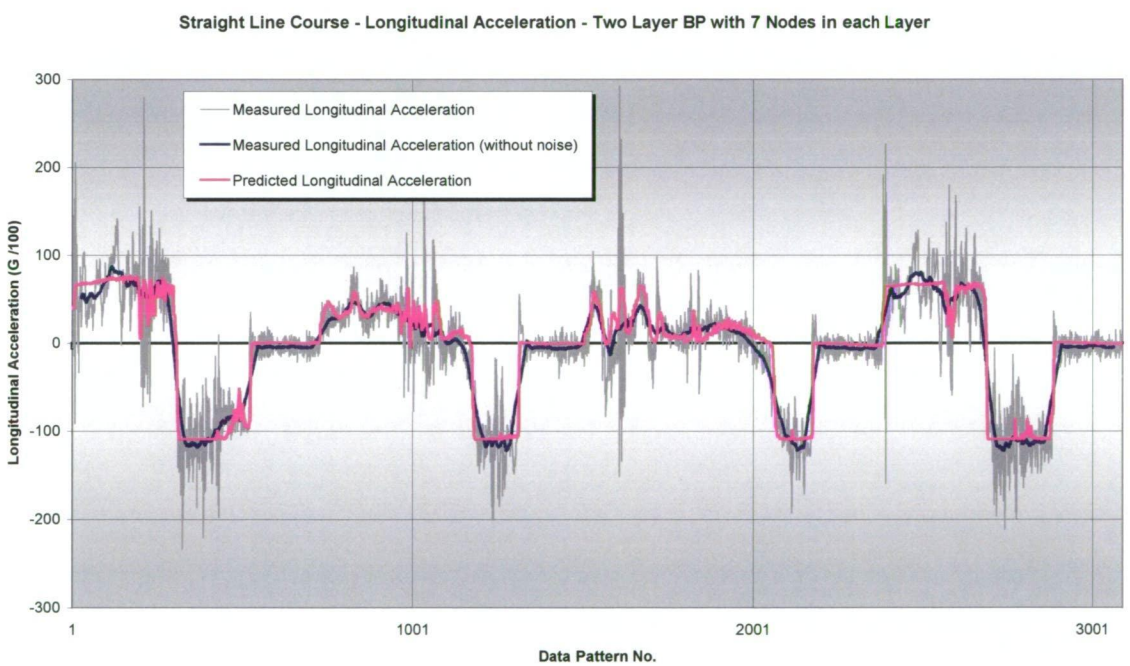

Figure 6.3: Longitudinal acceleration prediction during network training – course 1

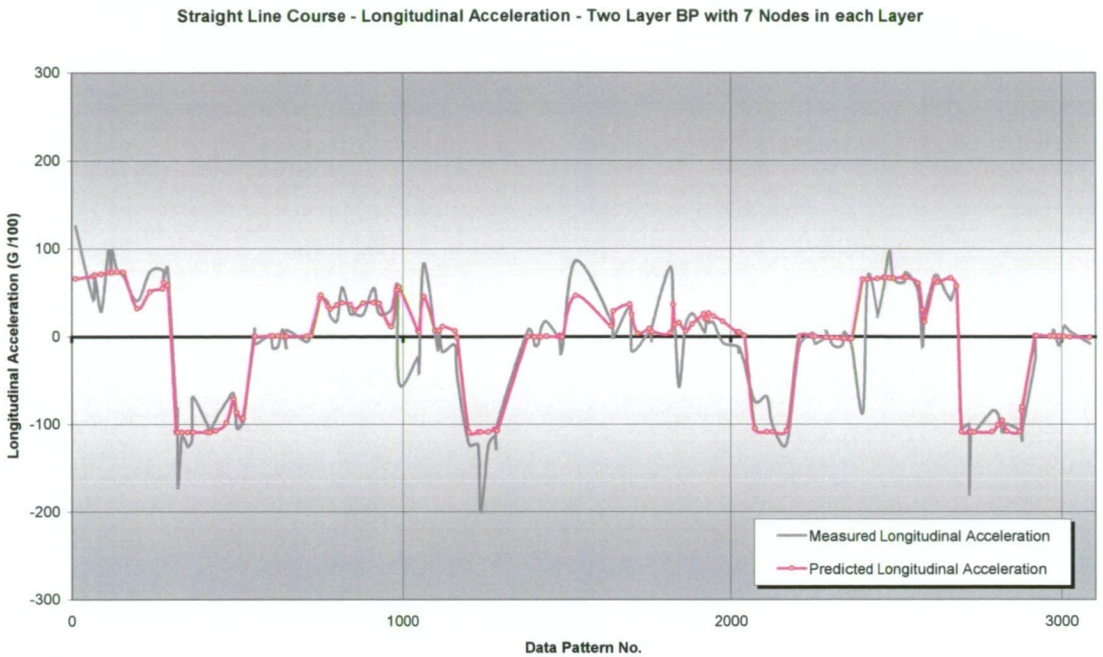

Figure 6.4: Longitudinal acceleration prediction during network testing – course 1

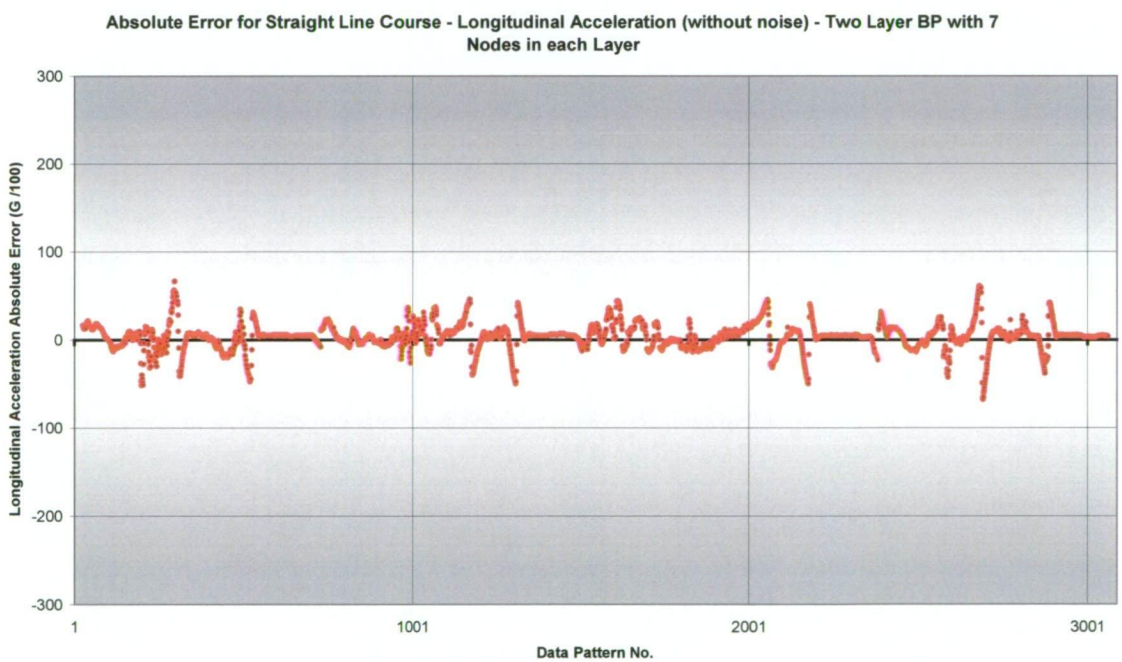

Figure 6.5: Longitudinal acceleration prediction error – course 1

The graph of longitudinal acceleration on the straight line course given in Figure 6.3 shows the measured acceleration (grey) used to train the network, the measured acceleration with the noise removed (blue) and the ANN predicted acceleration (pink). Looking at the measured acceleration it can be seen that the noise within it has, in some

places, amplitude that is numerous magnitudes larger than the averaged value. These noise 'spikes' can be shown to correspond to vibrations within the frame and also in the acceleration sensor at their resonant frequencies. It can also be seen that the noise under acceleration (positive G) experience much larger and erratic peaks than under braking (negative G). This suggests that the vibrations induced from high engine speed, excessive rear wheel slip and gear change can combine to produce large oscillation within the car and acceleration sensor, while the vibrations under braking produce a more uniform and lower magnitude oscillation.

Looking at the ANN predicted values it can be seen that this two layer BP, with 7 nodes in each hidden layer and trained to 100 iterations, follows the noiseless measured trend quite well. Under acceleration it can be seen that the curve follows the measured values well in most areas, but in some places either exaggerates peaks or flattens them out. It can also be seen that on a couple of places (pattern no. 200 and 1000) the network predicts a little of the noise induced in the sensor. This may indicate that the network has gone part of the way to being able to predict the vibration process that produces the noise, but it is also possible that insufficient data was gathered in these regions, resulting in under-training at these points.

Under braking it can be seen that the predicted curve flattens out much more than the measured data. It can be seen that it consistently approximates the measured data to a curve similar to a step function, but in doing so still follows the curve reasonably well. However, it should be noted that deceleration under brakes lies more in the realms of ABS, and since traction control is the focus of this study, it has little consequence on the final results (unless, of course, the engine braking provided though traction control is being used as a form of active brake control).

The testing graph given in Figure 6.4 also verifies that the network has learnt the vehicle dynamics trends well. By comparing the two graphs it can be seen that the majority of the deviation is due to noise within the results. The predicted values still follow the trends given by the measured values once noise is removed, which indicates that the network has learnt, rather than overfit, the data patterns.

Further, the longitudinal acceleration error graph given in Figure 6.5 shows an offset of 0.012G, indicating that the values vacillate around the mean so that there is no significant under or over bias within the model, and an absolute RMS error of 0.152G. When considering that the longitudinal acceleration field of the test vehicle is from 1.3G to –1.4G this equates to a full scale RMS error in the predicted values of just 5.6%. Further, it can be seen that the large errors in the graph are induced when the vehicle makes the transition from accelerating to braking, meaning that the majority of the error arises outside of the region where traction control operates.

6.3.2. Lateral Acceleration Prediction

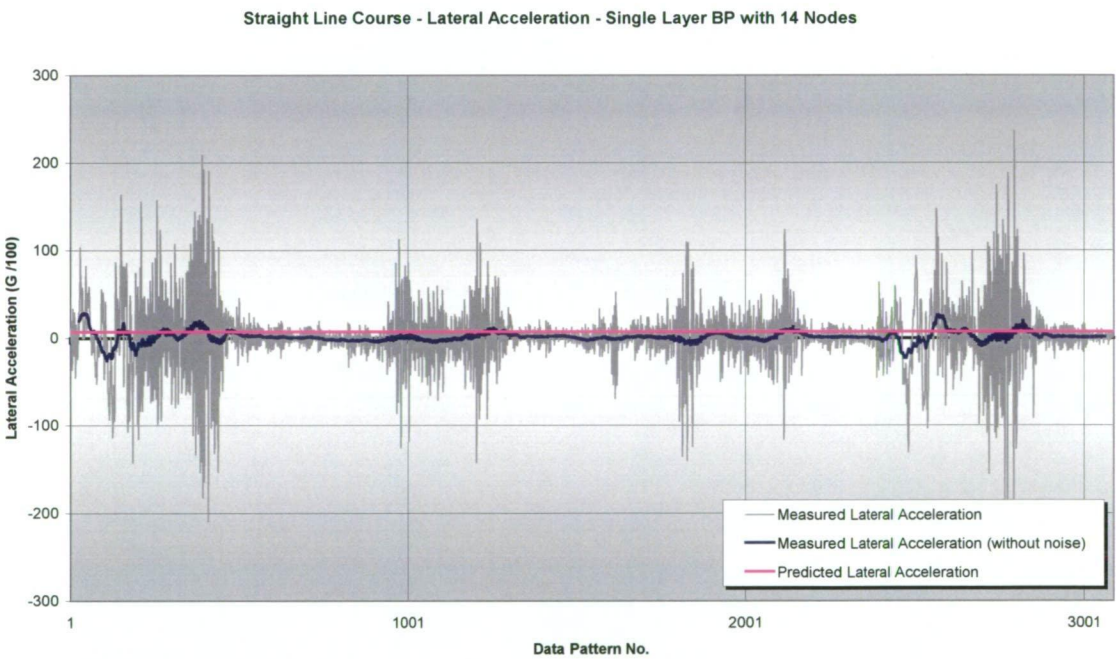

Figure 6.6: Lateral acceleration prediction during network training – course 1

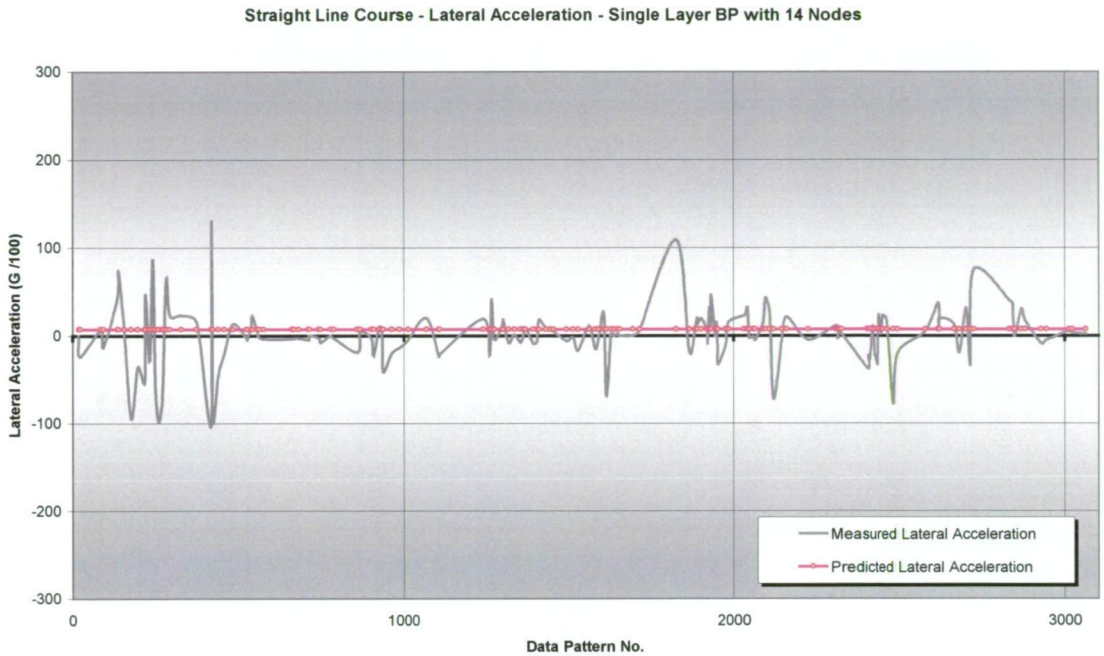

Figure 6.7: Lateral acceleration prediction during network testing – course 1

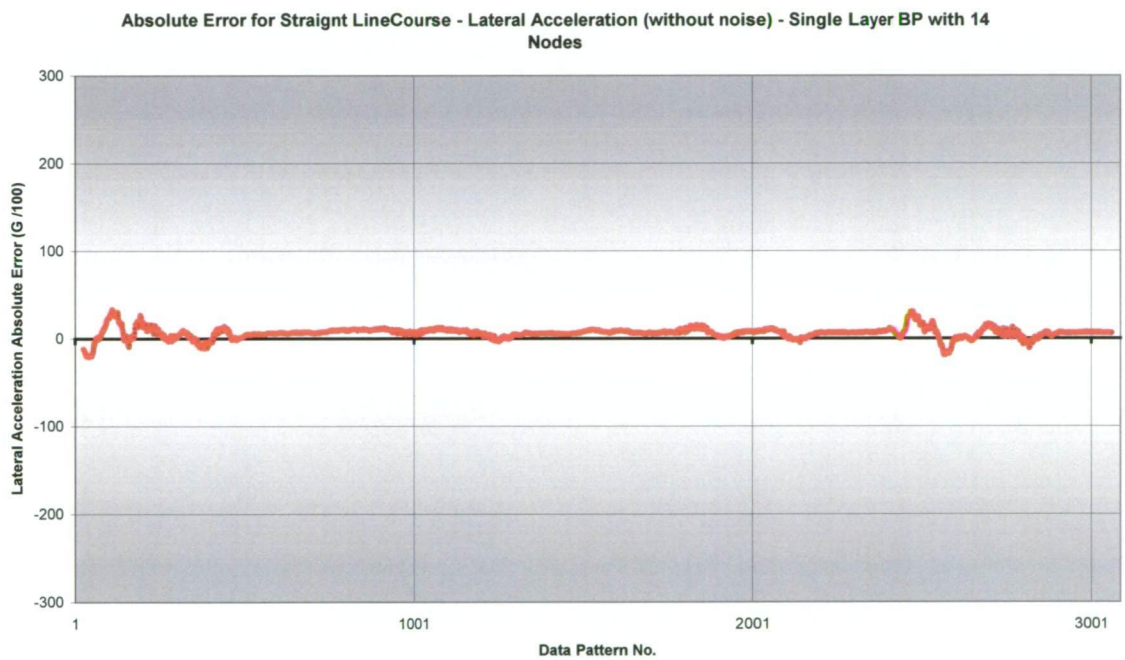

Figure 6.8: Lateral acceleration prediction error – course 1

The lateral acceleration graph for straight line running is given in Figure 6.6. As expected on a course that promotes only longitudinal acceleration, the lateral accelerating values are extremely small. It can be seen from the data with the noise removed that small lateral accelerations are only experienced due to the small driver

corrections required to maintain a straight course as the vehicle moves around laterally as a result of slip and small surface fiction coefficient variations. Of note, however, is the proportionally very large noise displayed in the results, again induced through chassis and sensor vibrations. It is the extent of this noise that makes it difficult for the ANN to identify the data trends, as can be seen in Figure 6.7, and is the reason why the ANN (chosen this time as a single layer 14 node BP network trained to 100 iterations) produced an output that was constant throughout the results. However, in this case, the use of a constant value still provides a reasonably accurate representation of the lateral acceleration. Figure 6.8 shows the error between the measured and predicted results, and it can be seen that it has an absolute RMS error of only 0.085G and an offset of 0.044G. Considering that the lateral acceleration field extends to 1.5G in either direction this corresponds to a full scale RMS error of just 2.8%. It should be noted at this stage, however, that the use of an ANN that simply predicts a single, constant value defeats the purpose of its use, and so further work should be conducted to provided a model that provides some sort of trend in relation to the data.

6.3.3. Yaw Angle Prediction

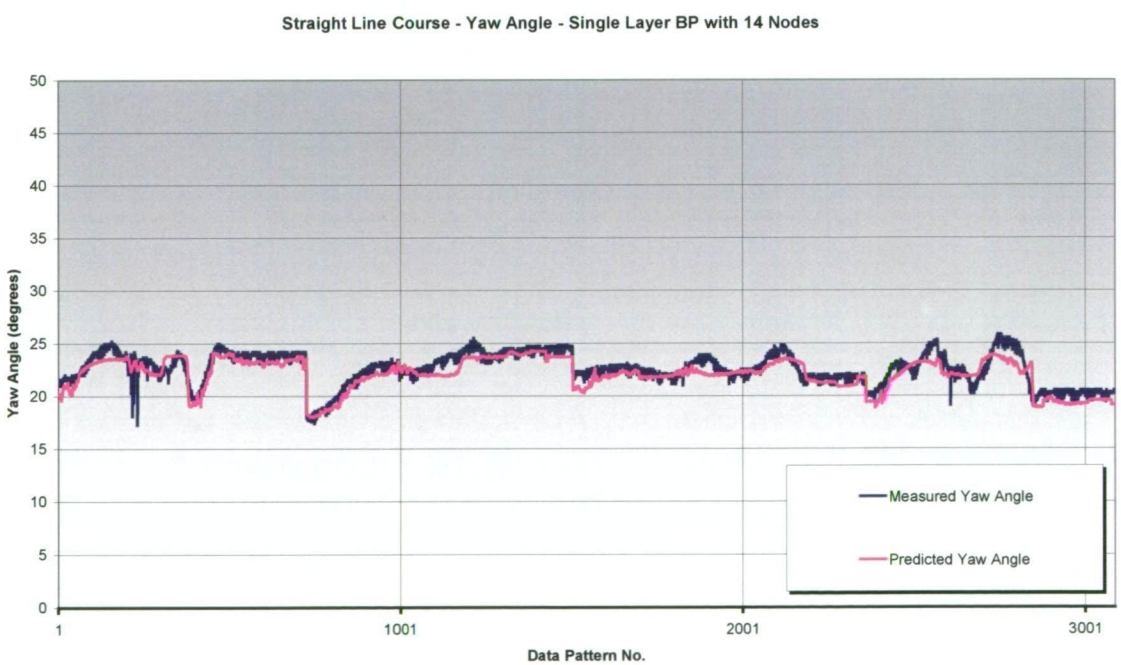

Figure 6.9: Yaw angle prediction during network training – course 1

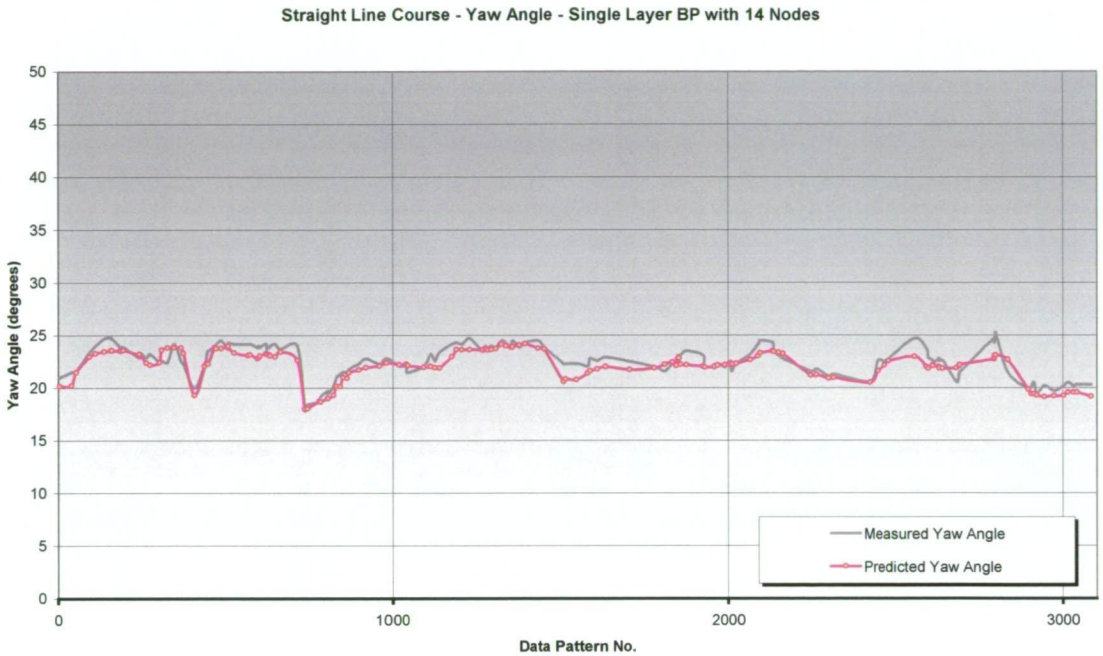

Figure 6.10: Yaw angle prediction during network training – course 1

Figure 6.11: Yaw angle prediction error – course 1

Again, because the course being run in this case is a straight line, one would expect the yaw angle to vary very little. Indeed this is the case, as shown in Figure 6.9. It can be

seen that the yaw angle varies by only approximately 5°, with a three small 'jumps' between runs as a result of the way the data was collated.

Comparing the measured and predicted values in both Figure 6.9 and 6.10, the two curves follow the trends of each other closely. While the predicted values consistently do not quite reach the peaks of the measured data, they still follow their general tendencies. Figure 6.11 shows that the error is very low, with absolute RMS error of 0.8°, offset of –0.3° and full scale RMS error of 0.2%, with the majority of the error produced during braking and gear changing.

6.4. BP Network Model - Course 2

6.4.1. Longitudinal Acceleration Prediction

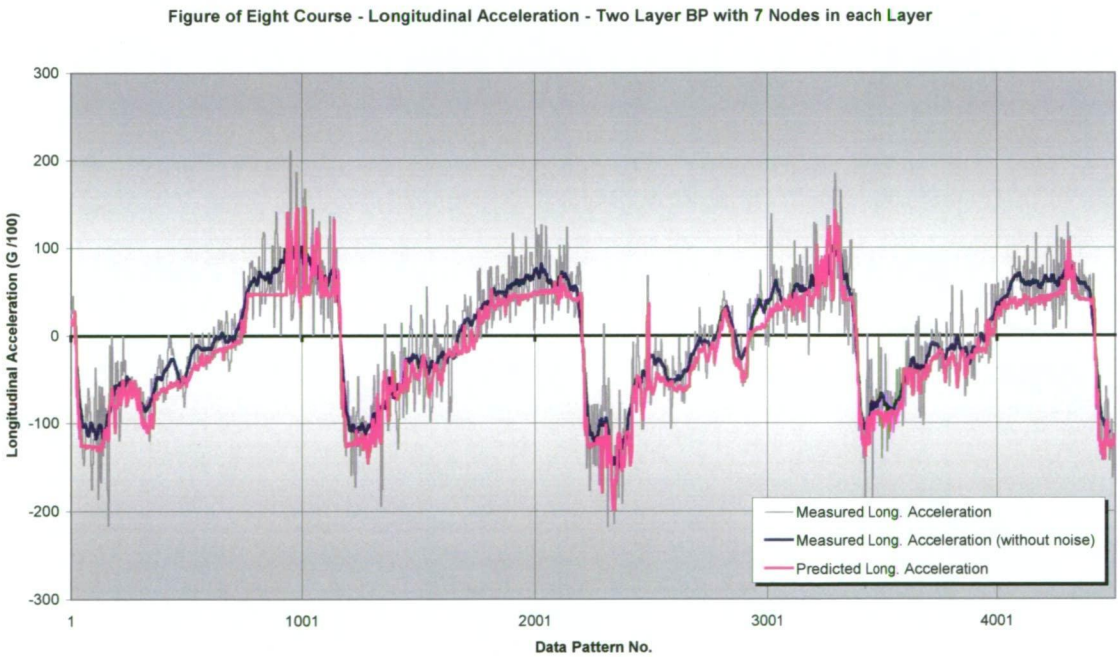

Figure 6.12: Longitudinal acceleration prediction during network training – course 2

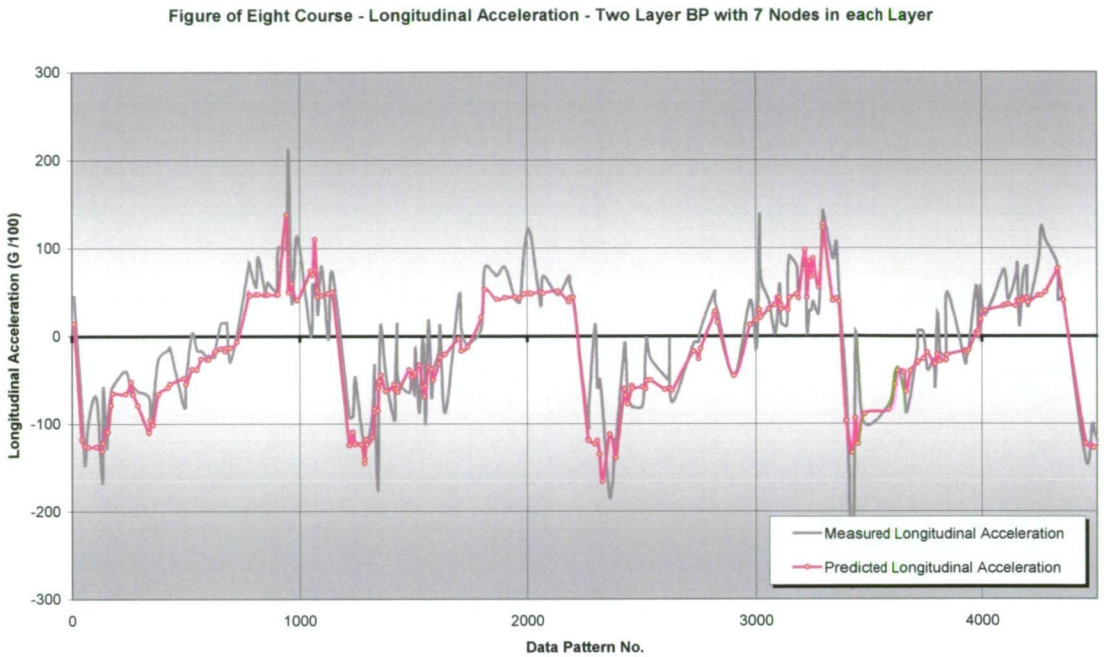

Figure 6.13: Longitudinal acceleration prediction during network testing – course 2

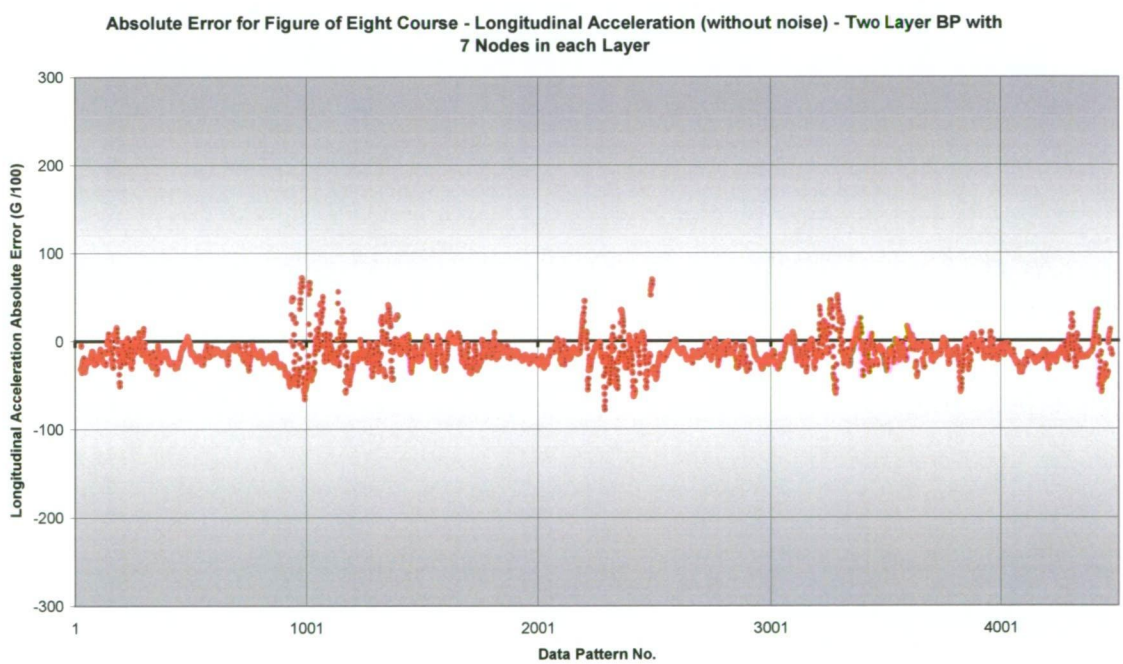

Figure 6.14: Longitudinal acceleration prediction error – course 2

As mentioned above, the figure eight course data was compiled from a single, continuous data set and incorporates both longitudinal and lateral acceleration as well as yaw angle. Looking at the longitudinal results in Figure 6.12 it can be seen that noise in

the measured values has a smaller magnitude and is more uniform than in the straight line case. This may be because the sampling rate was halved between courses, reducing peak sizes, but may also be because the operating conditions of the vehicle were not conducive to creating excessive vibration.

Looking at the driving style (shown in the results in "Appendix I") it can be seen that when approaching a corner the driver went hard on the brakes to slow the vehicle into the corner. The driver then stayed on the brakes into the beginning of the corner as they turned the steering wheel, before then moving to the throttle which was progressively increased throughout the remainder of the corner. Once out of the corner, the driver then accelerated along the straight to the next corner. This style would have reduced the engine speed range, number of gear changes and also the amount of wheel slip in both accelerating and braking, all of which were identified previously as possible sources of excessive vibration, and thus data noise.

The ANN use to predict the longitudinal accelerations was chosen as a two layer BP, operating with 7 nodes in each layer and trained to 100 iterations. It can be seen that the resulting predictions again follow the measured values closely. Looking at the graph it can be seen that the predicted values are consistently offset but still follow the data trends through the majority of the sample range. It can also be seen that the main deviations arise at maximum acceleration and deceleration, where the network seems to be predicting noise. Again, this may be because the network has gone part of the way to being able to predict the vibration process that produces the noise, but in this instance it seems more likely that that insufficient data was gathered for these regions.

With reference to Figure 6.13, it can be seen that the predicted data also follows the measured trends very well. Disregarding the effects of excessive noise in the results it can be seen that the testing predicted values have the same form as the training ones. It can also be seen, however, that it is still trying to predict some of the noise within the testing data which gives rise to the possibility of overfitting within this region, in addition to the other factors already mentioned.

Considering all of these factors, the network still shows admirable predictive accuracy. Figure 6.14 shows very small errors for the majority of the data, peaking only when the model becomes confused due to noise. As a result, the prediction accuracy of the model can be shown to give absolute RMS error of 0.212G, full scale RMS error of 7.8% and prediction offset of –0.139G which are still considerably small.

6.4.2. Lateral Acceleration Prediction

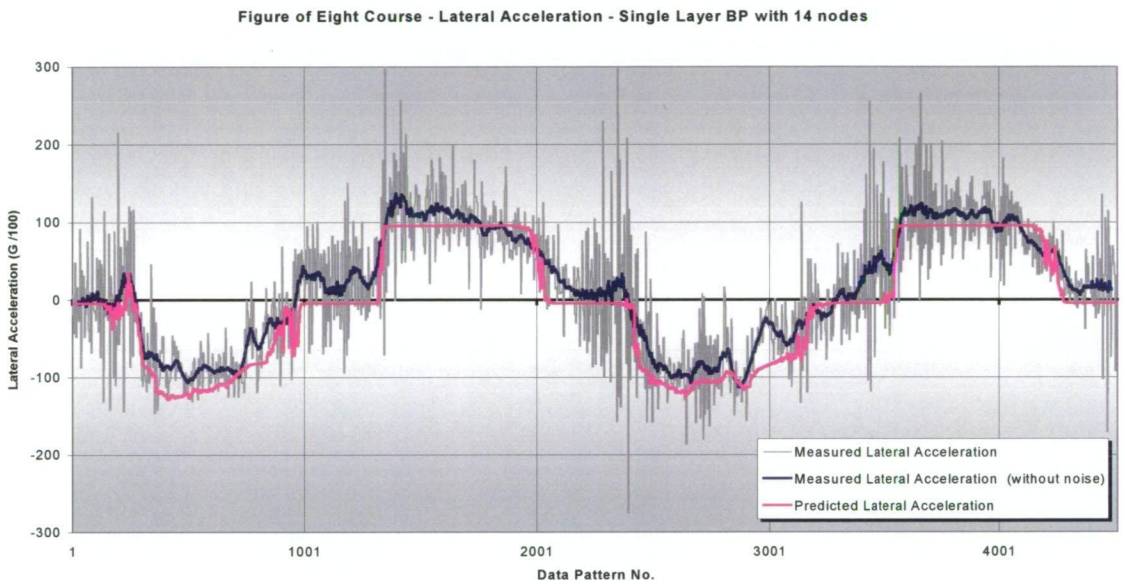

Figure 6.15: Lateral acceleration prediction during network training – course 2

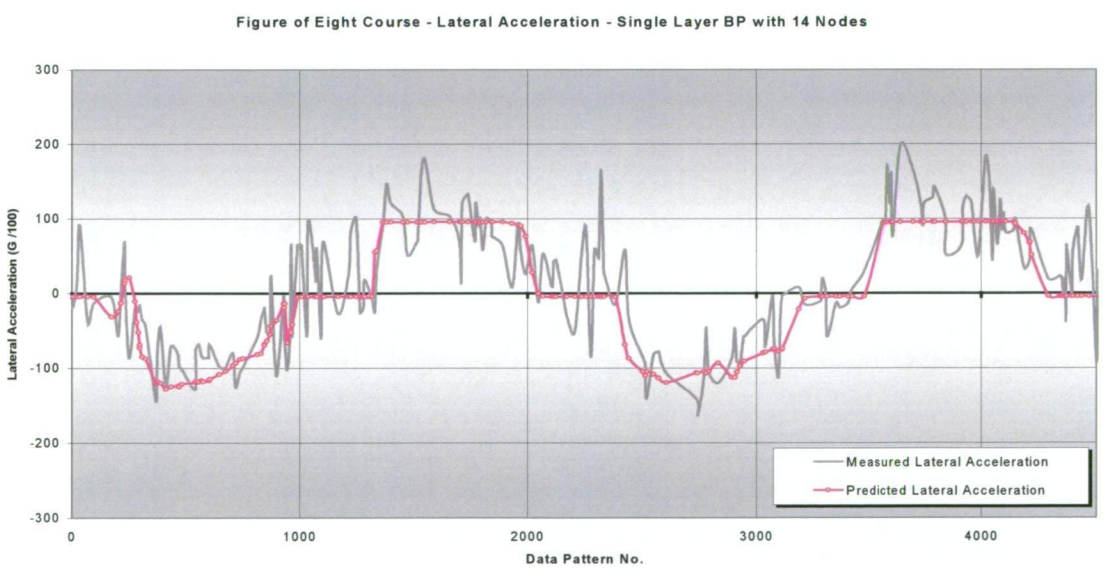

Figure 6.16: Lateral acceleration prediction during network testing – course 2

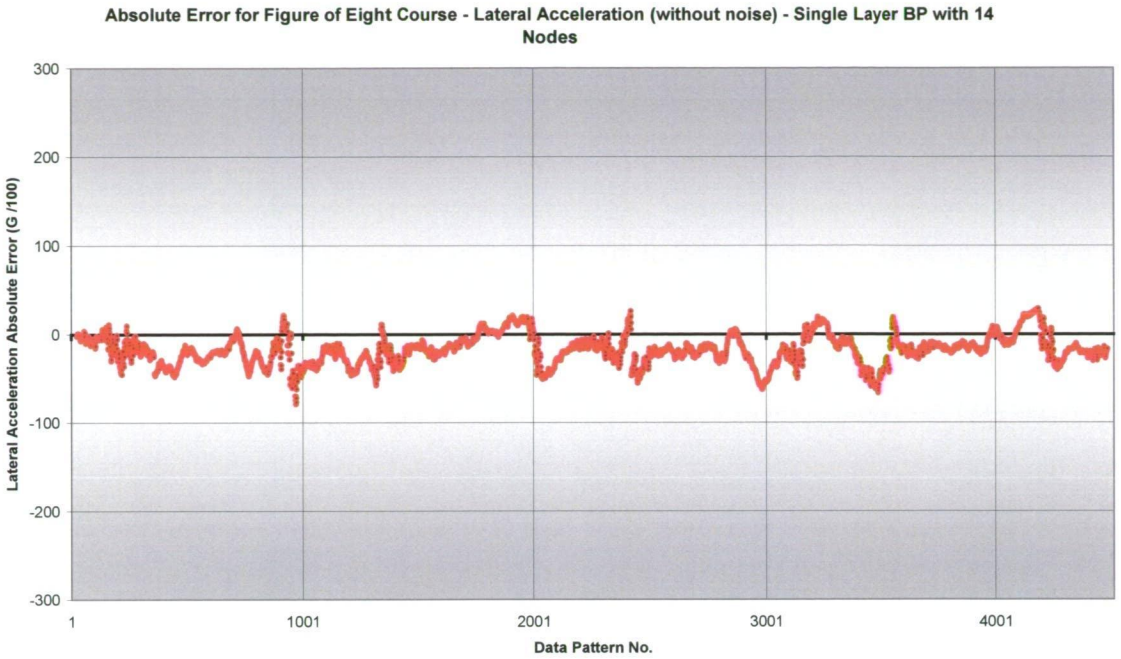

Figure 6.17: Lateral acceleration prediction error – course 2

Figure 6.15 shows the lateral acceleration results for the figure of eight course. Unlike in the straight line case, it can be seen that lateral accelerations vary as the vehicle completes its turning manoeuvres. It can also be seen that the data collected contains significant noise, with a near uniform distribution and peaks that frequently reach amplitudes of 3 to 4G. This represents a similar noise relationship as in the course 1 results, varying with chassis and sensor vibrations as resonant frequencies are reached, as well as the effects of the vehicle dynamics highlighted in section 6.4.1. In this case however, the noise seems so severe that the method used to remove the noise by averaging the results over 50 sampling periods still produces data that contains moderate oscillation. Looking at the single layer, 14 node BP network predicted values, however, it can be seen that despite the noise the curve follows the training data quite well when turning into the negative G range and approximating a step function when turning in the other direction. This may be due to the vehicle characteristics, but is most likely a fault in this preliminary network architecture. These predicted curve characteristics are also highlighted in the testing data depicted in Figure 6.16 and the error graph shown in Figure 6.17. Here it can be seen that despite the high levels of noise the network predicts with high accuracy of –0.181G offset and 0.248G absolute and 8.3% full scale RMS error.

6.4.3. Angle Prediction Yaw

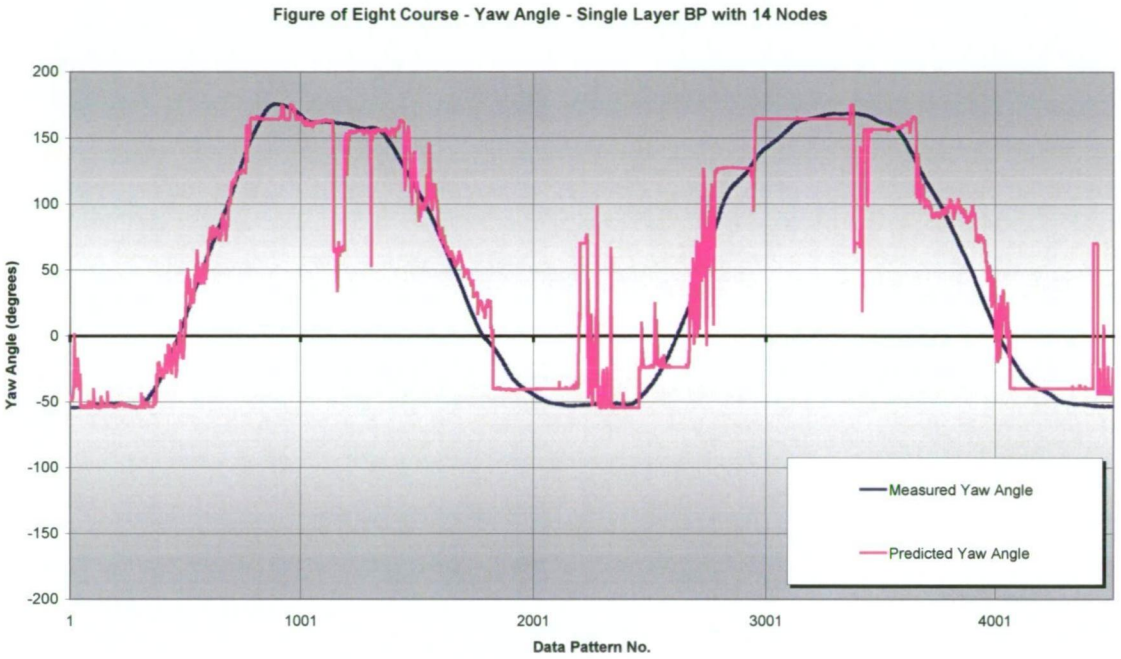

Figure 6.18: Yaw angle prediction during network training – course 2

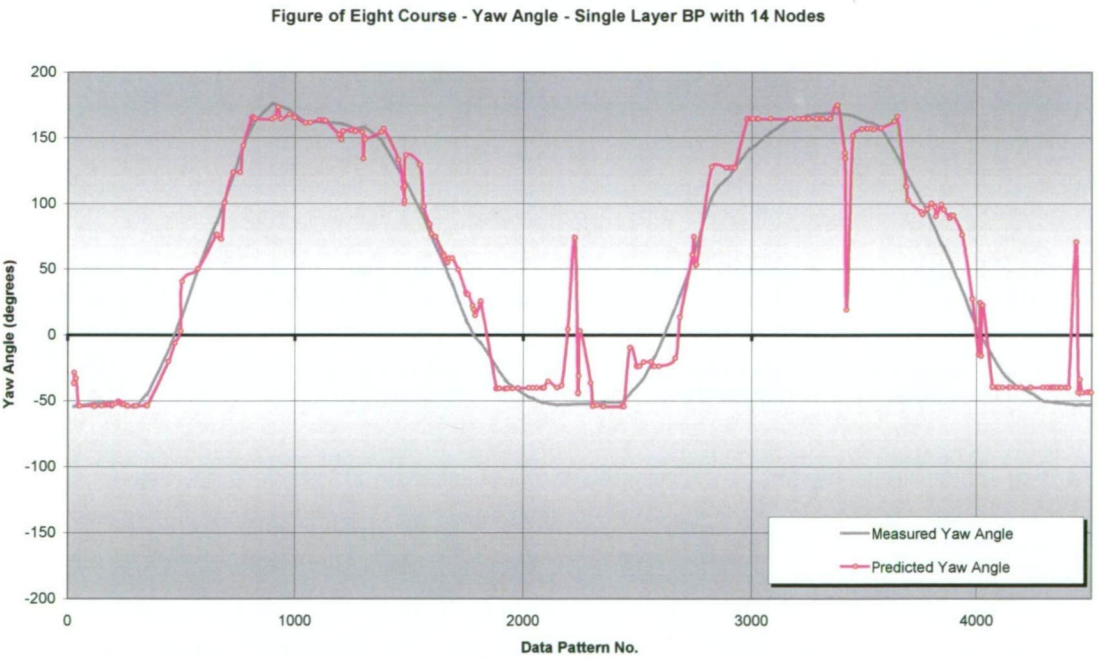

Figure 6.19: Yaw angle prediction during network testing – course 2

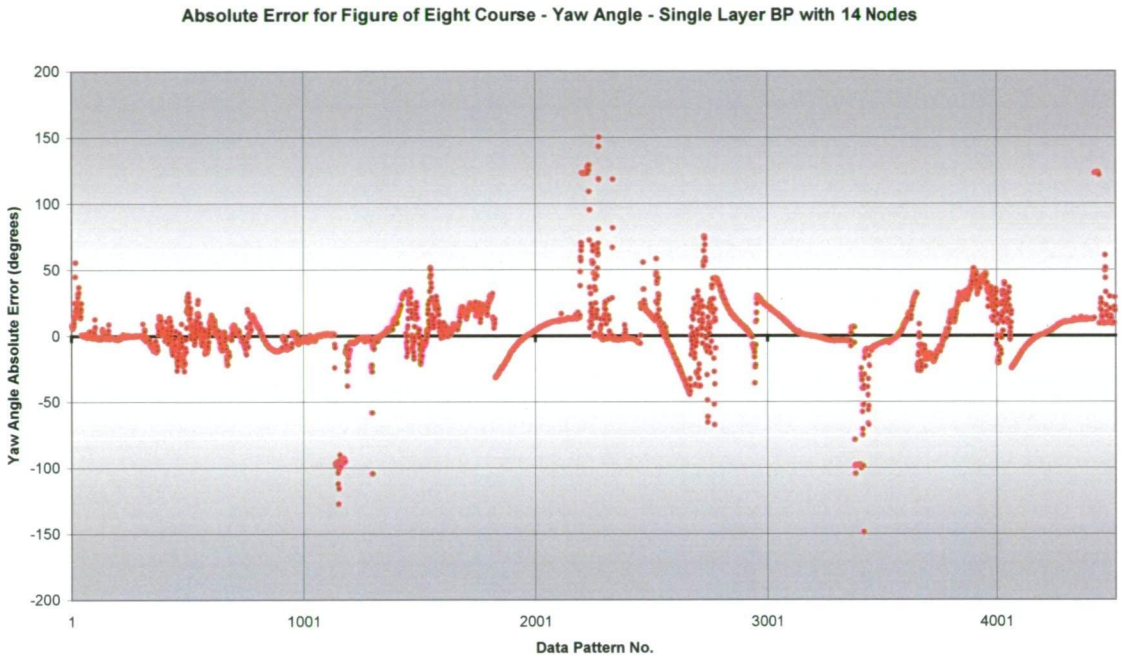

Figure 6.20: Yaw angle prediction error – course 2

Since on a figure of eight course the vehicle turns in one direction at one end of the course and in the other at the opposite end, the yaw angles for course 2 are as shown in Figure 6.18. It can be seen here that the training data, which displays very little in the way of noise, follows a sinusoidal type curve that represents the characteristics of the test track, with very little in the way of purely straight runs. Further inspection also shows that there are some periods where the curve deviates from this simple shape, and is the result of excessive lateral slip – mainly on the approach and departure to the corners. Looking at the predicted values it can be seen that curve again generally follows the measured values in both Figure 6.18 and Figure 6.19, except with two marked attributes. The most obvious is the occasional large deviation from the measured values, while the second is the scattered nature of the data which prevents the smooth prediction curves that are so obvious within the measured values. There is obviously room for improvement in all aspects within this model, from increasing data quality and providing additional sensor measurements to improving ANN architecture and training characteristics. Nonetheless, Figure 6.20 gives the absolute and full scale RMS errors to be only 25.14° and 7.0% receptively, with an offset if just 3.97°, which is still a very promising result.

6.5. GRNN Model – Course 1

As stated previously, the results for all of the GRNN models are given in "Appendix J" to avoid repetition. Additionally, the training and testing data for these models was taken from the same data set used within the BP models, and as such the results will not be discussed in as greater detail as was the case above.

6.5.1. Longitudinal Acceleration Prediction

Figure J.1 and J.2 show the training and testing data for the longitudinal acceleration predictions respectively. It can be seen that the 40 node GRNN trained with $\sigma = 0.4$ also produces predictions for the straight line course that are similar in quality to the BP case, except with a larger offset in some places. This offset causes the network to constantly predict the longitudinal acceleration to be slightly negative when the vehicle is at rest and also to regularly under predict acceleration. However, it can be seen from Figure J.3 that the major source of the error in this model stems from the moment the driver comes off the accelerator and on to the brake, when the accelerations go from positive to negative. In this case the model s slow to predict the change and significant error results. With this in mind though, the absolute and full scale RMS error for the GRNN model is still just 0.206G and 7.6% respectively, despite the 0.108G offset, making it a little less accurate than the BP model.

6.5.2. Lateral Acceleration Prediction

The first thing that is noticed when comparing the lateral acceleration predictions for GRNN, depicted in Figures J.4 and J.5, with the BP results is that the GRNN model has not approximated the results to a constant value. However, in doing so it can be seen that the network has developed some erroneous trends, sometimes exaggerating the predicted values and other times giving results that seem to bare little resemblance to the measured values. These errors are highlighted in Figure J.6, with deviations of close to 1G common. The result is a network that displays significantly higher error than the

BP model, with an absolute and full scale RMS error of 0.217G and 7.2% respectively, and an offset of 0.099G.

6.5.3. Yaw Angle Prediction

Again, the yaw angles in this case see very little variation. However, the GRNN predictions follow the trends quite well throughout the majority of the data, with the main deviation the result of the significant jump at about data pattern number 800 due to the 'cut and pasting' technique used to condition the data, as can be seen in Figures J.7 and J.8. In this case the deviation would be considered the fault of the data conditioning quality, rather than model performance, and since it is the significant cause for the model RMS error the result is an underestimate of model accuracy. This said, however, the network still displays an offset of 0.27° and an accuracy of just 1° absolute RMS error – equating to 0.3% full scale RMS error.

6.6. GRNN Model – Course 2

6.6.1. Longitudinal Acceleration Prediction

While the BP results for longitudinal acceleration on the figure of eight course was shown to follow the data well, except for the occasional period where it predicted noise, the GRNN results shown in Figure J.10 and J.11 can be seen to cope well in terms of noise prediction, but deviate from the measured values in some areas. It can be seen in a number of positions within the training data that there are two significant deviations with no obvious explanation, but become less pronounced in the testing data. Since the deviation continue over so many data patterns this has a marked effect on the model accuracy, as shown in Figure J.12. Here it can be seen that the GRNN model has a much smaller offset than the BP one, of just 0.028G, but has in total a larger RMS error of 0.261G absolute and 9.7% full scale.

6.6.2. Lateral Acceleration Prediction

The differences between the BP and GRNN models are distinct in this case of lateral acceleration prediction. As discussed above the BP network approximates the curve to a 'step function' style shape, whereas the GRNN model displays characteristics of exaggerated features, as can be seen in Figure J.13 and J.14. It can be seen that in some cases the model significantly under predicts value, while in others it over predicts, often to high magnitudes of error as is the case near pattern number 2300. It seems that this effect is due to the noise within the measured results, often occurring at the noise 'spikes', and so may be able to be solved by increasing the lateral acceleration sensor accuracy. As it stands, however, the model displays significant error, as shown in Figure J.15. It can be seen that the afore mentioned 'spike' represents a significant proportion of the total RMS error of 0.450G absolute and 15.0% full scale (which is starting to get quite large) but the network manages to maintain a small offset of just – 0.032G.

6.6.3. Yaw Angle Prediction

It can be seen from Figure J.16 to J.18 that the GRNN yaw angle predictions are extremely erroneous, with an absolute RMS error of 64.9°, full scale RMS error of 18.0% and offset of 1.90. The predictions only follow a vague trend, with many unwarranted deviations mainly as the yaw angles reach their maximum and minimum values (ie when cornering). This may represent a significant flaw in the model during cornering manoeuvres and could be improved with the adoption of any of the measures mentioned throughout this chapter.

6.7. BP and GRNN Comparison

The results giving throughout the bulk of this chapter highlight a number of issues. The first is that the majority of the ANN models discussed here seem to operate with high levels of accuracy, despite being only preliminary models that can be improved upon in many respects. The second is that the BP and GRNN models display different

characteristics in the way they predict the data. It can be seen in Table 6.1 that the BP networks consistently have lower RMS errors, but that the GRNNs produce marginally less offset data. It should be noted, however, that these two models represent the 'tip of the iceberg' and there are many more ANNs to test before a decision can be made as to which is the best for this application.

	BP Network			GRNN		
	Average Abs. Error (Offset)	Absolute RMS Error	Full Scale RMS error	Average Abs. Error (Offset)	Absolute RMS Error	Full Scale RMS error
Course 1						
Long. Accel. (G)	0.0116	0.1517	5.6%	0.1082	0.2060	7.6%
Lateral Accel. (G)	0.0445	0.0853	2.8%	0.0986	0.2172	7.2%
Yaw Angle (°)	-0.33	0.79	0.2%	0.27	1.00	0.3%
Course 2						
Long. Accel. (G)	-0.1385	0.2119	7.8%	0.0282	0.2613	9.7%
Lateral Accel. (G)	-0.1813	0.2476	8.3%	-0.0321	0.4495	15.0%
Yaw Angle (°)	3.97	25.14	7.0%	1.90	64.93	18.0%

Table 6.1: Summary of model absolute error properties

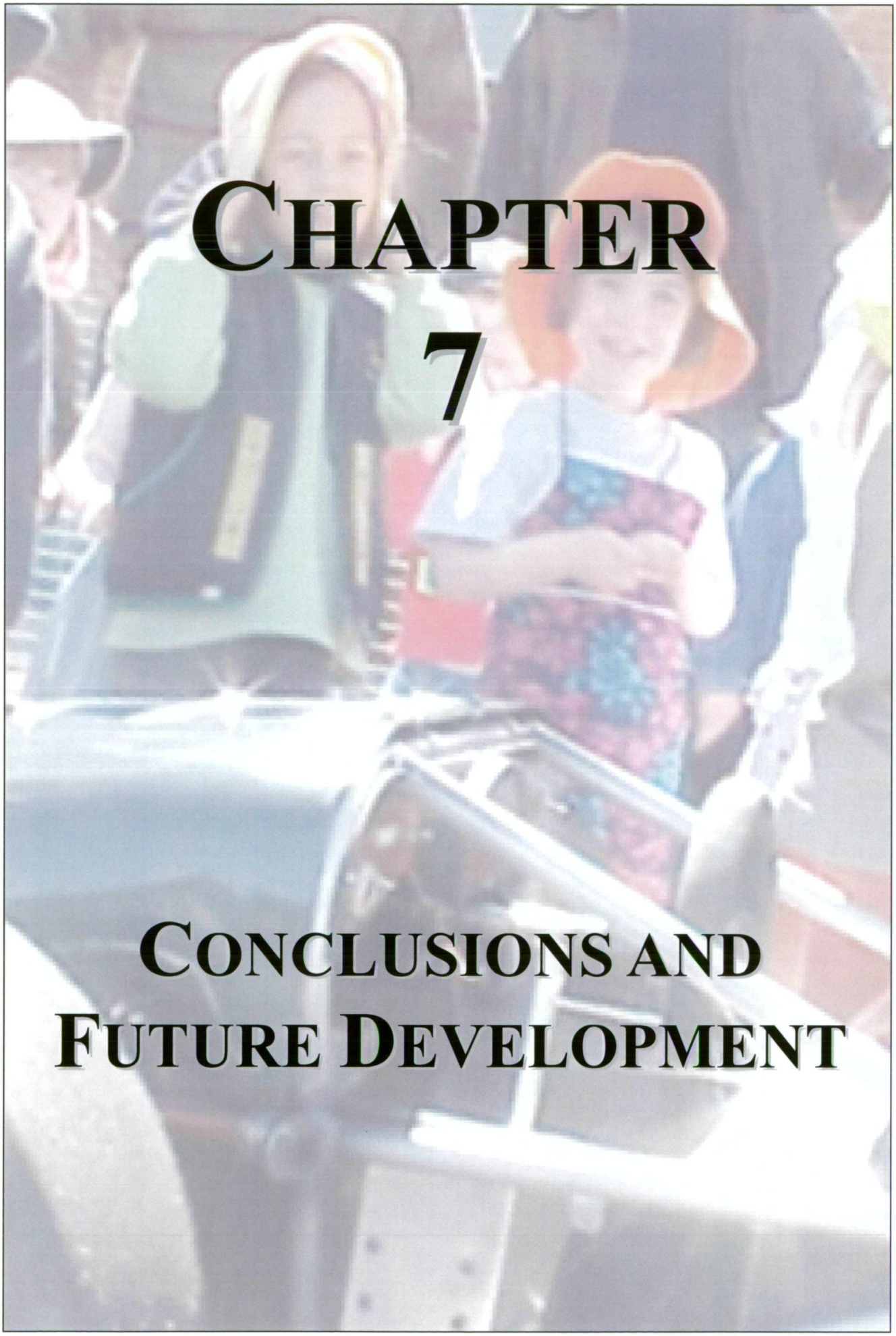

CHAPTER 7

CONCLUSIONS AND FUTURE DEVELOPMENT

From the extensive literature review carried out, it has been shown that there is a need for intelligent traction control in modern cars. It can be seen that the extent to which modern automobiles use conventional models for traction control is limited from both sensory and adaptability points of view, and can lead to erroneous control in some conditions. This work highlights the need for reliable quantitative predictions for longitudinal acceleration, lateral acceleration and yaw angles in all conditions for effective and robust traction control for use in a wider range of driving situations. Neural network modelling has previously been found to be a successful tool for performance estimation in complex manufacturing applications, and so was experimented with here for the prediction of these parameters.

It can be seen from the artificial neural network results that this preliminary investigation into the possible applications of ANNs in dynamic vehicle parameter prediction, with the aim of providing an effective traction controller, proved very promising. The ability of the majority of the networks to gain accuracies of less than 8% full scale RMS error shows that in these selected conditions ANNs can have high levels of accuracy, which could be further improved upon in future development. As already highlighted in the main body, significant improvements can be made to the ANNs to provide additional levels of accuracy.

In this work extensive research was also carried out into the design and development of the test vehicle, an open wheeler racecar build to the broad F-SAE specifications. Finite element analysis and structural modelling are a few of the techniques used in the design and construction of the chassis and other components of the vehicle. These include the suspension arrangement, the wheel assemblies, the steering system and the drivetrain, with each often utilising unconventional designs that proved highly effective. Other sub-systems such as the electrical circuitry, engine management system and data acquisition components were also installed through the coordination with other members of the 'Intelligent Car' team.

The use of artificial neural networks as predictive tools was found to be extremely satisfactory with both backpropagation (BP) and general regression neural networks (GRNN) giving excellent quantitative predictive capability given the preliminary nature of this investigation. The network training data was collected over a number of different driving conditions, with data acquisition completed on straight line and figure

of eight courses on a near homogeneous surface to provide information over a range of simplified driving conditions. The level of care for intricate instrumentation and data acquisition has resulted in reliable quantitative measurements for network modelling and testing, with BP networks providing acceleration predictions with RMS accuracies ranging from ± 0.085G to ± 0.25G and yaw angle predictions limited to ± 25° RMS error. While the results are encouraging, here is still significant room for improvement to optimise the networks for minimum training times and increased accuracy.

In terms of the acceleration prediction, the reduction of acceleration sensor noise due to vibrations was identified repeatedly as an important enhancement, as was the quality of all of the sensory data used throughout the training and testing processes. Improvements were also suggested in the selection of sampling rates and input parameters to enable the compression of as much relevant data as possible into small data sets. This would enable the networks to train themselves much more efficiently, and with many more driving conditions than possible within the scope of this study. The choice of network architecture was also mentioned as another way to improve network accuracy. As show within the results, the choice of network type and structure can have a large effect. Therefore, future work will involve conducting testing on a number of additional ANN models, as well as optimising each by experimenting with different network characteristics. These include trials in network properties such as the amounts of nodes and their arrangement, trying a number of training convergence parameters, altering the number of iterations to convergence and investigating the effects of different transfer functions. Combing all of these factors together produces significant scope ANN improvement beyond what has been covered within this study and should result in considerable improvements in predictive accuracy.

It is hoped that, once further work has been done to increase the ANN modelling accuracy, models will exist that can simulate the dynamics of a vehicle in regard to longitudinal acceleration, lateral acceleration and yaw angle in a broad range of conditions. This will provide models that can be compared to the actual running of the vehicle and can be used in on-line control.

The first stage of the integration of on-line control will most likely use just engine control, since the arrangement of the MoTeC M4 ECU makes this the easiest option for initial work and also requires the control of only one parameter; engine power. Control

of individual brakes, etc. could be included in the future once the system has proven itself. From this stage the ANN control could be set up in a number of ways. The most promising method, however, seems to be using the ANN to predict how close to the traction peak (Figure 2.3 & 2.10) each of the driven wheels are and adjusting driven wheel speed to suit. Considering only longitudinal acceleration as a special case, the ANN could be used to predict the longitudinal acceleration at a very slightly reduced driven wheel speed (reduced slip). If the acceleration of the vehicle is predicted to improve then there is obviously a need to reduce wheel speed, and engine power will be reduced, if not then the vehicle can be deemed in control with no intervention necessary. This principle can also be applied to lateral acceleration, providing a combination that covers all 2D motion of the vehicle, and yaw angle to prevent spin.

The ANN control data could then be used gain further estimates of the optimum sensor sampling rate for effective control, as well as providing a tool to test the effectiveness of different types of control logic, etc. The aim being to provide a robust system that can provide optimum traction on all surfaces likely to be encountered by an automobile.

- References -

[1] H. BAUER. "ESP Electronic Stability Program", Technical Instruction, Robert Bosch GmbH, 1999.

[2] H. BAUER. "Driving Safety Systems", Robert Bosch GmbH, Society of Automotive Engineers, 1999.

[3] R. K. JURGEN. "Automotive Electronics Handbook", 2nd Edition, Society of Automotive Engineers, 1999.

[4] D. R. McLELLAN, J. P. RYAN, E. S. BROWALSKI and J. W. HEINRICY. "Increasing the Safe Driving Envelope - ABS, Traction Control and Beyond", General Motors Corp, Society of Automotive Engineers, 1992.

[5] E. GOHRING. "Electronic Traction Control System ASR and its Integration in the Anti-Lock Braking Systems ABS to Form a Safety System ABS/ASR for Commercial Vehicles", Daimler-Benz AG, Society of Automotive Engineers, 1988.

[6] L. EVANS. "ABS and Relative Crash Risk Under Different Roadway, Weather, and Other Conditions", General Motors Corp, Society of Automotive Engineers, 1995.

[7] A. T. van ZANTEN, R. ERHARDT and G. PFAFF. "VDC, The Vehicle Dynamics Control System of Bosch", Robert Bosch GmbH, Society of Automotive Engineers, 1995.

[8] D. E. SCHENK, R. L. WELLS and J. E. MILLER. "Intelligent Braking for Current and Future Vehicles", Delco Chassis, Society of Automotive Engineers, 1995.

[9] T. MATHUES. "ABS Extending The Range", ITT Automotive Brake Systems, Society of Automotive Engineers, 1994.

[10] S. K. MOHAN and R. C. WILLIAMS. "A Survey of 4WD Traction Control Systems and Strategies", New Venture Gear, Society of Automotive Engineers, 1995.

[11] G. BROOKS. "Auto Engineer", Issue 6, Society of Automotive Engineers, 2001.

[12] R. BANNATYNE. "Future Developments in Electronically Controlled Braking Systems", Motorola Inc, Transportation Systems Group, 1998.

[13] V. V. VANTSEVICH, M. S. VYSOTSKI and S. V. KHARITONT. "Control of Wheel Dynamics", International Congress & Exposition, Society of Automotive Engineers, 1998.

[14] A. van ZANTEN, W. RUF and A. LUTZ. "Measurement and Simulation of Transient Tire Forces", Robert Bosch GmbH, Society of Automotive Engineers, 1989.

[15] K. C. CHEOK, F. B. HOOGTERP, W. K. FALES, K. KOBAYASHI and S. SCACCIA. "Fuzzy Logic Approach to Traction Control Design", Oakland University, Society of Automotive Engineers, 1996.

[16] Z. FAN, Y. KOREN and D. WEHE. "Practical Rule-Based Vehicle Traction Control", University of Michigan, Society of Automotive Engineers, 1994.

[17] A. SIGL and H. DEMEL. "ABS - Traction Control, State of the Art and Some Prospects", Robert Bosch GmbH, Society of Automotive Engineers, 1990.

[18] K. ISE, F. FUJITA, Y. INOUE and S. MASUTOMI. "The Lexus Traction Control (TRAC) System", Toyota Motor Corp, Society of Automotive Engineers, 1990.

[19] R. K. JURGEN. "Electronic Braking, Traction, and Stability Control", Society of Automotive Engineers, 1999.

[20] T. BACH, H. SCHMITT, W. SCHWANKE and H. TUMBRINK. "Roadrunner-Real-Time Simulation in Anti-Lock Brake System Development", Lucas Braking Systems, Society of Automotive Engineers, 1995.

[21] M. J. SCHEIDER. "Use of a Hazard and Operability Study for Evaluation of ABS Control Logic", Ford Motor Company, Society of Automotive Engineers, 1997.

[22] T. SHINOMIYA, T. TODA, M. NISHIKIMI, H. SAITO, H. TANKA and F. MANKINO. "The Sumitomo Electronic Anti-lock System", Sumitomo Electric Industries, Society of Automotive Engineers, 1988.

[23] H. DEMEL and H. HEMMING. "ABS and ASR for Passenger Cars - Goal and Limits", Robert Bosch GmbH, Society of Automotive Engineers, 1989.

[24] "Vehicle Dynamics Control", www.whnet.com/4x4/abs.html, 2002.

[25] H. SAITO, N. SASAKI, T. NAKAURA, M. KUME, H. TANAKA and M. NISHIKAWA. "Acceleration Sensor for ABS", Sumitomo Electric Industries, Society of Automotive Engineers, 1992.

[26] G. MAUER, G. GISSINGER and Y. CHAMAILLARD. "Fuzzy Logic Continuous and Quantising Control of an ABS Braking System", University of Nevada, Society of Automotive Engineers, 1994.

[27] W. SHOEBOTHAM. "Comprehensive Traction Control", Atlas F1, www.atlasf1.com/2000/dec27/shoebotham.html, 2000.

[28] R. HOLZWARTH and K. MAY. "Analysis of Traction Control Systems Augmented by Limited Slip Differentials", Zexel-Gleason Inc, Society of Automotive Engineers, 1994.

[29] W. MAISCH, W. JONNER, R. MERGENTHALER and ALFFRED SIGL. "ABS5 and ASR5: The New ABS/ASR Family to Optimize Direction Stability and Traction", Robert Bosch GmbH, Society of Automotive Engineers, 1993.

[30] T. IWATA, T. MURAKAMI and M. TAMURA. "Development and Analysis of New Traction Control System with Rear Viscous LSD", Nissan Motor Co. Ltd, Society of Automotive Engineers, 1991.

[31] K. HOSOMI, N. AKIRA and S. YAMAMOTO. "Development of Active-Traction Control System", Automotive Dynamics & Stability Conference, Society of Automotive Engineers, 2000.

[32] B. A. JAWAD, N. A. HACHEM and S. CIZMIC. "Traction Control Applications in Engine Control", International Truck & Bus Meeting & Exposition, Society of Automotive Engineers, 2000.

[33] K. ASAMI, Y. NOMURA and T. NAGANAWA. "Traction Control (TRC) System for 1987 Toyota Crown", Toyota Motor Corp, Society of Automotive Engineers, 1989.

[34] H. IGATA, K. UCHIDA, T. NAKATOMI and K. KOMATSUZAKI. "Development of New Control Methods to Improve Response of Throttle Type Traction Control System", Toyota Motor Corp, Society of Automotive Engineers, 1992.

[35] B. BONNING, R.FOLKE and K. FRANZKE. "Traction Control (ASR) Using Fuel-Injection Suppression - A Cost Effective Method of Engine-Torque Control", Robert Bosch GmbH, Society of Automotive Engineers, 1992.

[36] K. LYON, M. PHILIPP and E. GROMMES. "Traction Control for a Formula 1 Race Car: Conceptual Design, Algorithm Development and Calibration Methodology", Robert Bosch GmbH, Society of Automotive Engineers, 1994.

[37] A. STRICKLAND and K. DAGG. "ABS Braking Performance and Steering Input", Royal Canadian Mounted Police, Society of Automotive Engineers, 1998.

[38] A. T. van ZANTEN, R. ERHARDT, A. LUTZ, W. NEUWALD and H. BARTELS. "Simulation for the Development of the Bosch-VDC", Robert Bosch GmbH, Society of Automotive Engineers, 1996.

[39] "Artificial Neural Networks Technology", www.dacs.dtic.mil/techs/neural.

[40] F. FROST. "Neural Network Applications to Aluminium Manufacturing", PhD, University of Tasmania, 2001.

[41] V. KARRI and F. FROST. "Selecting Optimum Network Conditions In BP Neural Networks with respect to Computation Time and Output Accuracy", Comalco Aluminium Ltd, University of Tasmania, CR/01/1999.

[42] V. KARRI. "ANN for performance estimation in wood turning", ICMA '97, Hong Kong, Apr 29, pp 618.

[43] C. M. ATKINSON. "Virtual Sensing: a Neural Network-based Intelligent Performance and Emissions Prediction System of On-Board Diagnostics and Engine Control", Society of Automotive Engineers,

[44] C. ALIPPI, C. DE RUSSIS and V. PIURI. "A Fine Control of the Air-to-Fuel Ratio with Recurrent Neural Networks", Instrumentation and Measurement Technology Conference, IEEE, 1988.

[45] R. HECHT-NIELSEN. "Neurocomputing", University of California, Addison-Wesley Publishing, 1989.

[46] K. JAYAKUMAR, K. V. RAJARAM and M. A. FARUQI. "Machine Intelligence for Crisis Handling in Navigation Vehicles using Neuro-Controllers", 6th International Conference on Neural Information Processing, Institute of Electrical and Electronics Engineers, 1999.

[47] "2001 Formula SAE Rules", Society of Automotive Engineers, 2000.

[48] H. HEISLER. "Advanced Vehicle Technology", 1st Edition, Edward Arnold, 1989.

[49] M. PLATT. "Elements of Automobile Engineering", 2nd Edition, Sir Isaac Pitman & Sons, 1959.

[50] L. TERRY and A. BAKER. "Racing Car Design and Development", 1st Edition, Robert Bentley, 1973.

[51] C. CAMPBELL. "Design of Racing Sports Cars", 1st Edition, Chapman and Hall, 1973.

[52] D. HODGES and M. LAWRENCE. "A-Z of Formula Racing Cars (1945-1990)", 1st Edition, Bay View Books, 1990.

[53] M. COSTIN and D. PHIPPS. "Racing and Sports Car Chassis Design", 2nd Edition, B. T. Batsford, 1966.

[54] C. P. NAKRA. "Basic Automobile Engineering", 8th Edition, Dhanpat Rai Publishing, 1999.

[55] K. SINGH. "Automobile Engineering Vol. 1", 8th Edition, A. K. Jain, 2000.

[56] K. SINGH. "Automobile Engineering Vol. 2", 8th Edition, A. K. Jain, 2000.

[57] "Strand 7 - Finite Element Analysis System", Software, G+D Computing, 1999.

[58] "CADKey", Software, Baystate Technologies Inc., 1998.

[59] T. P. NEWCOMB and R.T. SPURR. "A Technical History of the Motor Car", 1st Edition, IOP Publishing, 1989.

[60] J. E. DUFFY, M. T. STOCKEL and M. W. STOCKEL. "Automotive Mechanics Fundamentals", 1st Edition, Gregory's Scientific Publications, 1985.

[61] "Design of Rolling Bearing Mountings", Catalogue WL 00 200/5 EA, FAG OEM und Handel AG, 1998.

[62] J. BRANDLEIN, P. ESCHMANN, L. HASBARGEN and K. WEIGAND. "Ball and Roller Bearings: Theory, Design and Application", 3rd Edition, Wiley.

[63] "FAG Rolling Bearings", Catalogue WL 41 520/2 EA, FAG OEM und Handel AG, 1998.

[64] "Technical Information", Catalogue WL 43 1190 EA, FAG OEM und Handel AG, 1997.

[65] R. L. NORTON. "Design of Machinery", 2nd Edition Mechanical Engineering Series, McGraw-Hill, 1999.

[66] D. BUTLER and V. KARRI. "Design Analysis Between On and Off-Centre Bearing for Racecar Wheel Using Finite Element Method", University of Tasmania, 2001.

[67] M. WATSON. "Common LISP Modules", Science Applications International Corp., Springer-Verlag Inc., 1991.

[68] D. HEBB. "Organisation of Behaviour", McGill University, John Wiley & Sons, Inc., 1964.

[69] M. ARBIB and J. ROBINSON. "Natural and Artificial Parallel Computation", Massachusetts Institute of Technology, 1990.

[70] M. ZEIDENBERG., "Neural Networks in Artificial Intelligence", University of Wisconsin, Ellis Horwood, 1990.

[71] M. CAUDILL and C. BUTLER. "Understanding Neural Networks", Volume 1, The MIT Press, 1994.

[72] "Gefran Online Catalogue", http://www.gefran.com/ing/istituzionale/m_map.htm, 2002.

[73] "Crossbow Online Catalogue", http://www.xbow.com/html/gyros/dmuahrs.htm, 2002.

[74] "Honeywell Online Catalogue", http://content.honeywell.com/sensing/prodinfo/auto/wheelspeed.asp, 2002.

[75] R. NEBEN. "Sensor Fusion as a Means to Identify Dynamical Behaviour on a Race Car", University of Tasmania, 2001.

Appendix A - Frame Design -

A-1: FEA of frame under normal driving

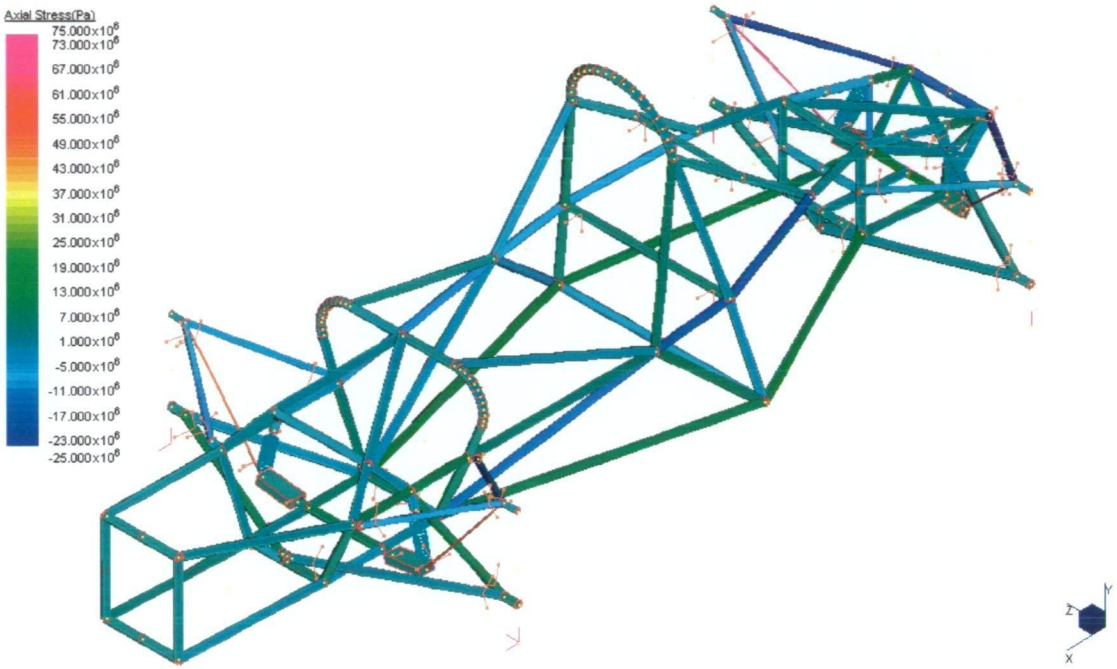

A-2: FEA of frame under acceleration

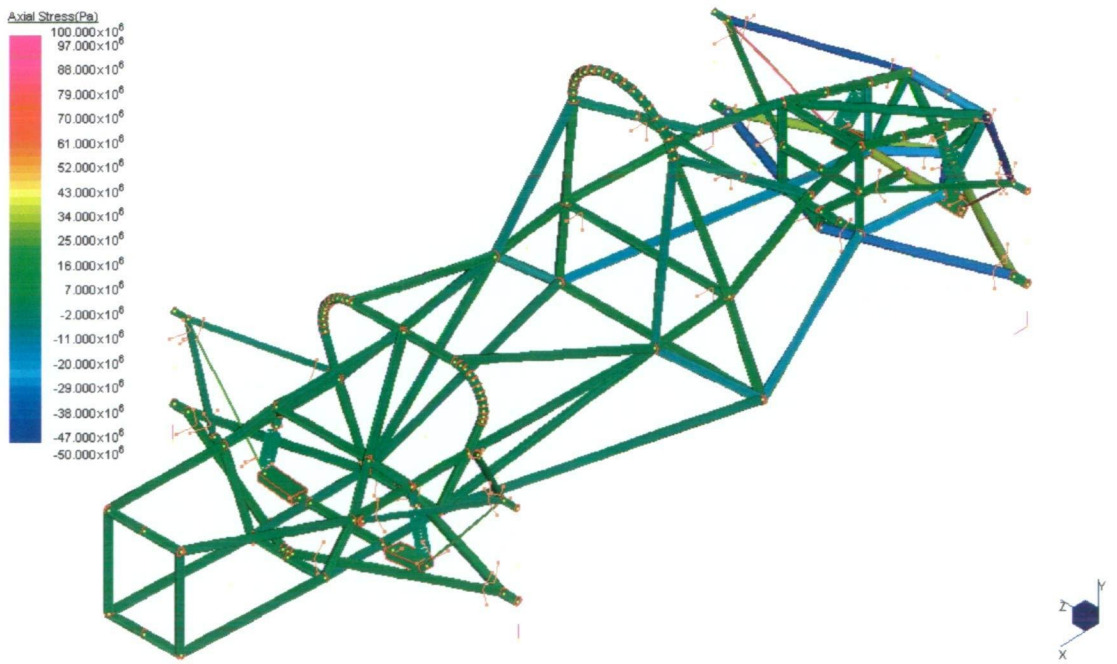

A-3: FEA of frame under braking

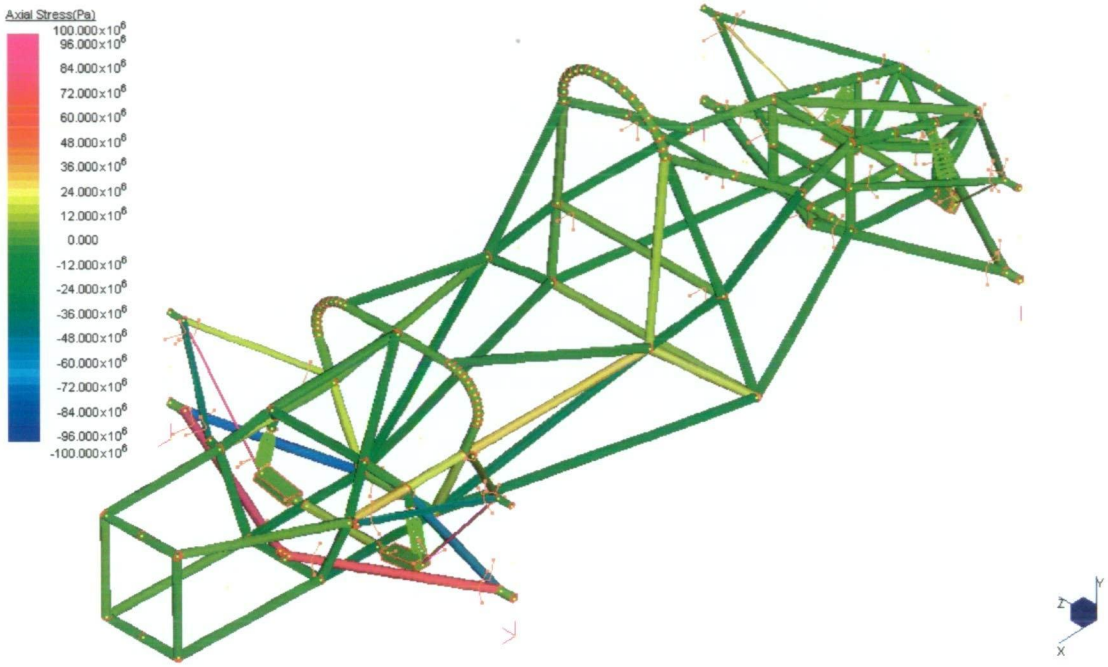

A-4: FEA of frame during cornering

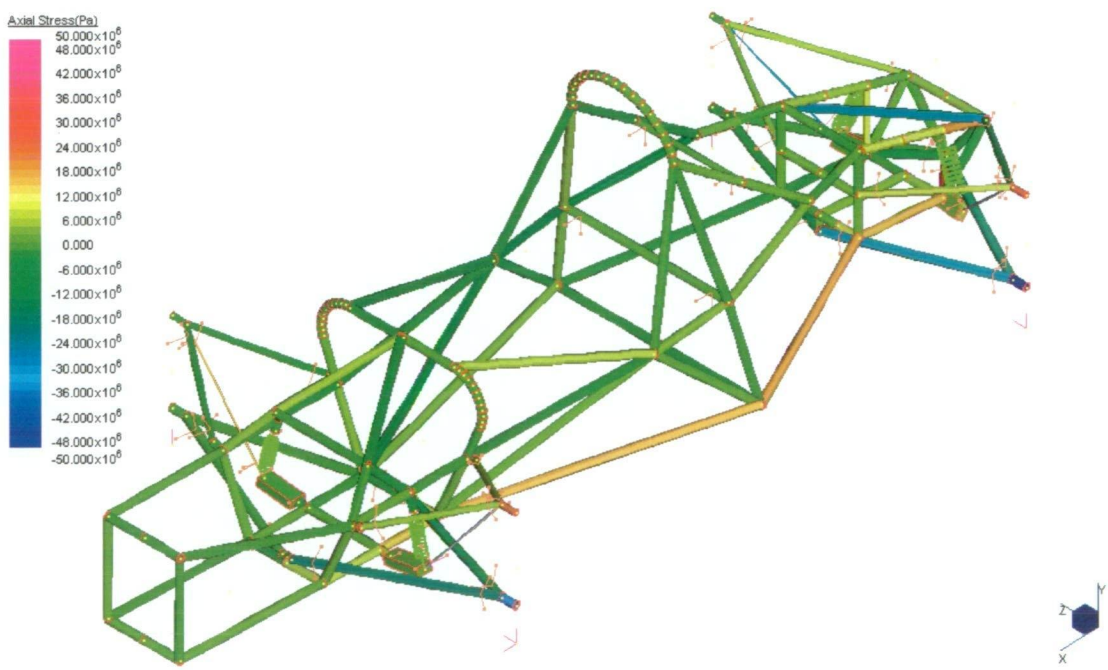

A-5: FEA of frame during cornering under acceleration

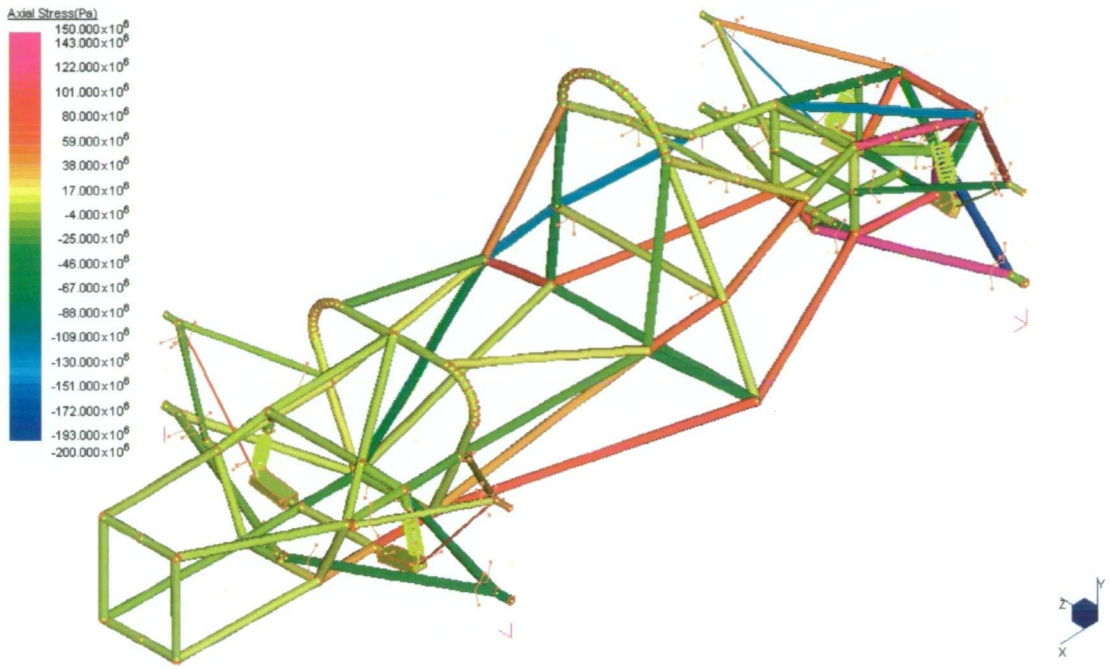

A-6: FEA of frame during cornering under acceleration

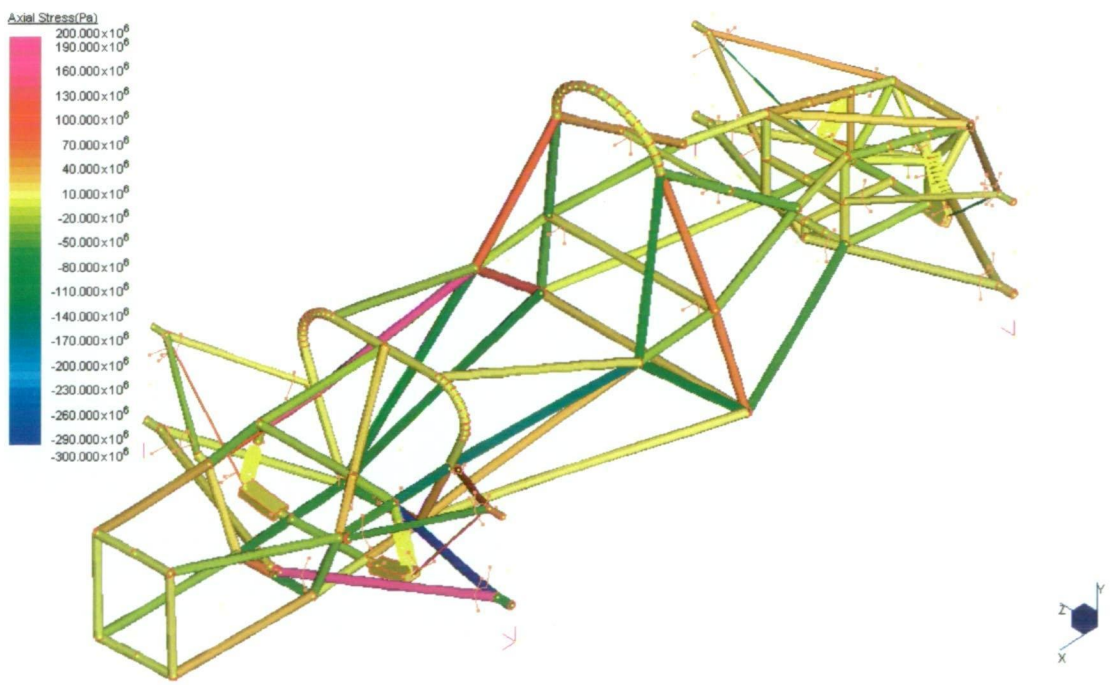

A-7: FEA torsional results under 1 Nm

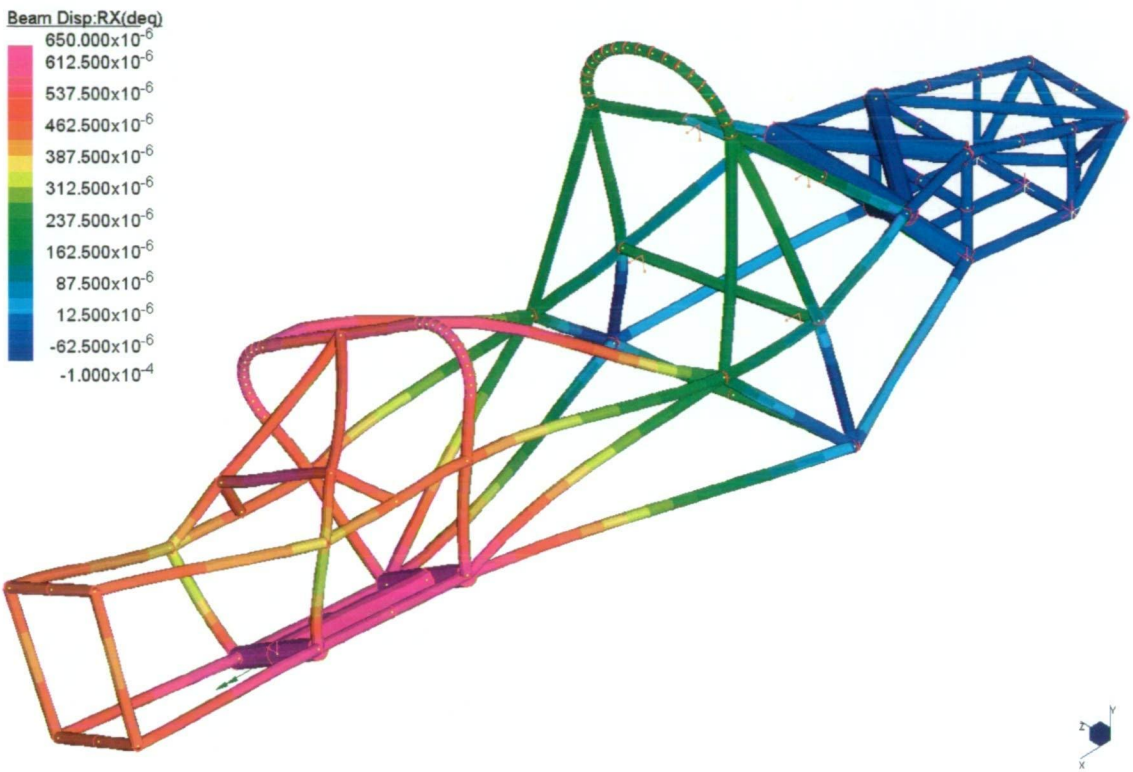

A-8: Left view of frame (1st set of dimensions)

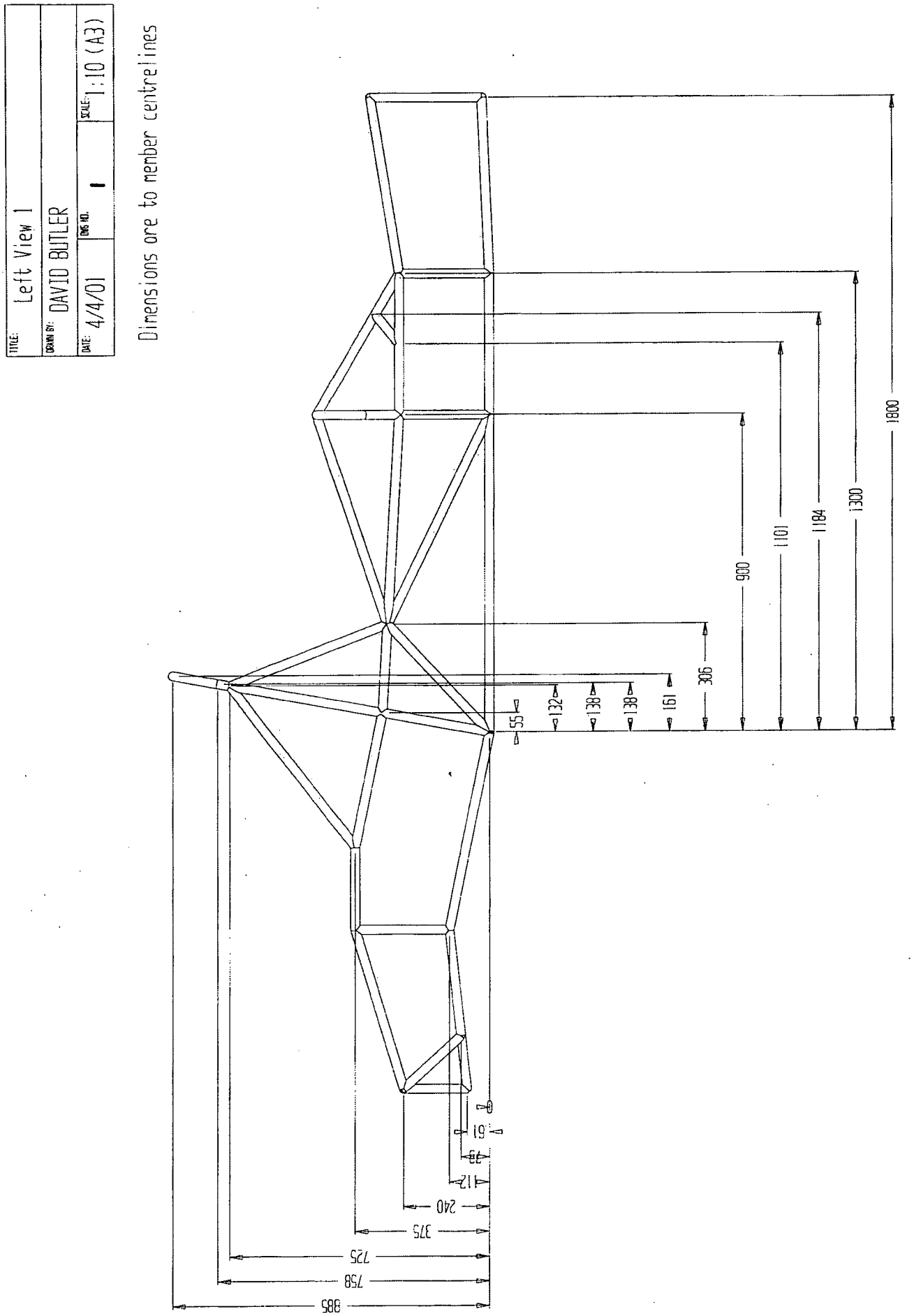

A-9: Left view of frame (2nd set of dimensions)

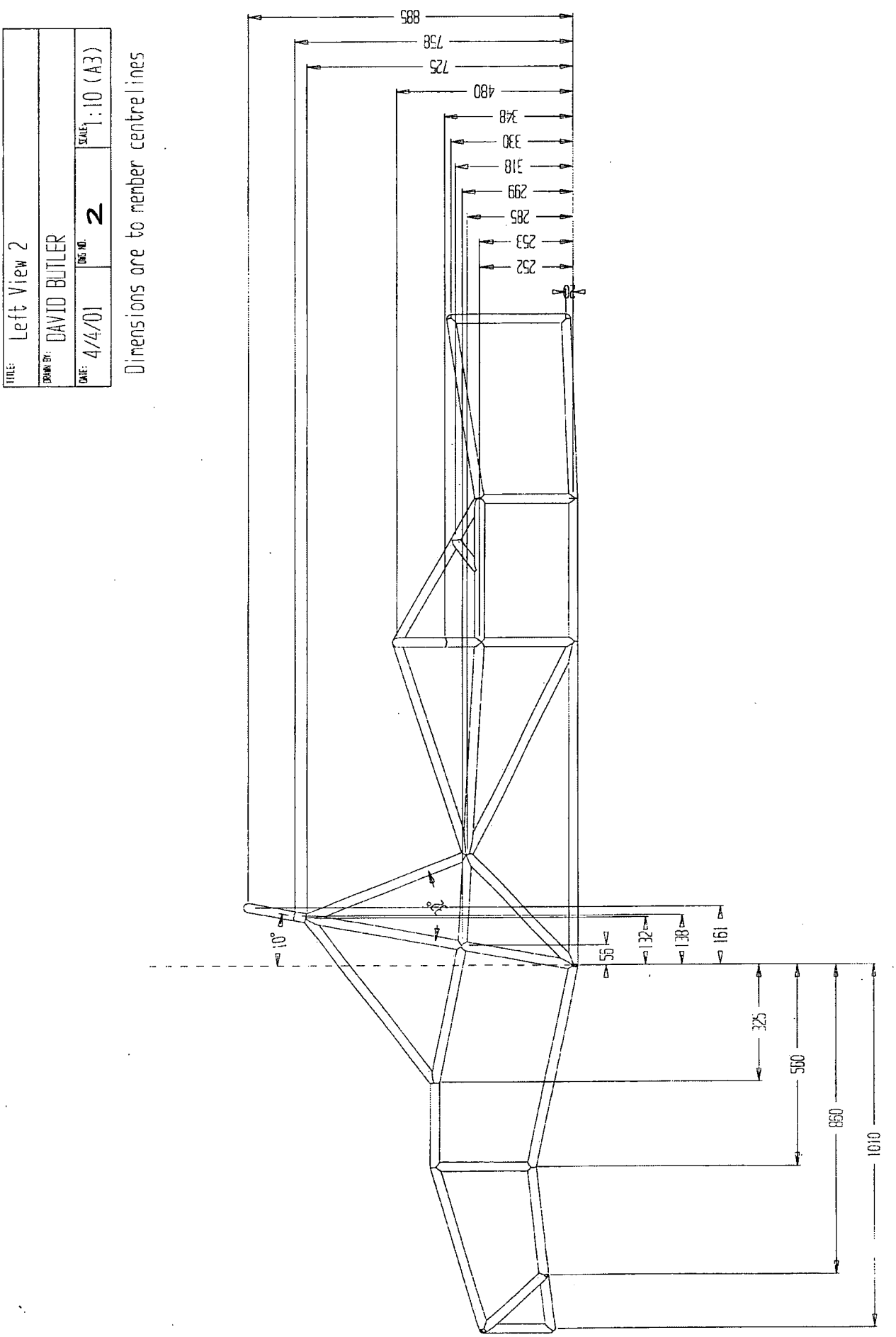

A-10: Left view of frame (member angles)

TITLE: Left View with Angles			
DRAWN BY: DAVID BUTLER		DWG NO. 3	SCALE: 1:10 (A3)
DATE: 4/4/01			

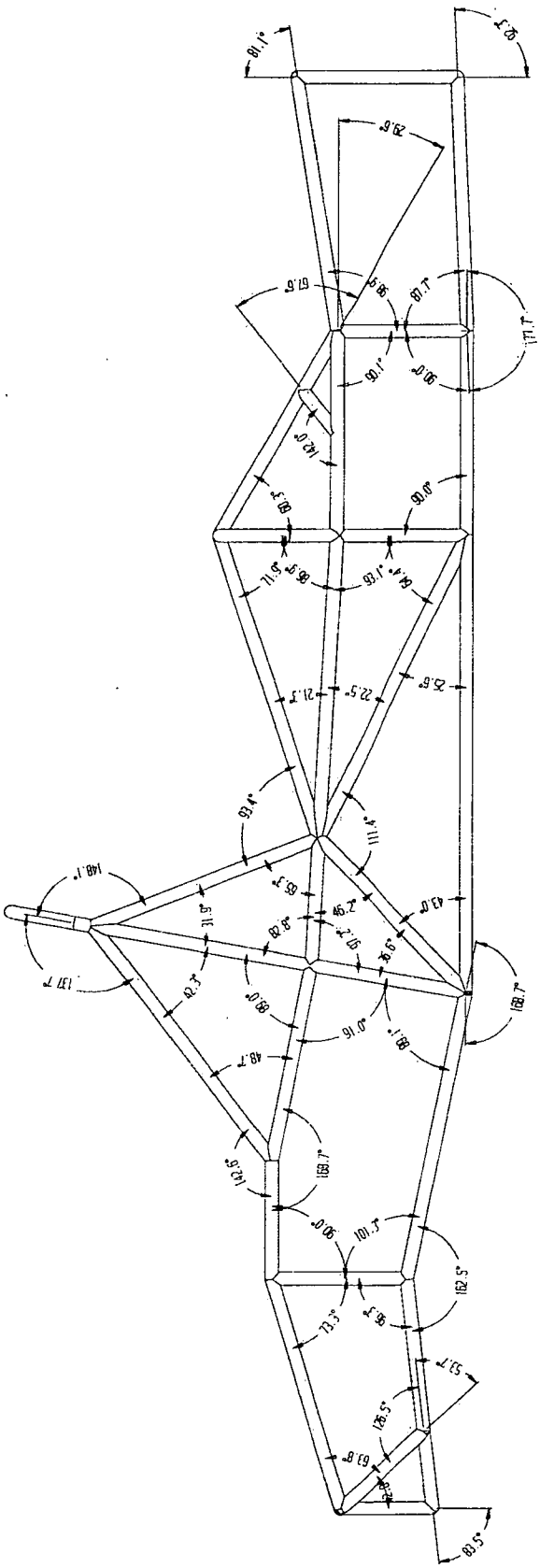

A-11: Left view of frame (three dimensional member lengths)

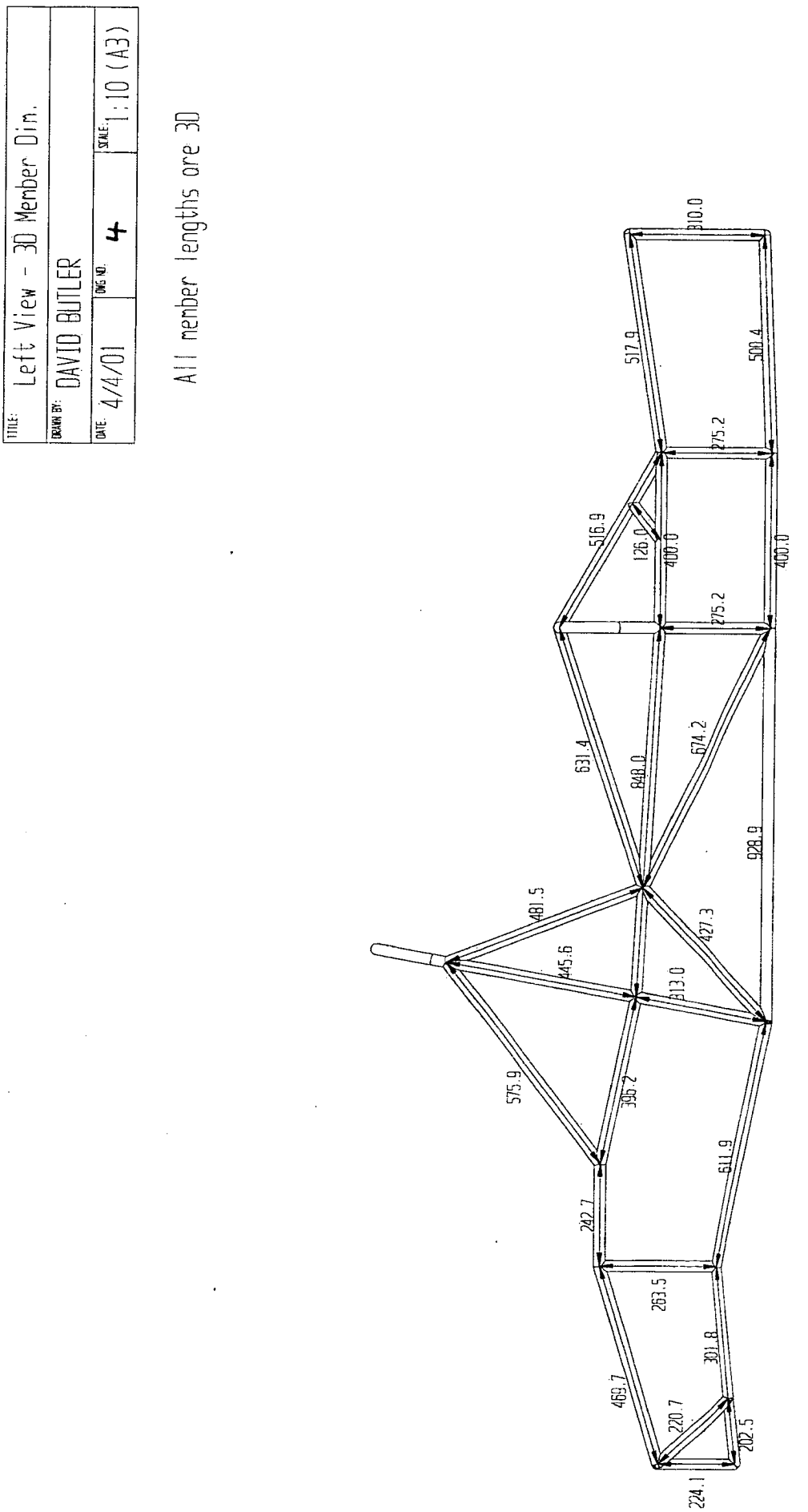

A-12: Top view of frame (first set of dimensions)

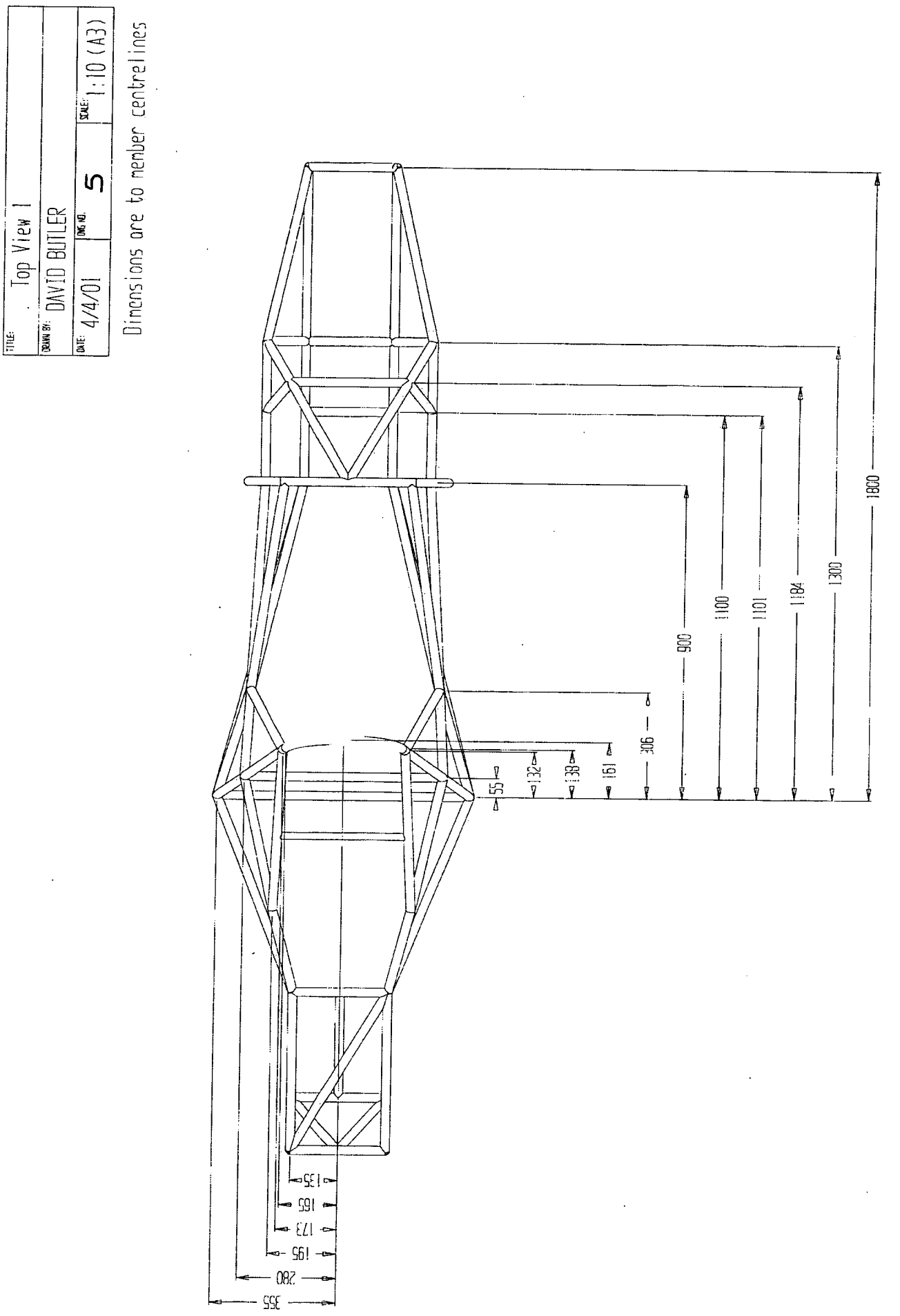

A-13: Top view of frame (second set of dimensions)

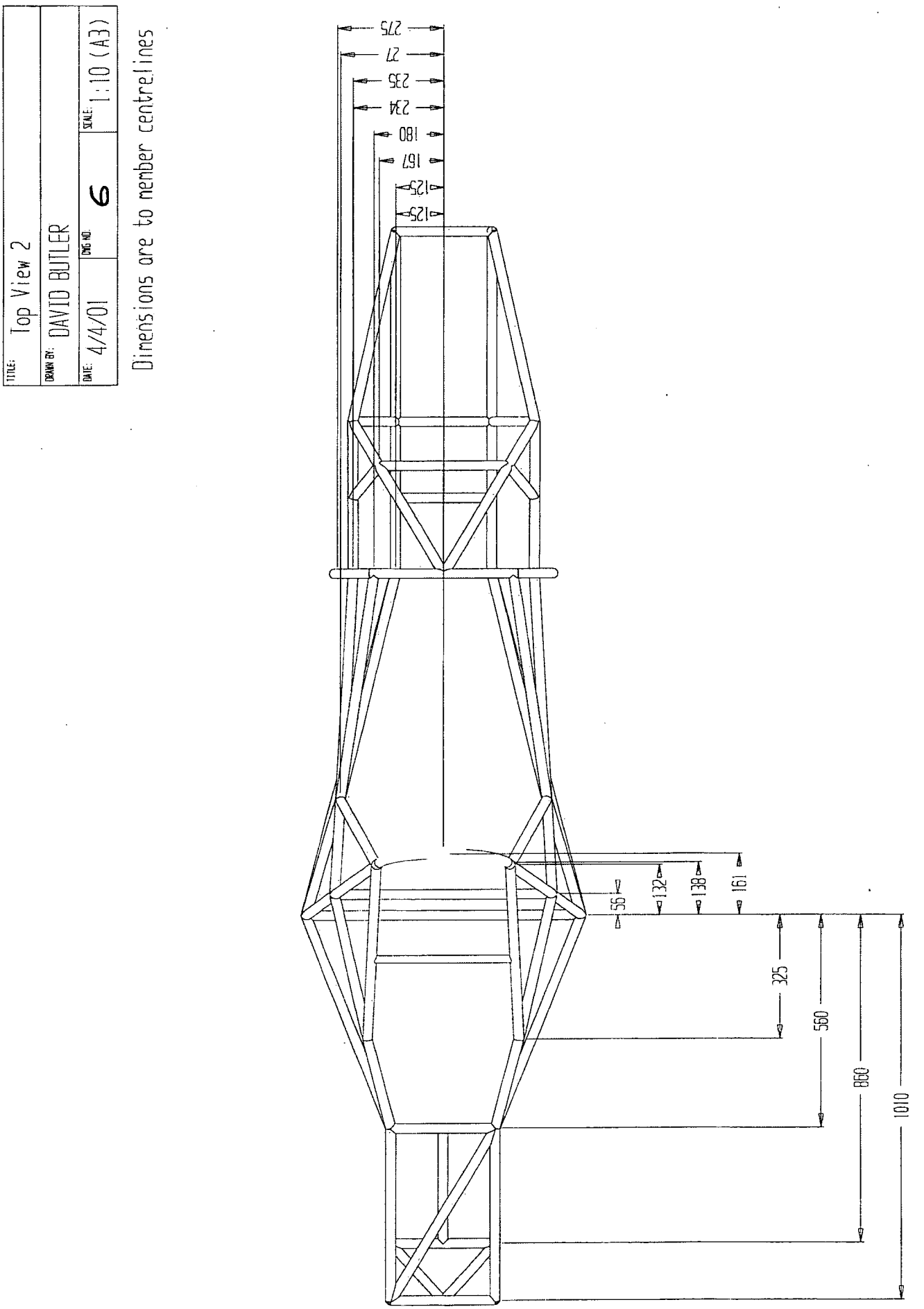

A-14: Top view of frame (member angles)

TITLE:	Top View Angles
DRAWN BY:	DAVID BUTLER
DATE:	4/4/01
DWG NO.	7
SCALE:	1:10 (A3)

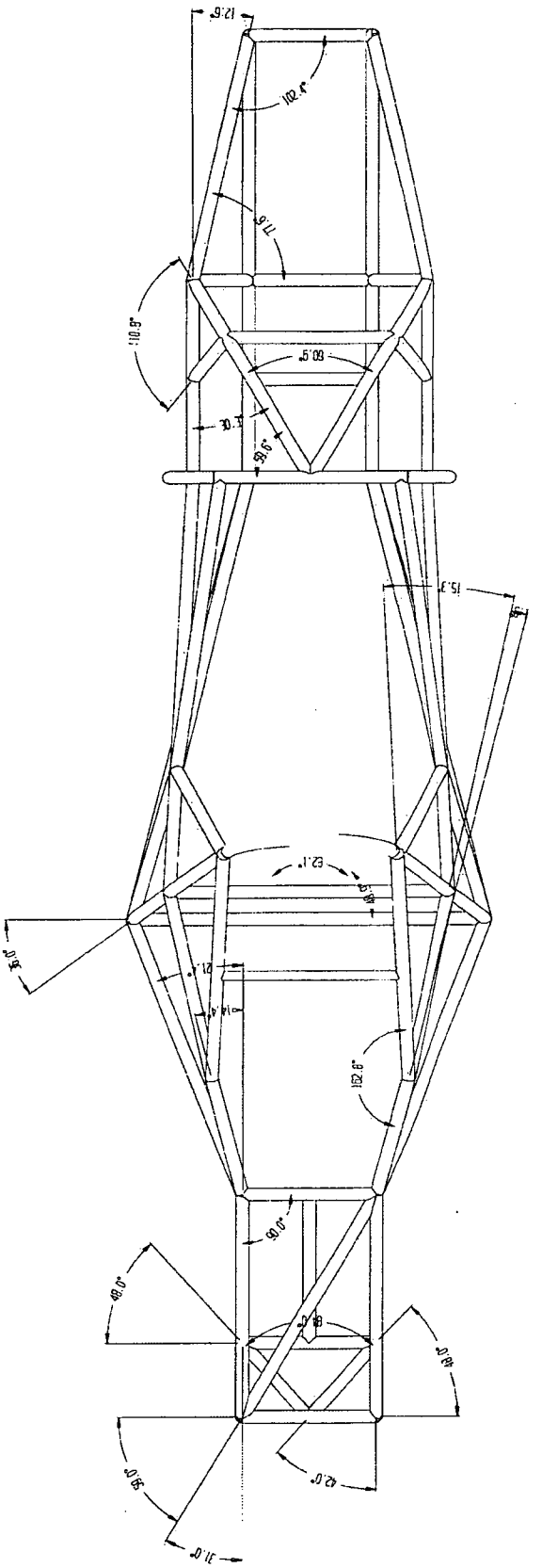

A-15: Top view of frame (member angles of mid-section)

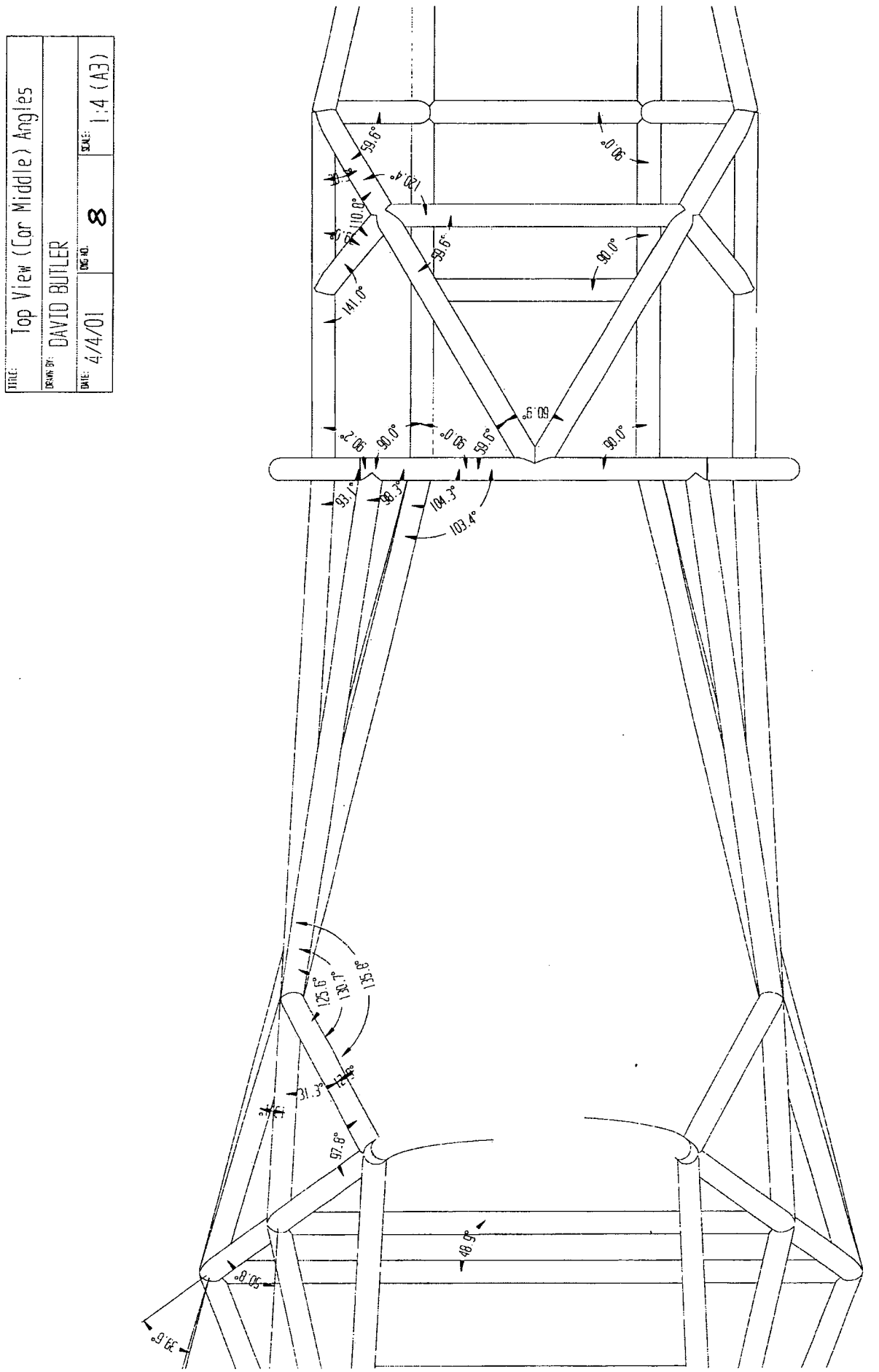

A-16: Front view of frame

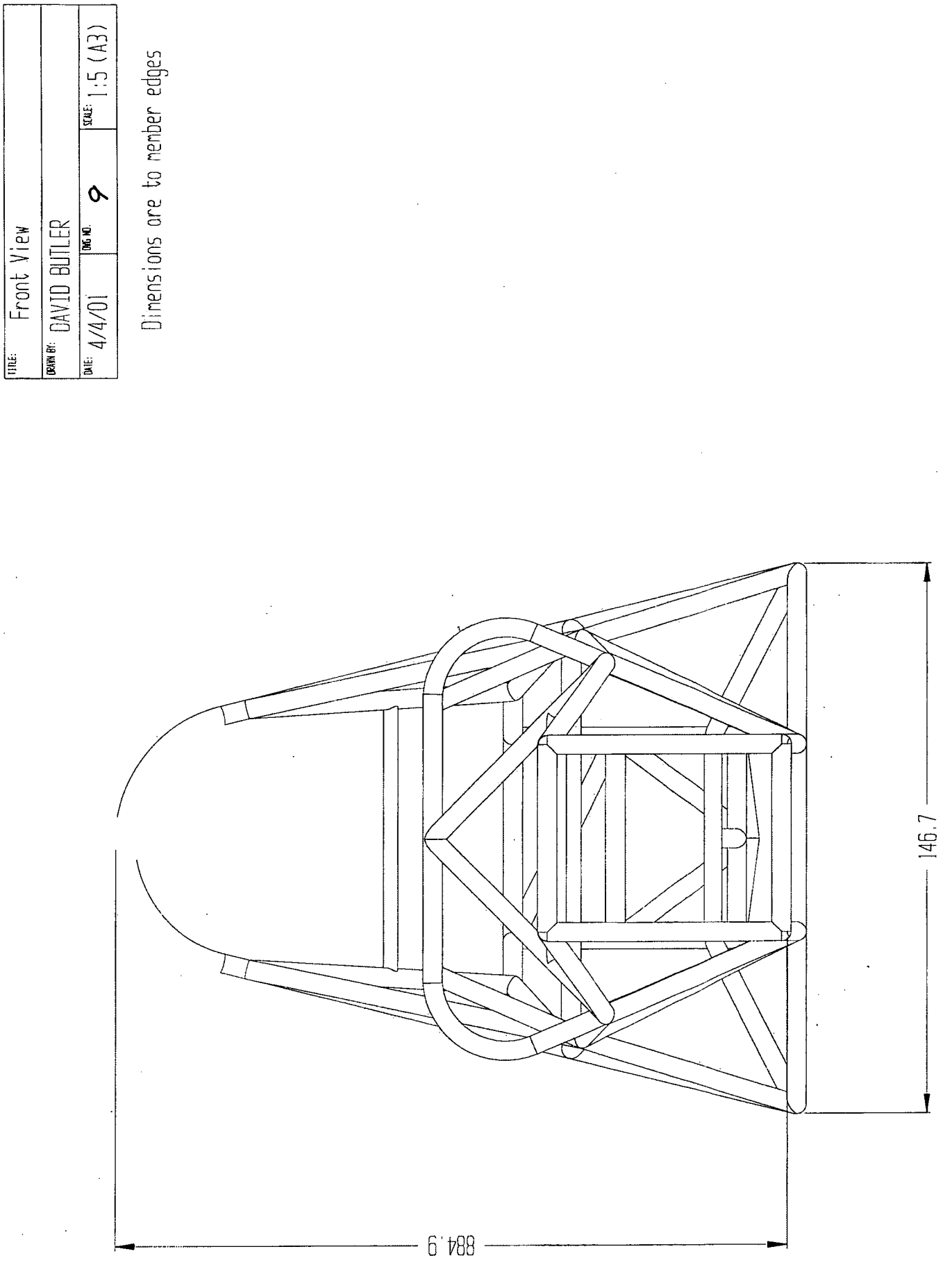

A-17: Roll hoop dimensions

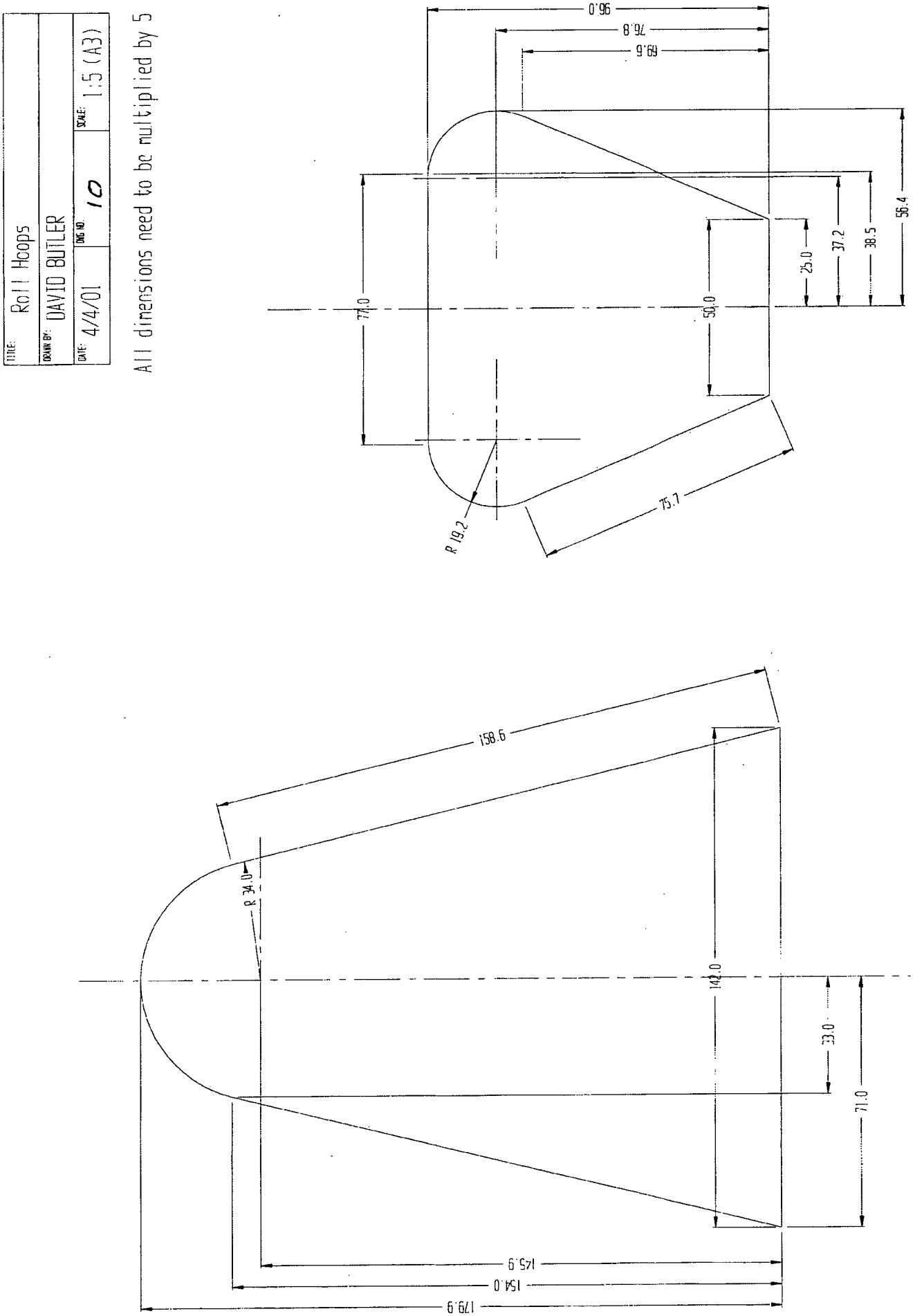

Appendix B - Suspension Design -

B-1: Example calculation of effect of track width on slalom performance

Example calculation

Consider a course of 10 cones at 10 m apart, and for a vehicle with a track width of 2m. The roll over threshold lateral acceleration is given by:

$$a = \frac{1}{2 \cdot h} \cdot trackwidth = 3.5G$$

This means that since the maximum lateral acceleration obtainable from the tyres is about 1.3G, this vehicle will spin out rather than roll over when the cornering limit is exceeded. The minimum the radius of the arc required to complete the slalom course is then calculated with:

l_1 = ½ wheelbase + cone clearance (say 0.1m)

l_2 = ½ cone spacing

Thus:
$$r = \frac{\left(l_1^2 + l_2^2\right)}{2 \cdot l_1} = 11.9m$$

With the total distance travelled given by:

$$Arc\ length = 2 \cdot r \cdot \sin^{-1}\left(\frac{l_2}{r}\right) = 10.32m$$

$$Distance\ travelled = Arc\ length \cdot No.\ cones = 103.2m$$

And the maximum speed at which the vehicle can travel through the slalom by:

$$v = \sqrt{a \cdot r} = 12.3ms^{-1} = 44.4km/hr$$

Gives the minimum time required to complete the course of:

$$t = \frac{distance}{velocity} = 8.37s$$

B-2: Preliminary front suspension geometry

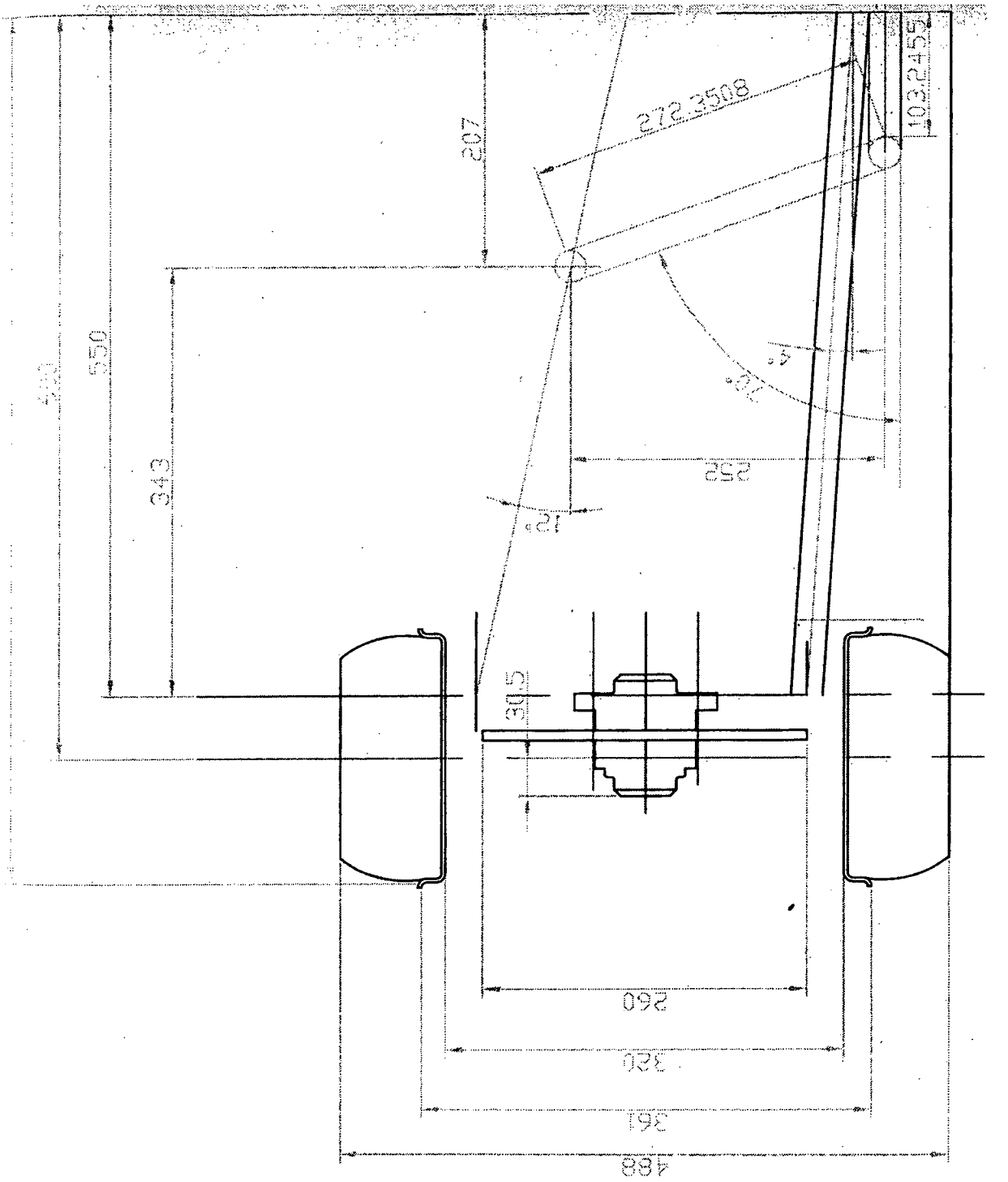

B-3: Front suspension geometry

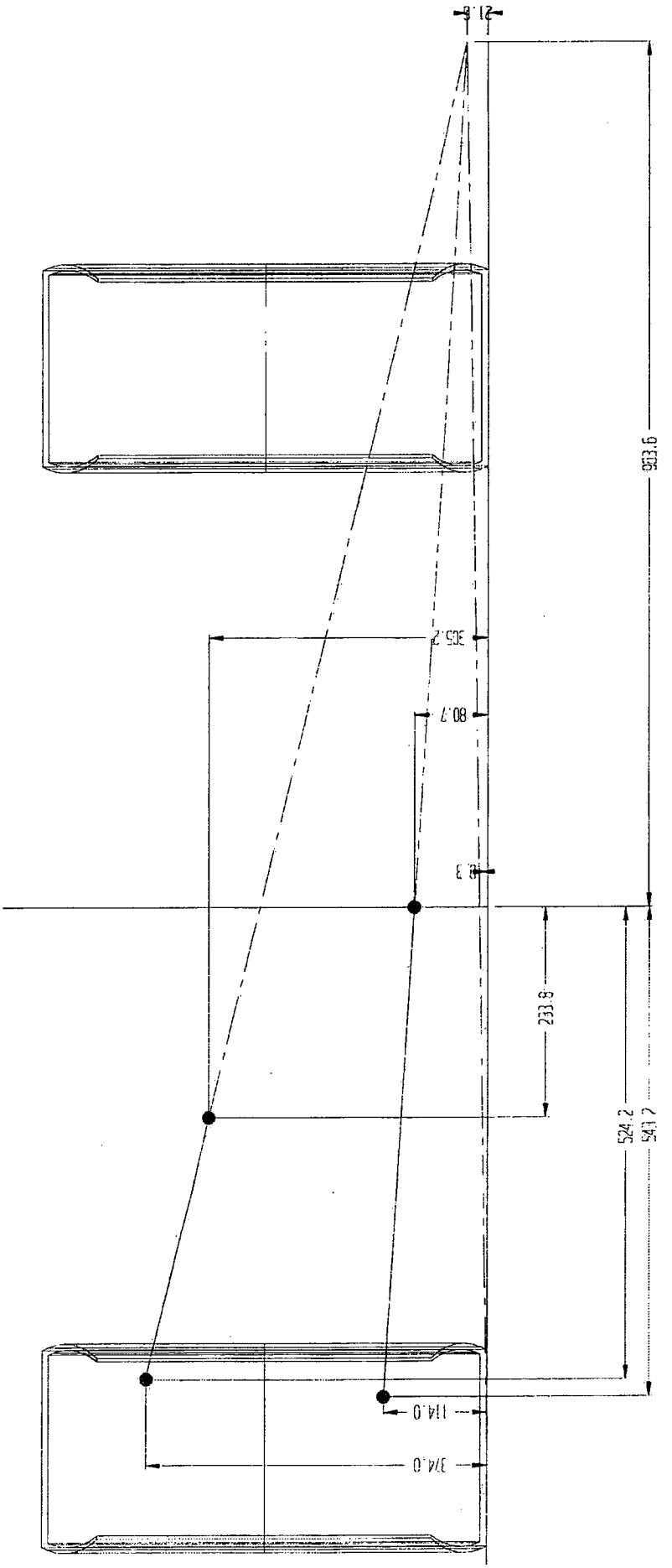

B-4: Preliminary rear suspension geometry

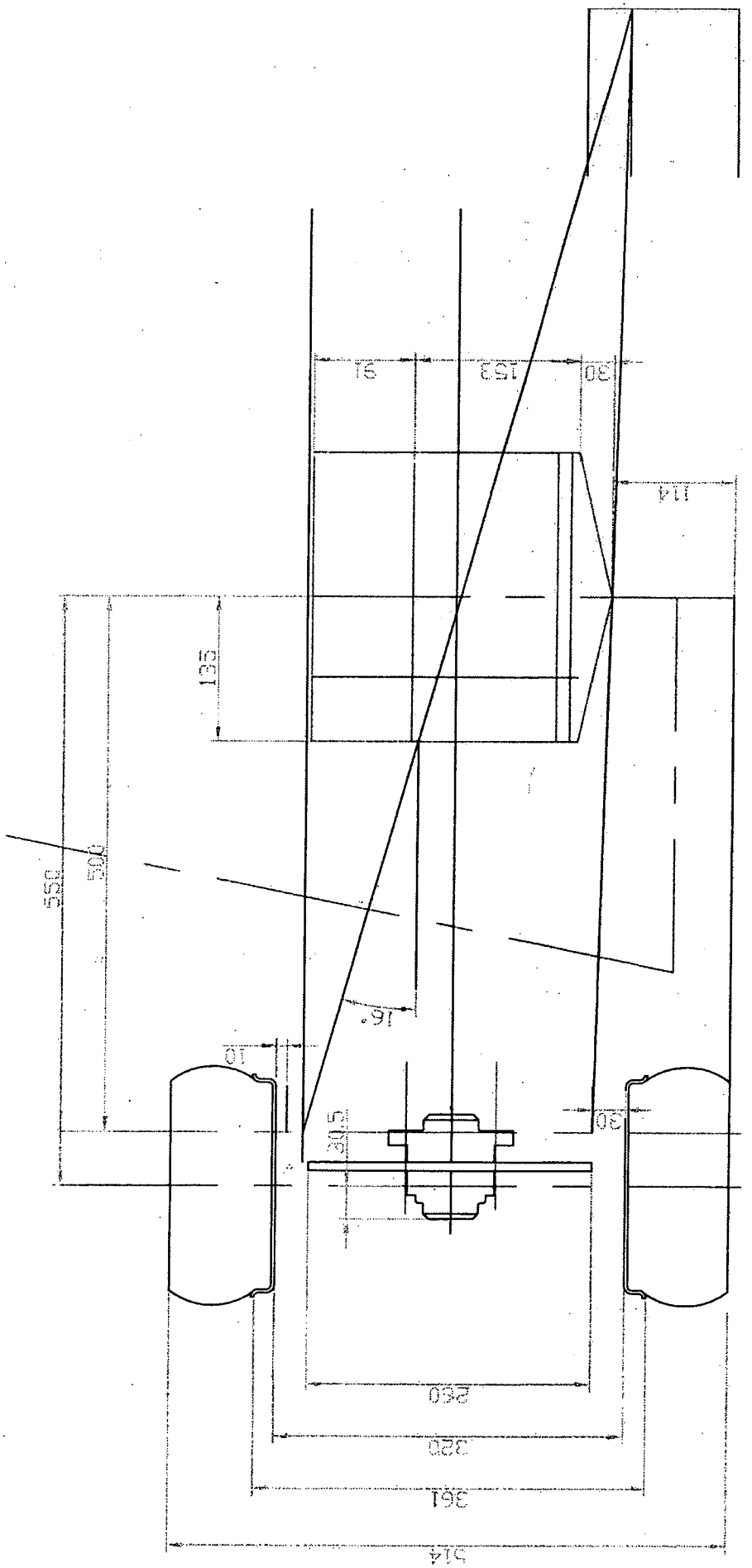

B-5: Rear suspension geometry

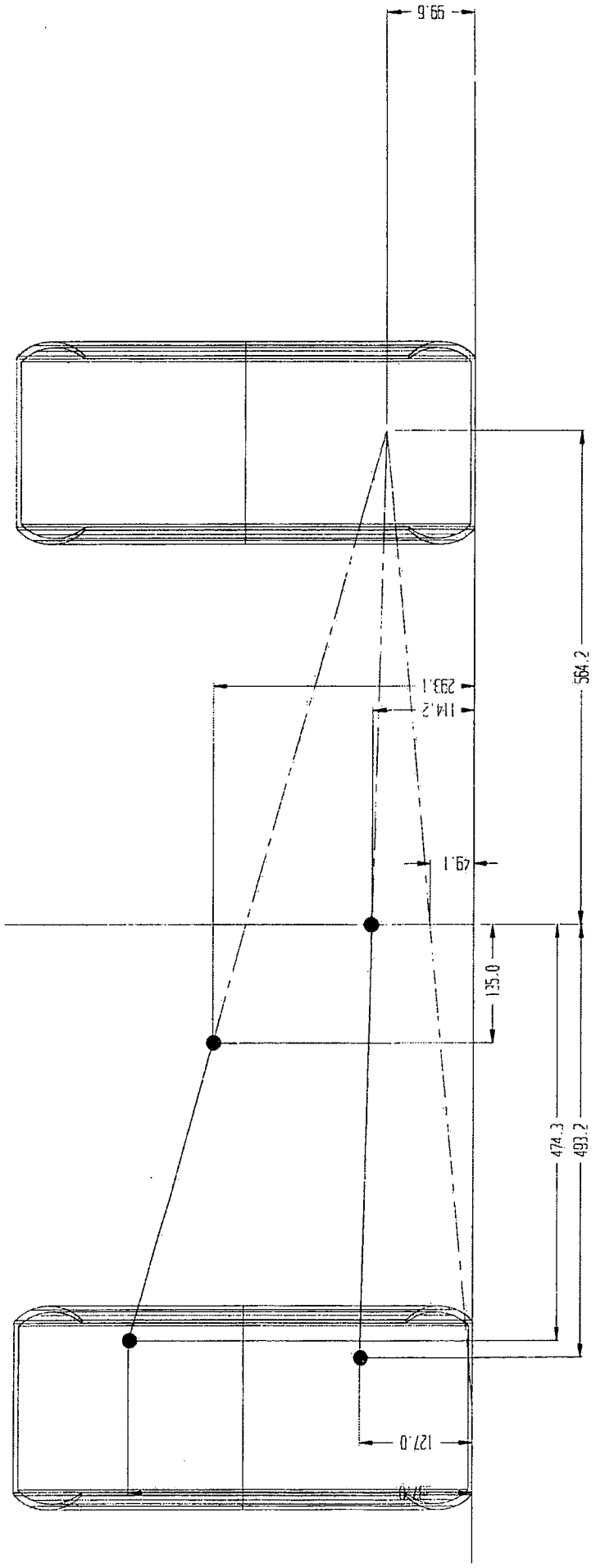

B-6: 7/16" high capacity rod ends

High Capacity Rod Ends

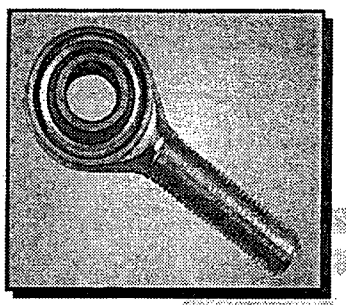

RM SERIES • CHROME MOLY STEEL HOUSING, BALL AND RACE • PLATED FOR CORROSION RESISTANCE

Alinabal's High Capacity Series combines high strength material with three piece construction to produce increased static load ratings.

Materials:

Housing: Chrome moly or low carbon steel - heat treated - plated for corrosion resistance
Ball: Heat treated chrome moly steel - plated for corrosion resistance and wear
Race: Heat treated chrome moly steel - plated for corrosion resistance
Liner: Self lubricating woven Teflon fabric (optional)

Notes:

1. Add letter "L" to prefix to indicate left hand thread (examples: RML-6-X5)
2. Add letter "T" to prefix to indicate permanently bonded Teflon material to the race I.D. (examples: RMLT-6-X5)

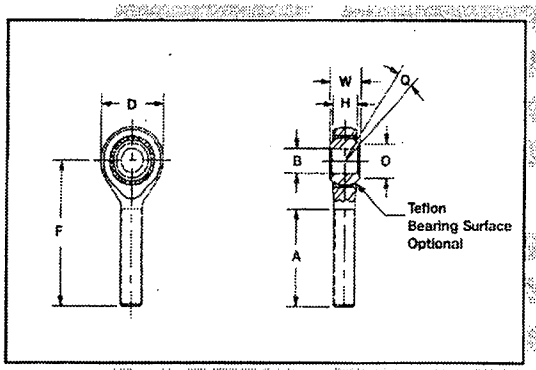

Other variations can be supplied as specials. For additional information and ordering instructions, contact ALINABAL CUSTOMER SERVICE

Rod End Numbers High Capacity (Chrome Moly Steel)	Dimension in Inches										Approx Weight	Ultimate (Radial)Static Load Rating (lbs)
	B	W	H	A	F	D	O	Ball Dia	Thread	Q		
	+.0025 -.0005	±.005	(REF)	±.060	±.030	±.010	(REF)	(REF)	Class UNF-2	(REF)	lbs/ Piece	High Strength
RM-5-X5	.3125	.437	.344	1.250	1.875	.875	.438	.618	5/16-24	±14°	.07	3,940
RM-6-X5	.3750	.500	.406	1.250	1.938	1.000	.508	.713	3/8-24	±15°	.12	6,800
RM-7-X5	.4375	.562	.437	1.375	2.125	1.125	.578	.806	7/16-20	±16°	.16	8,830
RM-8-X5	.5000	.625	.500	1.500	2.438	1.312	.690	.931	1/2-20	±16°	.24	13,990
RM-8/6-X5	.3750	.500	.406	1.500	2.438	1.312	.508	.713	1/2-20	±15°	.24	20,850
RM-10-X5	.6250	.750	.562	1.625	2.625	1.500	.801	1.098	5/8-18	±15°	.38	16,110
RM-10/8-X5	.5000	.625	.500	1.625	2.625	1.500	.690	.931	5/8-18	±16°	.38	26,280
RM-12-X5	.7500	.875	.687	1.750	2.875	1.750	1.010	1.336	3/4-16	±12°	.65	21,950
RM-12/10-X5	.6250	.750	.562	1.750	2.875	1.750	.801	1.098	3/4-16	±12°	.65	35,900

B-7: 1/4" aircraft grade rod ends

LINEAR BEARINGS PTY LTD

IMPERIAL ROD ENDS MALE

Bronze lined	Nylon lined	Steel on steel	Teflon lined heavy duty aircraft quality	Teflon lined light duty stainless steel	Basic size reference	Eye diameter d	UNF thread diameter g x pitch	Thread length G	Centre of eye to thread end H	Head diameter D	O/A ball width B	Studded see page 2 P	Studded see page 2 K
VM-G	PM-G	AM-G	ART-E	AHMT	* 3	3/16	3/16 X 32	.750	1.250	.750	.312	.500	.500
					* 4	1/4	1/4 X 28	1.000	1.562	.750	.375	.500	.562
					5	5/16	5/16 X 24	1.250	1.875	.875	.437	.562	.687
					6	3/8	3/8 X 24	1.250	1.938	1.000	.500	.625	.875
					7	7/16	7/16 X 20	1.375	2.125	1.125	.562	.875	1.125
					8	1/2	1/2 X 20	1.500	2.438	1.312	.625	.875	1.125
					10	5/8	5/8 X 18	1.625	2.625	1.500	.750	1.000	1.500
					12	3/4	3/4 X 16	1.750	2.875	1.750	.875	1.250	1.812
					16	1	1¼ X 12	2.375	4.125	2.750	1.375	-	-

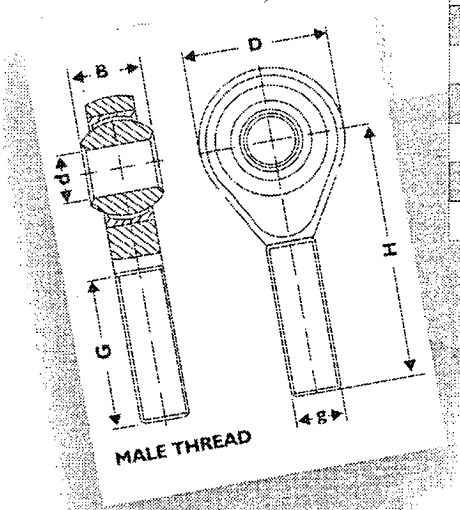

* For ART-E sizes 3 & 4 thread is .312 diameter x 24TPI

Ordering example: **VM10G** (Bronze lined, male, right hand 5/8" basic size)
For left hand versions add **L** to prefix letters **VML10G.**

IMPERIAL ROD ENDS FEMALE

Bronze lined	Nylon lined	Steel on steel	Teflon lined light duty stainless steel	Basic size reference	Eye diameter d	UNF thread diameter g x pitch	Thread length G	Centre of eye to thread end H	Head diameter D	O/A ball width B	Studded see page 2 P	Studded see page 2 K
VF-G	PF-G	AF-G	AHFT	3	3/16	3/16 X 32	.562	1.062	.750	.312	.500	.500
				4	1/4	1/4 X 28	.750	1.312	.750	.375	.500	.562
				5	5/16	5/16 X 24	.750	1.375	.875	.437	.562	.687
				6	3/8	3/8 X 24	.937	1.625	1.000	.500	.625	.875
				7	7/16	7/16 X 20	1.062	1.812	1.125	.562	.875	1.125
				8	1/2	1/2 X 20	1.87	2.125	1.312	.625	.875	1.125
				10	5/8	5/8 X 18	1.500	2.500	1.500	.750	1.000	1.500
				12	3/4	3/4 X 16	1.750	2.875	1.750	.875	1.250	1.812
				**16	1	1¼ X 12	2.125	4.125	2.750	1.375	-	-

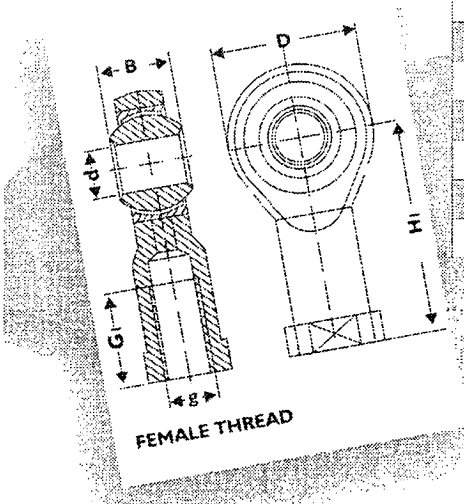

** 1" x 12 UNF thread also available. Please enquire

Ordering example: **PF8G** (Nylon lined, female, 1/2" basic size)
For left hand versions add **L** to prefix letters: **PFL8G.**

B-8: Suspension spring specifications

RST 58

Coil spring with internal hydraulic floating piston

A6061-T6 aluminum body

Spring pre-load adjustment

Spring standard color : black

	58
COMPRESS DAMPING ADJUSTMENT	YES
COMPRESS LOCKOUT	YES
REBOUND DAMPING ADJUSTMENT	YES
EYE TO EYE LENGHT	155mm~190mm
TRAVEL	26mm~37mm

RST 58

★This information is for reference Only. please contact RST local agent or RST web site to get fully product information.

No	Description	Qty
1	Body pivot	1
2	Pivot spacer	4
3	Spring collar	1
4	Shaft pivot	1
5	Adjuster knob	1
6	Adjuster screw	1
7	Spring	1
8	Spring retainer	1

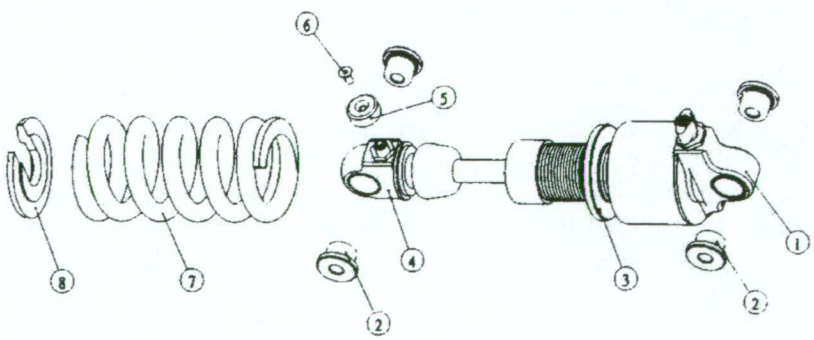

Appendix C - Wheel Assembly Design -

C-1: Brake aluminium rotor dimensions

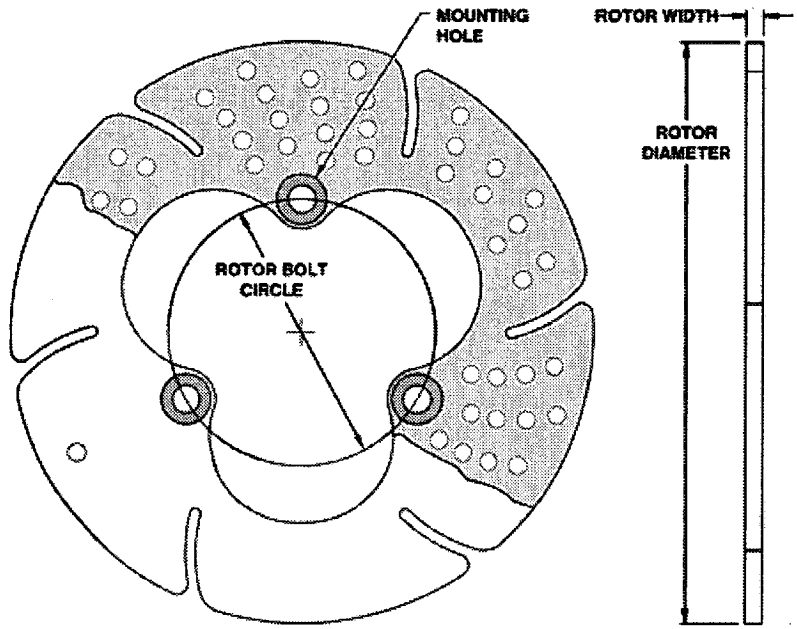

WIDTH	DIAMETER	BOLT CIRCLE	HOLE TYPE
7.9mm	259.1mm	127.0mm	13.1mm

C-2: Brake caliper aluminium rotor pad dimensions

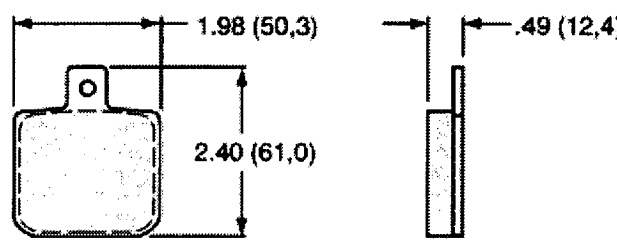

PURPLE PADS FOR ALUMINIUM ROTORS

C-3: Brake caliper dimensions

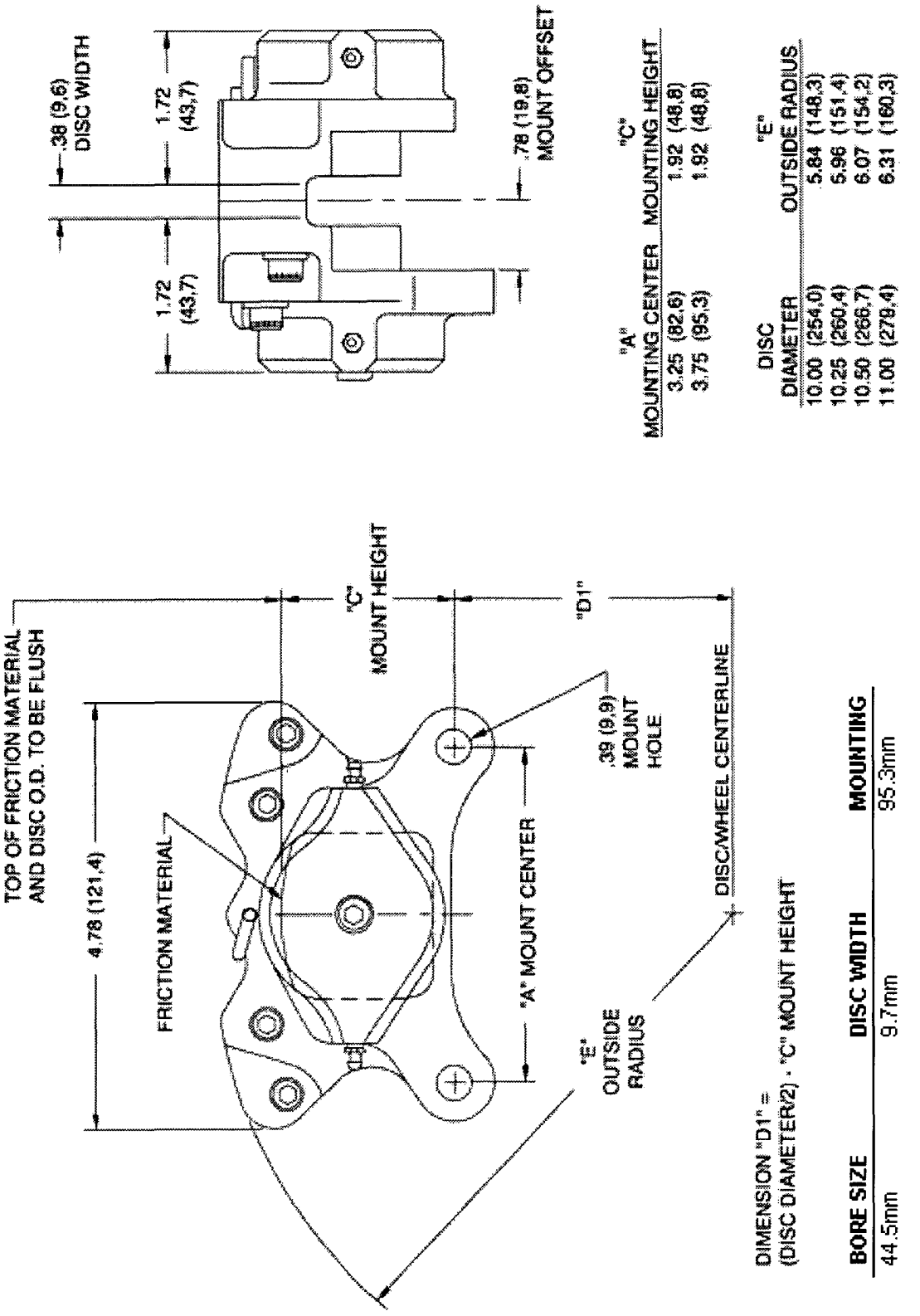

C-4: Stub axle (30mm dia.) FEA for centred bearing design

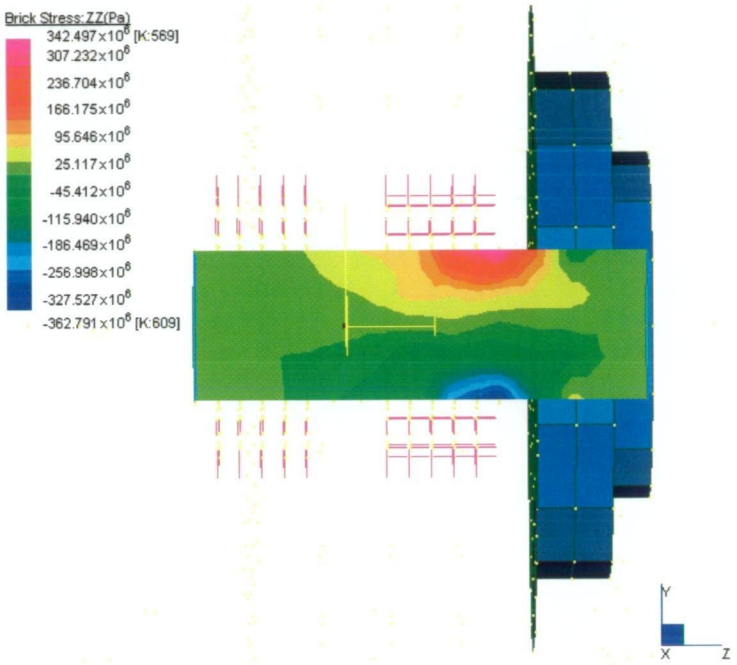

C-5: Stub axle (35mm dia.) FEA for off centre bearing design

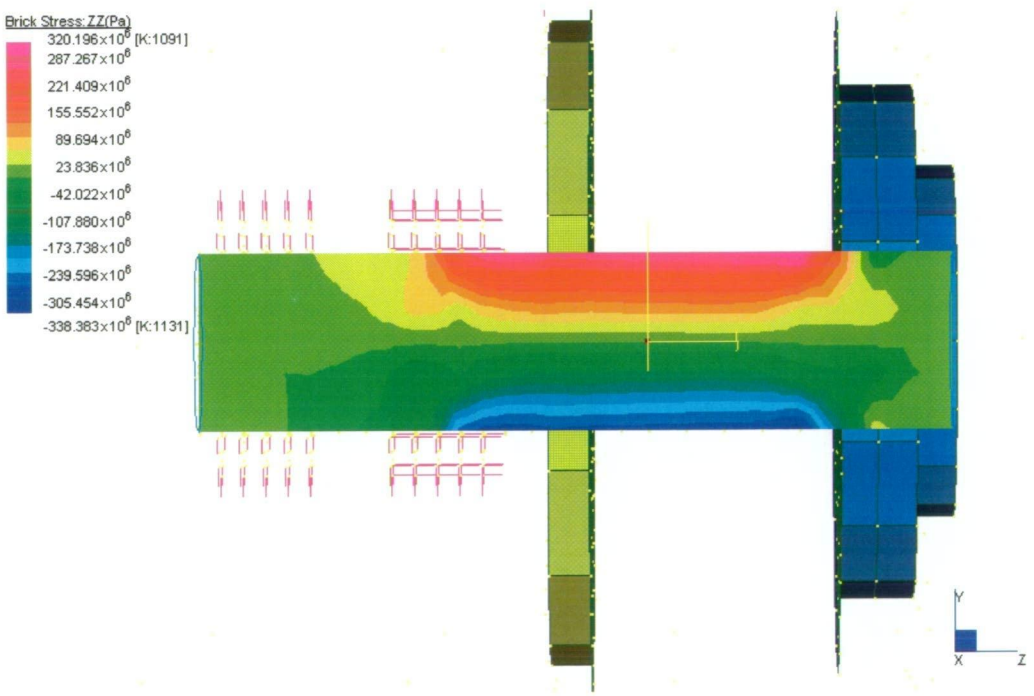

C-6: FEA stub axle bearing loads for centred design

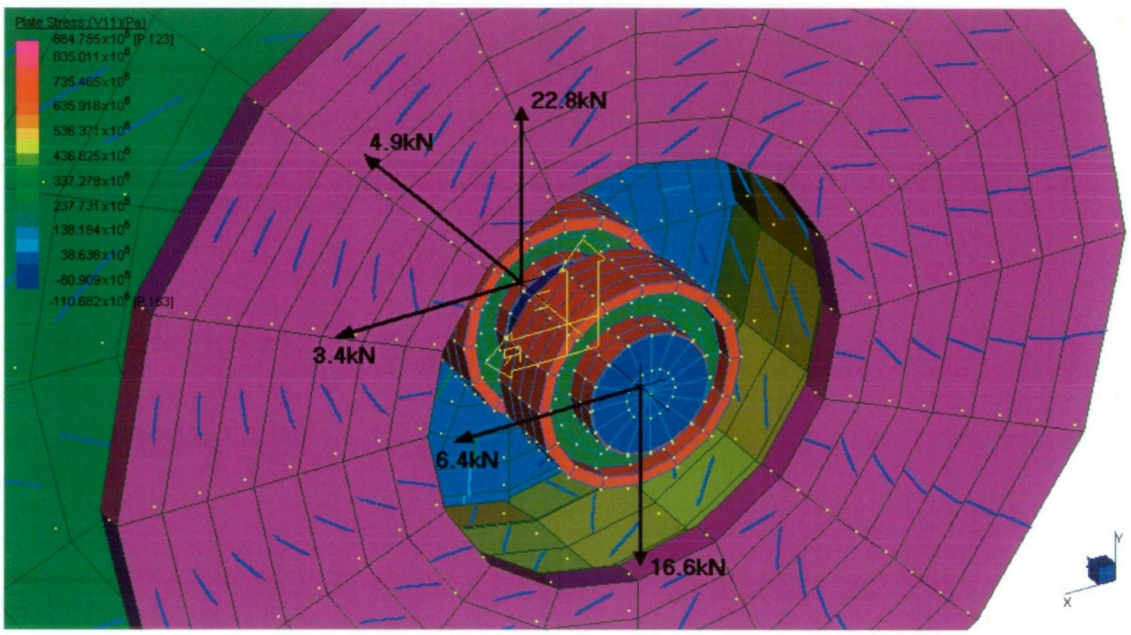

C-7: FEA stub axle bearing loads for off centre design

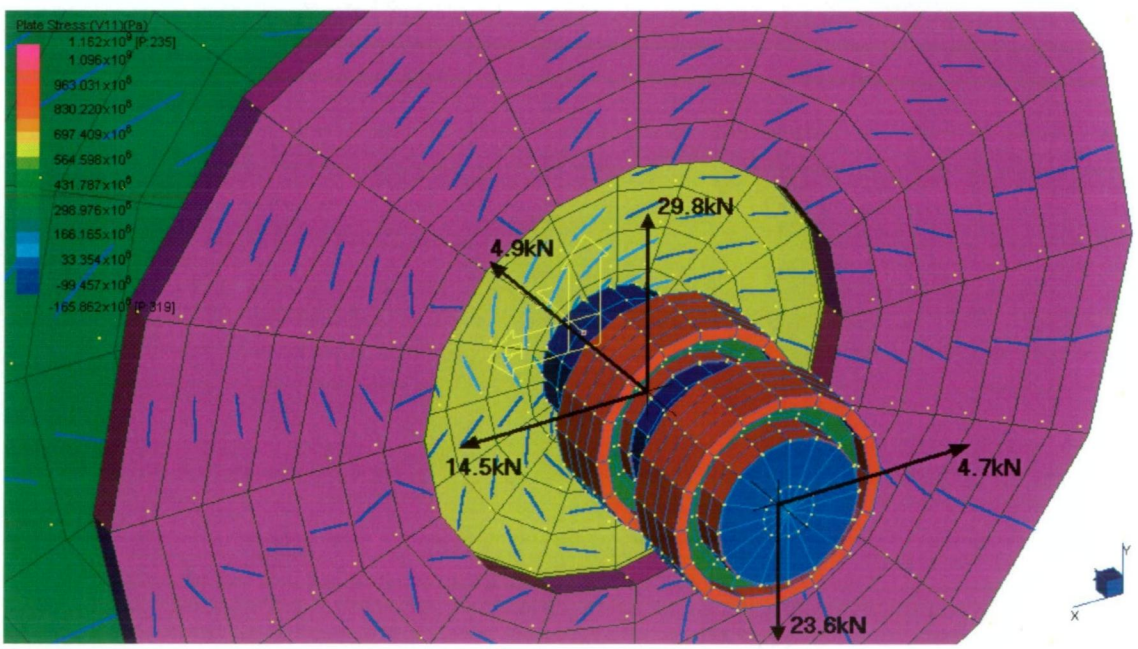

C-8: Upright dimensions

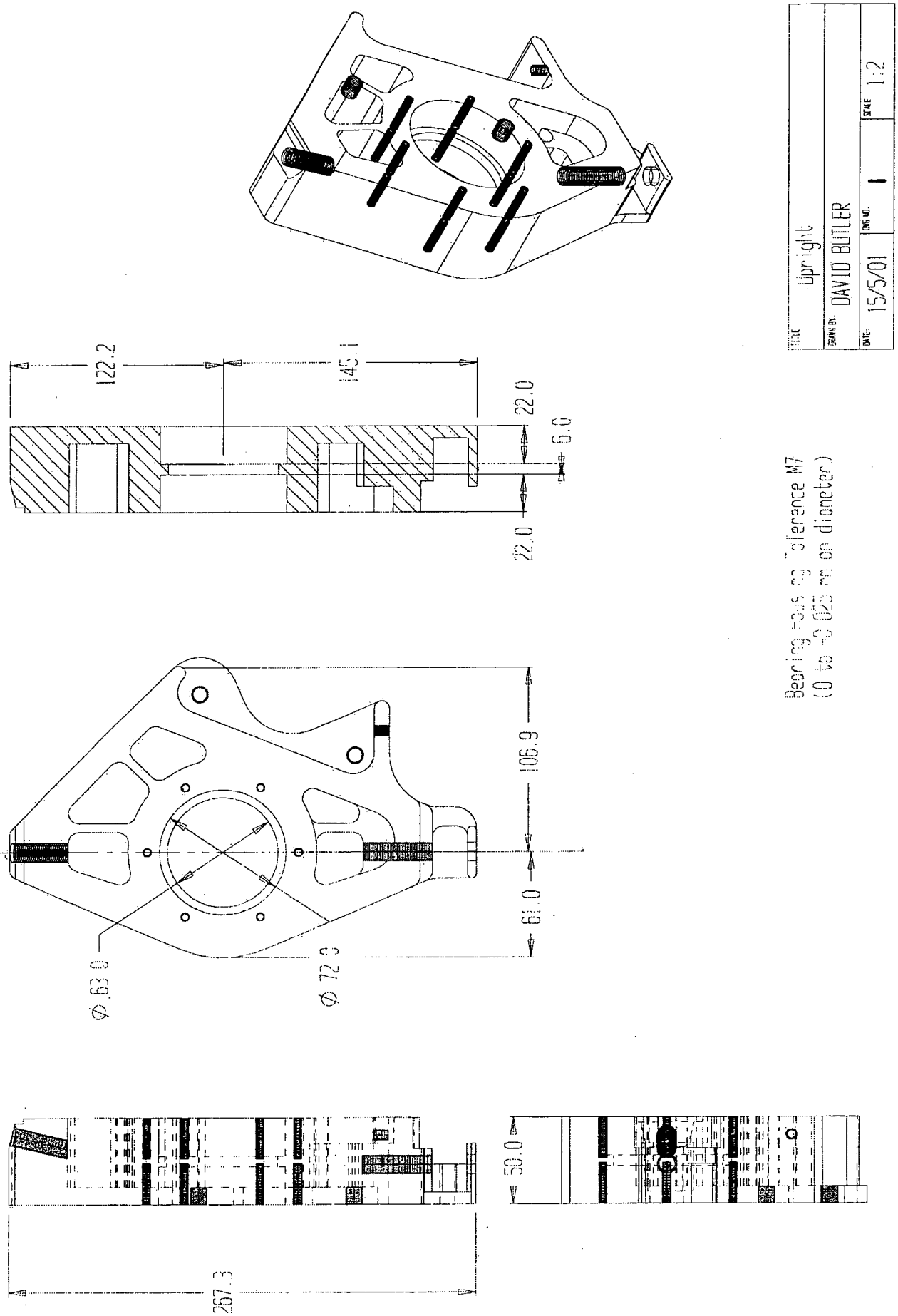

C-9: Oil seal dimensions

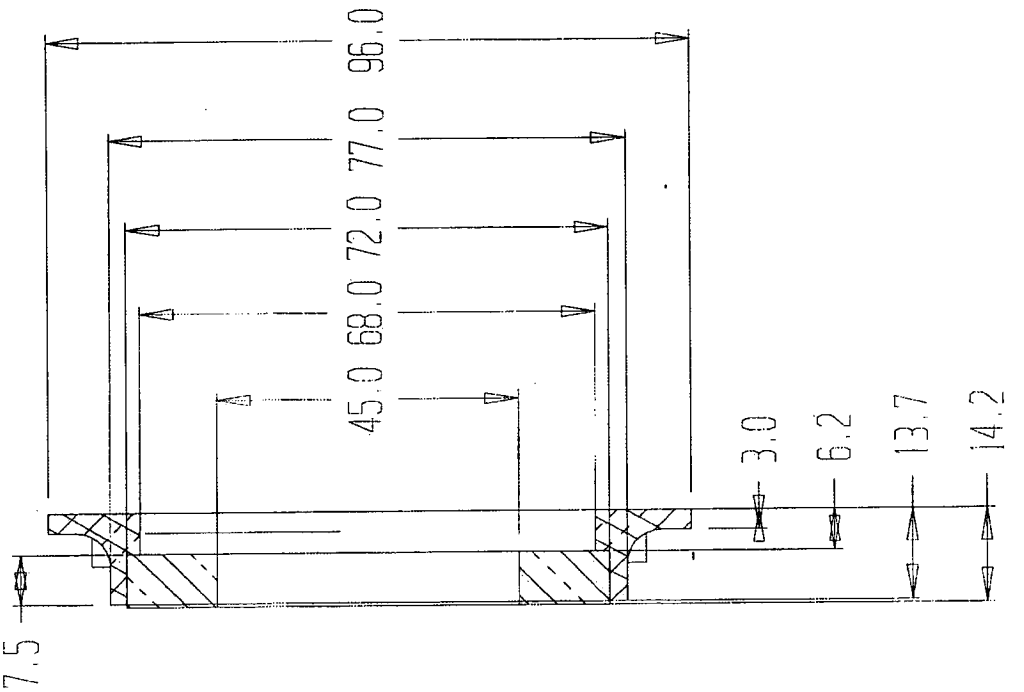

TITLE:	Oil Seal
DRAWN BY:	DAVID BUTLER
DATE:	6/6/01
DWG NO.	2
SCALE:	1 : 1 (A4)

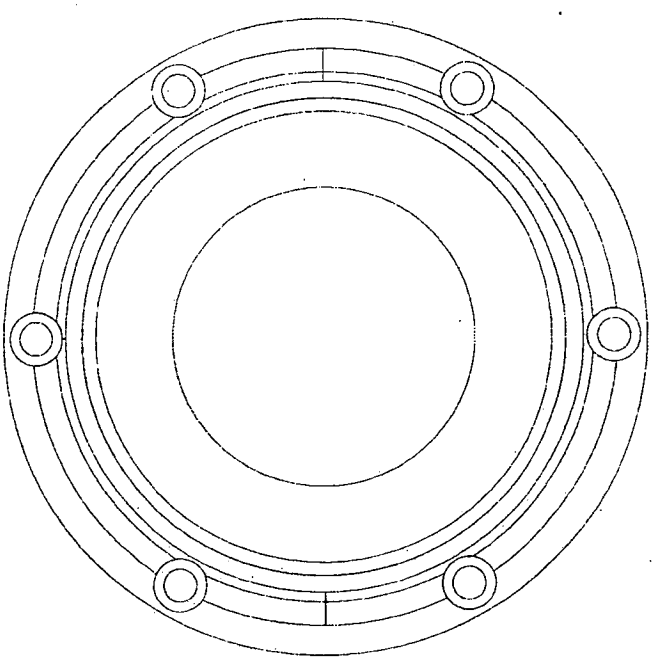

C-10: Stub axle dimensions

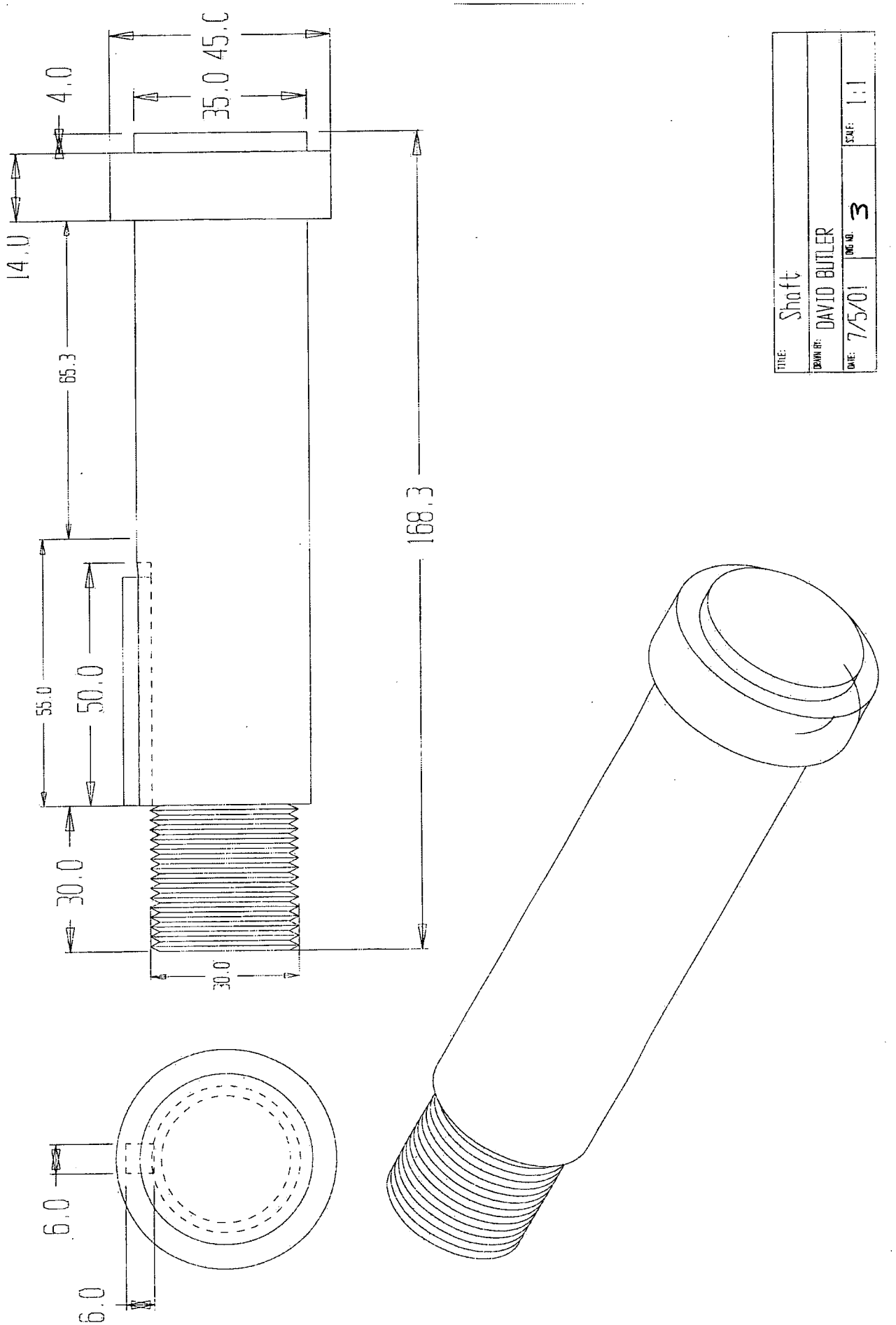

C-11: Wheel hub dimensions

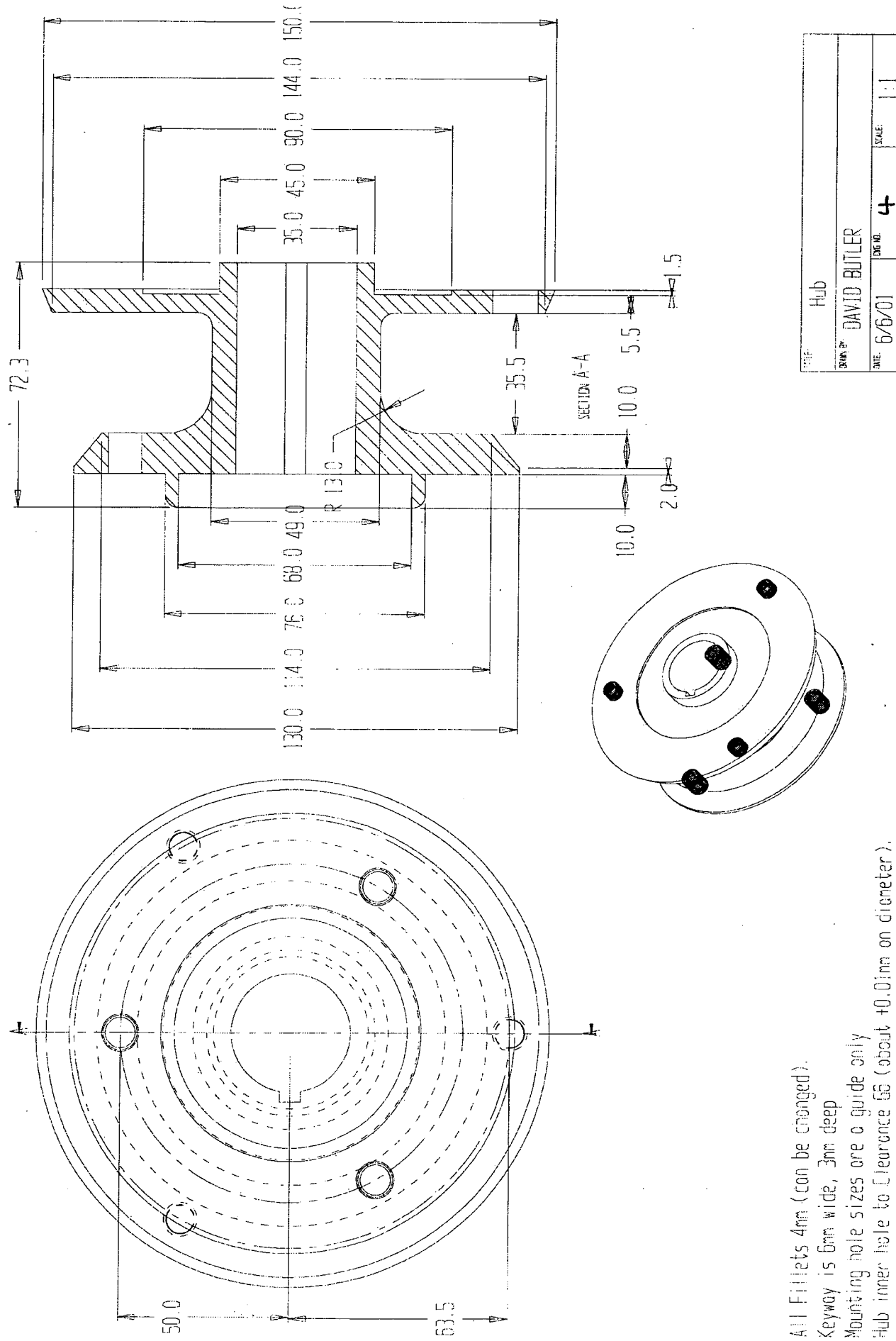

C-12: King pin and caster reference angles

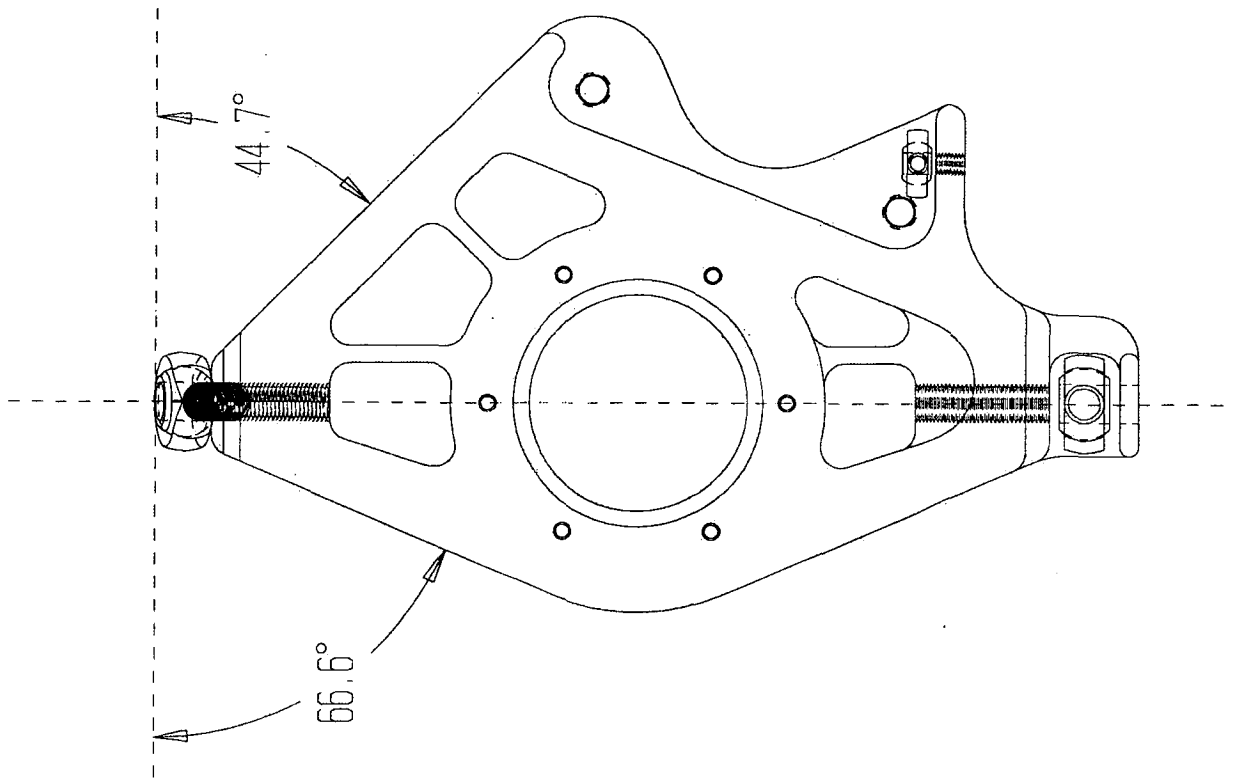

Appendix D - Cockpit Design -

D-1: Brake pedal dimensions with balance bar

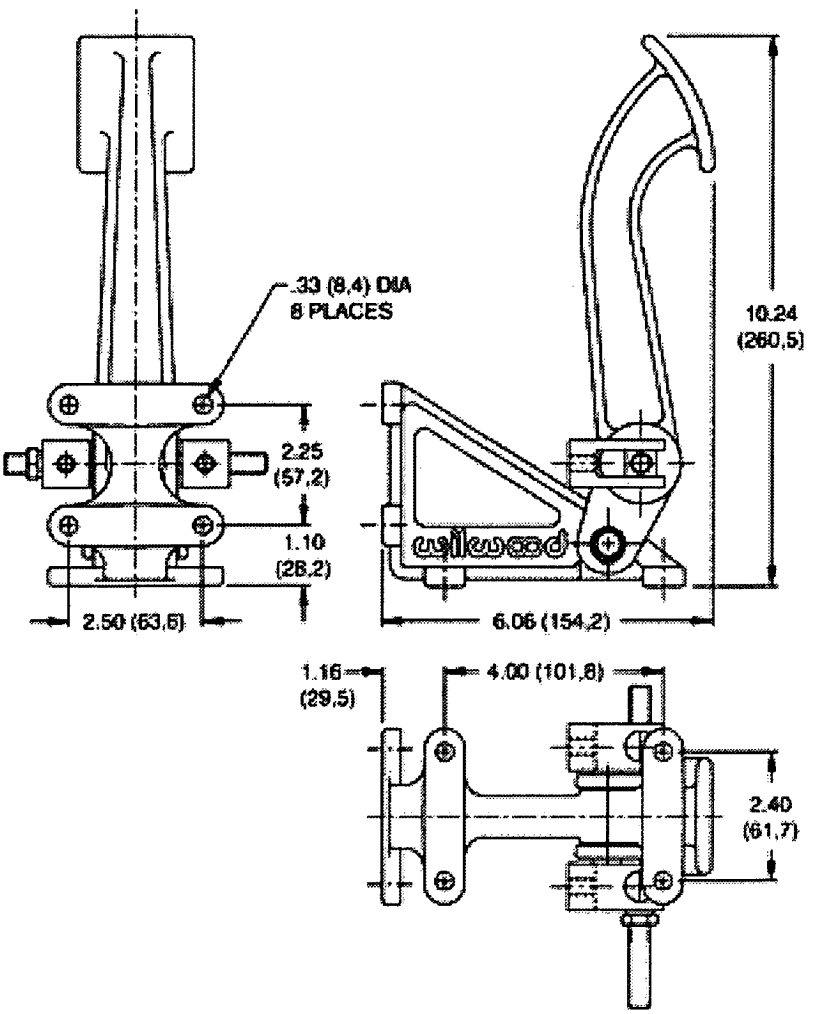

D-2: Brake master cylinder dimensions

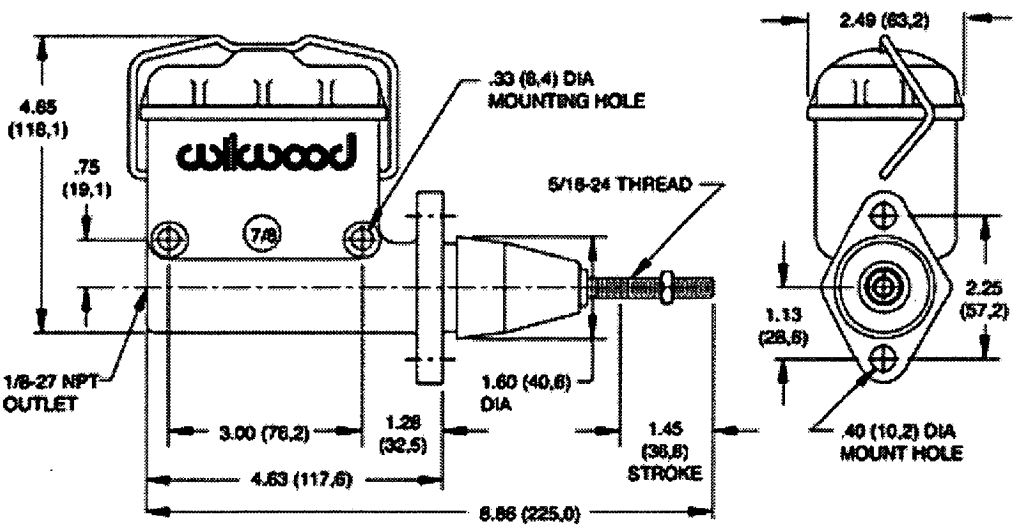

Appendix E - Engine Systems Design -

E-1: Engine specifications

Engine:		
Type		4-stroke, DOHC, 4-cylinder
Cooling system		Liquid-cooled
Bore and stroke		66 x 43.8 mm
Displacement		599 mL
Compression ratio		12.8
Maximum horsepower		81.6 kW (111 PS) @12 500 r/min (rpm), (AS) 80.6 kW (109.6 PS) @12 500 r/min (rpm), (PR) 78.2 kW (106.3 PS) @12 500 r/min (rpm), (US) - - -
Maximum torque		65.6 N·m (6.7 kg·m, 48 ft·lb) @10 000 r/min (rpm), (AS) 64.6 N·m (6.6 kg·m, 48 ft·lb) @10 000 r/min (rpm) (FR)(US) - - -
Carburetion system		Carburetors, Mikuni BDSR 36R x 4
Starting system		Electric starter
Ignition system		Battery and coil (transistorized)
Timing advance		Electronically advanced(digital igniter)
Ignition timing		From 12.5° BTDC @1 300 r/min (rpm) to 42.5° BTDC @5 000 r/min (rpm)
Spark plug		NGK CR9E
Cylinder numbering method		Left to right, 1-2-3-4
Firing order		1-2-4-3
Valve timing:		
Inlet	Open	56° BTDC
	Close	80° ABDC
	Duration	316°
Exhaust	Open	61° BBDC
	Close	33° ATDC
	Duration	274°
Lubrication system		Forced lubrication (wet sump with cooler)
Engine oil:		
Grade		SE, SF or SG class
Viscosity		SAE10W-40, 10W-50, 20W-40, or 20W-50
Capacity		3.8 L

E-2: Engine top end exploded view

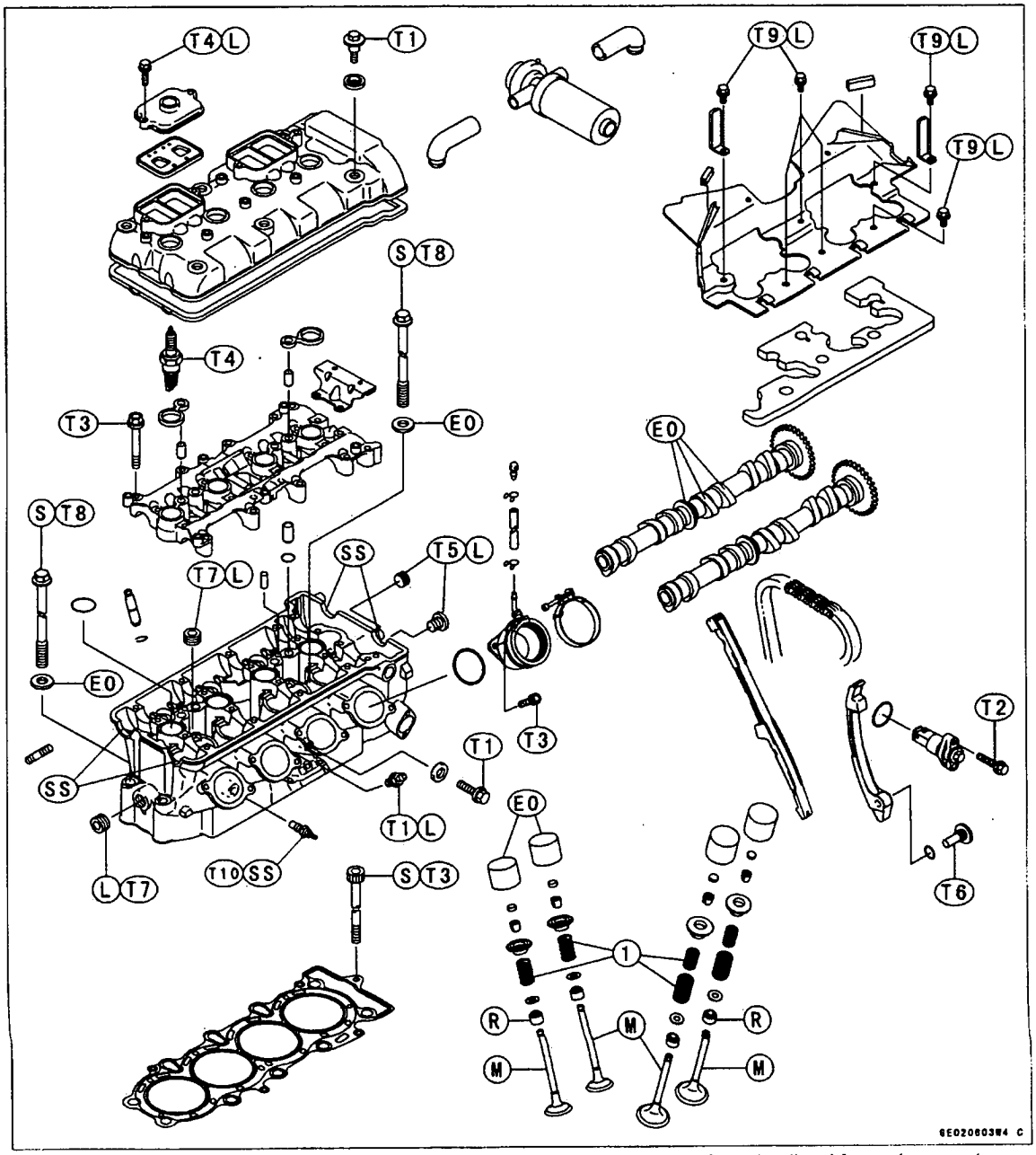

T1: 9.8 N·m (1.0 kg·m, 87 in·lb)
T2: 11 N·m (1.1 kg·m, 95 in·lb)
T3: 12 N·m (1.2 kg·m, 104 in·lb)
T4: 13 N·m (1.3 kg·m, 113 in·lb)
T5: 15 N·m (1.5 kg·m, 11.0 ft·lb)
T6: 25 N·m (2.5 kg·m, 18.0 ft·lb)
T7: 20 N·m (2.0 kg·m, 14.5 ft·lb)
T8: 49 N·m (5.0 kg·m, 36 ft·lb)
T9: 5.9 N·m (0.60 kg·m, 52 in·lb)
T10: 7.8 N·m (0.8 kg·m, 69 in·lb)

1. Closed coil end faces downward.
L: Apply a non-permanent locking agent.
M: Apply molybdenum disulfide grease.
EO: Apply engine oil.
SS: Apply silicone sealant.
R: Replacement Parts
S: Follow the specific tightening sequence.

E-3: Engine crankshaft exploded view

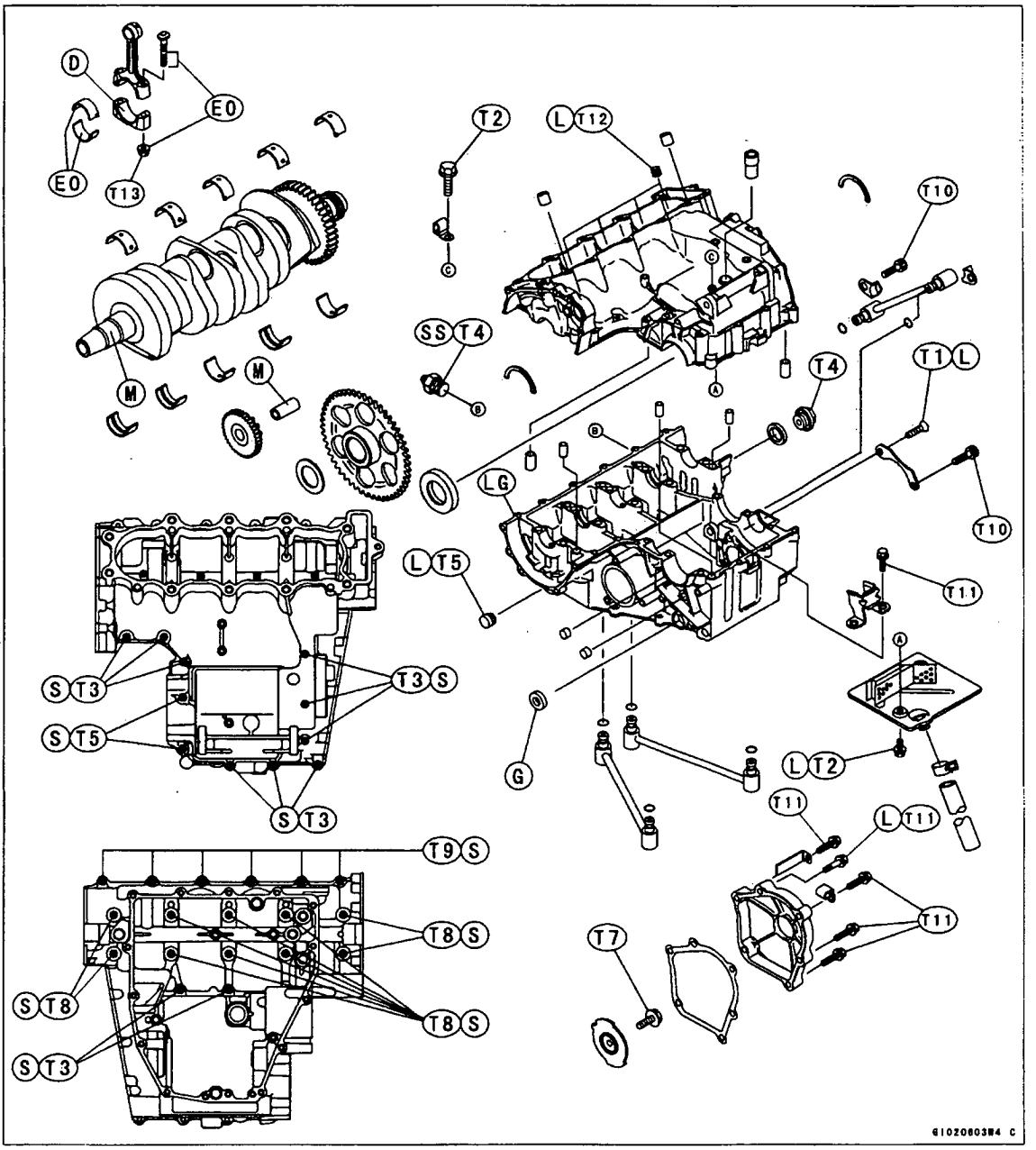

T1: 5.4 N·m (0.55 kg·m, 48 in·lb)
T2: 9.8 N·m (1.0 kg·m, 87 in·lb)
T3: 12 N·m (1.2 kg·m, 104 in·lb)
T4: 15 N·m (1.5 kg·m, 11.0 ft·lb)
T5: 20 N·m (2.0 kg·m, 14.5 ft·lb)
T6: 28 N·m (2.9 kg·m, 21 ft·lb)
T7: 40 N·m (4.0 kg·m, 29 ft·lb)
T8: 30 N·m (3.0 kg·m, 22 ft·lb)
T9: 18 N·m (1.8 kg·m, 13.0 ft·lb)
T10: 13 N·m (1.3 kg·m, 113 in·lb)
T11: 11 N·m (1.1 kg·m, 95 in·lb)
T12: 6.9 N·m (0.70 kg·m, 61 in·lb)
T13: See the text.

E-4: ECU installation

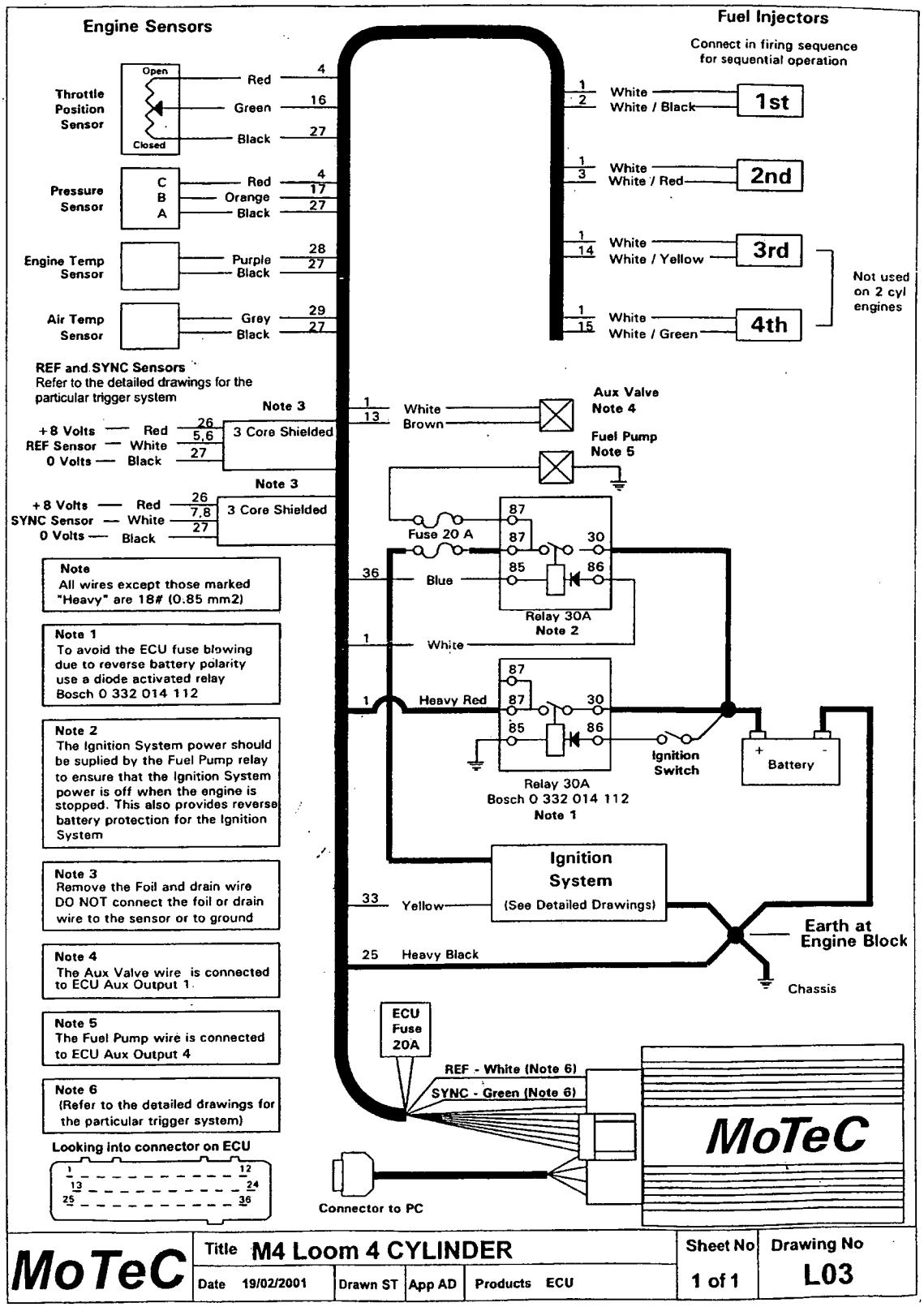

Appendix F - Drivetrain Design -

F-1: Gearbox specifications

Drive Train:		
Primary reduction system:		
Type		Gear
Reduction ratio		2.022 (89/44)
Clutch type		Wet multi disc
Transmission:		
Type		6-speed, constant mesh, return shift
Gear ratios:		
	1st	2.923 (38/13)
	2nd	2.062 (33/16)
	3rd	1.631 (31/19)
	4th	1.380 (29/21)
	5th	1.217 (28/23)
	6th	1.083 (26/24)
Final drive system:		
Type		Chain drive
Reduction ratio		2.666 (40/15)
Overall drive ratio		5.843 @Top gear

F-2: Clutch assembly exploded view

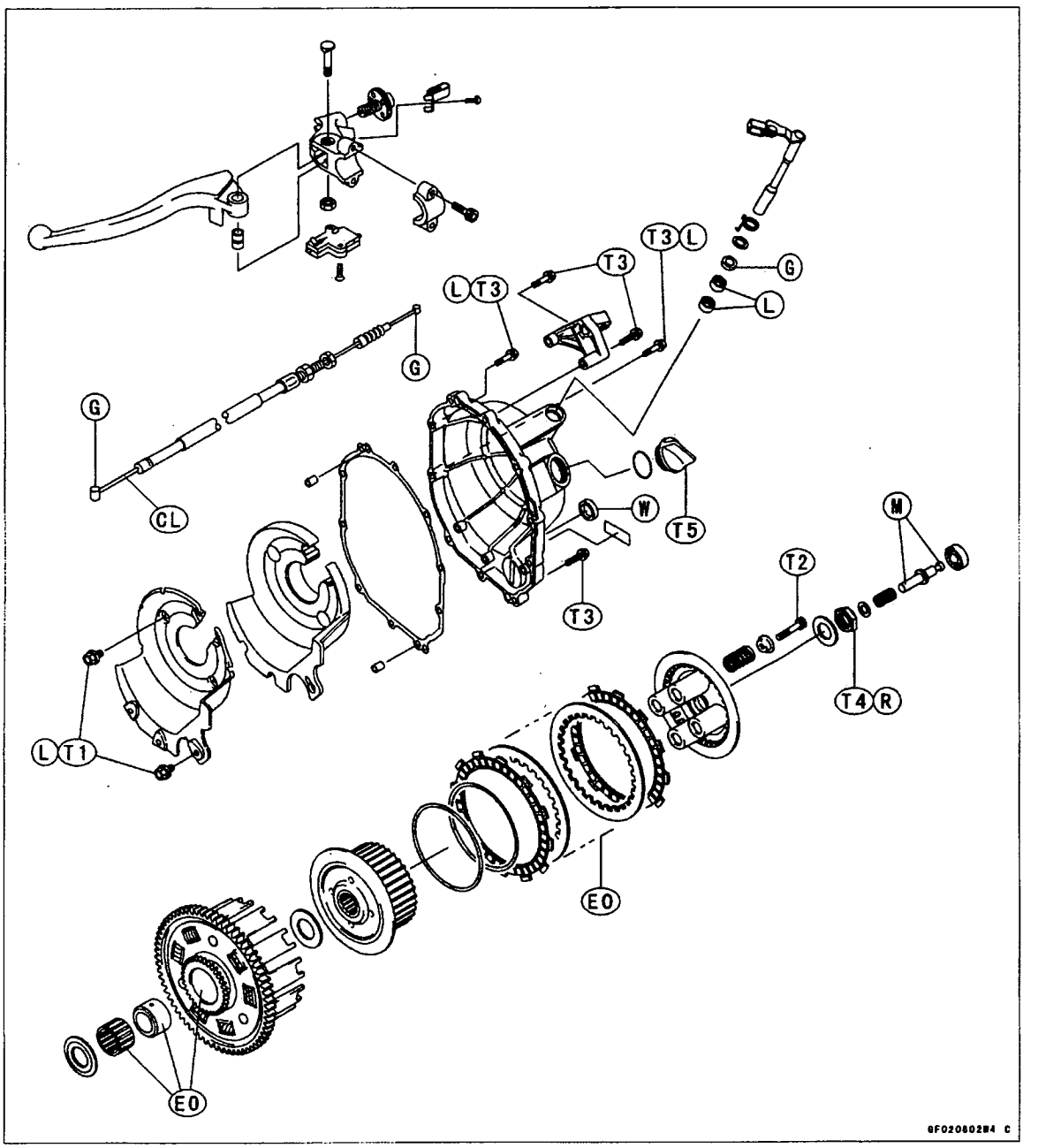

CL: Apply cable lubricant.
G: Apply grease.
EO: Apply engine oil.
L: Apply a non-permanent locking agent.
M: Apply molybdenum disulfide grease.
R: Replacement Parts
W: Apply water.

T1: 5.9 N·m (0.60 kg·m, 52 in·lb)
T2: 8.8 N·m (0.90 kg·m, 78 in·lb)
T3: 12 N·m (1.2 kg·m, 104 in·lb)
T4: 130 N·m (13.5 kg·m, 98 in·lb)
T5: 1.5 N·m (0.15 kg·m, 13 in·lb) or Hand-Tight

F-3: Transmission exploded view

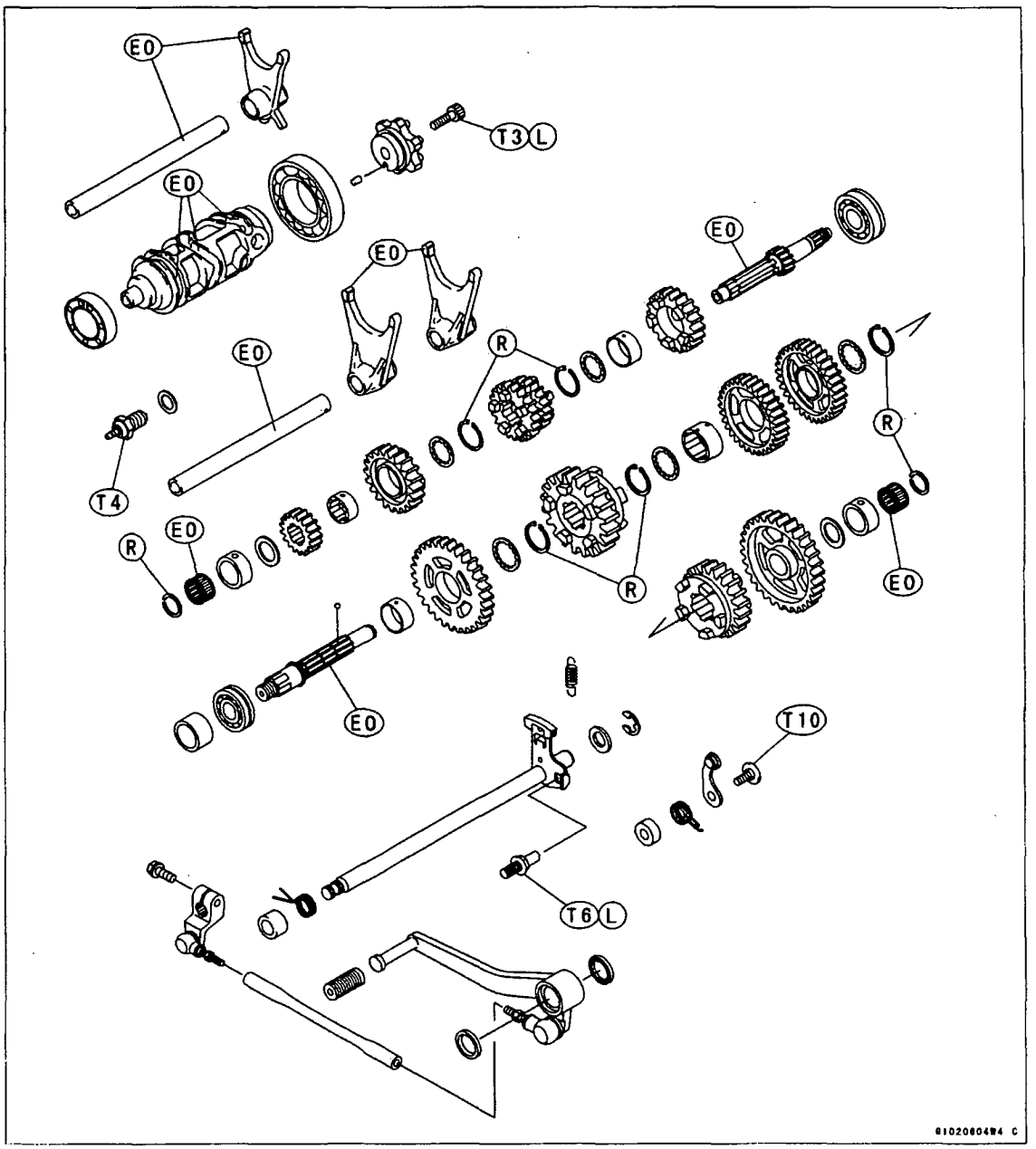

D: Do not apply any grease or oil.
G: Apply grease.
L: Apply a non-permanent locking agent.
M: Apply molybdenum disulfide grease.
SS: Apply silicone sealant (56019–120).
LG: Apply silicone sealant (92104–1063).
EO: Apply engine oil.
R: Replacement parts.
S: Tighten the fasteners following the specified sequence.

Quaife Automatic Torque Biasing Differential for Added Traction

Design

The Quaife ATB Differential is designed to prevent the complete loss of drive that occurs with a conventional differential when one wheel slips.

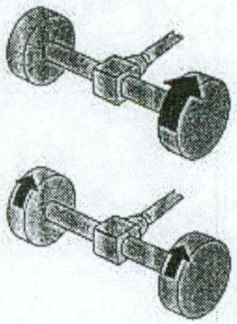

Whilst requiring some torque in the slipping wheel the Quaife unit is progressive in action but never locks - controlled power is transmitted to all the driving wheels. Although ideally suited to high-powered front-wheel drive systems, Quaife ATB differentials are used in rear and four-wheel drive vehicles where optimum traction is required. The four-wheel drive layout includes a centre differential as well as one in each axle.

The torque capacity of the Quaife unit is increased or decreased by varying the helix and pressure angles of the gear teeth. A combination is available to meet user requirements varying from Formula One racing to high mileage Ambulance fleets.

The operation is automatic, normal axle lubrication is retained and the unit is interchangeable with the conventional differential.

Operation

The Quaife Differential is an automatic gear-operated Torque Biasing Differential. Sets of floating helical gear pinions (1) mesh to provide the normal speed differential action. To pre-load the gear packs there is a selection of centre spring discs (2) available. In the event of wheel

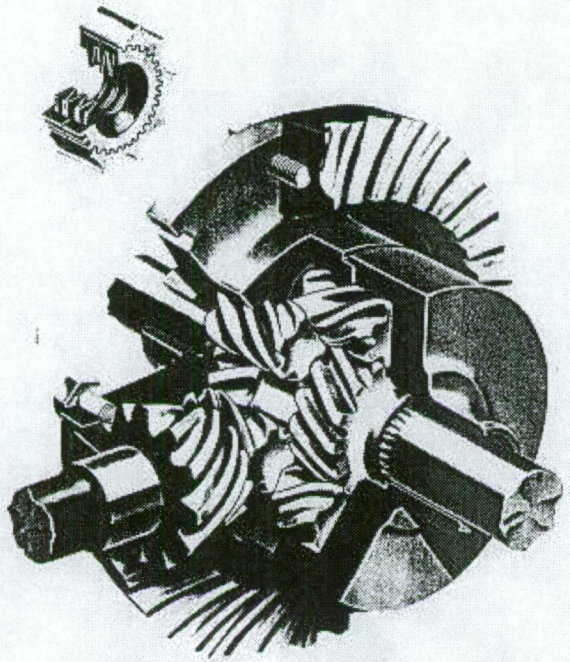

slip torque bias is generated by the axial and radial thrusts (red) of the pinions in the pockets (3). The resultant friction force enables the driving road wheel and sun-gear (4) to transmit a greater proportion of the torque. This effect is progressive, but at no stage does the differential lock solid. Hence the inherent safety of the Quaife Automatic Torque Biasing Differential.

Fitting and Maintenance

Installation is identical to the normal differential with bearing pre-loads and pinion mesh being restored to the original manufacturers' recommendation. Servicing of the unit is simple as all

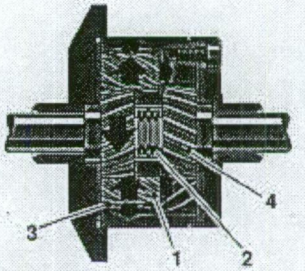

KEY
1 Helical gear pinions
2 Centre spring discs
3 Pocket
4 Sun Gear

gear pinions are free fitting and normal final drive lubrication oils are retained. Due to the internal design of the Quaife differential, all driving wheels must be elevated when servicing brakes, tyres, etc.

Applications

Quaife differentials are used in all forms of motor sport from circuit to rallying in two and four-wheel drive systems. A wide variety of emergency vehicles, where all-weather mobility is essential, also use Quaife differentials. Major users being Ambulance, Police, HM Coastguard, MOD, Forestry Commission and Public Utilities where the addition of a Quaife ATB differential improves vehicle handling and stability without compromising service life or operating costs. The benefits being available all year round whatever the traction conditions.

Company Profile

R.T. Quaife Engineering (established 30 years in UK) manufactures racing gear boxes (car and motor cycle), differentials, steering components and drive line power take-offs. The Differential design is patented and the Quaife name is a registered mark.

R. T. Quaife Engineering Ltd

Vestry Road, Otford, Sevenoaks, Kent.
TN14 5EL. England
Tel: 01732 741144
Fax: 01732 741565

F-5: Quaife ATB differential operation

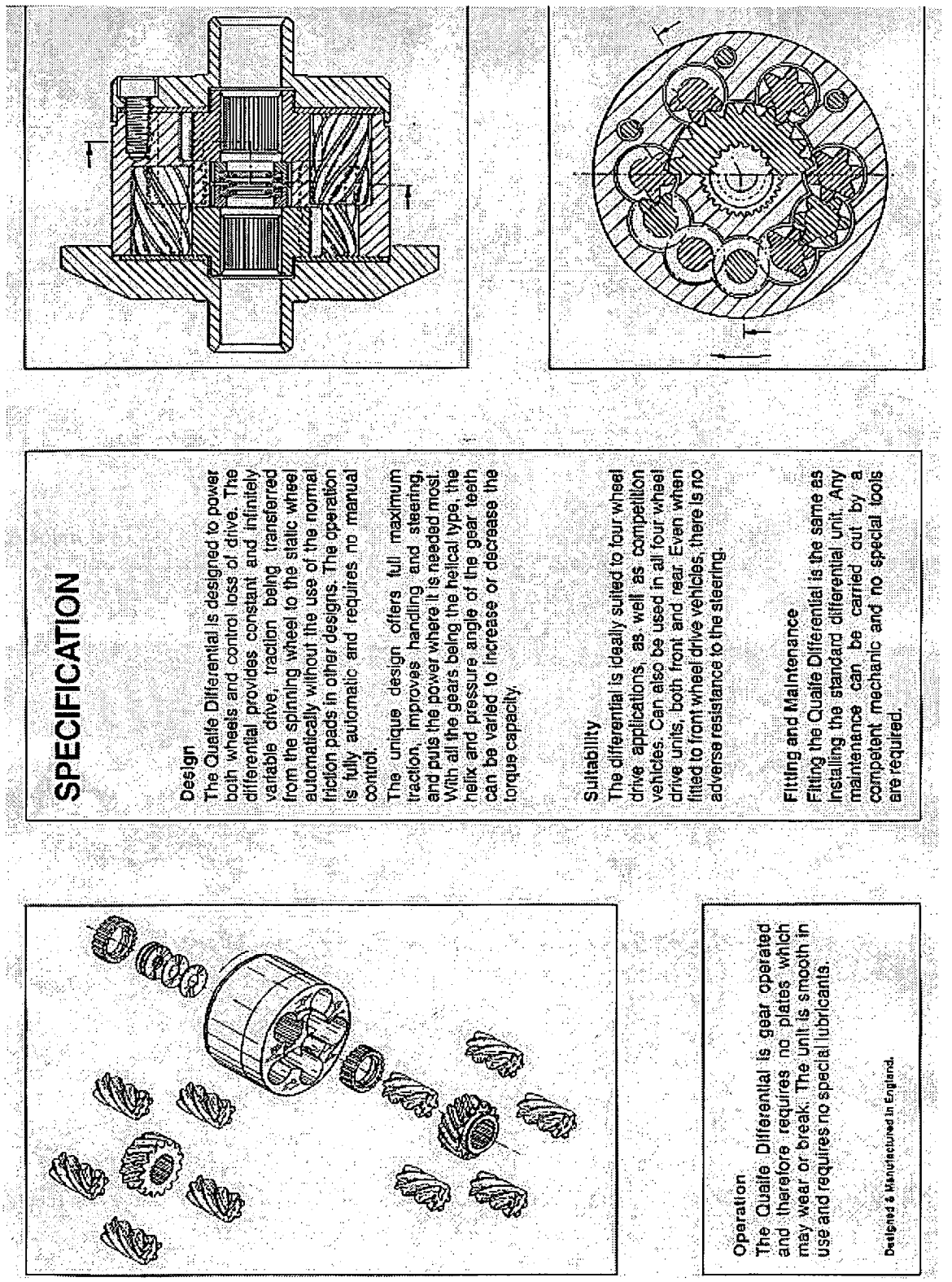

F-6: Quaife ATB differential specifications

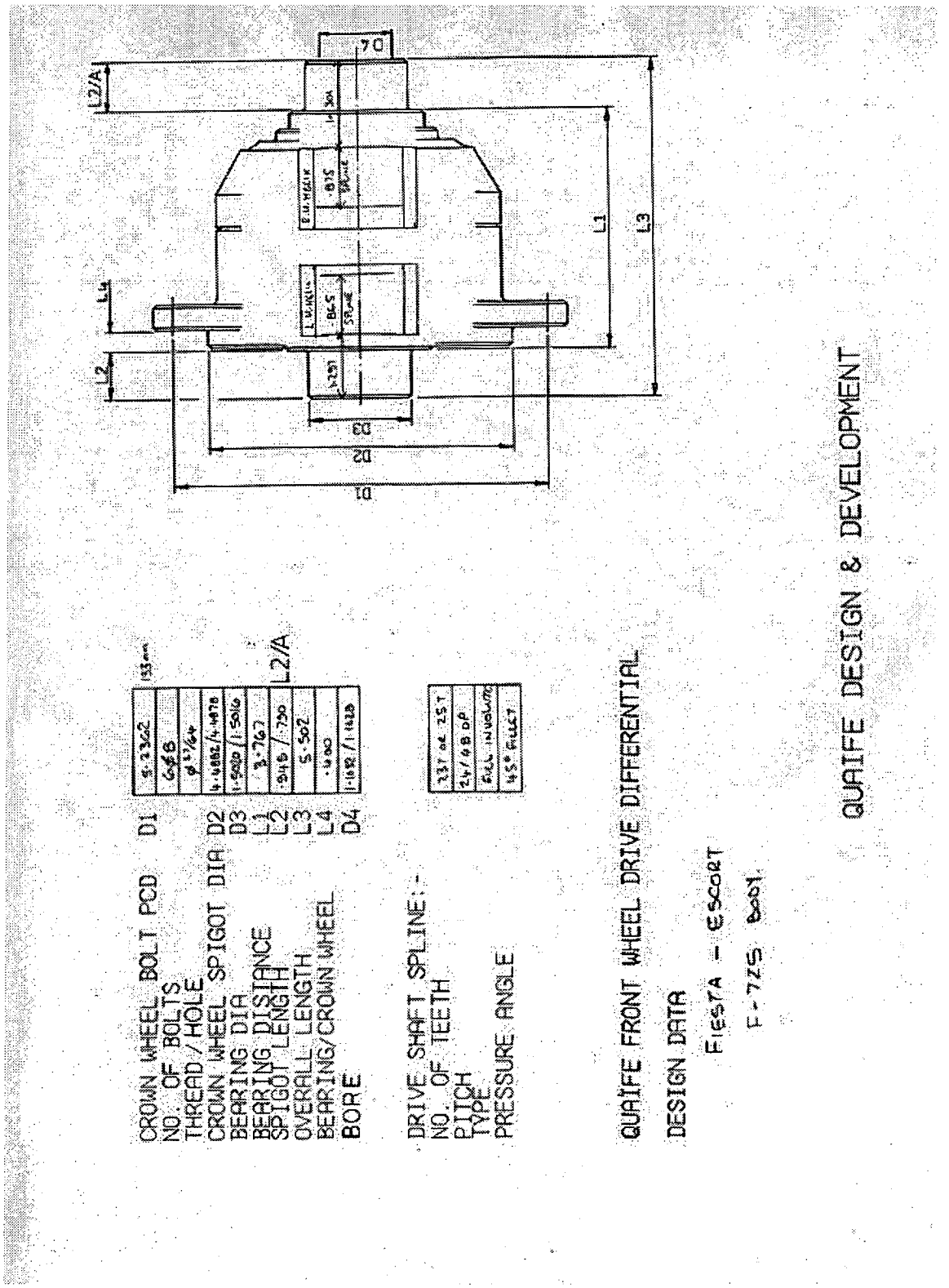

F-7: Quaife ATB differential dimensions

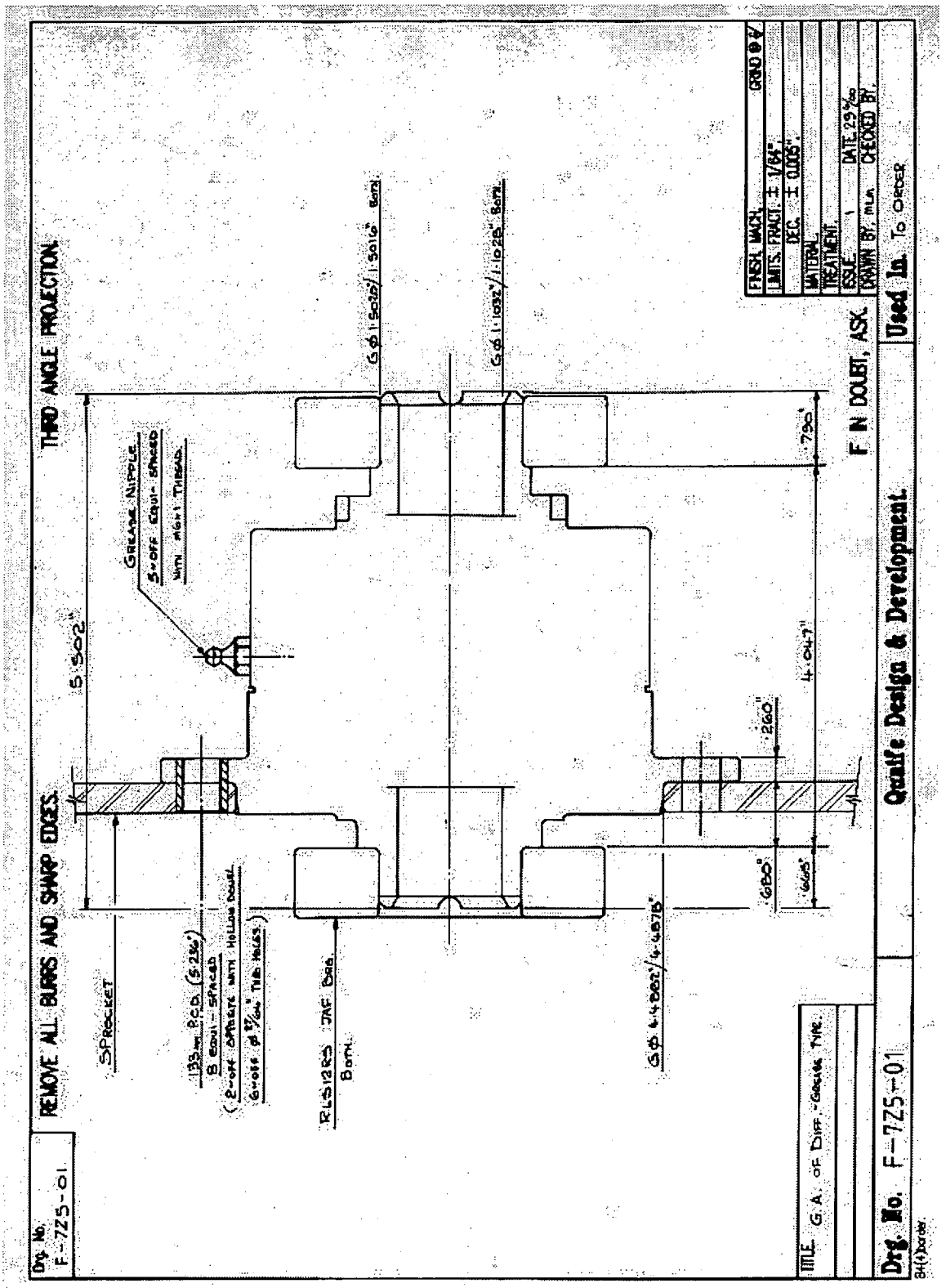

F-8: Composite disc dimensions

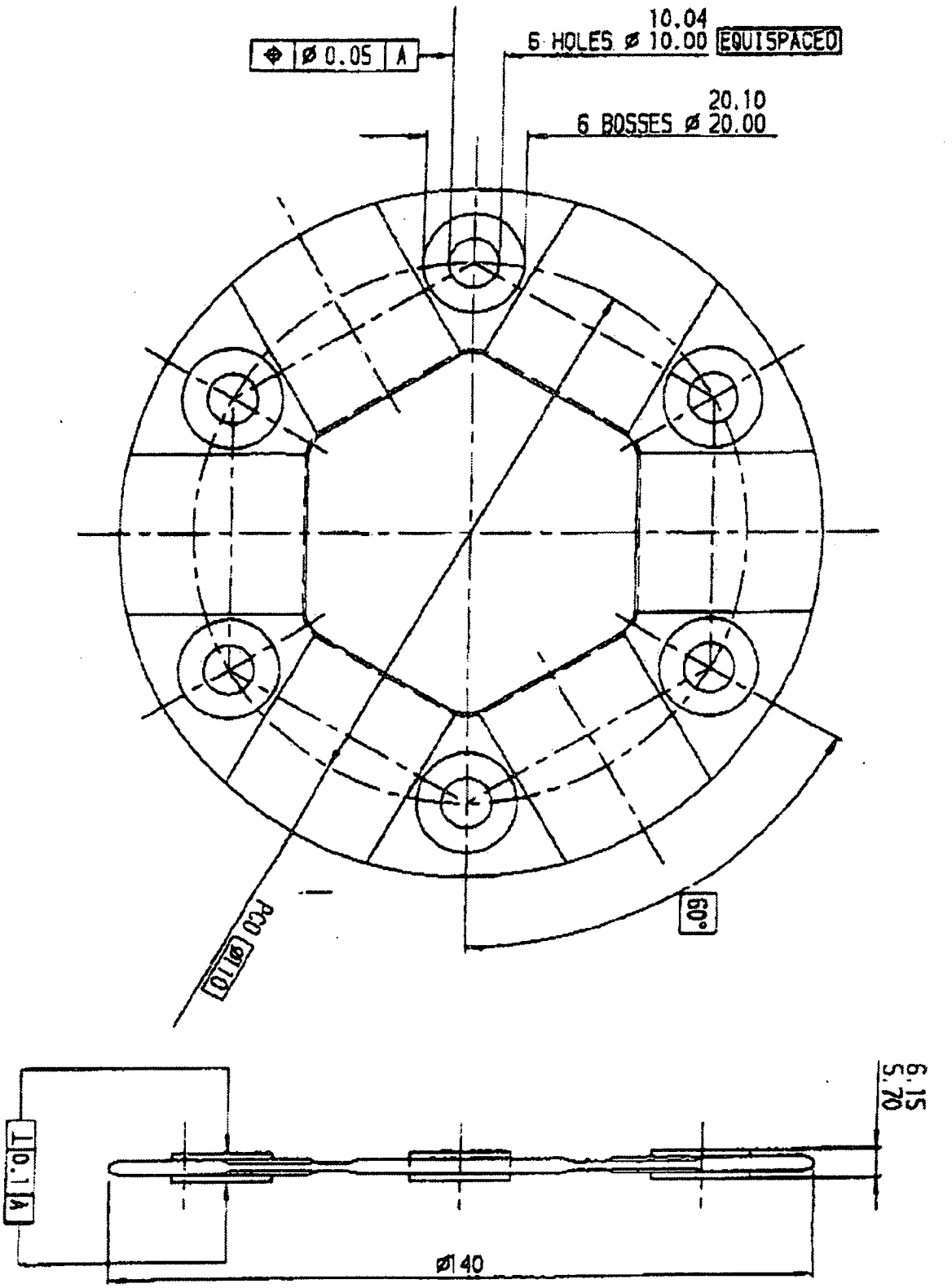

Appendix G - Electrical Systems Design -

G-1: Electrical system specifications

Battery	
Type	Gel cell
Capacity	15 Ah
Voltage	12.6 V
Charging System	
Type	Three Phase AC
Alternator output voltage	45 V
Stator coil resistance	0.2-0.6 Ohm
Charging Voltage	14 – 15 V
Electric Starter System	
Starter motor	12 V
Brush length	12mm

G-2: Alternator exploded view

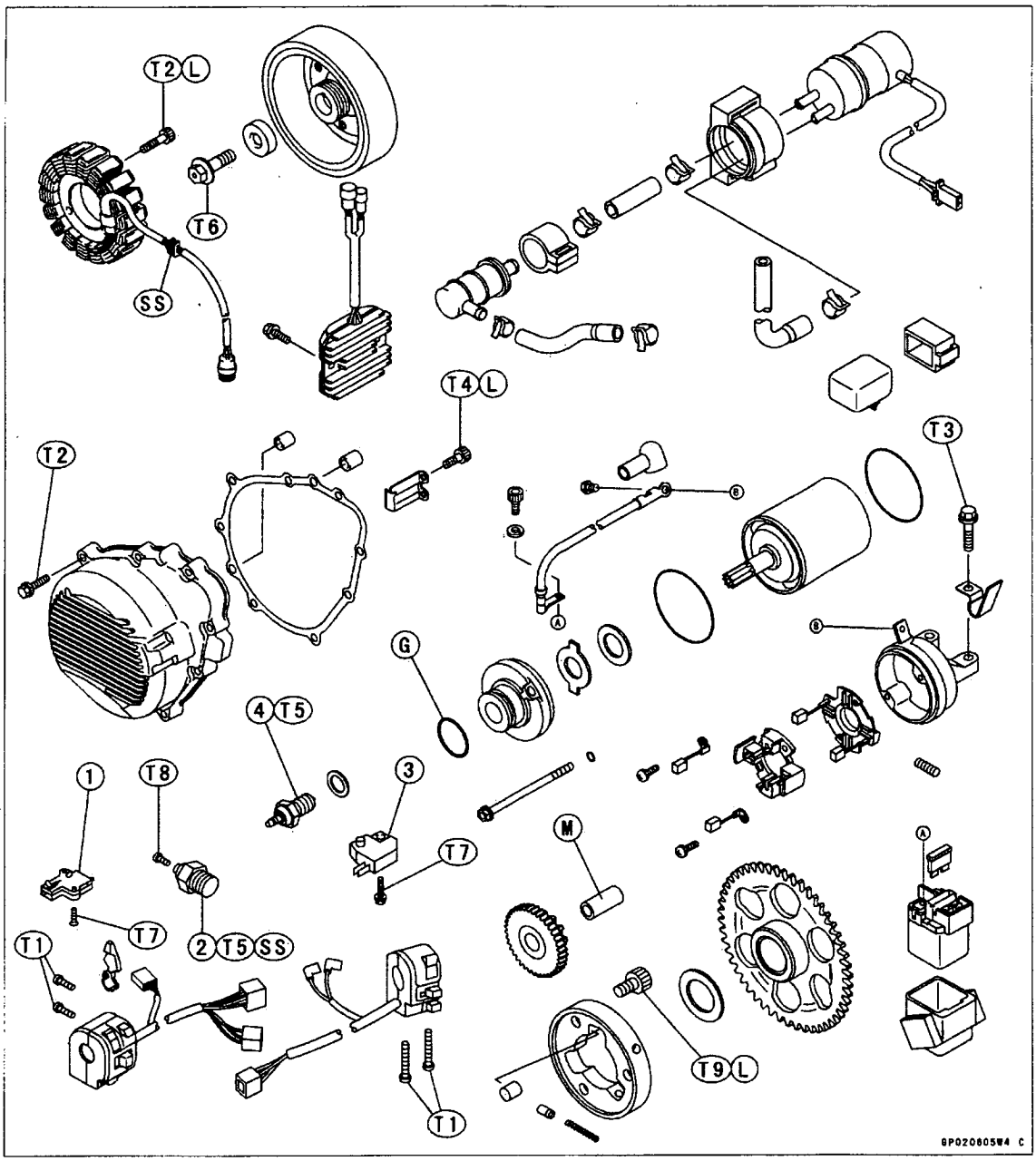

1. Starter Lockout Switch
2. Oil Pressure Switch
3. Front Brake Light Switch
4. Neutral Switch

L: Apply a non–permanent locking agent.
SS: Apply silicone sealant
M: Apply molybdenum disulfide grease.
G: Apply grease or engine oil.

T1: 3.5 N·m (0.35 kg·m, 30 in·lb)
T2: 12 N·m (1.2 kg·m, 104 in·lb)
T3: 11 N·m (1.1 kg·m, 95 in·lb)
T4: 7 N·m (0.7 kg·m, 62 in·lb)
T5: 15 N·m (1.5 kg·m, 11.0 ft·lb)
T6: 120 N·m (12 kg·m, 87 ft·lb)
T7: 1.0 N·m (0.1 kg·m, 9 in·lb)
T8: 1.5 N·m (0.15 kg·m, 13 in·lb)
T9: 33 N·m (3.4 kg·m, 24 ft·lb)

G-3: Fuse box wiring diagram

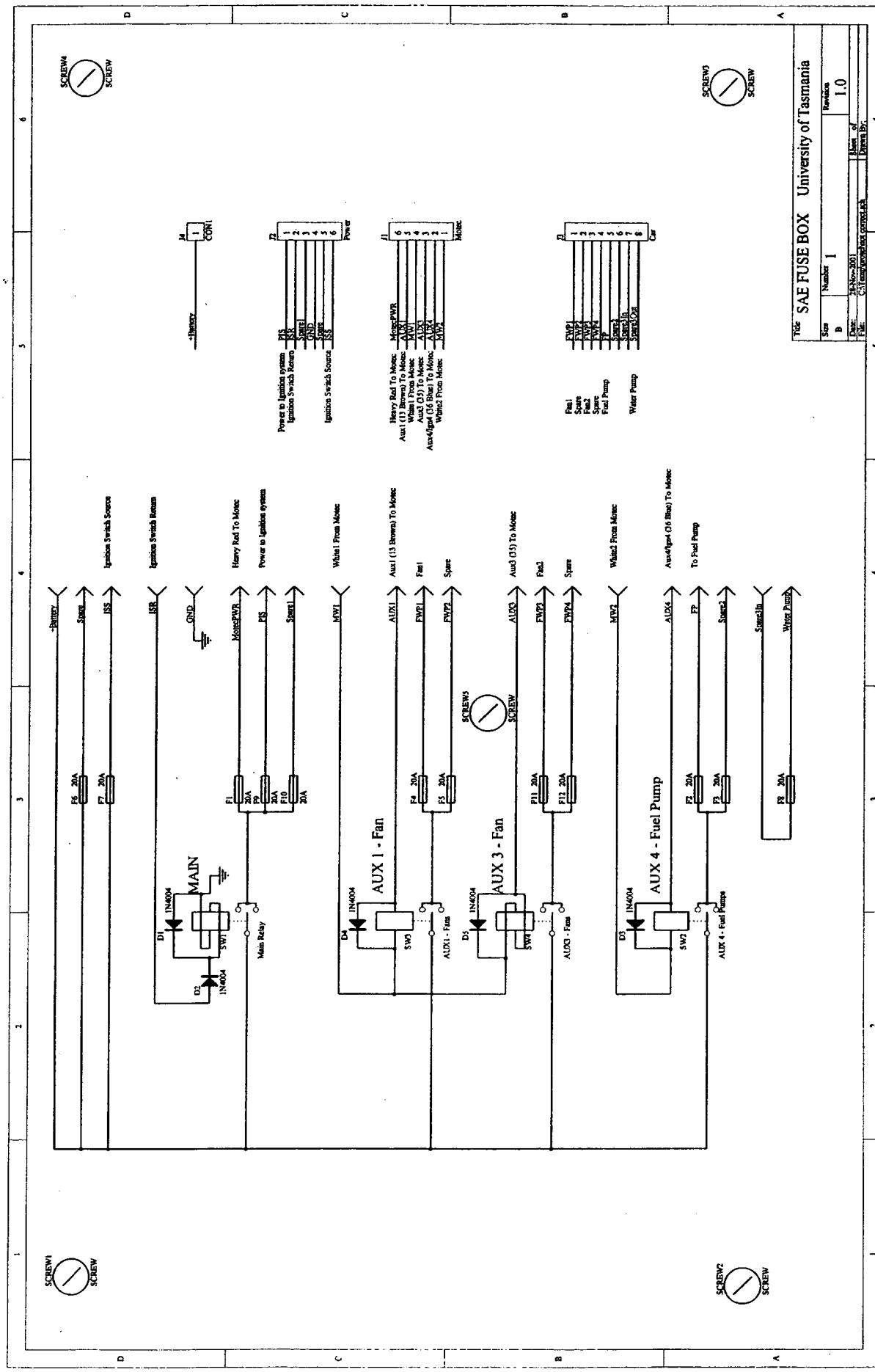

G-4: Fuse box circuit layout

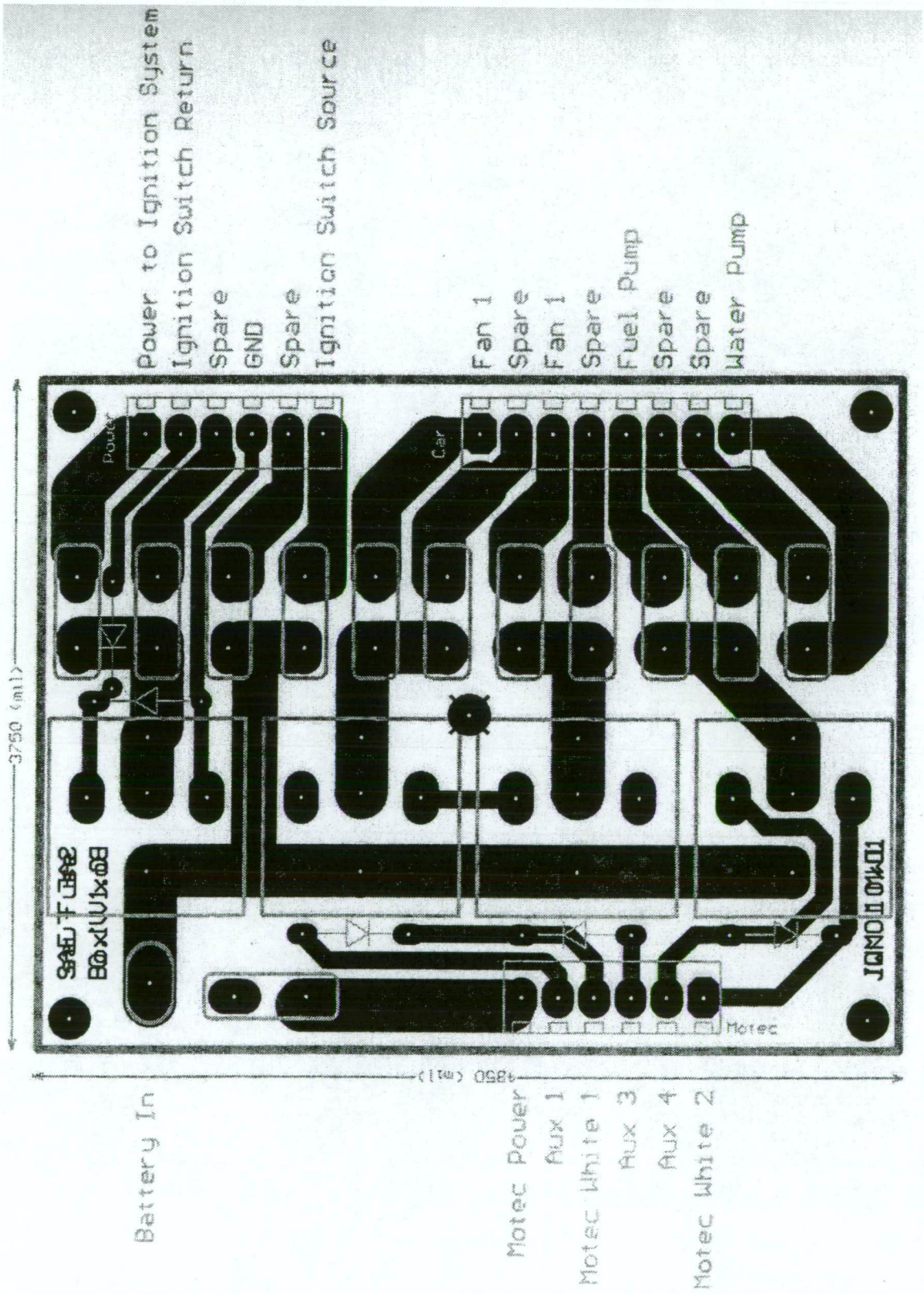

Appendix H - Sensor Specifications -

H-1: Advanced dash logger - description

MoTeC Advanced Dash Logger (ADL)

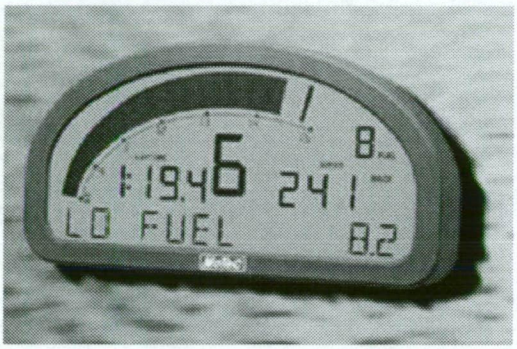

The MoTeC Advanced Dash Logger (ADL) is a fully featured and self contained, programmable logger. The key difference between the MoTeC ADL and other products is its flexibility to be adapted to any application.

Many vehicle, marine and industrial applications require separate products to perform the logging, controlling and displaying. However, the MoTeC ADL offers seamless integration of all three functions.

All aspects of the ADL are fully configurable, including which sensor is connected to which input, what to log, how fast to log it, which channels to display, warning alarms and control outputs.

The MoTeC ADL uses a high speed 32 bit microprocessor and incorporates a 79 pin autosport connector. The ADL is built to internationally recognised quality and manufacturing standards and is back by a full 2 year worldwide warranty.

Data Logging

Data logging allows for readings taken from Analog, Digital, Serial, CAN or Calculated channels, to be stored in the ADL for later analysis on a computer. The ADL uses permanent non-volatile Flash memory. Data memory may be unloaded at very high speeds (approx. 19 seconds per Mbyte). Different logging options allow 384k, 1MB or the full 8MB to be accessed.

The ADL can store channels at up to 1000 times per second per channel, this can be individually set for each channel. Four logging modes may run concurrently (Normal, Fastest Lap and two Burst Modes) each with selectable start and stop logging parameters. Memory can operate in stack or circular buffer mode.

Analog and Digital Channels

In total the ADL can accommodate over 200 channels derived from any mixture of Analog, Digital, RS232 Serial and CAN bus data channels.

The ADL directly supports up to 28 analog inputs, 12 digital/speed inputs, 8 auxiliary outputs and 2 high accuracy Wideband Lambda (Air/Fuel ratio) inputs.

The analog channels sample at up to 1000 samples per second per channel, with a measurement range of 0 to 15 VDC.

Digital inputs are used for state monitoring, counting and pulse width measurement. They accept switch, logic, open collector (Hall Effect), or magnetic signals.

The auxiliary outputs can be configured to operate as simple off/on outputs, duty cycle control or frequency based outputs.

Serial Communications

The RS232 serial port is programmable up to 115k baud and can be used as either a telemetry data output port or serial data input port.

As a telemetry port; devices such as Modems, GSM & Satellite Phones, Radio Modems etc. can be connected to facilitate remote communication.

As a serial data input port; serial communication devices can be connected for displaying and logging purposes. These include Engine Management Systems (MoTeC and other), bar code devices, keypads, GPS Systems or other serial communications devices.

Display

The MoTeC ADL display is a high contrast, high temperature, custom designed reflective LCD. Its unique design makes it viewable in direct sunlight or artificial light.

The display has 3 modes of operation, where each mode is fully programmable and independent of the other. Each mode may be selected by pressing a button or activated by a condition.

The 70 segment bar graph display is programmable to display any channel, with an optional peak hold marker and setpoint marker. Each numerical display item can be programmed to display any channel value as required. The 13 digit alphanumeric display area has 20 lines available to scroll through and may be used to display any channel value or to display warning messages.

Lap times may be displayed when connected to a MoTeC Lap Beacon (or a driver activated switch). Other performance information may be displayed, including minimum corner and maximum straight speed, fuel used or fuel remaining, and many more.

Alarms

Warning alarms may be defined for any analog, digital, serial or calculated channel. Alarm limits are fully programmable and may include up to 6 conditions to ensure that the alarms are only activated at the correct time.

When an alarm condition has been detected, a message can be shown on the display and an auxiliary output activated. These outputs can be used for warning lights or the control of other devices.

The alarms remain active until they are acknowledged, either by activating a switch or automatically after a definable period of time.

Controller Area Network (CAN)

The CAN bus is a high speed communication standard operating at speeds up to 1Mbit.

CAN allows many devices to be connected by a common bus, allowing all devices to share information as part of a larger system.

CAN devices include: automatic transmission controllers, sensors, multi-channel input/output modules, engine management systems etc.

Host Software

The ADL is supplied with software packages for managing the ADL, analysing the logged data and monitoring a telemetry link.

Ease of use is one of the most attractive aspects of the MoTeC ADL software. There is no complex language to learn, just simple menu driven windows.

A full online help system is easily accessible and is integrated throughout the software.

Dash Manager Software

The Dash Manager Software is used to configure the ADL and download logged data. It is logically laid out, giving the user access to the power of the ADL without requiring high levels of computer knowledge or intense training.

Interpreter Software

The Interpreter software contains predefined configurations for easy data analysis. Screen display formats may be varied to suit all preferences, including user defined graphs, histograms and statistical summaries. By utilising these different display methods, users can view data in many formats to obtain accurate, meaningful analysis.

Data can also be exported into ASCII CSV file format for analysis in other software packages.

The Pro Logging option includes graph overlays, virtual instruments, mathematical functions, XY graphs (scatter plots), track maps (shows minimum and maximum speeds, gear change point and breaking points) and other advanced features.

Telemetry Monitor (Optional)

The Telemetry Monitor software allows for realtime viewing of the telemetry data either via direct serial communications, modems or radio modems. Data can be viewed in various formats such as charts, bar graphs, dial gauges, numerics, lights, XY graphs and scroll charts. All objects are definable by the user.

Upgrades and Accessories

The MoTeC ADL is completely field updateable by the user. The control software and logged data is stored in FLASH memory. No programming interface is required, simply send to the ADL the new program and the latest features are immediately available.

Upgrade Options

The ADL has field upgradeable options using a password enabling system. Upgrade options include:

Extended inputs & Outputs, Pro Logging (advanced data analysis), Medium Logging (1Mbyte), Large Logging (4Mbyte), Telemetry Support, Remote Logging and Wideband Lambda measurement.

Three wiring options are available for the ADL:

Separate I/O Terminal Module with plug-in screw terminals. Includes a Realtime Clock, additional RS232 port and wide ranging power supply.

Standard (vehicle style) wiring loom for specific permanent installations.

Custom wiring looms for complex installations.

Accessories

A wide range of sensors are available for use with the ADL including: linear position, accelerometers, pressure, resistive and thermocouple temperature sensors, hall and magnetic speed sensors and many others.

The MoTeC Lap Beacon transmitter and receiver has been designed in conjunction with the ADL. It features high channel count (990), improved optics, low power consumption and multi beacon capability.

And for peace of mind the MoTeC ADL offers a full 2 year worldwide warranty.

H-2: Advanced dash logger - specifications

ADL Specifications

General

- Microprocessor: 32 Bit High Performance
- Manufacturing Quality standard to ISO9001
- Field updateable Operating System
- Non-volatile FLASH memory for data & operating system
- High RFI Immunity
- Rugged Aluminium Housing (IP-55, NEMA 4)
- 79 pin Autosport connector
- Operating Temperature: -10 to 70 DegC
- Operating Voltage: 7 to 22 VDC
- Operating Current: 0.3 A max.
- Weight: 385 gms (0.85 lbs)
- Size: 180mm x 91mm x 18mm (excluding connector)
- Reverse Battery and Transient Protection
- Warranty: 2 years Parts and Labour

Measurement Inputs

- 28 Analog Inputs (10 Standard):
  - 20 Analog Voltage (6 Standard)
  - 8 Analog Temperature (4 Standard)
  - 12 bit resolution, 0 to 15 VDC range
  - Update rate (Max. 8 channels): up to 1000 times/sec
  - Other inputs: up to 500 times/sec

- 4 Digital Inputs (2 Standard)
- 4 Speed Inputs (2 Standard)

  Digital & Speed
  - Switch to OV, logic signal, open collector (Hall Effect), or Magnetic
  - State & Counting (1MHz)
  - Period (1 micro sec)
  - Pulse width (1 micro sec)

- 4 Switch Inputs (4 Standard
- User definable sensor calibrations

Auxiliary Outputs

- 8 Digital Outputs (4 standard)
  - Open Collector (drives to ground) with pullup (10k ohms) to battery positive
  - On/Off or Pulse Width Modulation with variable Frequency and Duty Cycle

Air Fuel Ratio Measurement (Optional)

- 2 high accuracy Wideband Lambda (Air/Fuel ratio) inputs

- Resolution: 0.01 Lambda
- Temperature compensated
- Range: 0.75 to 1.2 Lambda

Data Logging

- Memory: 384k, 1MB, 2MB, 4MB, 8MB
- Non-volatile FLASH, field upgradeable
- Logging of any Analog, Digital, Serial, CAN bus or Calculated channel
- Maximum Logging throughput: 20k/sec
- 2 Burst Logging buffers with pre triggering (Large logging option only)
- Typical Unload Speed: 19 sec/MB, using parallel port of PC to CAN bus RS232 unload rates dependent on baud rate

Calculations

- Timers (0.01s, 0.1s, & 1s resolution)
- 2D and 3D Tables
- User conditions
- Math Functions: Differentiate, Integrate, Absolute, Min/Max
- Lap Time and Number
- Lap Gain/Loss
- Speed and Distance
- Gear Detection
- Fuel Prediction
- Tell-tales
- Running Min/Max

Display

- Custom LCD, High Contrast, High Temperature, Reflective
- Display any Analog, Digital, Serial, CAN bus channel or Calculated channel
- 3 Display Modes
- 70 Segment Bar graph
    - Definable Range
    - Programmable Setpoint and Peak Hold point
- 4 Numeric Display Items
- 13 Digit Alpha Numeric Display area, 1,2 or 3 channels per line (20 scrollable lines per display mode)
    - Alarm messages
    - Channel display
    - Descriptive text

Communication

- Serial RS232 Coms. (1200 to 115k baud)
- CAN data link (250Kbit to 1Mbit)
- Telemetry Link output (RS232)

Host Software

1. Dash Manager Software
2. Interpreter Analysis Software
3. Telemetry Software (Optional)

Computer Requirements

- IBM PC compatible running Windows 95/98 or NT4.0
- Pentium (Min.) 90MHz, 16MB RAM

Upgrades

The MoTeC ADL in its base configuration includes:

- 10 Analog Inputs
- 8 Digital Inputs
- 4 Digital Auxiliary Outputs
- RS232 and CAN bus support
- Software: Dash Manager and Interpreter
- User's Manual

Upgrades Available *(field updateable by the user)*:

- **Extended Inputs & Outputs**
  - 28 Analog Inputs (10 standard)
  - 12 Digital Inputs (8 standard)
  - 8 Digital Auxiliary Outputs (4 standard)

- **Pro Logging** - Advanced Analysis Software
  - Graph Overlays
  - XY Plots
  - Maths functions
  - Virtual Instruments display
  - Track Mapping

- **Medium Logging**
  - 384k to 1MB Memory

- **Large Logging** *(requires Medium Logging Upgrade)*
  - 1MB to 8MB with Burst mode logging

- **Lambda Measurement**
  - 2 Wideband Lambda inputs

- **Telemetry**
  - Enables realtime viewing of data via a telemetry link

- **Remote Logging** *(requires Telemetry Upgrade)*
  - Allows Remote Logging via a telemetry link or hand held computer

Accessories

- PC Communications Cable (High Speed CAN)
- Wiring Looms
- Input/Output Terminal Module
- Lambda (Air/Fuel ratio) Sensors and Kits
- Telemetry Products
  - GSM mobile phones, radio modems etc
- Sensors and transducers
  - a full range of sensors, amplifiers, transducers, lights and buttons are available
- Lap Beacon: Transmitter and Receiver (990 channel)

H-3: ADL wiring loom

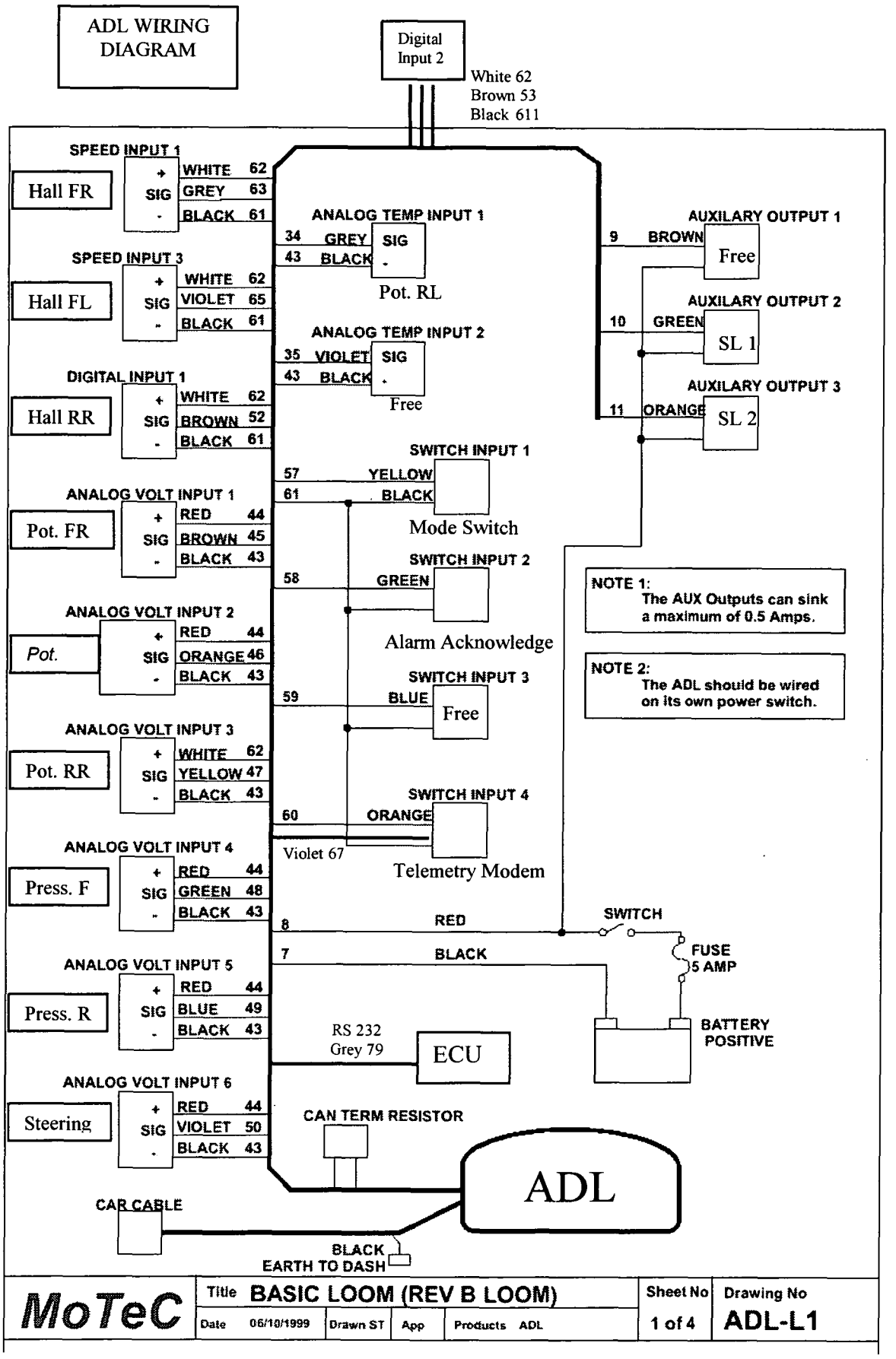

H-4: Radio modem – specifications

RF INNOVATIONS

HIGH SPEED RADIO MODEM

RFI 9256 *Series 3*

SPREAD SPECTRUM 900MHz RADIO MODEM

The RFI 9256 is a license free high performance data radio capable of functioning in hostile RF environments with data throughput of 115 Kbps. Receiver design provides superior rejection of unwanted signals in hostile crowded spectrum environments.

Features

- Economical
- Dual RS-232 ports
- Suitable for voice and data
- Forward error correction
- ARQ is software selectable
- Air data speeds 115 Kbps
- In built diagnostic channel
- Up to 30 Kms point to point
- User friendly intuitive software
- Interface speeds 110 to 115000 bps
- RF power up to 1 Watt software selectable
- Programmable I/O for SCADA applications
- Front panel indicators for RSSI, TX power and status
- Can be installed and commissioned without test equipment

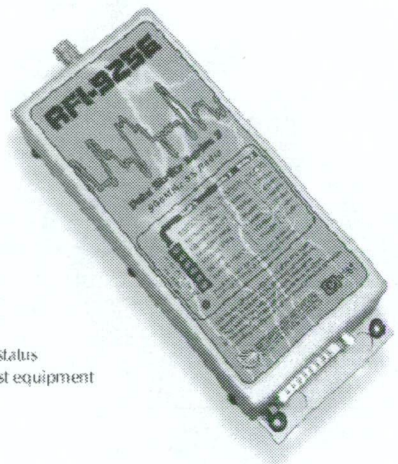

Applications

Point to Multipoint Data Acquisition and Control

Intelligent built in Modem can interface with virtually any standard Data logger, PLC, computer; i.e. any RS232 device. In built buffers handshake with input/output devices at data speeds up to 115,000 bps and transparently move data to the other end.

Linking of local and remote RS232 serial ports

Depending upon the geography and terrain, the Radio modems can communicate reliably over considerable distances. Good line of site paths from mountain top to hill can extend useful range up to 30 km. The RFI 9256 can be used as a repeater to extend range indefinitely.

Parallel digital I/O and expansion

8 parallel digital I/O in addition to the standard RS232 serial port are provided in the RFI 9256 model Radio modems. Expansion radio interface modules (RIM) permit very large SCADA capability. For more details regarding interface parameters, contact the manufacturer.

Diagnostics functions

The second RS 232 port can be used as a diagnostics channel for monitoring network performance, and for additional data routing if required.

RF INNOVATIONS PTY LTD ABN 97 065 523 579
22 Boulder Road, Malaga WA 6090
Telephone +61 8 9209 0900 • Facsimile +61 8 9248 2833
Email: sales@rfinnovations.com.au • Web: www.rfinnovations.com.au

Specifications
MODEL RFI 9256 Series 3

PHYSICAL

Dimensions	190mm L x 80mm W x 35mm H
Weight	260 grams
Construction	Alodined aluminium chassis and cover, with integrated display

GENERAL

Operating voltage	9 to 16VDC negative ground
Operating current	
Standby mode	150 mA
Transmit mode (1Watt)	Averages 350mA
Operating temperature range	-10 to +60 deg C
Operating Humidity range	Up to 95% non-condensing RH @ 50 deg C
Parameter and mode settings	In built software

TRANSMITTER

Output Power	1mW to 1 Watt software selectable
Spurious emissions	<-60 dBc
Output protection	Transmitter is fully protected for any load @ full power @ 60 deg C

RECEIVER

Sensitivity	<-108dBm for BER 1 part in 10^-4
End to end performance	Better than 1 in 10^-6 BER for S/N 20 dB or better
Frequency range	915-928 MHz (Australia) 902-928 MHz (FCC) 921-929 MHz (NZ)
RSSI display range	-110 to -60 dBm in 5 dB steps

DATA SYSTEM

RS 232 handshaking	Hardware/ software/ none software selectable
Protocol modes	All common variants / PLCs supported including point / point, point / multipoint and Hayes modes
Interface data speed	110 to 115,000 bps, software selectable all modes

Distributed by:

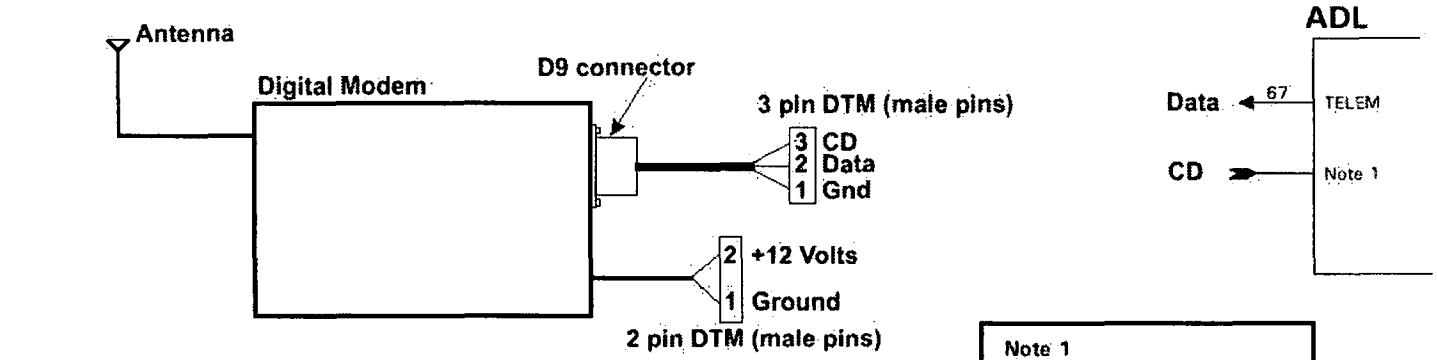

Note 1

The following pins can be used:
Switched Inputs (normally sw4)
Speed Inputs, Digital Inputs

D9 Connector Wiring Details

Male D9 Viewed from loom end

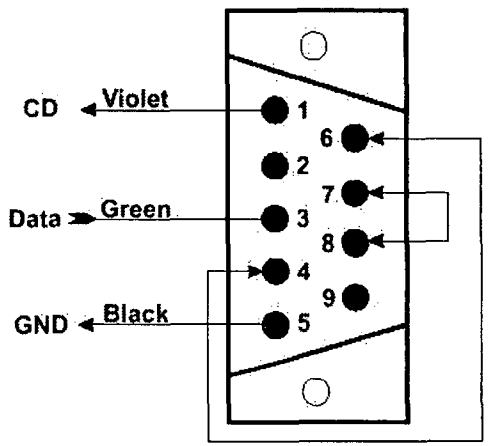

Motec Part No. 61071

ADL Setup

1. Set Input pin's channel to "Carrier Detect"
2. Select one of the templates in the RS232 Communications Setup screen.

NOTE: The modem may need configuration before it will connect.

MoTeC	Title: Digital Telemetry Connection				Sheet No	Drawing No
	Date 04/03/1999	Drawn ST	App	Products ADL	1 of 1	TEL01

H-6: Wheel speed hall effect sensor – specifications

Solid State Sensors

GT1 Series

Hall Effect Gear Tooth Sensors

TYPICAL APPLICATIONS

Automotive and Heavy Duty Vehicles:

- Camshaft and crankshaft speed/ position
- Transmission speed
- Tachometers
- Anti-skid/traction control

Industrial:

- Sprocket speed
- Chain link conveyor speed and distance
- Stop motion detector
- High speed low cost proximity
- Tachometers, Counters

FEATURES

- Senses ferrous metal targets
- Digital current sinking output (open collector)
- Better signal-to-noise ratio than variable reluctance sensors, excellent low speed performance, output amplitude not dependent on RPM
- Sensor electronically *self-adjusts* to slight variations in runout and variations in temperature, simplifying installation and maintenance
- Fast operating speed – over 100 kHz
- EMI resistant
- Reverse polarity protection and transient protection (integrated into Hall I.C.)
- Wide continuous operating temperature range (–40° to 150°C), short term to 160°C

GENERAL INFORMATION

1GT1 Series Gear Tooth Sensors use a magnetically biased Hall effect integrated circuit to accurately sense movement of ferrous metal targets. This specially designed I.C., with discrete capacitor and bias magnet, is sealed in a probe type package for physical protection and cost effective installation.

Units will function from a 4.5 to 24 VDC power supply. Output is digital, current sinking (open collector). Reverse polarity protection is standard. If power is inadvertently wired backwards, the sensor will not be damaged. Built-in protection against pulsed transients to +60V, –40V is also included.

Optimum sensor performance is dependent on the following variables which must be considered in combination:

- Target material, geometry, and speed
- Sensor/target gap
- Ambient temperature
- Magnetic material in close proximity

GT1 ORDER GUIDE

Catalog Listing	Description
1GT101DC	Gear Tooth Sensor

MOUNTING DIMENSIONS (For reference only)

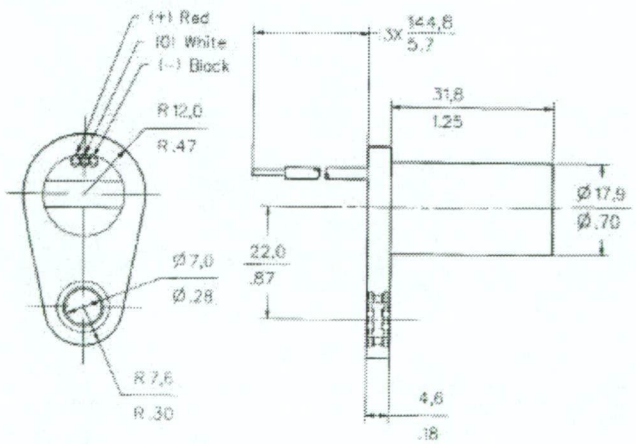

Solid State Sensors

GT1 Series

Hall Effect Gear Tooth Sensors

SENSOR SPECIFICATIONS

All values were measured using 1 K pull-up resistor.

Electrical Characteristics	Supply Voltage	4.5 to 24 VDC
	Supply Current	10 mA typ., 20 mA max.
	Output Voltage (output low)	0.4 V max.
	Output Current (output high)	10 µA max. leakage into sensor
	Switching Time	
	Rise (10 to 90%)	15 µsec. max.
	Fall (90 to 10%)	1.0 µsec. max.
Absolute Maximum Ratings*	Supply Voltage (Vs)	±30 VDC continuous
	Voltage Externally Applied To Output (output high)	−0.5 to +30 V
	Output Current	40 mA sinking
	Temperature Range	
	Storage	−40 to 150° (−40 to 302°F)
	Operating	−40 to 150° C (−40 to 302°F)
Switching Characteristics**	Operate Point	3.7±1.25° (3.28±1,13 mm)
	Release Point	4.7±2.50° (4,16±2,21 mm)
	Differential Travel	8.4±3.70° (7.45±3.34 mm)

* As with all solid state components, sensor performance can be expected to deteriorate as rating limits are approached; however, sensors will not be damaged unless the limits are exceeded.
** See Reference Target table.

TARGET GUIDELINES

The Target Guidelines table provides basic parameters when an application is not restricted to a specific target.

Any target wheel that exceeds the following minimum specifications can be sensed over the entire temperature range of −40° to 150°C with any sensing gap up to .080 in. (2.0 mm). This data is based on a 4 in. (102 mm) diameter wheel, **rotating 10 to 3600 RPM.**

Reference Target Dimensions

Tooth Height:	.200 in. (5.06 mm) min.
Tooth Width:	.100 in. (2.54 mm) min.
Tooth Spacing:	.400 in. (10.16 mm) min.
Target Thickness:	.250 in. (6.35 mm)

Sensor Output (with pull-up resistor added to output circuit)

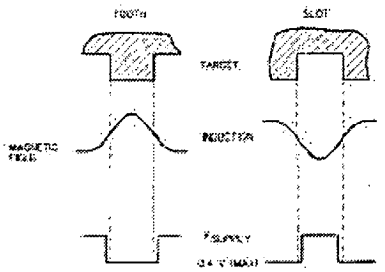

REFERENCE TARGET/CONDITIONS

Characteristics will vary due to target size, geometry, location, and material. Sensor specifications were derived using a cold-rolled steel reference target. See table, right, for reference target configuration and evaluation conditions.

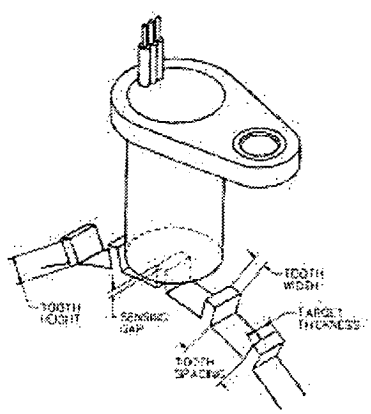

Target	
Diameter:	4 in. (101.6 mm)
Tooth Width:	.350 in. (8,89 mm)
Thickness:	.250 in. (6,35 mm)

Test Conditions	
Air Gap:	.040 to .080 in. (1,02 to 2,03 mm)
V Supply:	4.5 to 24 V
RPM:	10 min., 3600 max.

Operating Temp -40 to +150 deg C
Output States Air : High
Metal : Low (8 sec Hold Typ)

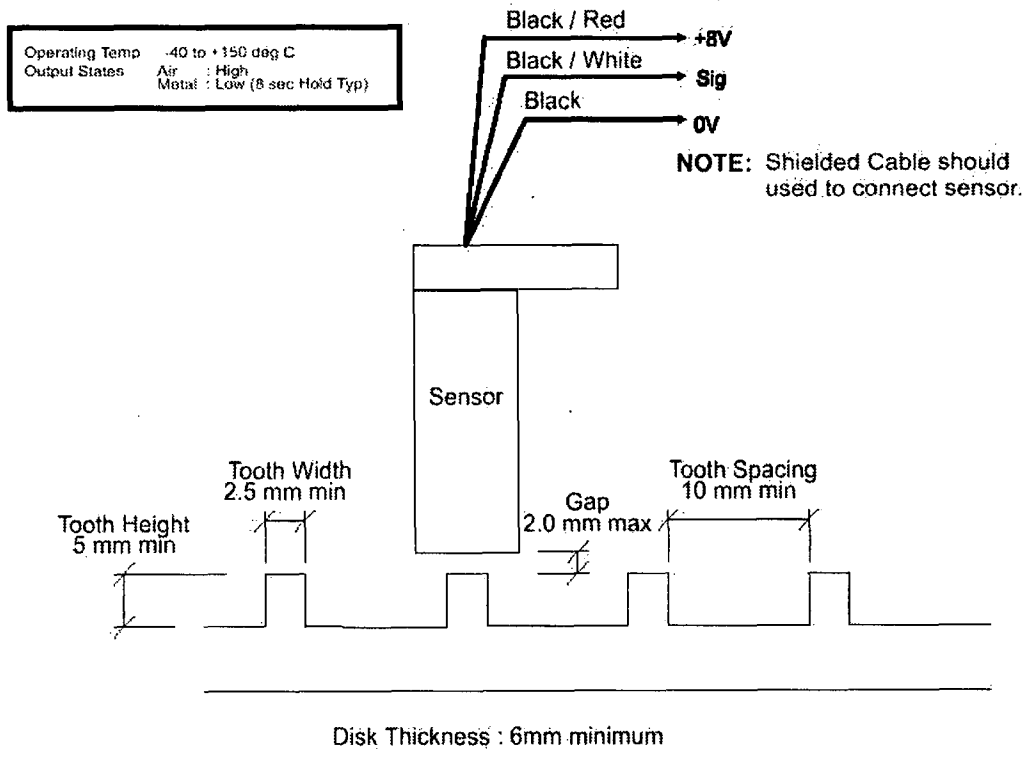

NOTE: Shielded Cable should used to connect sensor.

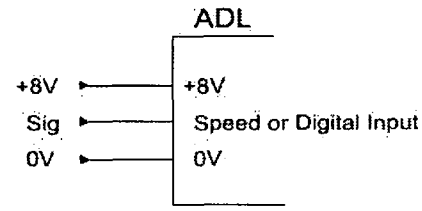

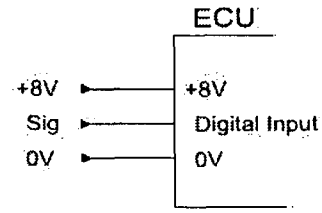

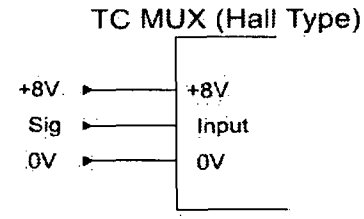

ADL Setup

Speed setup.
Select "HALL" Sensor type

When used for Traction Control the edge variation of the teeth must be less than 0.5% (to give 1 KPH in 200KPH accuracy)

eg. If the edge spacing is 20mm then the variation must be less than 0.1 mm.

MoTeC	Title GT101 Hall Effect Sensor				Sheet No	Drawing No
	Date	Drawn ST	App	Products ADL, ECU, TC MUX	1 of 1	X02

H-8: Suspension position linear potentiometer – specifications

GEFRAN

PZ12

RECTILINEAR DISPLACEMENT TRANSDUCER WITH CYLINDRICAL CASE

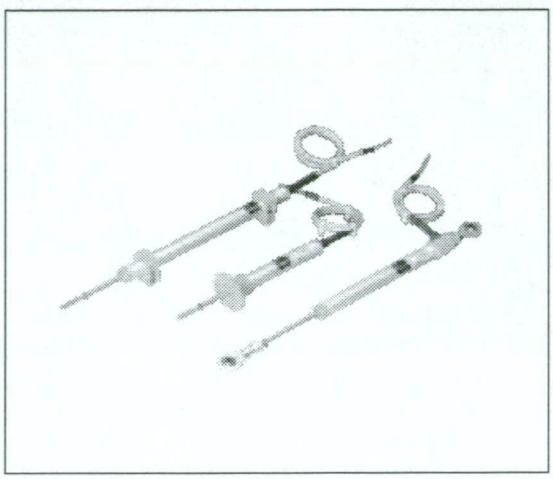

Main features

- *25 to 150 mm. stroke*
- *Mechanical fixing using brackets, selfaligning ball-joints or flange*
- *Independent linearity up to ± 0,05%*
- *Infinite resolution*
- *No variation of electrical signal outside theorical electrical stroke*
- *Displacement speed up to 10 m/s*
- *Working temperature: -30...+100°C*
- *Electrical connection: 3-pole screened cable (1m length)*
- *Life duration: > 25x10⁶ meters or >100x10³ operations whichever is the smaller (within C.E.U.)*
- *Grade of protection IP60*

TECHNICAL DATA

Useful electrical stroke (C.E.U.)	25/50/75/100/125/150
Independent linearity (within C.E.U.)	see table
Displacement speed	≤ 10 m/s
Displacement force	≤ 0.5N
Vibrations	5...2000Hz, Amax =0,75 mm amax. = 20 g
Shock	50 g, 11ms.
Tolerance on resistance	± 20%
Recommended cursor current	< 0,1 µA
Maximum cursor current	10mA
Maximum applicable voltage	see table
Electrical isolation	>100MΩ at 500V=, 1bar, 2s
Dielectric strength	< 100 µA at 500V~, 50Hz, 2s, 1bar
Dissipation at 40°C (0W at 120°C)	see table
Temp. Coeff. of the resistance	-200 ± 200ppm/°C
Actual Temperature Coefficient of the output voltage	< 1,5ppm/°C
Working temperature	-30...+100°C
Storage temperature	-50...+120°C
Case material	Anodised aluminium Nylon 66 GV 40
Control rod material	Stainless steel AISI 303
Fixing	Brackets, selfaligning ball-joints or flange

MECHANICAL DIMENSIONS

PZ12-S

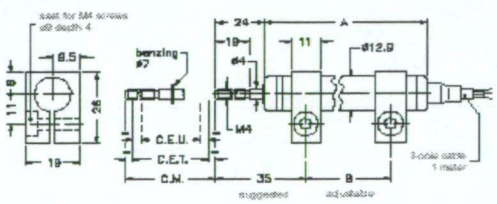

PZ12-A

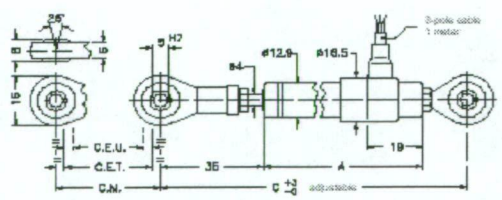

PZ12-F

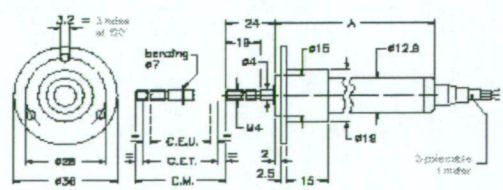

Important: all the data reported in the catalogue linearity, lifetime, temperature coefficient are valid for a sensor utilization as a ratiometric device with a max current across the cursor Ic ≤ 0.1 µA.

MECHANICAL / ELECTRICAL DATA

MODEL			25	50	75	100	125	150
Useful electrical stroke (C.E.U.) + 1 / -0		mm	25	50	75	100	125	150
Theoretical electrical stroke (C.E.T.) ± 1		mm	C.E.U. +1					
Resistance (C.E.T.)		kΩ	1	2	3	4	5	6
Independent linearity (within C.E.U.)		± %	0,2	0,1	0,1	0,1	0,05	0,05
Dissipation at 40°C (0W at 120°C)		W	0,5	1	1,5	2	2,5	3
Maximum applicable voltage		V	20	40	60			
Mechanical stroke (C.M.)		mm	C.E.U. +5					
Case length (A)	mod. PZ12 - S	mm	74,5	99,5	124,5	149,5	174,5	199,5
	mod. PZ12 - A	mm	102	127	152	177	202	227
	mod. PZ12 - F	mm	74,5	99,5	124,5	149,5	174,5	199,5
Recommended distance between brackets (B)		mm	42	67	92	117	142	167
Minimum distance between ball-joints (C)		mm	153	178	203	228	253	278
Weight	mod. PZ12 - S	g	45	55	65	75	85	95
	mod. PZ12 - A	g	70	80	90	100	110	120
	mod. PZ12 - F	g	60	70	80	90	100	110

ELECTRICAL CONNECTIONS

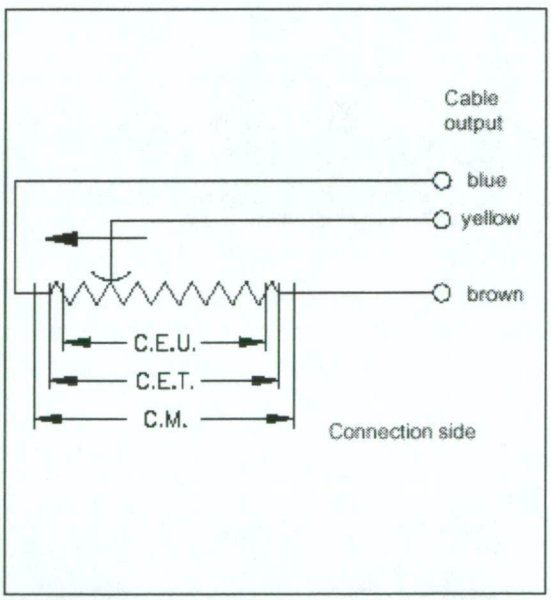

ORDER CODE

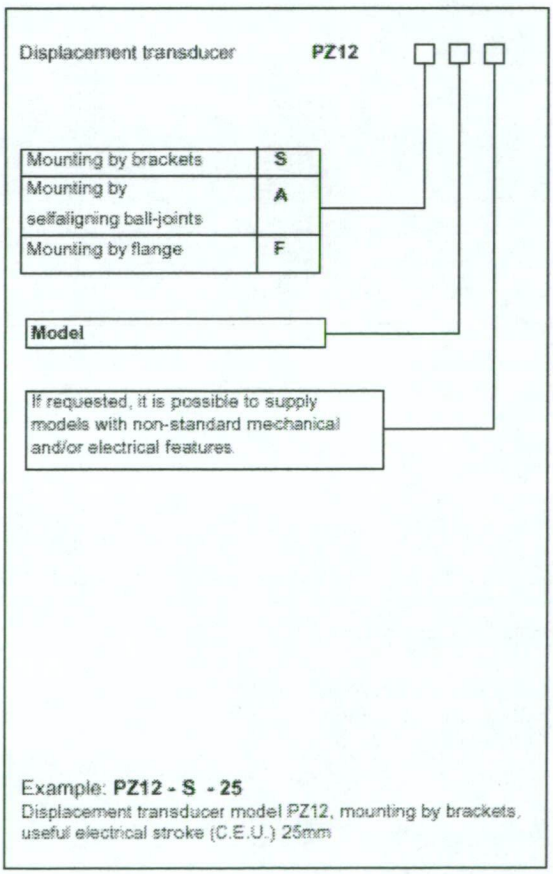

Example: **PZ12 - S - 25**
Displacement transducer model PZ12, mounting by brackets, useful electrical stroke (C.E.U.) 25mm

STANDARD ACCESSORIES

	Code
2 mounting brackets for PZ12-S	**STA074**

GEFRAN spa reserves the right to make any kind of design or functional modification at any moment without prior notice

GEFRAN spa
via Sebina, 74
25050 PROVAGLIO D'ISEO (BS) - ITALIA
ph. 0309888.1 - fax. 0309839063
Internet: http://www.gefran.com

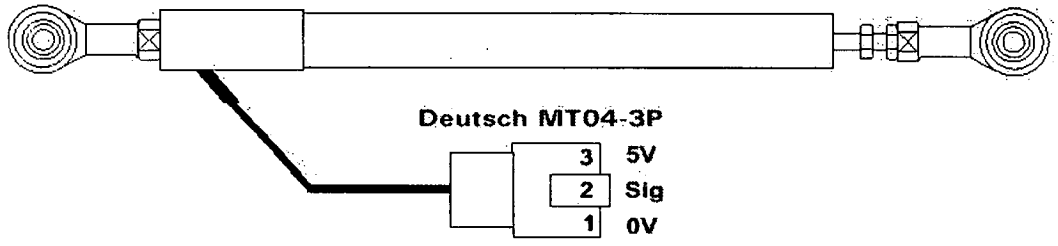

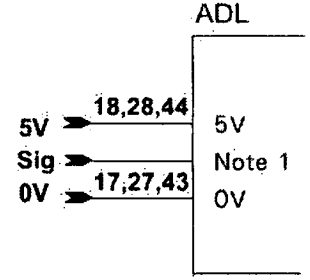

ADL Setup (to measure distance)

Channel Assignments

Assign a distance channel ie: Brake Pedal position

Sensor Calibration

1. In Calibration, select change.
2. Select Ratiometric(5V).
3. In calibration table enter the distance the pedal has moved and press "Read Value". You will end up with a table like the example.

V	mm
1.23	0
1.99	5
2.34	10
2.89	15
3.04	20

Note 1
Analog Voltage (Pins 1,2,3,4,5,19,20,21,22,23,24,25,26 45,46,47,48,49,50) or Analog Temp (Pins 34,35,36,37,38, 39,41,42) input may be used.

MoTeC	Title: Linear Position Sensor				Sheet No	Drawing No
	Date: 21/09/1999	Drawn: ST	App: AD	Products: ADL	1 of 1	X24

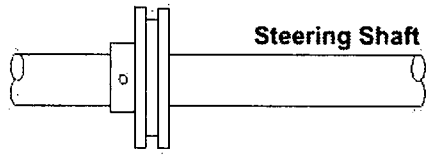

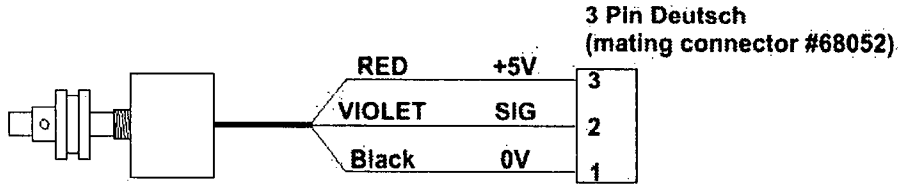

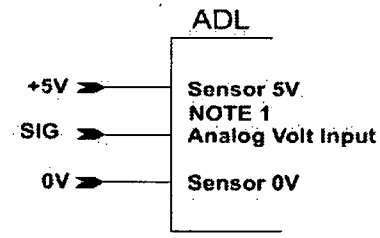

ADL Setup

Channel Assignments
Assign a Steering Channel to the appropriate pin

Sensor Calibration
Measurement method = Ratiometric
Turn wheel to desired angle & enter angle in deg table. Then click on read value to read sensor.,
Right turn = positive angles
Left turn = negative angles
Straight = 0 degree

NOTE 1

ADL PINS

+ 5V Analog Pins are 18, 28, 44
0V Analog Pins are 17, 27, 33, 40, 43
Analog Volt Input Pins are 1, 2, 3, 4, 5, 19, 20, 21, 22, 23, 24, 25, 26, 45, 46, 47 48, 49, 50

MoTeC	Title MoTeC STEERING ANGLE SENSOR				Sheet No	Drawing No
	Date 12/12/2000	Drawn ST	App	Products ADL	1 of 1	X21

H-11: Brake pressure transducer - specifications

ECLIPSE® • *OEM PRESSURE TRANSDUCER*

APPLICATIONS

- HYDRAULIC / PNEUMATIC CONTROLS
- AIR COMPRESSORS
- ENERGY MANAGEMENT: "SMART" COMPRESSORS, REFRIGERATION/ CHILLER CONTROL
- PROCESS CONTROL SYSTEMS
- ENGINE CONTROLS AND MONITORS

The Eclipse® is designed for high volume OEM's needing a low cost pressure transmitter for industrial or other heavy duty applications. The Eclipse's combination of rugged packaging, internal signal amplification and price make it ideal for many applications.

The pressure media is contained by a brazed assembly of stainless steel. There are no hidden O-rings or elastomers containing the media. A plated steel case protects the internal electronics.

It is available with either a 0.5 to 4.5 volt or 4 to 20 mA output. The 4 to 20 mA output is useful for applications where electrical noise may be a concern. Many units are CE compliant.

FEATURES	*BENEFITS*
• Voltage or current output	• Flexibility for the designer
• 15 PSIG through 7100 PSIS ranges	• Suitable for many applications
• High performance at low price	• Reduces OEM system cost
• CE versions available	• Ready for Europe
• Weatherproof type connector	• High reliability and user flexibility
• Reverse polarity protection	• Not damaged by reversed wiring
• Low excitation voltage	• Suitable for ORV or marine use
• IP65 sealed steel case	• Complete environmental protection for electronics

ECLIPSE® • *OEM PRESSURE TRANSDUCER*

TECHNICAL SPECIFICATIONS

RANGE

	0-15, 25, 50 PSIG 0-100, 250, 500, 1000, 2000, 3000, 5000, 7100 PSIS 0-1, 2, 4, 7 bar g (0-10, 15, 20, 35, 50, 100, 200, 350, 700 bar s)

PHYSICAL

Proof Pressure	1.5 x rated range
Burst Pressure	5 x rated range
Material In Contact With Media	300 series stainless steel, braze compound
Shock	50 g's peak (5 milliseconds)
Vibration	Meets MIL-STD-810-C, Figure 514.2-6, Curve AK, 20.7 g rms minimum

ELECTRICAL

	Voltage output	**Current output**
Full Scale Output	4.00 Vdc nominal (0.5 - 4.5 Vdc)	16 mA into 0 to 1400 Ω loop resistance (4-20 mA)
Zero Output	0.5 V nominal	4 mA nominal
Excitation	5.0 Vdc ± 0.25 Vdc @ 20mA	10 to 40 Vdc (linear derating to 35 Vdc from 25°C to 100 C°)
Reverse Polartiy Protection	Yes	
Insulation Resistance	1000 MΩ @ 50 Vdc	
Electrical Connection	Standard Packard Metri-Pack™ Requires Packard #12065287 mating connector, not included. Optional Hirschmann connector, mate included.	

PERFORMANCE

Accuracy	±1% of FSO from best fit straight line including effects of nonlinearity, hysteresis and nonrepeatability
Operating Temperature Range	-40° to 105°C (-40° to 221°F)
Compensated Temperature Range	-1° to 82°C (30° to 180°F)
Total Error	±4% of full scale. Includes the effects of zero output error, calibration error, temperature, nonlinearity, hysteresis, and repeatability.

DIMENSIONS

xx.xx = inches
(xx.x) = mm

Eclipse with Packard

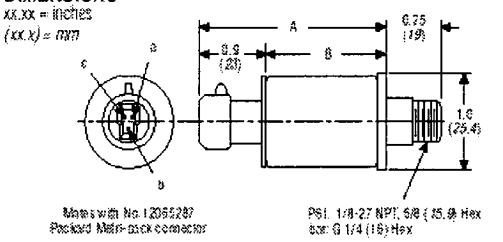

Eclipse with Hirschmann

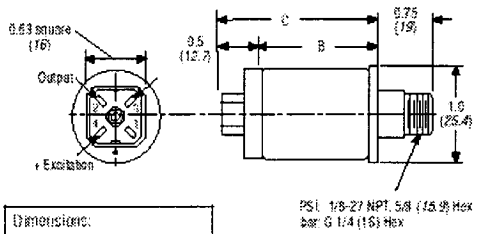

Dimensions:		
	Voltage	**Current**
A	2.4 (61)	2.6 (66)
B	1.5 (38)	1.7 (43)
C	2.0 (51)	2.2 (56)

Load resistance in current loop

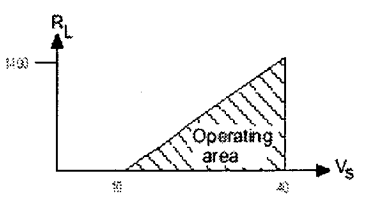

Ratiometric Output

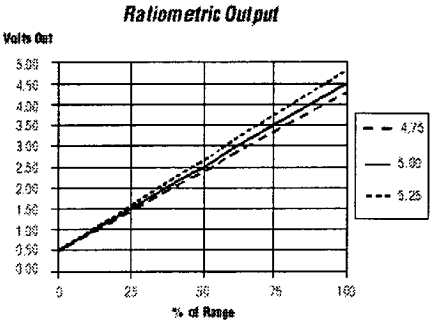

PACKARD CONNECTOR PINS

	Voltage	**Current**
a	+ Excitation	+ Excitation
b	Output	- Excitation (Return)
c	Common	NC

HIRSCHMANN CONNECTOR PINS

	Voltage	**Current**
Pin 1	NC	NC
Pin 2	Signal Output	NC
Pin 3	Common	- Excitation (Return)
Pin 4	+ Excitation	+ Excitation

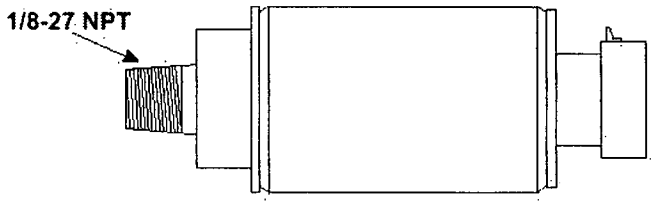

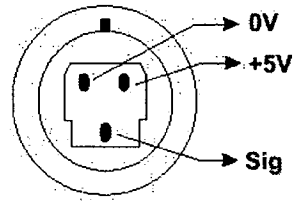

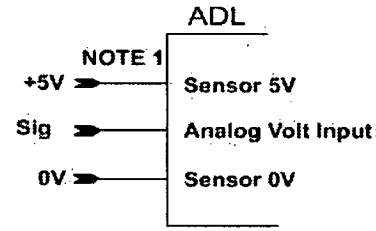

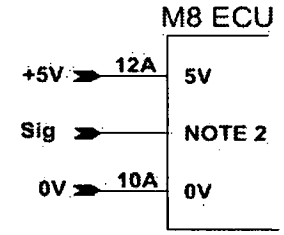

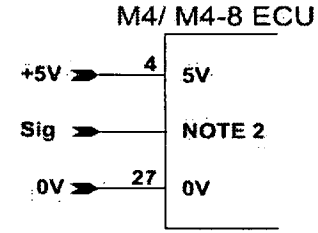

ADL Setup

Channel Assignments
Assign the pressure Channel to the appropriate pin

Sensor Calibration
Press "Select" and choose correct calibration file for the sensor
For example, Data Inst Eclipse 100 psi MAP.C1P

NOTE 1:
+ 5V Analog Pins are 18, 28, 44
0V Analog Pins are 17, 27, 33, 40, 43
Analog Volt Input Pins are 1, 2, 3, 4, 5, 19, 20, 21, 22, 23, 24, 25, 26, 45, 46, 47 48, 49, 50

ECU Setup M8	
Sensor Calibration	**100 PSI sensor**
Display in KPA	17
Display in PSI	23
Display in InHg	29

NOTE 2:
M8 input pins are 28A,27A,13B,7B,8B,9B 14B, 15B & 16B
M4 and M4-8 input pins are 17,18 & 30

ECU Setup M4 M4-8	
Sensor Calibration	**100 PSI sensor**
MAP PIN	-1*
AUX TEMP PIN	-4*
AUX VOLT PIN	-3*

*** = DISPLAY IN KPA**

100 PSI Sensor CalibrationTables for M4-M4-8

Map Pin	0	10	20	30	40	50	60	70	80	90	100	110	120	130	140	150	160	170	180	190	200	210	220	230	240	250
	102	114	125	137	149	161	172	184	196	208	219	231	243	254	266	278	290	301	313	325	337	348	360	372	384	395
	260	270	280	290	300	310	320	330	340	350	360	370	380	390	400	410	420	430	440	450	460	470	480	490	500	
	407	419	430	442	454	466	477	489	501	513	524	536	548	559	571	583	598	606	618	630	642	653	665	677	689	

Aux Temp & Aux VoltPin	0	40	80	120	160	200	240	280	320	360	400	440	480	520	560	600	640	680	720	760	800	840	880	920	960	1000
	102	149	196	243	290	336	383	430	477	524	571	618	665	711	758	805	852	899	940	981	1018	1054	1091	1127	1164	1200

MoTeC	Title DATA INSTRUMENTS (ECLIPSE)				Sheet No	Drawing No
	Date 28/07/1999	Drawn ST	App AD	Products ADL, ECU	1 of 1	X22

H-13: Attitude & heading reference sensor – specifications and installation

New

AHRS

ATTITUDE & HEADING REFERENCE SYSTEM

- Roll, Pitch and Heading Angle in Dynamic Environments
- Enhanced Performance Kalman Filter Algorithm
- High Stability MEMS Sensors
- High Range Gyro and Accel Options

Applications

- UAVRPV Control
- Platform Stabilization
- Avionics

AHRS400CA (DMU-HDX-AHRS)

The Crossbow AHRS400CA is a high performance, solid-state attitude and heading reference system intended for airborne applications such as UAV control, Avionics, and Platform Stabilization. This high reliability, strap-down inertial subsystem provides attitude and heading measurement with static and dynamic accuracy comparable to traditional spinning mass vertical and directional gyros.

This AHRS400 series product builds on the performance of the AHRS300 series. It features higher performance sensors, including silicon MEMS accelerometers and gyroscopes with lower noise and improved bias stability.

The AHRS400CA achieves its excellent performance by employing proprietary Kalman Filter algorithms to determine stabilized roll, pitch, and heading angles in static and dynamics conditions. The Kalman Filter implementation results in a continuous on-line gyro bias calibration, and an adaptive attitude and heading measurement that is stabilized by the long term gravity and magnetic north references. Output data is provided in both analog and digital (RS-232) formats.

Each Inertial System comes with a User's Manual offering helpful hints on programming, installation, and product information. In addition, Crossbow's GYRO-VIEW software is included to assist you in system development and evaluation, and allows you to perform data acquisition.

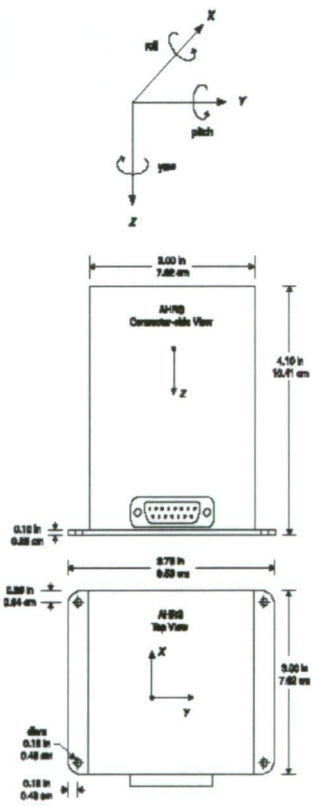

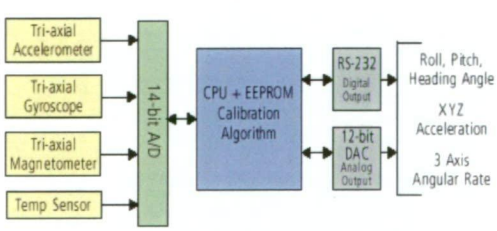

AHRS Block Diagram

inertial systems

Crossbow

Specifications		AHRS400CA-100	AHRS400CA-200	Remarks
Performance				
Update Rate (Hz)		> 60	> 60	Continuous update mode
Start-up Time Valid Data (sec)		< 1	< 1	
Fully Stabilized Data (sec)		< 60	< 60	
Heading				
Range (°)		± 180	± 180	
Static Accuracy (°)		<± 1.5	<±2	
Dynamic Accuracy (° rms)		± 3	± 4	
Resolution (° rms)		< 0.1	< 0.1	
Attitude				
Range: Roll, Pitch (°)		± 180, ± 90	± 180, ± 90	
Static Accuracy (°)		<± 0.5	<±1	Measured on level surface
Dynamic Accuracy (° rms)		± 2.0	± 2.5	
Resolution (°)		< 0.1	< 0.1	
Angular Rate[1]				
Range: Roll, Pitch, Yaw (°/sec)		± 100	± 200	
Bias: Roll, Pitch, Yaw (°/sec)		<± 1.0	<± 1.0	Scaled sensor mode
Bias: Roll, Pitch, Yaw (°/sec)		<± 0.05	<± 0.05	Angle mode
Scale Factor Accuracy (%)		< 1	< 1	
Non-Linearity (% FS)		< 0.3	< 0.3	
Resolution (°/sec)		< 0.025	< 0.05	
Bandwidth (Hz)		> 10	> 10	-3 dB point
Random Walk (°/hr$^{1/2}$)		< 0.85	< 1.7	
Acceleration				
Input Range: X/Y/Z (g)		± 2	± 10	
Bias: X/Y/Z (mg)		<± 8.5	<± 12	
Scale Factor Accuracy (%)		< 1	< 1	
Non-Linearity (% FS)		< 1	< 1	
Resolution (mg)		< 0.25	< 1.25	
Bandwidth (Hz)		> 10	> 10	-3 dB point
Random Walk (m/s/hr$^{1/2}$)		< 0.1	< 0.5	
Environment				
Operating Temperature (°C)		-40 to +71	-40 to +71	
Non-Operating Temperature (°C)		-55 to +85	-55 to +85	
Non-Operating Vibration (g rms)		6	6	20 Hz - 2 KHz random
Non-Operating Shock (g)		1000	1000	1 ms half sine wave
Electrical				
Input Voltage (VDC)		9 to 30	9 to 30	
Input Current (mA)		< 300	< 300	
Power Consumption (W)		< 4	< 4	at 12 VDC
Digital Output Format		RS-232	RS-232	"See Digital Data Format"
Analog[2] Range (VDC)		± 4.096	± 4.096	Pins 8, 9, 10, 12, 13, 14
		0 to 5.0	0 to 5.0	Pins 5, 6, 7
Physical				
Size	(in)	3.0 x 3.75 x 4.10	3.0 x 3.75 x 4.10	Includ. mounting flanges
	(cm)	7.62 x 9.53 x 10.41	7.62 x 9.53 x 10.41	Includ. mounting flanges
Weight	(lbs)	< 1.4	< 1.4	
	(kg)	< 0.64	< 0.64	
Connector		15 pin sub-miniature "D" female		

Notes
[1]All analog outputs are fully buffered and are designed to interface directly to data acquisition equipment
Specifications subject to change without notice

15 Pin "D" Connector Socket Pinout

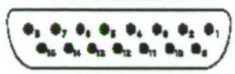

Pin	Signal
1	RS-232 Transmit Data
2	RS-232 Receive Data
3	Input Power
4	Ground
5	X-axis accel voltage[1]
6	Y-axis accel voltage[1]
7	Z-axis accel voltage[1]
8	Roll-axis angular rate[2]
9	Pitch-axis angular rate[2]
10	Yaw-axis angular rate[2]
11	NC - Factory use only
12	Roll angle/X-axis mag voltage[3]
13	Pitch angle/Y-axis mag voltage[3]
14	Not used/Z-axis mag voltage[3]
15	NC - Factory use only

Notes
1 The accelerometer voltage outputs are taken directly from the accelerometers without compensation or scaling.
2 The angular rate analog outputs are scaled to represent degrees/second. Outputs are created by a D/A converter.
3 Actual output depends on AHRS measurement mode. Axis magnetometer scaled analog voltage vs. angle.

Pin Diagram

inertial systems

Ordering Information

Model	Previous Model	Description	Gyro (°/sec)	Accel (g)
AHRS400CA-100	DMU-HDX-AHRS	Attitude & Heading Reference System	± 100	± 2
AHRS400CA-200	DMU-HDX-AHRS	Attitude & Heading Reference System	± 200	± 10

CALL FACTORY FOR OTHER CONFIGURATIONS

phone: 408.965.3300 ▼ fax: 408.324.4840 ▼ e-mail: info@xbow.com ▼ web: www.xbow.com

Appendix I - Testing Data -

I-1: Testing data, logged at the University carpark straight line course

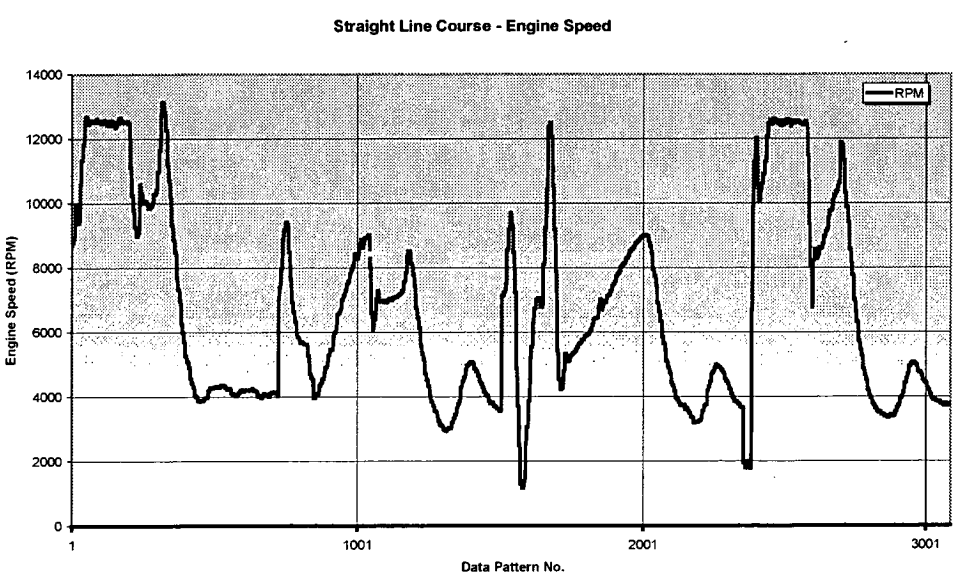

Straight Line Course - Gear

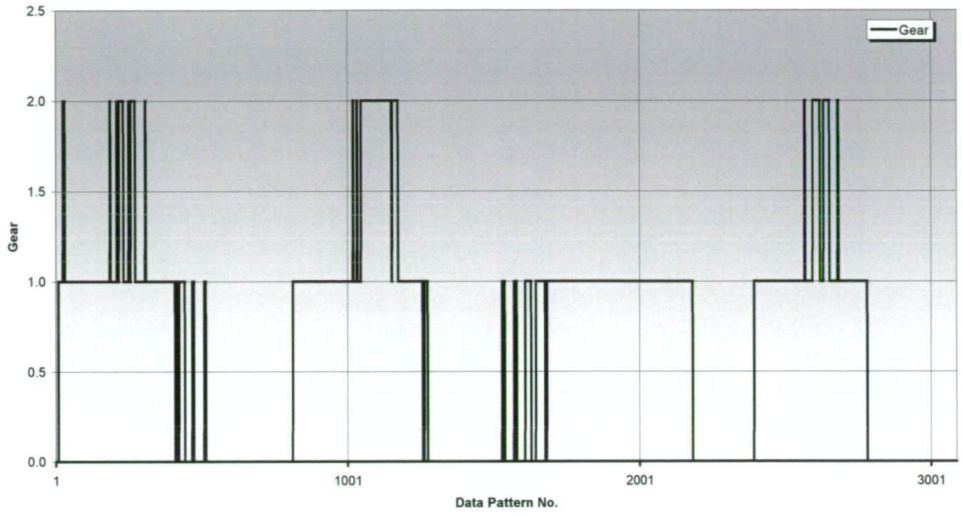

Straight Line Course - Steering Wheel Angle and Throttle Position

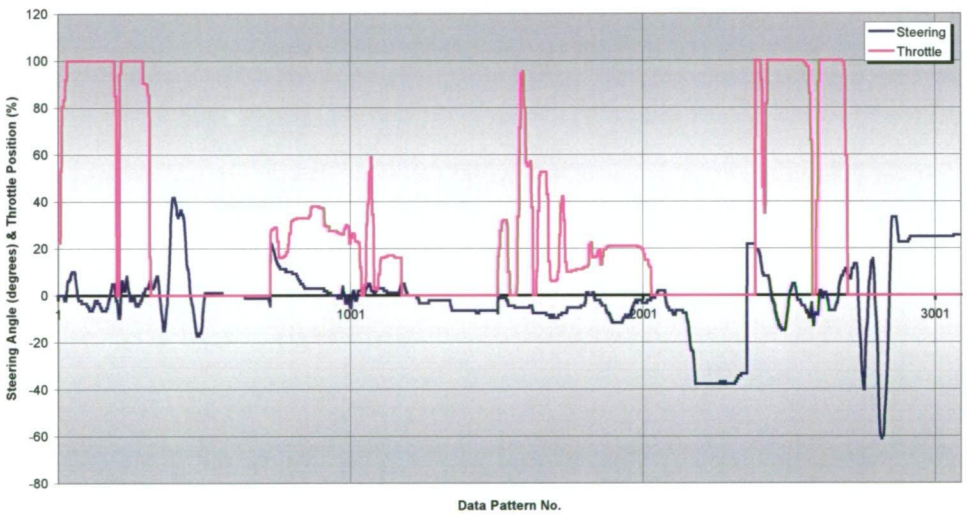

Straight Line Course - Hydraulic Brake Pressure

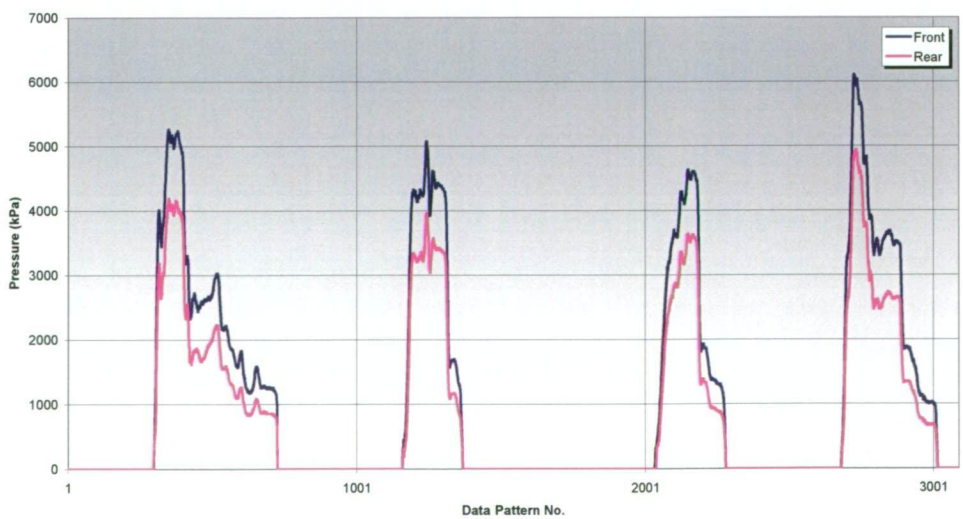

Straight Line Course - Acceleration

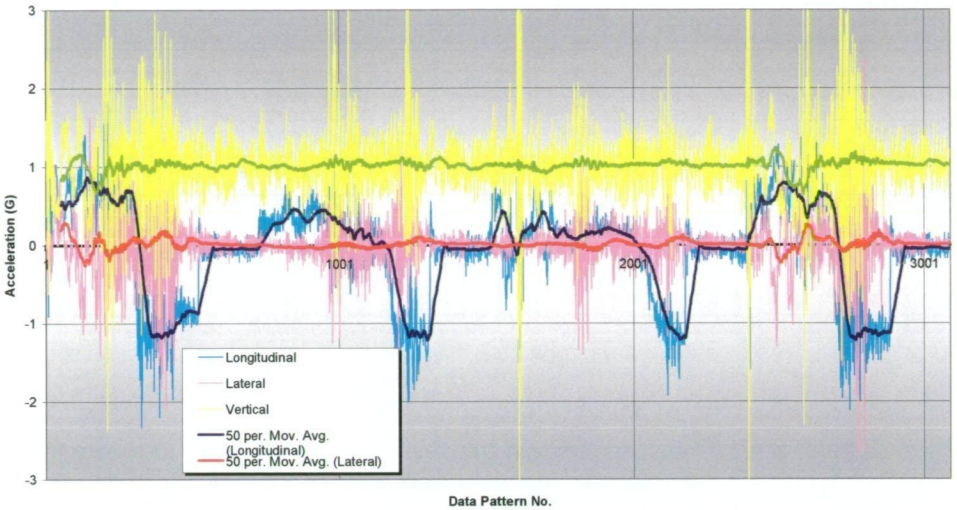

Straight Line Course - Heading Angle

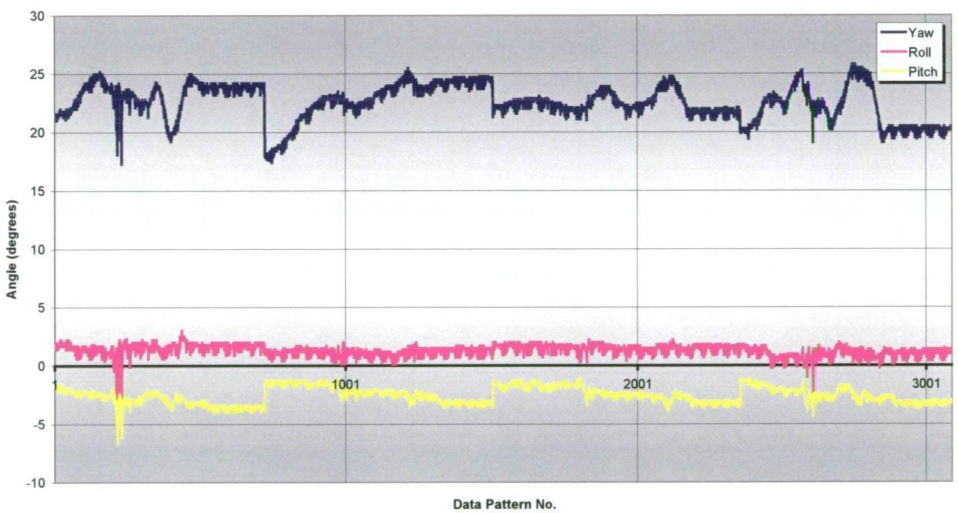

Straight Line Course - Heading Anglular Velocity

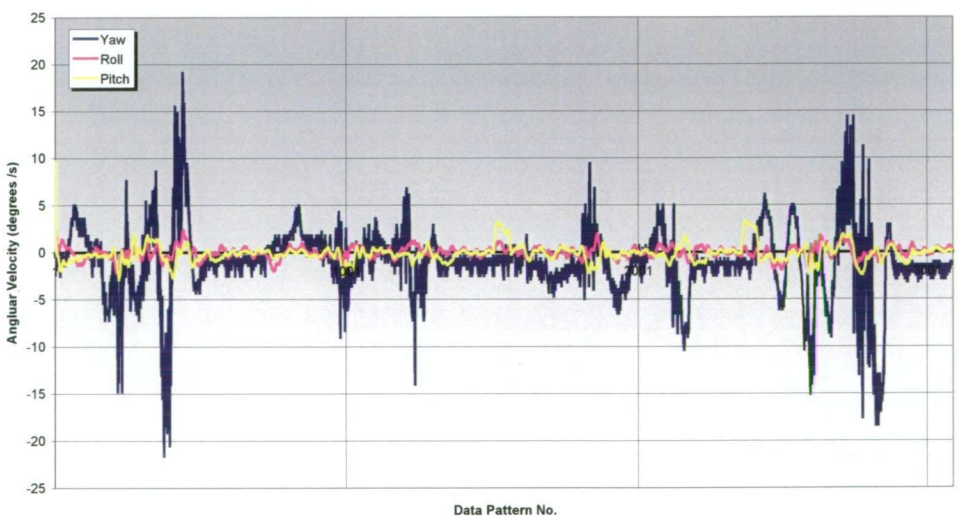

Straight Line Course - Wheel Speeds

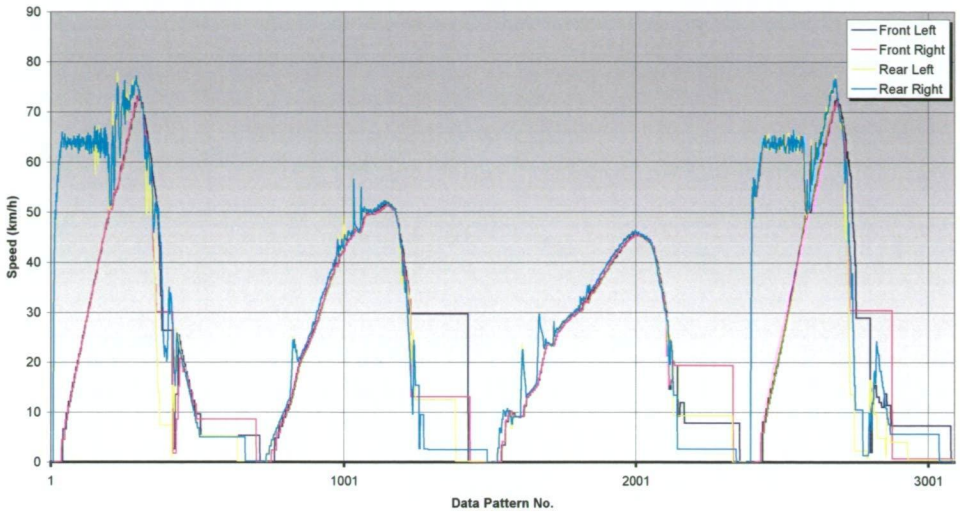

Straight Line Course - Wheel Acceleration

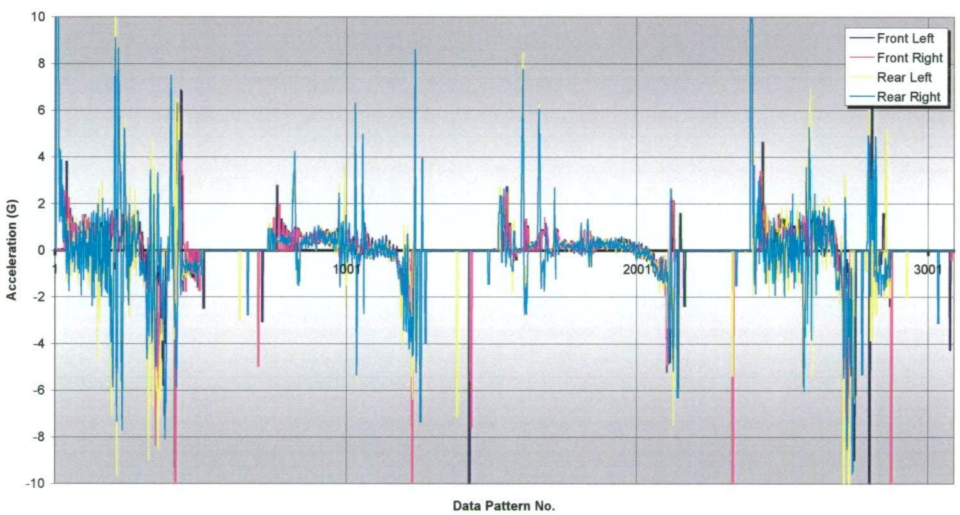

Straight Line Course - Ground and Drive Speed

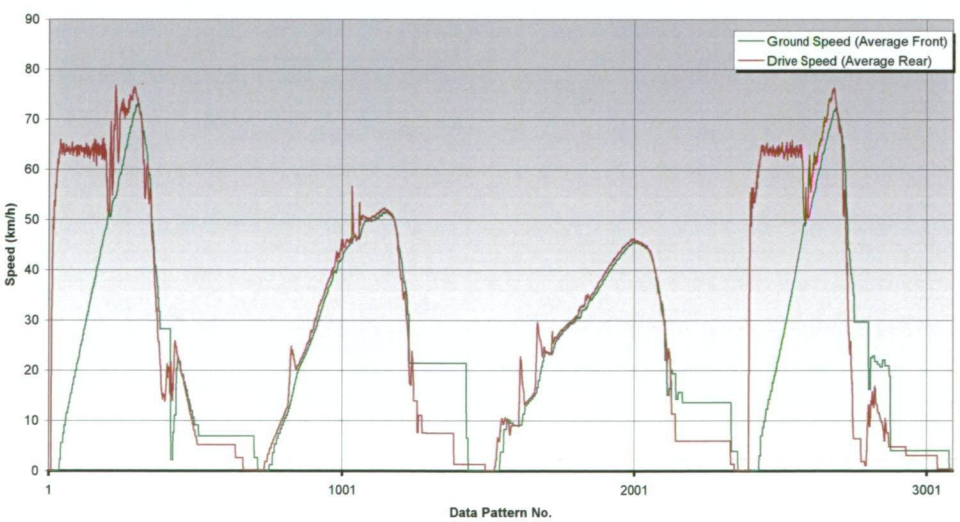

Straight Line Course - Rear Wheel Slip (under Acceleration)

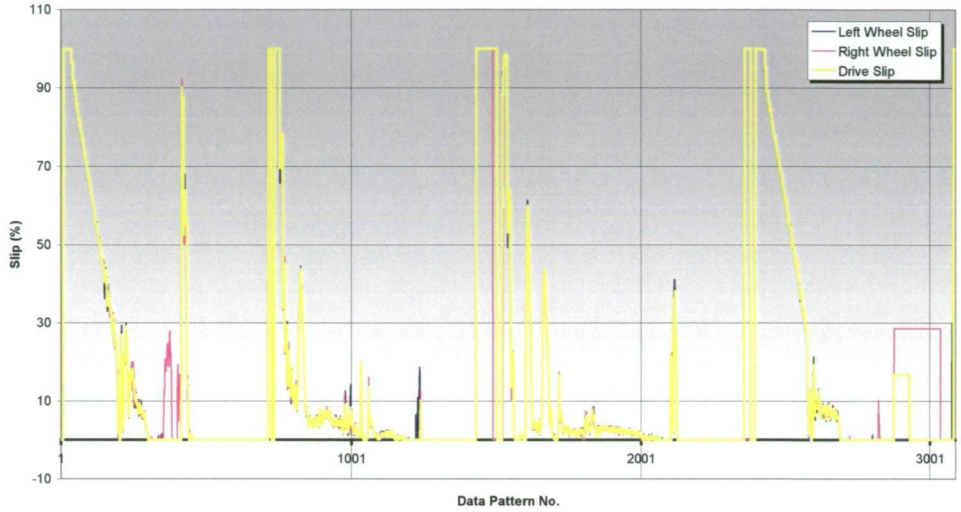

Straight Line Course - Suspension Positions

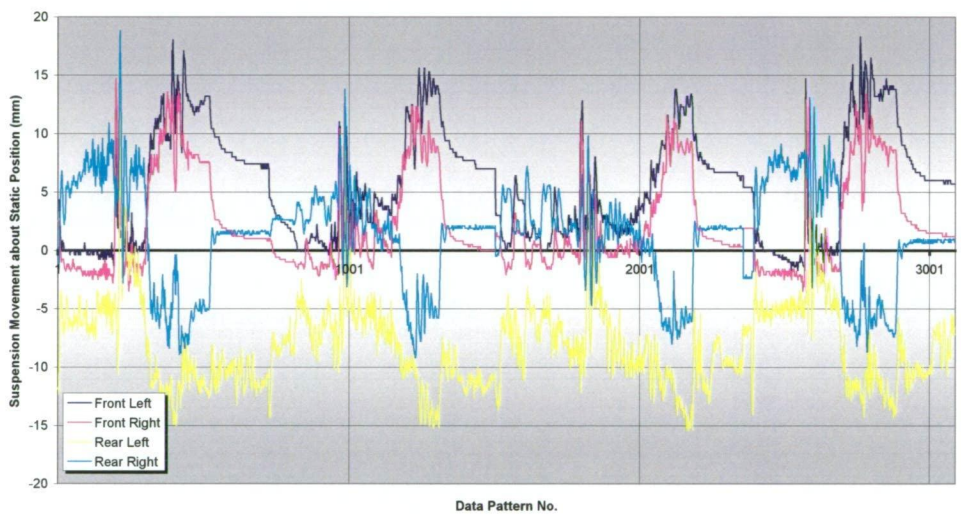

Straight Line Course - Suspension Velocities

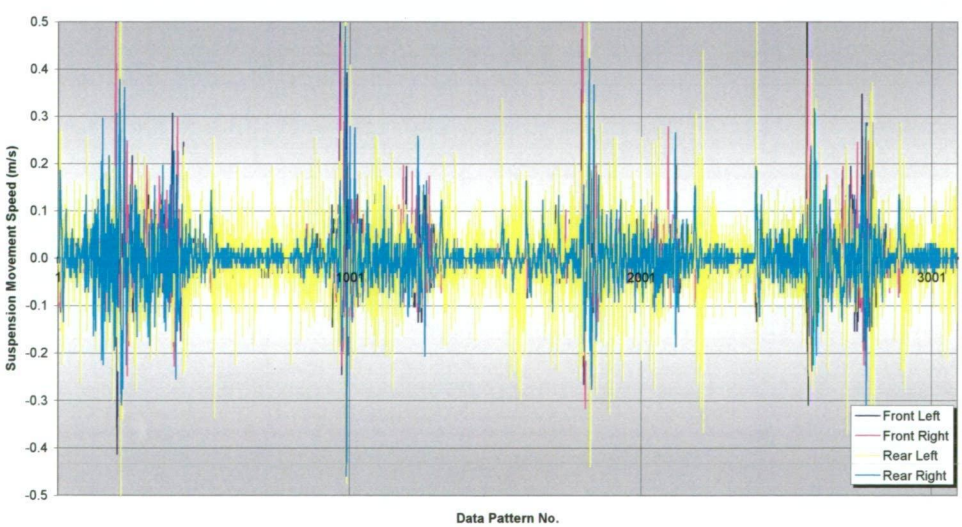

I-2: Testing data, logged at the University carpark figure 8 course

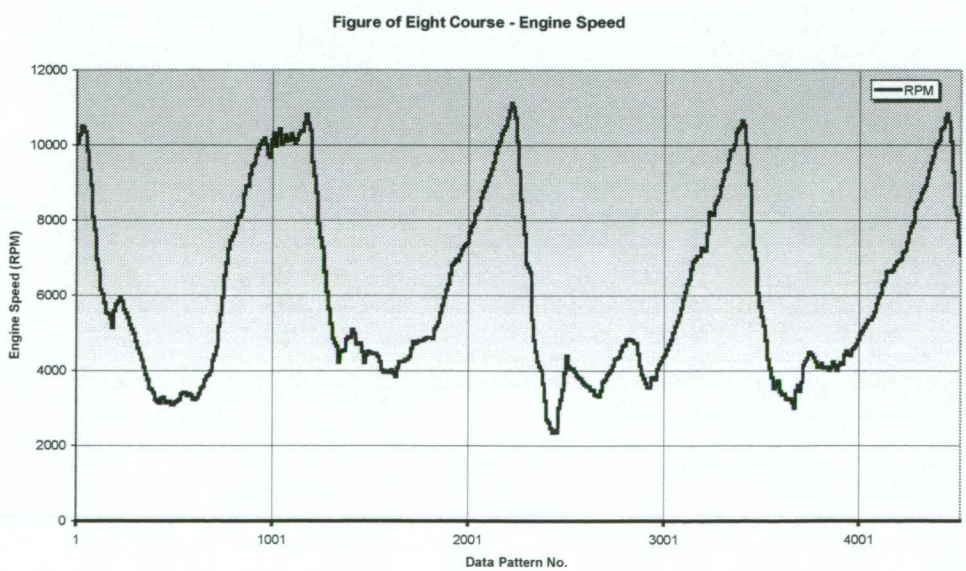

Figure of Eight Course - Gear

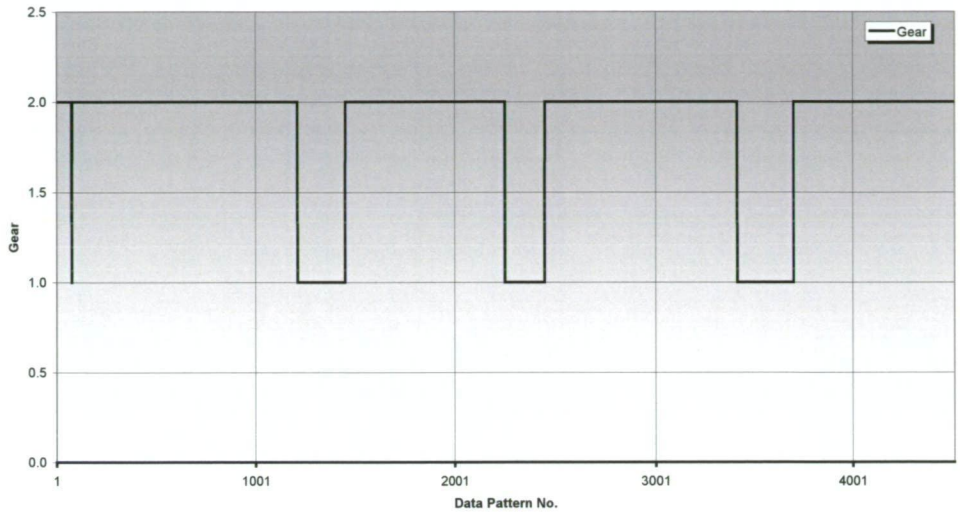

Figure of Eight Course - Steering Wheel Angle and Throttle Position

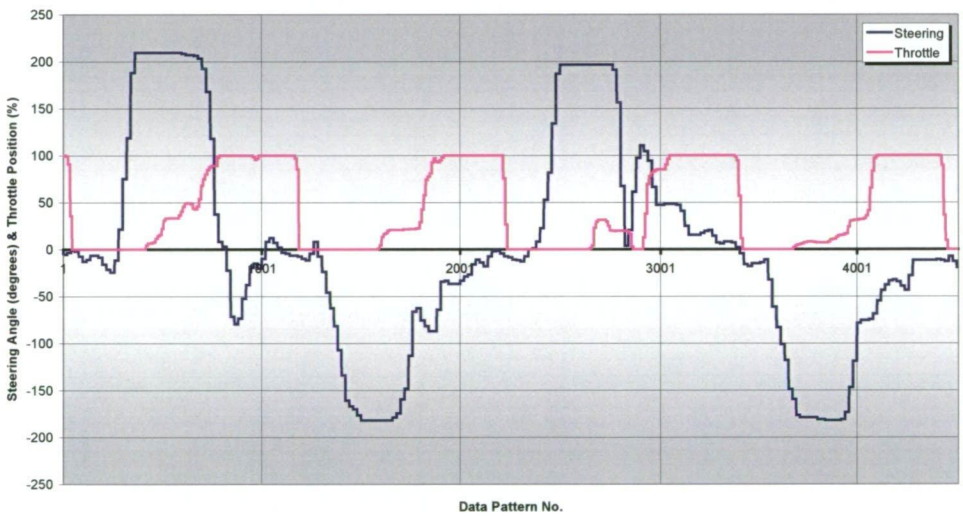

Figure of Eight Course - Hydraulic Brake Pressure

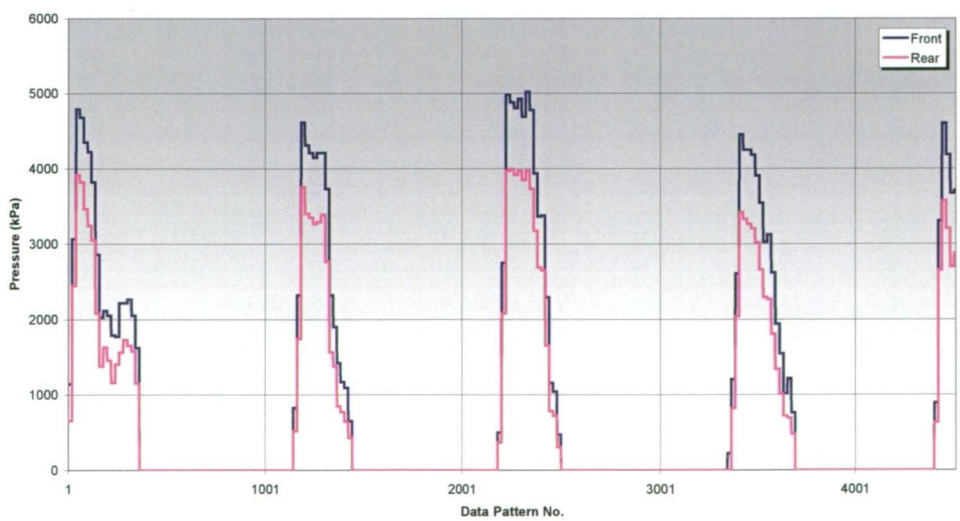

Figure of Eight Course - Acceleration

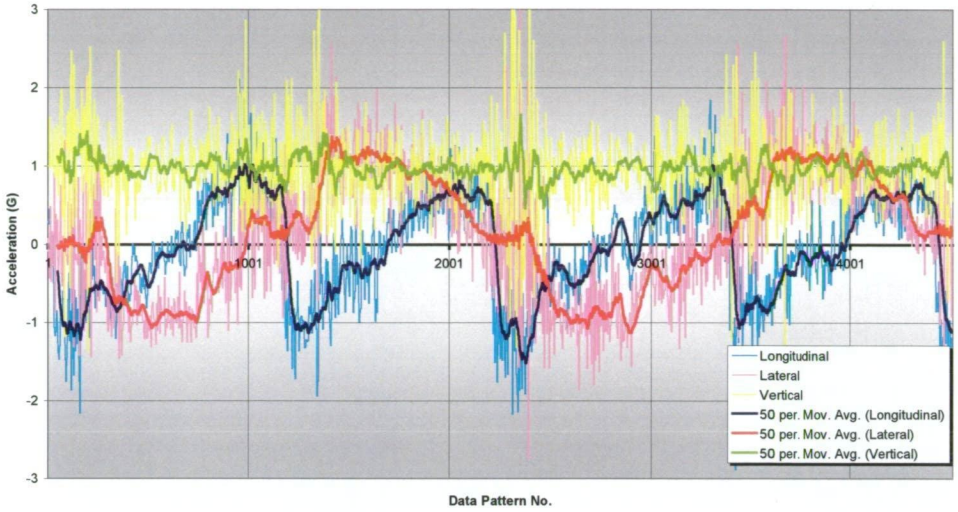

Figure of Eight Course - Heading Angle

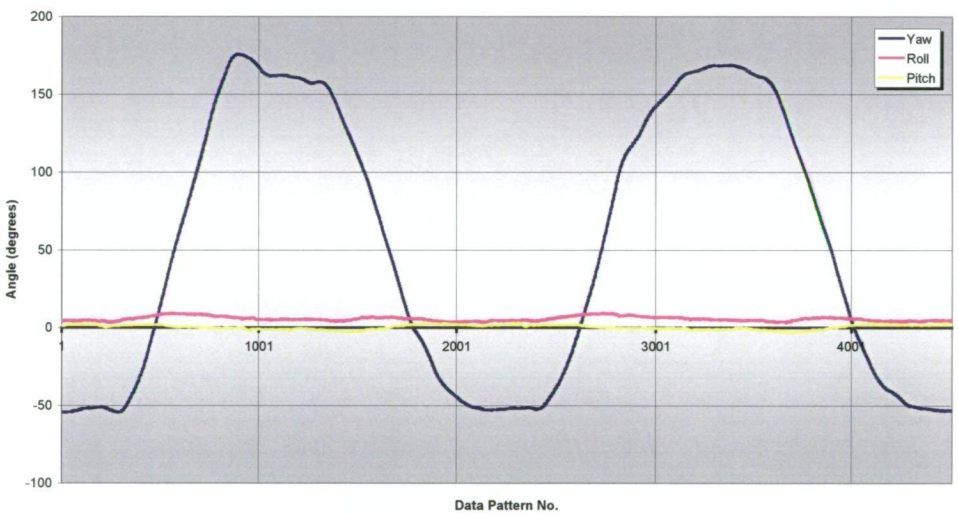

Figure of Eight Course - Heading Anglular Velocity

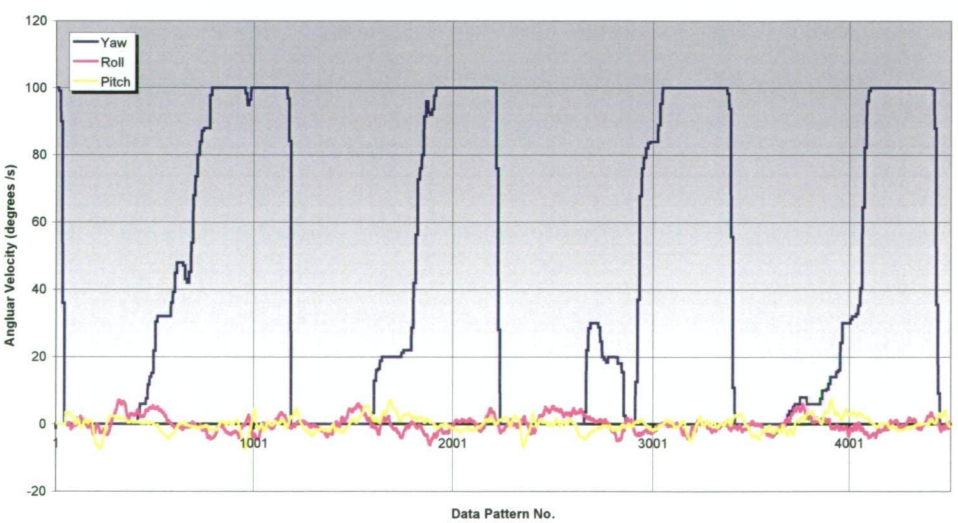

Figure of Eight Course - Wheel Speeds

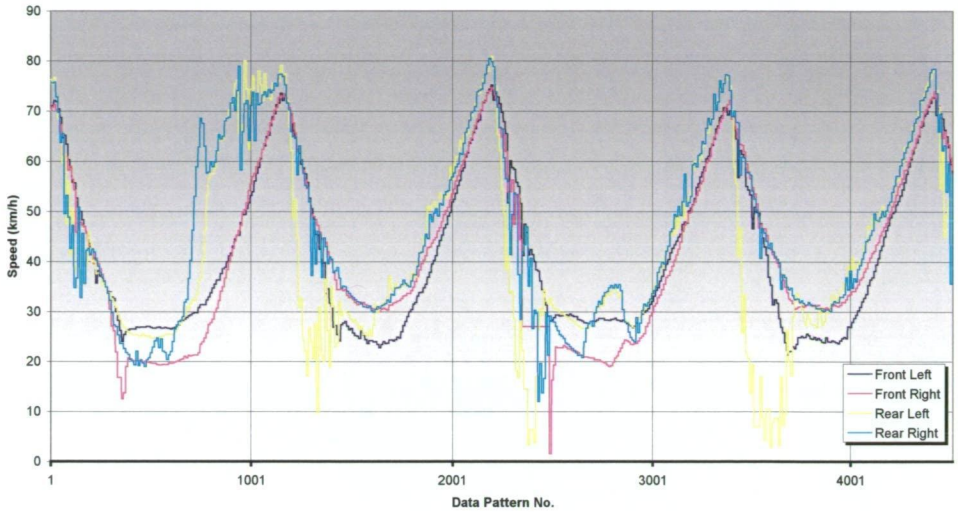

Figure of Eight Course - Wheel Acceleration

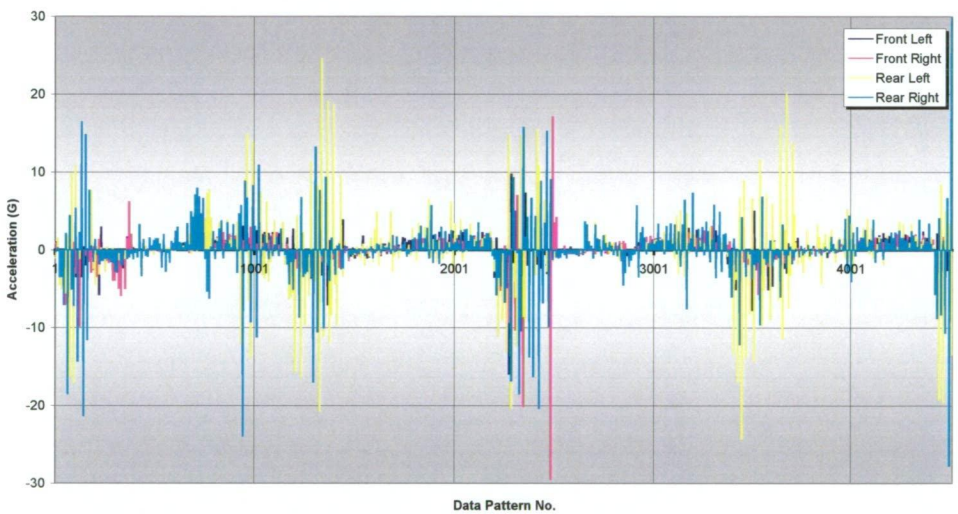

Figure of Eight Course - Ground and Drive Speed

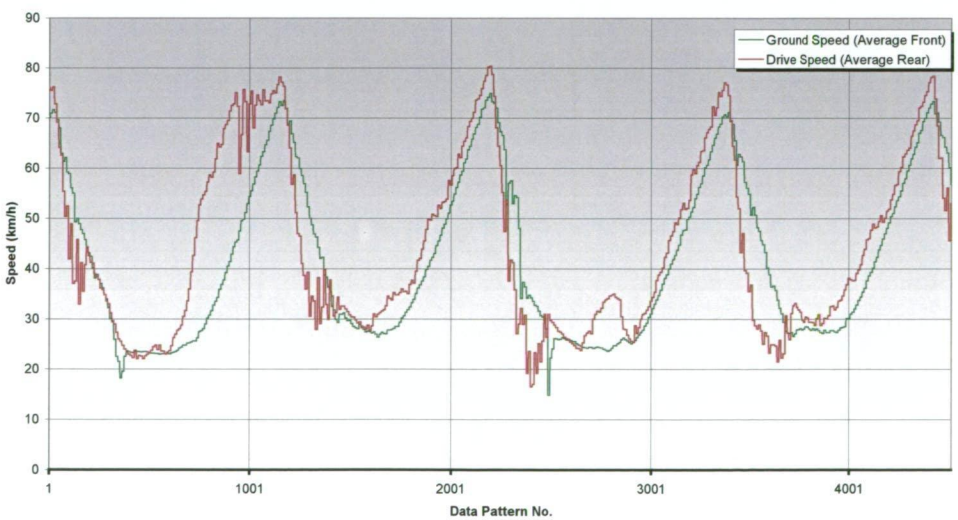

Figure of Eight Course - Rear Wheel Slip (under Acceleration)

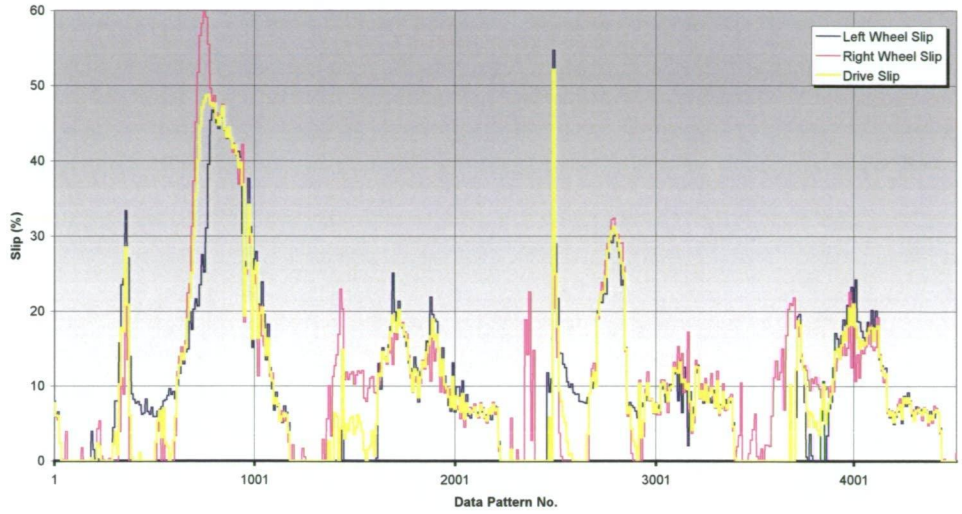

Figure of Eight Course - Suspension Positions

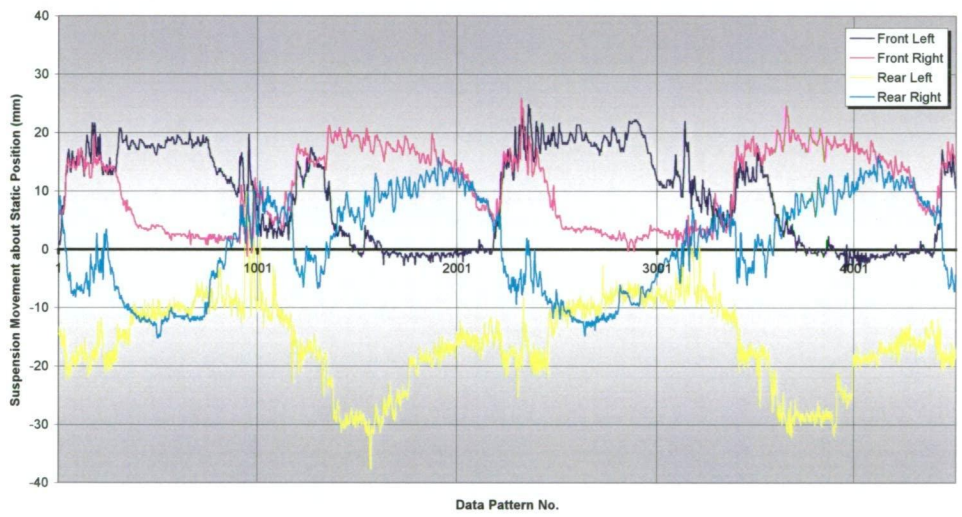

Figure of Eight Course - Suspension Velocities

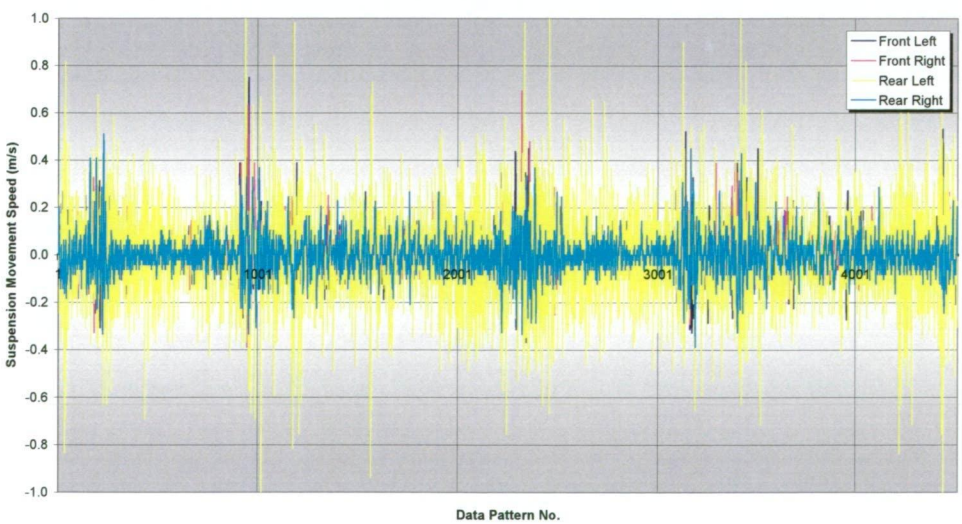

Appendix J - Neural Network Results -

J.1: Longitudinal acceleration GRNN prediction during network training – course 1

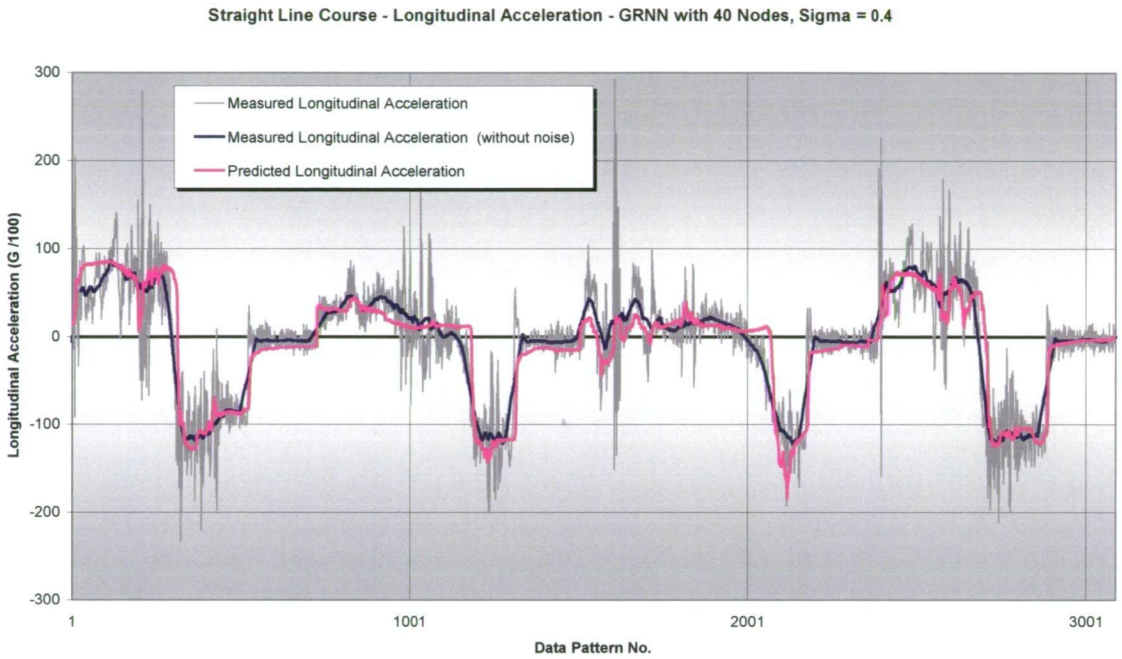

J.2: Longitudinal acceleration GRNN prediction during network testing – course 1

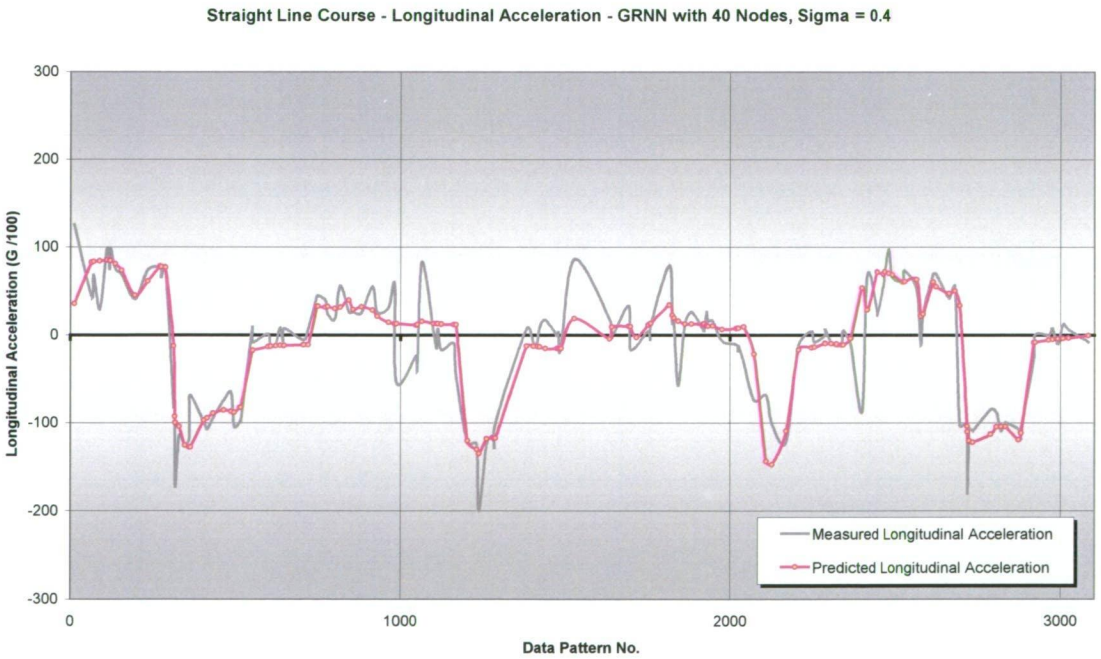

J.3: Longitudinal acceleration GRNN prediction error – course 1

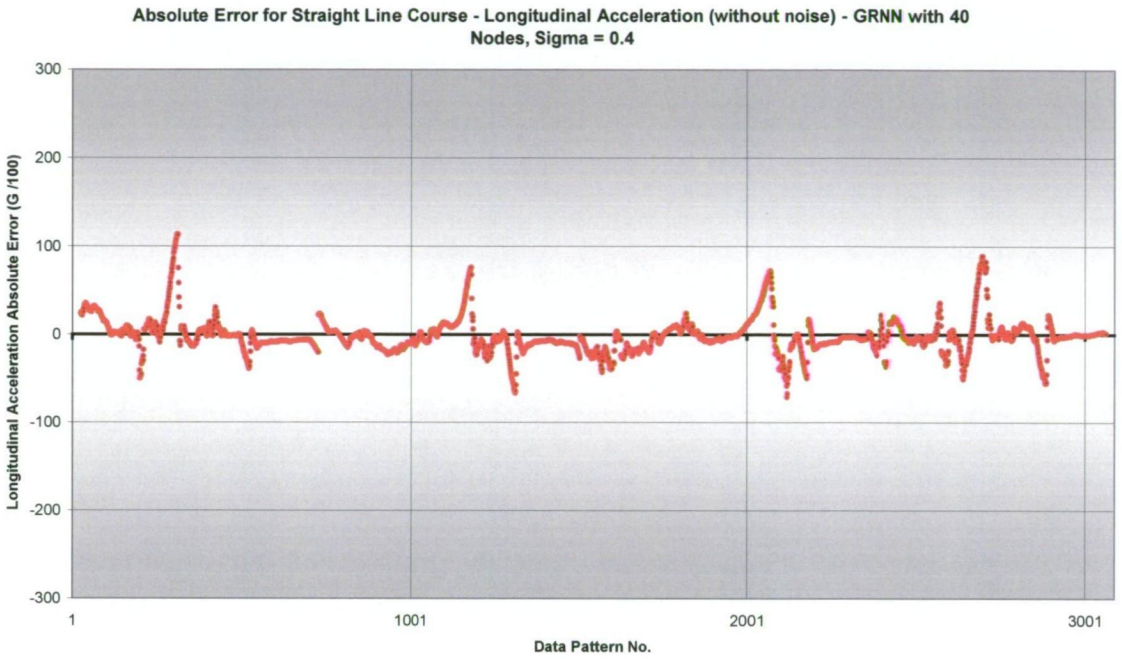

J.4: Lateral acceleration GRNN prediction during network training – course 1

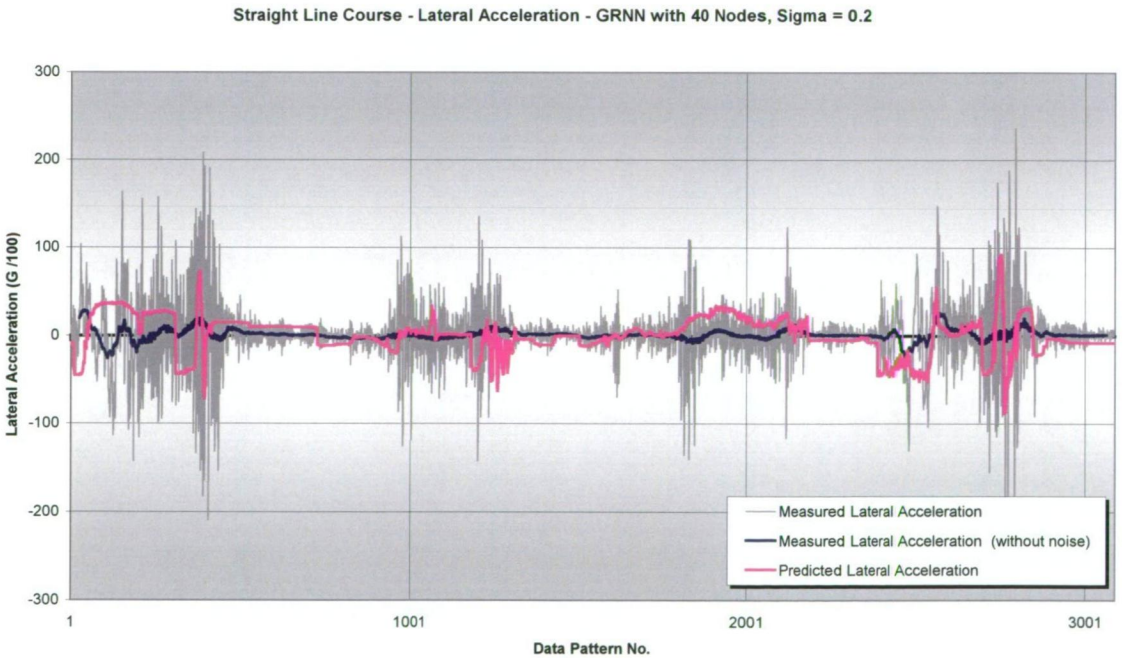

J.5: Lateral acceleration GRNN prediction during network testing – course 1

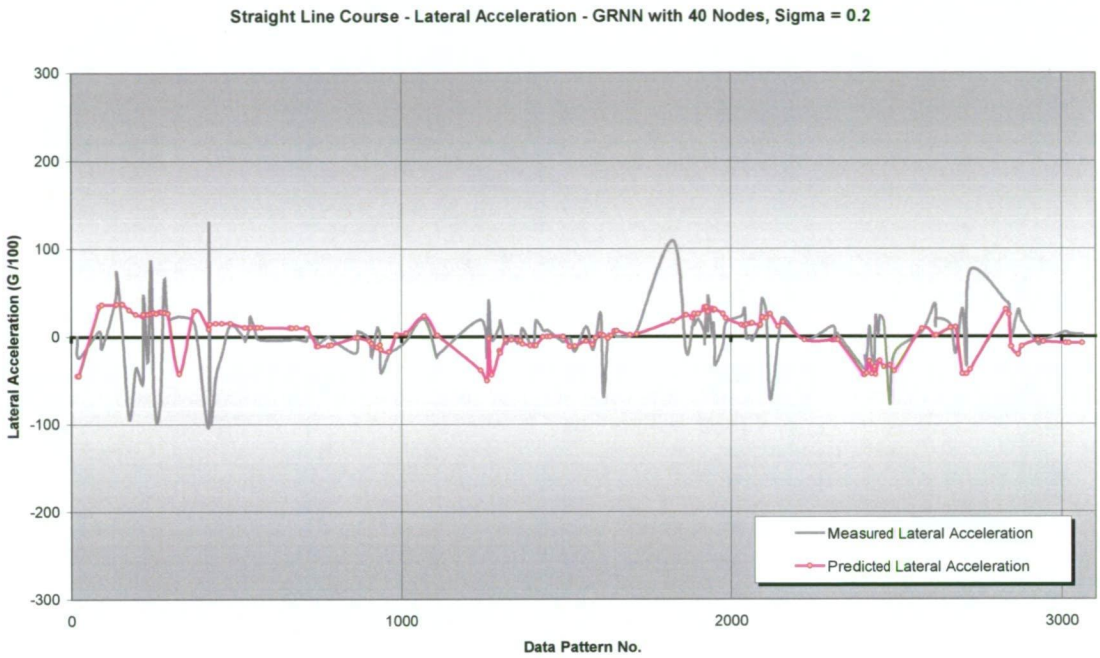

J.6: Lateral acceleration GRNN prediction error – course 1

J. 7: Yaw angle GRNN prediction during network training – course 1

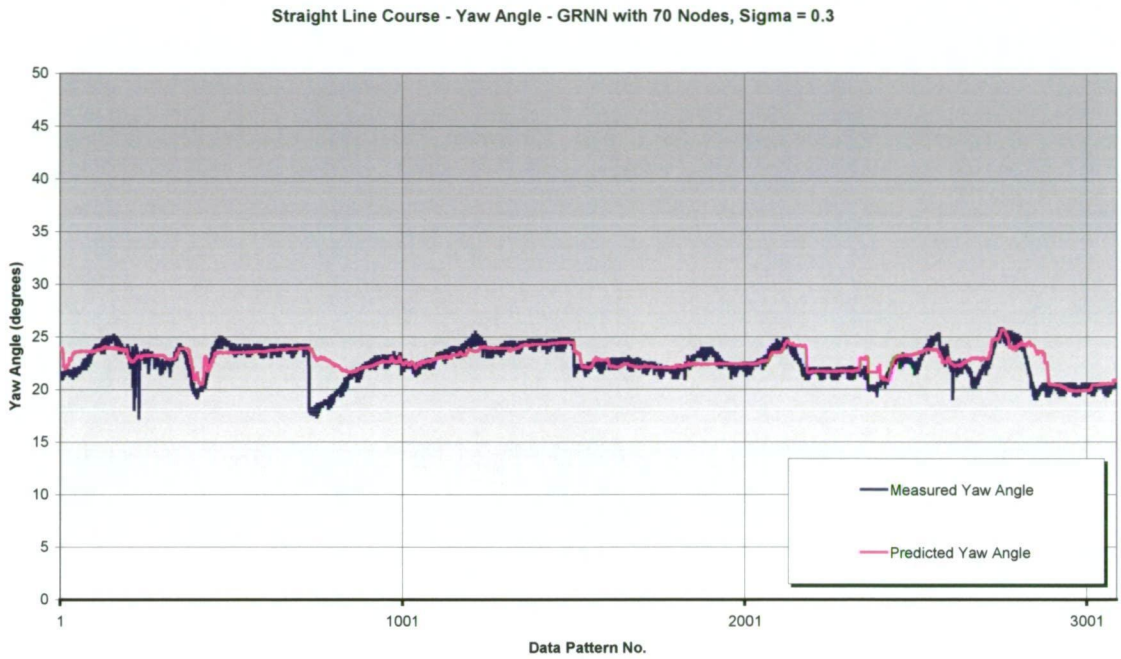

J. 8: Yaw angle GRNN prediction during network testing – course 1

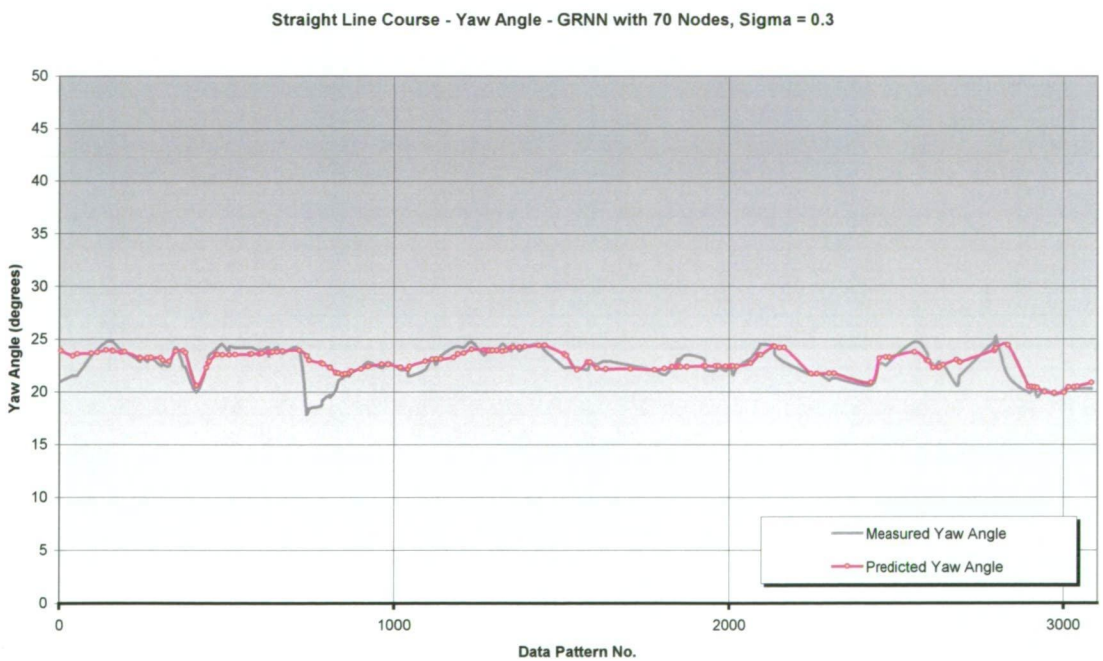

J.9: Yaw angle GRNN prediction error – course 1

J.10: Longitudinal acceleration GRNN prediction during network training – course 2

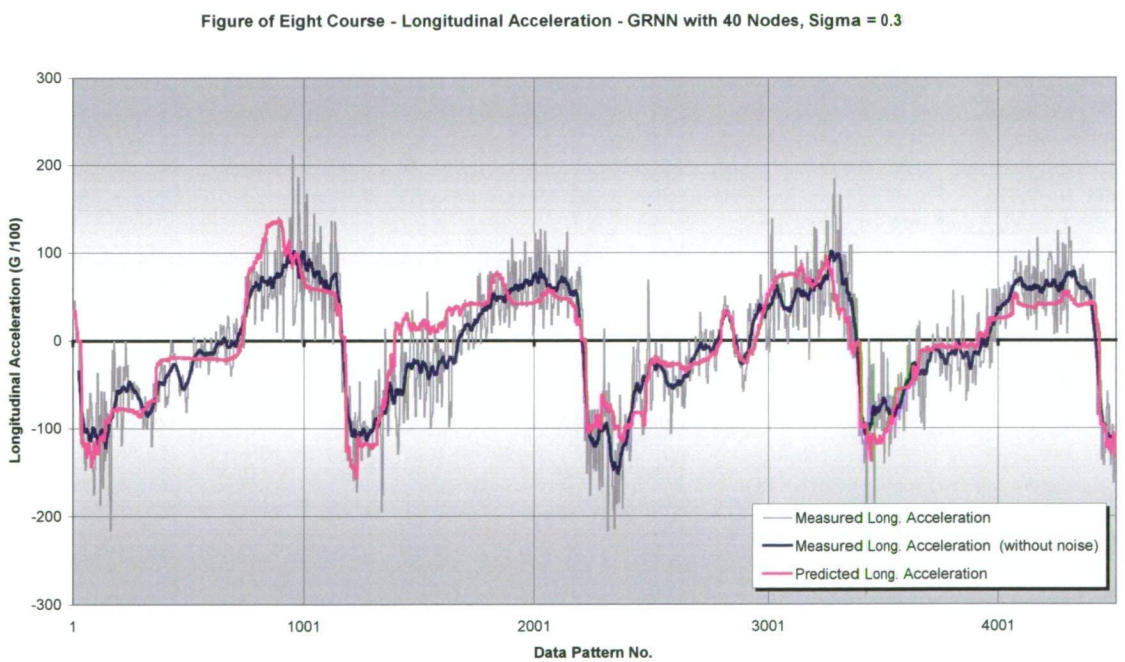

J.11: Longitudinal acceleration GRNN prediction during network testing – course 2

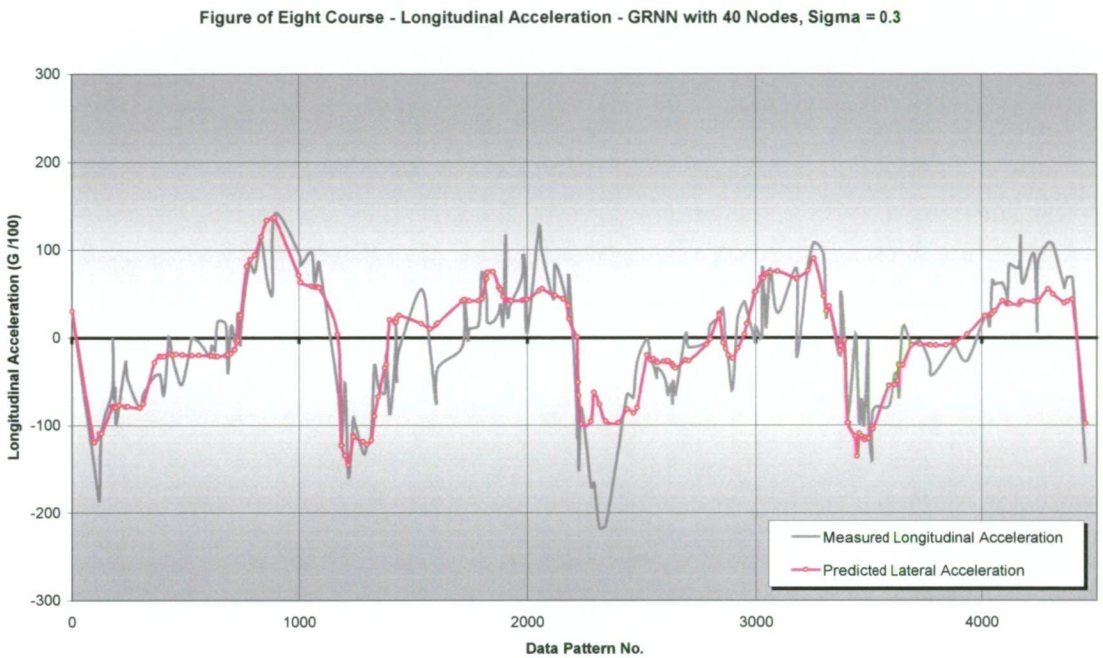

J.12: Longitudinal acceleration GRNN prediction error – course 2

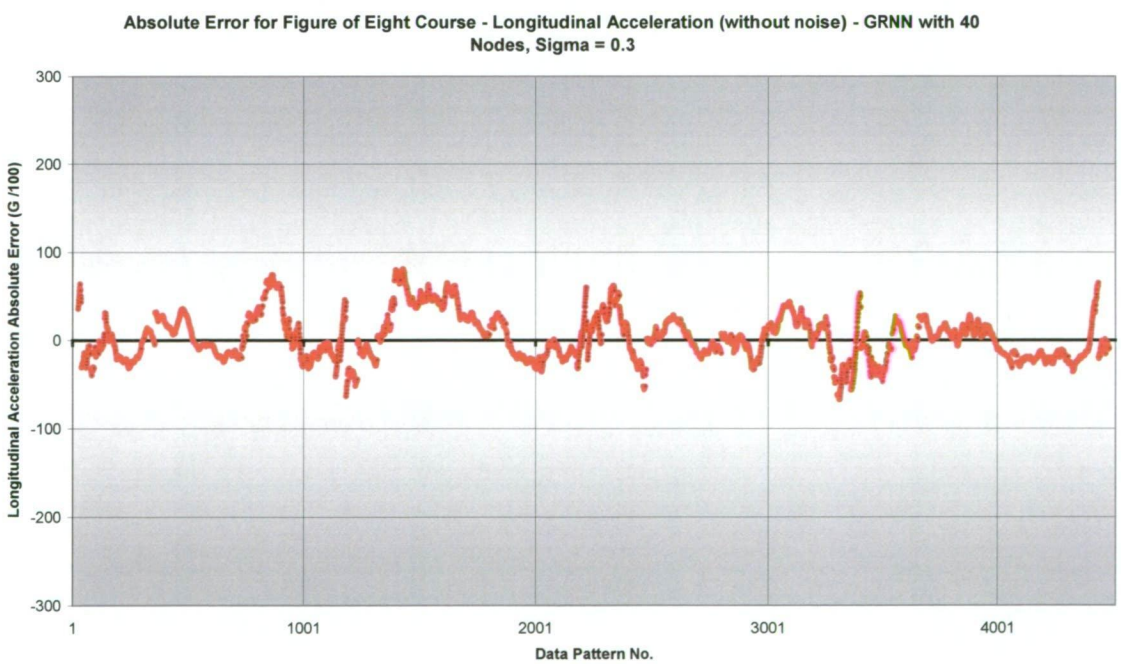

J.13: Lateral acceleration GRNN prediction during network training – course 2

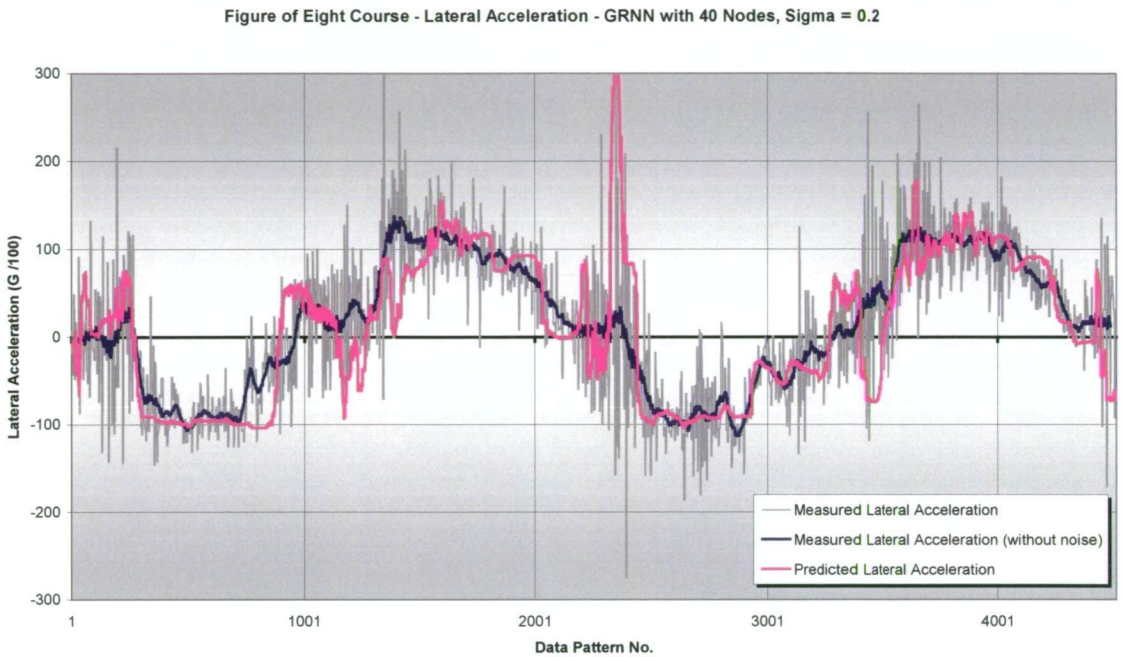

J.14: Lateral acceleration GRNN prediction during network testing – course 2

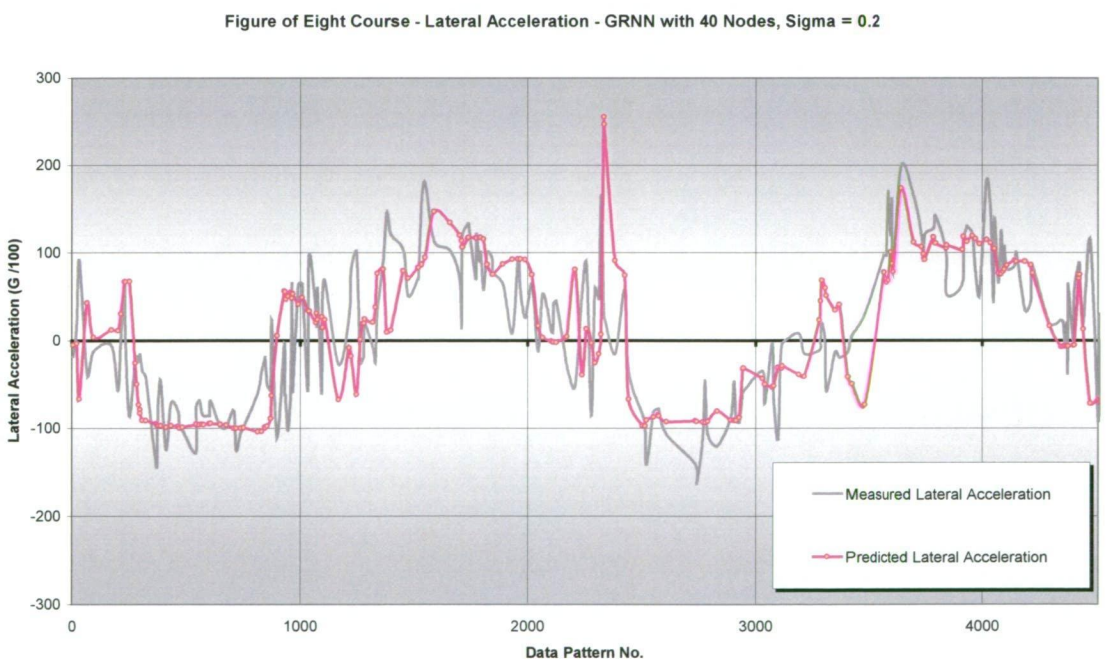

J.15: Lateral acceleration GRNN prediction error – course 2

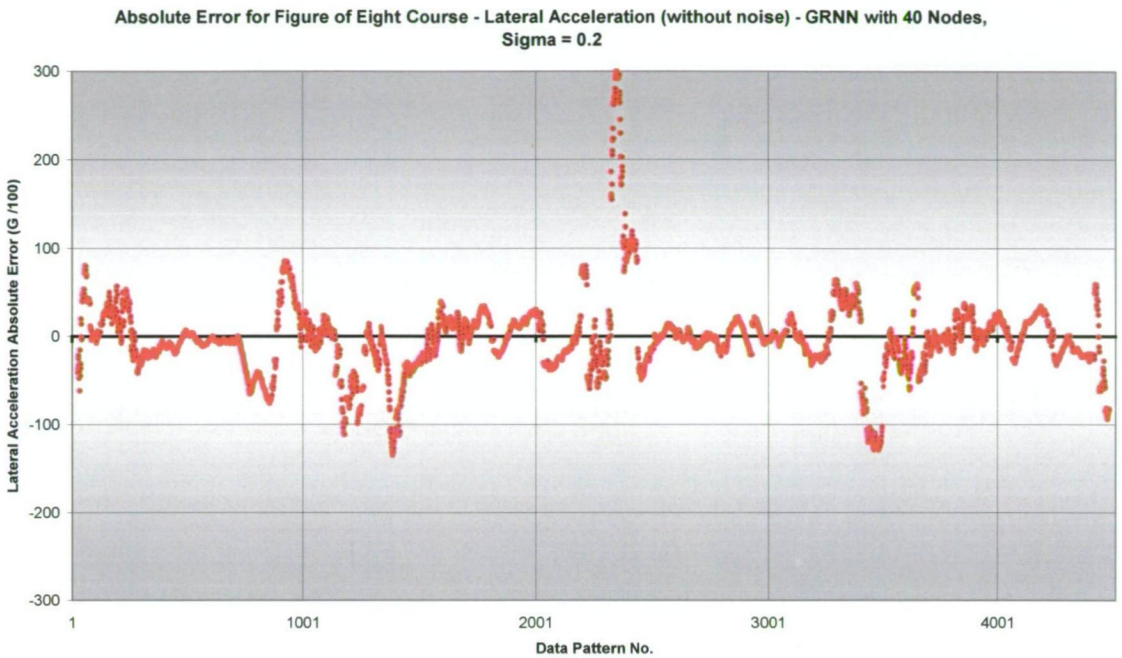

J.16: Yaw angle GRNN prediction during network training – course 2

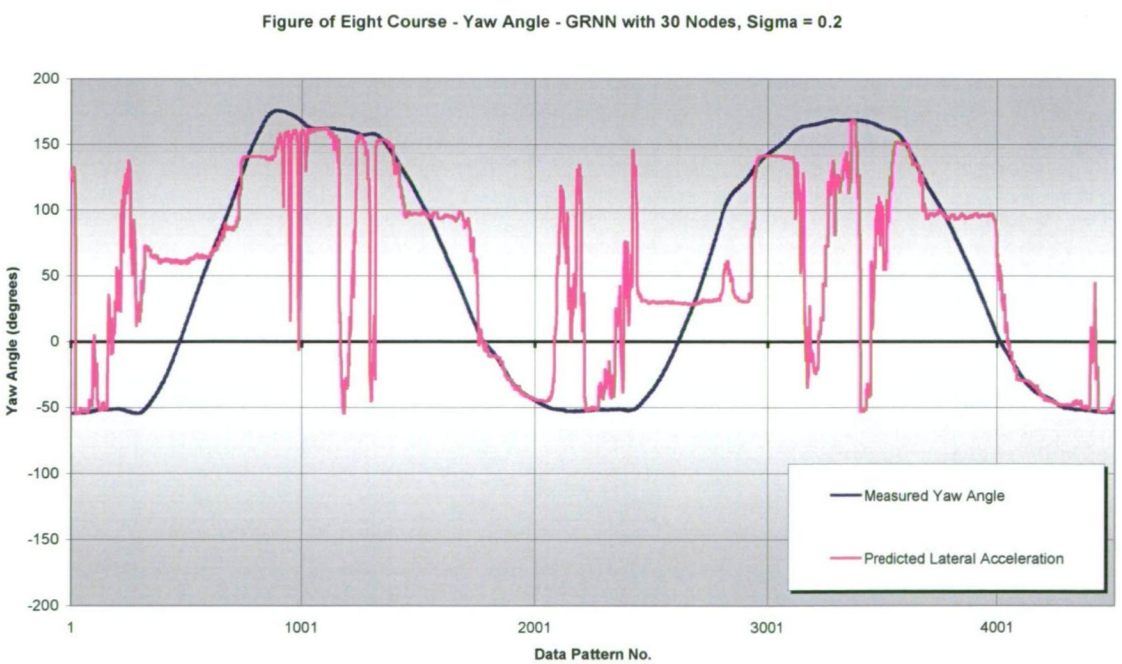

J.17: Yaw angle GRNN prediction during network testing – course 2

J.18: Yaw angle GRNN prediction error – course 2